Molecular and Cellular Studies of *Drosophila* Neuroserpin Spn4A and its Polymer-Forming Mutants

by

Christine Chieh-Lin Lai

B.Sc. University of British Columbia, 2008

A THESIS SUBMITTED IN PARTIAL FULFILLMENT OF
THE REQUIREMENTS FOR THE DEGREE OF

MASTER OF SCIENCE

in

THE FACULTY OF GRADUATE STUDIES

(Microbiology & Immunology)

The University of British Columbia

(Vancouver)

August 2010

Abstract

Serpins (**Ser**ine **P**rotease **In**hibitors) are expressed by most organisms and perform a variety of functions. Most serpins inhibit proteases by undergoing a unique conformational change. They are clinically relevant in two ways. First, introduction of single amino acid point mutations transforms the serpins' labile conformations into pathogenic, inactive polymers causing "serpinopathies". In particular, human neuroserpin is a brain-specific serpin that, when mutated, causes a debilitating early onset dementia through unknown cellular pathways. Second, serpins are currently under investigation as therapeutic inhibitors of proprotein convertases (PCs). PCs are associated with some bacterial and viral infections as well as cancer. However, no comprehensive investigation into the cellular effects of PC inhibitor expression in mammalian cells has been performed.

This thesis details the use of the *Drosophila* serpin, Spn4A, to address the cellular pathways mediated by serpin polymers or PC inhibition. Spn4A is a neuron-specific, secretory pathway serpin that inhibits *Drosophila* or human PCs. We hypothesized that Spn4A mutants, encoding homologous disease-causing mutations in human neuroserpin, would form pathogenic polymers and represent an ideal candidate for generating a cell-based and transgenic *Drosophila* serpinopathy model. Further, we hypothesized that we could evaluate the cellular response to PC inhibition and polymer accumulation by transcriptome profiling of H4 human neuroglioma cells expressing Spn4A wild-type and mutants.

We established an expression system using Spn4A and its mutants in H4s. Subsequently, we used microarray analysis to simultaneously address how serpin polymers may induce cytotoxicity as well as the effects of proprotein processing inhibition in neuroglioma cells. We demonstrated that Spn4A mutants formed polymers, were retained in the endoplasmic reticulum, and lacked inhibitory function, but induced few changes on the transcriptome (under 20 genes differentially regulated). To this end, we have developed transgenic *Drosophila* overexpressing Spn4A variants to further investigate the biological impact of Spn4A mutants. Next, we analyzed the response to the PC inhibitor, Spn4A, and found marked changes in genes related to malignancy. Our genome-wide gene expression studies have provided novel insights into cellular changes in response to polymeric or PC-inhibiting serpins, and establish the foundation for future functional studies.

Preface

Ethics certificates for transgenic *Drosophila* experiments were obtained by Dr. Carl Hashimoto at Yale University. All transgenic fly experiments were performed by Dr. Hashimoto. Phylogenetic analysis of Spn4A was performed and Fig. 2.2 was generated by Dr. Victoria Svinti (Dr. François Jean's lab). Catherine Verreault (Dr. Jean's lab) cloned four Spn4A variants (Spn4A-S S49P, S52R, H338R, and G392E). Adenoviruses Ad. Emp, Ad. Spn4A WT-S, Ad. RFP Spn4A WT-S, and Ad. RFP Spn4A WT-R were generated previously by Dr. Jean's lab. I prepared RNA for microarray experiments, Dr. Anne Haegart (Vancouver Prostate Center Microarray Facility, Vancouver, Canada) performed the microarray experiment and Dr. Robert Bell (Vancouver Prostate Center Microarray Facility, Vancouver, Canada) performed the statistical analysis and provided me with fold changes and p-values. I performed all the other experiments and prepared the figures.

Table of Contents

List of Tables

List of Figures

List of Abbreviations

Ad	Adenovirus
AhR	Aryl hydrocarbon receptor
AJAP1	Adherens junctions associated protein 1
ALPP	Alkaline phosphatase, placental (Regan isozyme)
ATF6	Activating transcription factor 6
BCL2	B cell lymphoma 2
BiP	Binding immunoglobulin protein
BMF	BCL2 modifying factor
C5ORF13	Chromosome 5 open reading frame 13, also known as P311
CCN	Cyclin
CD24	CD24 molecule
CD36	CD36 molecule (thrombospondin receptor)
CDC25A	Cell division cycle 25
CDK	Cyclin-depndent kinase
CDKN1C	Cyclin-dependent kinase inhibitor 1C
cDNA	Complementary deoxyribonucleic acid
CFSE	Carboxyfluorescein succinimidyl ester
CNS	Central nervous system
CT	Threshold cycle
DAVID	Database for Annotation, Visualization and Integrated Discovery
DCN	Decorin
DDIT3	DNA-damage-inducible transcript 3
DMEM	Dulbecco's modified eagle medium
E2F2	E2F transcription factor 2
ECM	Extracellular matrix
EDTA	Ethylenediaminetetraacetic acid
EI	Enzyme-inhibitor
eLF2α	Eukaryotic translation initiation factor 2 alpha
Emp	Empty
EOR	ER overload response
EPYC	Epiphycan
ER	Endoplasminc reticulum
ERAD	ER associated degradation
ERGIC	ER-Golgi Intermediate Compartment
ERRFI1	ERBB receptor feedback inhibitor 1
ES	Enrichment score
ETH	Ecdysis triggering hormone
ETV5	Ets variant 5
F	FLAG polypeptide tag
FC	Fold change
FENIB	Familial Encephalopathy with Neuroserpin Inclusion Bodies

FGF	Fibroblast growth factor
FLIP	Fluorescence loss in photobleaching
FRAP	Fluorescence recovery after photobleaching
G1	Gap1
G2	Gap2
GADD	Guanidinylated aryl 2,5-dideoxystreptamine derivatives
gB	Glycoprotein B
GDF15	Growth differentiation factor 15
GUCY1A3	Guanylate cyclase 1, soluble, alpha 3
HA	Hemagglutinin
hCMV	Human cytomegalovirus
HDEL	His-Asp-Glu-Leu
HEK293	Human embryonic kidney 293 cells
HERPUD1	Homocysteine-inducible, ER stress-inducible, ubiquitin-like domain member 1
HF	His and FLAG polypeptide tag
HGG	High grade gliomas
HIV-1	Human immunodeficiency virus 1
hNS	Human neuroserpin
Hsp47	Heat shock protein 47 kDa
HSPA5	Heat shock 70 kDa protein 5
IGF	Insulin growth factor
IGFR	Insulin growth factor receptor
IL8	Interleukin-8
IPA	Ingenuity Pathway Analysis
IRE1	Inositol requiring enzyme 1
ITGA	Integrin alpha
KDEL	Lys-Asp-Glu-Leu
Ki	Inhibition constant of the enzyme-inhibitor complex
KRT81	Keratin 81
LPC	Lymphoma proprotein convertase
M	Mitosis
MCM	Mini chromosome maintenance
MEF	Mouse embryonic fibroblast
MGP	Matrix gla protein
ML	Maximum likelihood
MMP	Matrix metalloproteases
MOI	Multiplicity of infection
mRNA	Messenger ribonucleic acid
MT1-MMP	Membrane type 1 matrix metalloprotease
MTS	3-(4,5-dimethylthiazol-2-yl)-5-(3-carboxymethoxyphenyl)-2-(4-sulfophenyl)-2H-tetrazolium inner salt
MYC	v-Myc myelocytomatosis viral oncogene homolog

Nek2	Never in mitosis gene A-related kinase 2
NFκB	Nuclear factor kappa-light-chain-enhancer of activated B cells
NI	Non-infected cells
OLR1	Oxidized low density lipoprotein (lectin-like) receptor 1
ORC	Origin of replication complex
PA	Protective antigen
PAGE	Polyacrylamide gel electrophoresis
PAI-1	Plasminogen activator inhibitor 1
PAS	Periodic acid/Schiff reagent
PBS	Phosphate buffered saline
PBS-S	PBS with 0.05% saponin
PC	Proprotein convertase
PCR	Polymerase chain reaction
PCSK-9	Proprotein convertase subtilisin kexin-9
PDB	Protein data bank
PDGF	Platelet-derived growth factor
PEA	Pseudomonas exotoxin A
PERK	PKR-like endoplasmic reticulum kinase
PI8	Proteinase inhibitor 8
PLAG-1	Pleiomorphic-adenoma gene 1
PLAT	Tissue type plasminogen activator
PLAUR	Urokinase plasminogen activator receptor
PPAP2A	Phosphatidic acid phosphatase type 2A
qPCR	Quantitative real-time polymerase chain reaction
RCL	Reactive center loop
RFP	Red fluorescent protein
RGS1	Regulator of G-protein signaling 1
ROS	Reactive oxygen species
RSL	Reactive site loop
S	Synthesis
S100A4	S100 calcium binding protein A4
SCID	Severe combined immunodeficiency
SDS	Sodium dodecyl sulfate
SEM	Standard error of the mean
Serpin	Serine protease inhibitor
SKI-1	Subtilisin/kexin-like isozyme-1
SMC	Structural maintenance of chromosome proteins
SOCS2	Suppressor of cytokine signaling 2
SP	Signal peptide
Spn4A	Serpin 4A
SPP1	Secreted phosphoprotein 1
SPRR2D	Small proline-rich protein 2D
STS	Staurosporine

TGFA	Transforming growth factor alpha
TGFβ	Transforming growth factor beta
TGFβR	Transforming growth factor beta receptor
TGN	Trans-Golgi network
TNF	Tumor necrosis factor
tPA	Tissue-type plasminogen activator
uPA	Urokinase-type plasminogen activator
UPR	Unfolded protein response
VEGF	Vascular endothelial growth factor
WAG	Whelan and Goldman
WT	Wild type
XBP1	X-box binding protein 1

Acknowledgements

I would like to acknowledge numerous people who have supported me through my Masters at UBC. I thank my supervisor, Dr. François Jean, for the opportunity to learn so much about serpins, guidance on how to present and write scientifically, and many discussions that left me with more questions than answers. Also, I thank my committee members, Dr. Michael Gold and Dr. Steven Hallam, for their time, advice on my projects, and encouragements.

I would like to thank Dr. Carl Hashimoto for his gift of the *Drosophila* Spn4A and human neuroserpin cDNA and collaboration to make transgenic flies.

I am grateful to the members of the Jean lab who are always available for questions, laughs, and chocolate. Especially Martine Boutin, who ordered reagents on short notice and lent me a hand when I was too ambitious with experiments. I also thank Catherine Verreault, a past co-op student, who cloned the first four serpinopathy-linked variants to start the project. Further, Dr. Victoria Svinti helped with the phylogenetic analysis of Spn4A. Lastly, I thank Steve McArthur, a Master student, who critically read my thesis.

I thank my family and friends for all their support; especially my dad, who rushed to fix my computer when it crashed while writing my thesis, and my mom, who brought me food when I was too tired to cook. I am thankful for my older brother, Ben, who helped me through my undergraduate and graduate years with advice on science and life. Also, I thank Mark for his emotional and technical support. The microarray analysis would not have been possible without his scripts.

Last, I am grateful for the Graduate Entrance Scholarship from the UBC Microbiology and Immunology Department and Master's Award from the Canadian Institute of Health Research (CIHR CGM-98317). This work is supported by a CIHR grant (III-94585) to Dr. François Jean.

Dedication

For my parents, brother, and puppeh.

Chapter 1: Introduction

1.1 Serpins

Serpins (**Ser**ine **P**rotease **In**hibitors) comprise a protein superfamily found in organisms ranging from humans and plants to viruses and prokaryotes (1-4), as identified by conserved sequence motifs (5). In humans, 36 serpins have been identified to date (2). These serpins can localize extracellularly or intracellularly and most inhibit serine proteases. A few others also inhibit cysteine proteases, or lack inhibitory activity altogether (2). Phylogenetic analyses categorize serpins into 16 clades labeled A to P, with 10 additional unclassified serpins (5). Generally, human serpins reside in clades A to I, while clades J to P group according to nonvertebrate species (5).

1.2 Serpin structure and inhibitory mechanism

Serpins are identified by a total of approximately 50 highly conserved amino acid residues and an ~30% amino acid sequence homology (5) to the prototypical serpin, α_1-antitrypsin, an inhibitor of neutrophil elastase (6). Despite low amino acid sequence homology, all serpins share a conserved tertiary structure (6). Most serpins have three β-sheets and nine α-helices like α_1-antitrypsin (Fig. 1.1A) (7). The reactive site loop (RSL) or reactive center loop (RCL) lies approximately 20 to 25 amino acids above the serpin core and contains a peptide sequence to bait target proteases (6). The native structure exists in a metastable or "stressed" state (8). Once a protease recognizes the pseudosubstrate peptide in the RCL, the P1-P1' bond is cleaved and an acyl ester bond forms between the protease and the serpin (6). Like a mousetrap, the serpin undergoes a conformation change that involves the end-to-end translocation of the protease by incorporation of the clipped RSL into the serpin's β-sheet A (9) (Fig. 1.1C). The conformational transition is accompanied by an increase in serpin stability, bringing it into the "relaxed" state (8). In the new conformation, the protease active site is distorted, preventing the deacylation step and the reaction from running to completion (9). Thus, serpins are suicide inhibitors, trapping the protease in an irreversible and heat- and SDS (sodium dodecyl sulfate)-stable covalent complex.

Aberrations such as mutations within the RSL limit its insertion rate into the β-sheet, resulting in serpin cleavage instead (10) (Fig. 1.1D). For example, the P14 position (14^{th} residue on the amino terminal side of the cleavage site), usually a serine or threonine, acts like a hinge

for RSL insertion (11). Mutations at P14 to charged or bulky amino acids force the serpin into the substrate pathway, producing active protease and non-inhibitory, cleaved serpin (11;12).

1.3 Human serpins

1.3.1 Function and localization

In humans, the majority of the serpins are inhibitory. Some are secreted into the circulating plasma to control extracellular proteolytic cascades such as inflammation (α_1-antitrypsin inhibition of elastase (13)), the complement pathway (C1 inhibitor and C1 esterase (14)), blood clotting (antithrombin and thrombin (15)), or tissue remodeling (neuroserpin and tissue plasminogen activator (16)). Other serpins localize to the cytoplasm to control inappropriate protease activities (cytoplasmic antiproteinase 9 inhibition of granzyme B (17;18)).

The small number of non-inhibitory serpins localize extracellularly or intracellularly. Non-inhibiting serpins may function as hormone precursors like angiotensinogen, which regulates blood pressure (19), or hormone transporters, such as thyroxine-binding globulin (20). Intracellularly, well studied and non-inhibitory serpins include the chaperone Hsp47 (heat shock protein 47 kDa) (21) and the tumor suppressor maspin (22). Non-inhibitory serpins may have regions beside the RSL that are involved in biological activities (6).

1.3.2 Serpinopathies

Serpin diseases can arise from mutations affecting the inhibitory mechanism or serpin stability. In the latter, point mutations cause serpins to fold into disease-causing conformations, known as pathogenic polymers. The new conformational transition involves domain swapping of one RSL and β-sheet strand from one serpin to the β-sheet of another serpin (23;24) (Fig. 1.2). The inactive long-chain polymers are known to cause several diseases, collectively known as "serpinopathies" (25;26).

Serpin polymers cause gain and/or loss of function diseases. The best studied example is α_1-antitrypsin deficiency. α_1-Antitrypsin is synthesized in liver cells and secreted into the plasma. It maintains the integrity of the lung tissue by inhibiting neutrophil elastase. The most common and clinically significant mutation of α_1-antitrypsin, called the Z allele, leads to polymer formation and subsequent retention of the serpin within hepatocytes. Inclusion body formation manifests physiologically as hepatitis, cirrhosis, and hepatocellular carcinoma (27;28). Further,

decreased serum levels and inhibitory activity expose lung tissue to uncontrolled elastase proteolysis, leading to emphysema.

Pathogenic polymers also underlie the hereditary dementia, Familial Encephalopathy with Neuroserpin Inclusion Bodies (FENIB). Central nervous system neurons secrete neuroserpin, which controls synaptic plasticity by inhibiting tissue plasminogen activator (29). Several point mutations identified in neuroserpin result in neuronal inclusion body formation. Clinically, the inclusion bodies are associated with dementia, which manifests as early as childhood (30) with mortality in early adulthood (31). The loss of extracellular neuroserpin and regulation of synaptic contact formation may also cause epilepsy (30).

1.4 *Drosophila* Spn4A

Fewer serpins are well characterized in other organisms compared to humans. Nonetheless, the study of serpins in model organisms has broadened our knowledge of their functional diversity and cellular localization. One of the best examples comes from the *Spn4* (Serpin 4) gene in *Drosophila*. *Spn4* can be alternatively spliced into eight protein isoforms (A-H) using four different RSL sequences. Isoforms A-D differ from E-H by the presence of an N-terminal signal peptide (SP) (32), targeting proteins to the secretory pathway. Spn4A contains an ER retention motif at the C-terminus (32), and unlike Spn4B-D, is not secreted to the extracellular space (33). Without the N-terminal targeting sequence, Spn4E-H are not secreted (33).

In vitro, Spn4A can inhibit *Drosophila* and human furin as well as *Drosophila* PC2 (proprotein convertase 2) (33-36), serine endoproteases important for activation of proproteins, such as hormones, in the secretory pathway. In *Drosophila*, Spn4A localizes to the central nervous system. Its overexpression leads to lethal larval molting defects (35) resembling the *Drosophila* PC2 (37) and ETH (ecdysis triggering hormone) (38) loss of function phenotype. This was the first demonstration of an endogenous serpin co-localizing and inhibiting a PC. Further evidence of the novel function was recently confirmed in a *Branchiostoma lanceolatum* serpin, B1-Spn1, which has an N-terminal signal peptide and ER retrieval signal and inhibits PCs (39).

The PC inhibitory activity of Spn4A is of therapeutic interest. PCs control the maturation of proteins such as growth factors and extracellular matrix proteins important for tumor

malignancy as well as the activation of viral proteins and bacterial toxins (40). The ability of Spn4A to inhibit PC activity under human pathological conditions has been demonstrated by our lab (unpublished data). Previous work showed that Spn4A blocked PC-mediated processing of viral coat proteins from HIV-1 (human immunodeficiency virus I) by Vesna Posarac (Jean lab, Master's student, 2008), hCMV (human cytomegalovirus) by Martine Boutin (Jean lab, technician), and H5N1, H7N3, and H7N7 influenza viruses by Dr. Sandra Diederich (Jean lab, postdoctoral researcher). Therefore, Spn4A may be an effective treatment for various PC-mediated pathologies including infectious diseases and cancer.

1.5 Project overview

The ability of polymer-forming serpin mutants to cause disease and the development of serpin PC inhibitors as cancer therapeutics are two clinically significant research fields. However, many questions remain regarding the pathogenesis of polymers (discussed in Chapter 2) and the potential of PC-targeted therapeutics (discussed in Chapter 3).

Drosophila Spn4A offers a unique vantage point in studying the pathobiology and therapeutic application of serpins. As a neuron specific serpin, Spn4A mutants encoding homologous FENIB-causing substitutions may be molecular tools for studying the cellular pathways associated with FENIB in cell culture and transgenic *Drosophila* models. Further, Spn4A has pharmacological significance as a potent inhibitor of PCs. We addressed these two different roles.

The overall objective of this thesis project was to use Spn4A variants to study the cellular responses to serpin polymers and furin inhibition (Fig. 1.3). Accordingly, we describe the development and transcriptome profile of a cellular model expressing Spn4A polymer forming-mutants (Chapter 2). We show that Spn4A mutants, with amino acid substitutions equivalent to those found in FENIB, formed polymers in human H4 neuroglioma cells. Gene expression profiling revealed that fewer than 20 genes were differentially regulated in response to Spn4A polymers. Further, to evaluate Spn4A as a therapeutic agent, we investigated the transcriptome profile of neuroglioma cells expressing Spn4A and found marked changes in cell proliferation and movement (Chapter 3). Consequently, we hypothesize mechanisms through which PC inhibition may block tumorigenesis and malignancy. Finally, we developed a non-inhibitory hinge mutant of Spn4A as a negative control to demonstrate functional specificity (Appendix 1).

Figure 1.1. Serpin structures and mechanisms. A) The structure of native SERPINA1 (α_1-antitrypsin, Protein Data Bank (PDB) code IQLP (41)) is shown. The A sheet is in red, the B sheet in green, the C sheet in yellow, helices in blue, and the reactive center loop (RCL) in magenta. The dashed magenta line indicates the path of RCL insertion. The breach and shutter region are as labeled. B) The multicoloured trypsin protease docks on the RCL of α_1-antitrypsin (PDB code IOPH (42)). C) The protease cleaves the peptide bond, releasing the serpin's C-terminal tail (not shown), and is translocated to the other end of the serpin, which traps the protease in an irreversible serpin-enzyme complex (PDB code IWZX (9)). D) Alternatively, serpins follow the substrate pathway, producing cleaved α_1-antitrypsin (PDB code 7API (43)) and active protease. Reprinted with permission from BioMed Central: Genome Biology, Law RA, Zhang Q, McGowan S, Buckle AM, Silverman GA, Wong W, Rosado CJ, Langendorf CG, Bird PI, and Whisstock JC, An Overview of the Serpin Superfamily (2), © 2006.

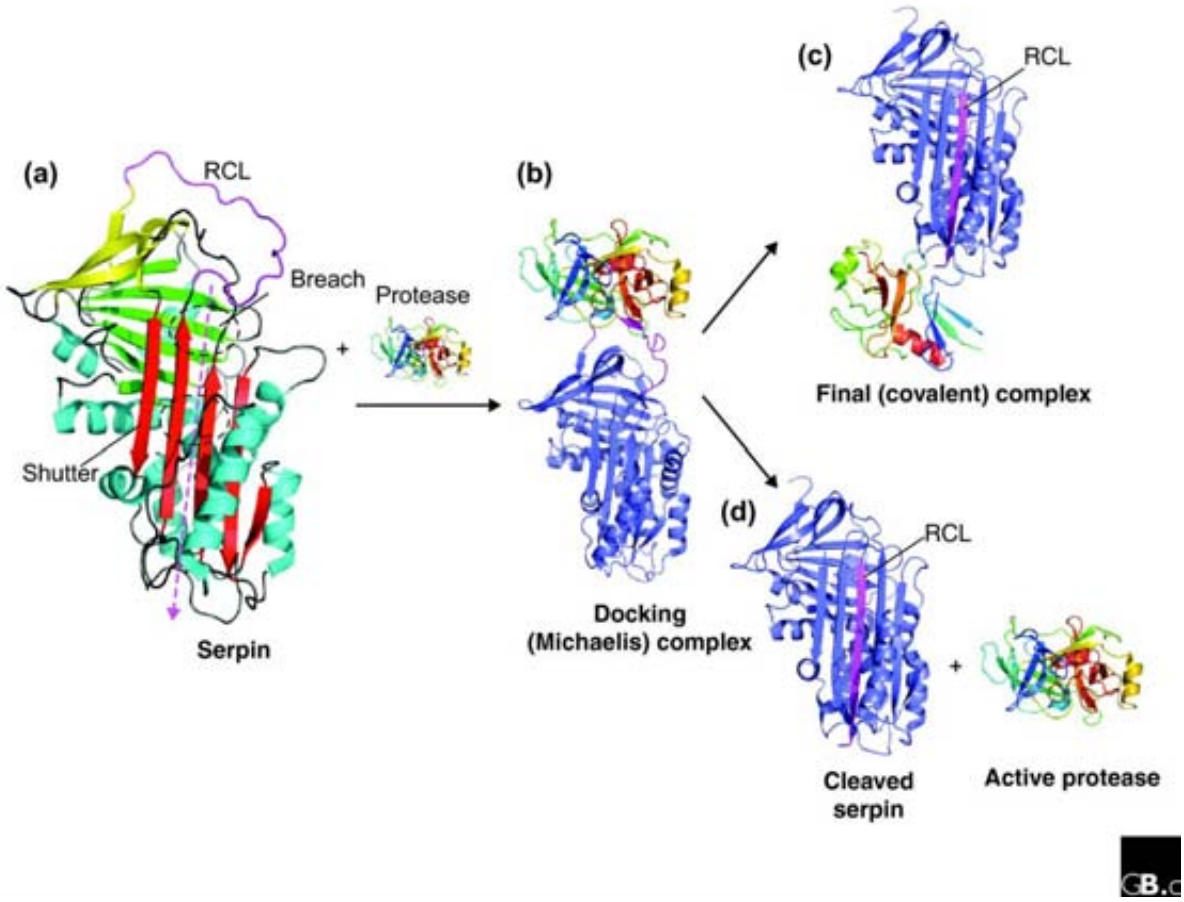

Figure 1.2. Serpin polymer formation. A) Unfolded serpins fold to a short-lived intermediate. B) In the native protein conformation, the β-strand s4A folds into β-sheet A. C) Mutations promote the insertion of one serpin's domain into another. Monomer 2 donates the RCL (reactive centre loop) and s5A into a neighbouring monomer. A third monomer could donate its β-strands to the empty space in monomer 2, allowing polymer growth. Reprinted by permission from Macmillan Publishers Ltd: Nature, Whisstock JC and Bottomley SP, Structural biology: Serpins' mystery solved (24), © 2008.

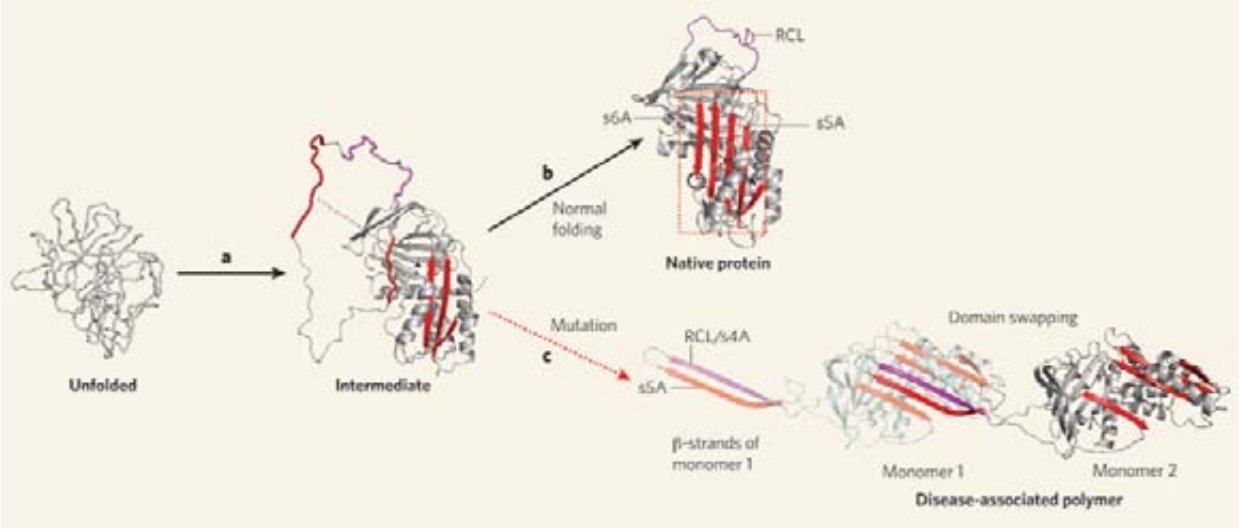

Figure 1.3. Flow chart of themes, questions addressed, and experimental approaches in this thesis project.

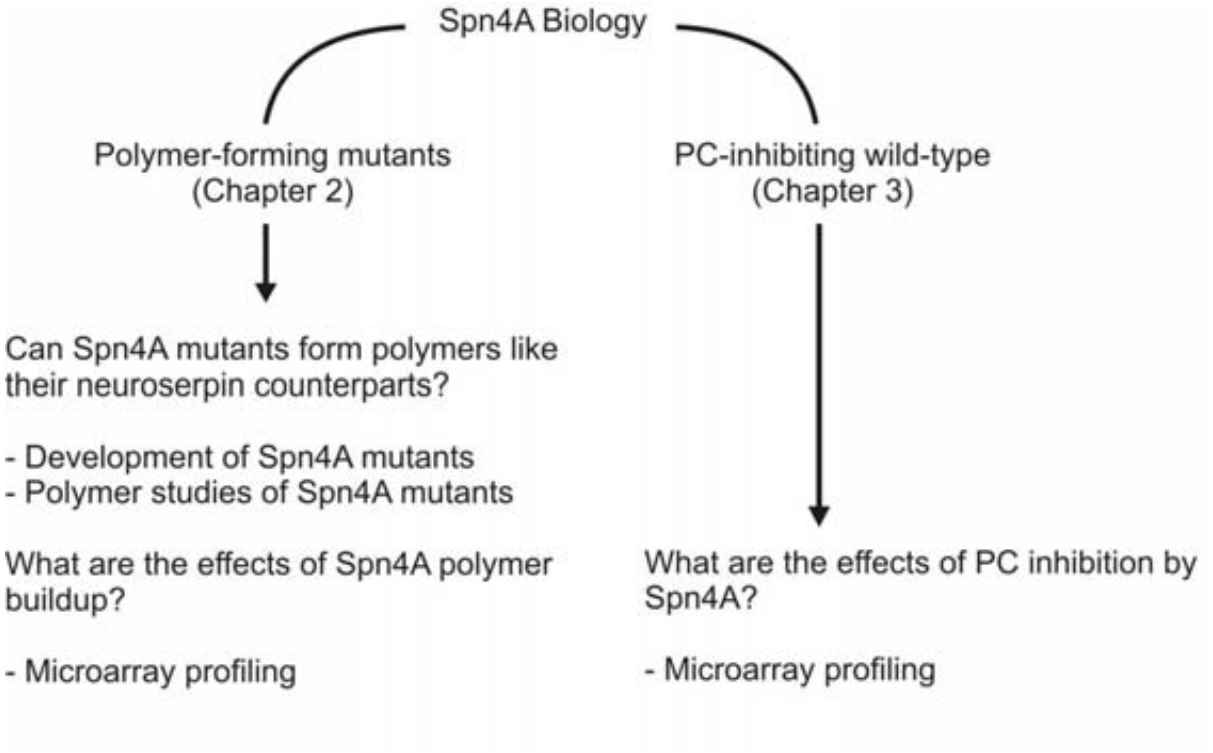

Chapter 2: Development and transcriptome profiling of a cell model expressing Spn4A polymer-forming mutants

2.1 Introduction

2.1.1 Serpinopathies and neurodegenerative diseases

Serpins (**Ser**ine **p**rotease **in**hibitors) are a superfamily of proteins that typically function in the control of proteolytic cascades (6). However, mutations in serpins can cause aberrant protein conformational transitions, resulting in inactive serpin polymers retained inside the cell. Disease is attributed to a toxic gain of function due to intracellular protein inclusion body formations and/or a loss of extracellular inhibitory function (25;26). Polymeric α_1-antitrypsin, C1 inhibitor, antithrombin, α_1-antichymotrypsin, and neuroserpin lead to liver cirrhosis and emphysema, angioedema, thrombosis, emphysema, and dementia and epilepsy, respectively. Together, they are known as the serpinopathies (25;26).

The most recently described serpinopathy is caused by mutations to neuroserpin, an inhibitor of tissue-type plasminogen activator (tPA) (29;44), that result in the formation of neuronal inclusion bodies. Familial Encephalopathy with Neuroserpin Inclusion Bodies (FENIB), described in six families to date, is a disorder characterized by early-onset dementia, seizures, and/or tremors (45). Although affecting only a handful of families worldwide, FENIB shares common disease hallmarks – conformational instability, oligomerization, and inclusion body deposition – with other neurodegenerative syndromes such as Alzheimer's, Parkinson's, and Huntington's diseases as well as the prion encephalopathy. Unlike other disorders, the causative protein and its function, mechanism, and native and disease-causing structures are clear in FENIB (29;46;47). Thus, models of FENIB are likely to provide insight into the pathogenesis of other neurodegenerative diseases (25;26;48).

2.1.2 FENIB

2.1.2.1 Human neuroserpin

Human neuroserpin (hNS) is expressed primarily in embryonic and adult neurons of the central nervous system (CNS), with low levels in the pancreas, heart, kidney, and testis (29). *In vitro*, neuroserpin has inhibitory activity toward tPA and to a lesser extent, urokinase-type plasminogen activator (uPA) and plasmin (29;44). Detection of an enzyme-bound serpin

complex from cultured cells expressing both neuroserpin and tPA suggest that the complex also occurs *in vivo* (49). In the brain, neuroserpin and tPA are both secreted from growth cones at the tips of axons especially during neurite outgrowth, synaptogenesis, and synaptic plasticity (50). Further, neuroserpin is neuroprotective in blocking tPA-dependent seizures (51) and stroke (52;53).

2.1.2.2 Human pathology of FENIB

First described in 1999, FENIB is an inherited, autosomal dominant disorder caused by mutations to hNS (46). It presents with myoclonus (muscle twitching) and pre-senile dementia, affecting individuals as early as eight years of age to as late as 50 years of age (45;46). FENIB patients have problems with shortened attention span and oral fluency in the early stages (54). Global cortical atrophy is found in more severe cases (54). Neuroserpin inclusion bodies, named Collins bodies, are histologically unique (periodic acid/Schiff reagent (PAS)-positive, but diastase-resistant), can be 1-50 μm in diameter (46;55), and deposit in the cerebral cortex and substantia nigra (located in the midbrain) (46). Isolated Collins bodies were shown to be composed exclusively of neuroserpin by amino-acid sequencing (46). Subsequent genetic sequencing of affected individuals revealed point mutations resulting in the following substitutions S49P, S52R, H338R, G392E, or G392R (30;31;46;56).

2.1.2.3 Biochemical studies of hNS mutants

To understand how single amino acid point mutations may lead to disease, neuroserpin mutants were cloned and expressed in *Escherichia coli* (57-59) or in mammalian cells (60;61). Polymers are identified by ladder formations on non-denaturing polyacrylamide gel electrophoresis (PAGE) (57-60) and punctate inclusions within the endoplasmic reticulum (ER) by confocal microscopy (60;61). Decreased levels of extracellular mutant serpins are found in the cultured media, demonstrating protein retention (61). Strikingly, the molecular instability of neuroserpin, assessed biochemically by polymer formation rate, is directly related to the amount of inclusion body formed in human brain histology samples and to disease severity (Table 2.1) (31). Further, neuroserpin mutants are poor inhibitors of tPA (the S49P mutant had a 100 fold difference in inhibitory constant compared to the wild type [WT] and the S52R mutant was not inhibitory at all) (57-59), which may intensify epileptic episodes and other neurological symptoms (30;45).

2.1.2.4 Cellular studies of hNS mutants

The cellular response to polymer accumulation is currently under investigation. Since the ER is the site of polymer retention, pathways within the ER may mediate toxic effects. The unfolded protein response (UPR), ER overload response (EOR), ERAD (ER associated degradation), or autophagy are pathways activated by cells to cope with increased intracellular protein load. Excessive signaling from these pathways, or lack thereof from ERAD, may lead to apoptosis (62;63).

The UPR includes the PERK (PKR-like endoplasmic reticulum kinase), IRE1 (inositol requiring enzyme 1), and ATF6 (activating transcription factor 6) signaling pathways in response to increased ER protein load or pathological stresses, such as the presence of misfolded proteins (Fig. 2.1). The ER molecular chaperone, BiP (binding immunoglobulin protein), normally binds to these three transmembrane signal transducers and is released when misfolded protein accumulates (64). Freed IRE1 then dimerizes, which activates its endonuclease activity leading to alternative splicing of the *XBP1* (X-box binding protein 1) mRNA (messenger ribonucleic acid), which produces an active transcription factor (65;66). Release of ATF6 leads to its translocation to the Golgi, where it is proteolytically processed to an active transcription factor (67). Last, PERK dimerizes and phosphorylates eLF2α (eukaryotic translation initiation factor 2 alpha) to attenuate general mRNA translation while promoting the translation of select mRNAs such as *ATF4* (68;69). These three transcription factors (Xbp1, ATF6, and ATF4) regulate stress-response genes, ultimately leading to protein translation attenuation, increased chaperone expression, and protein degradation through ERAD, enabling the cell to cope and recover from stress (62). The inability to resolve the excess load results in signaling from the transcription factor CHOP, which represses transcription of the anti-apoptotic protein Bcl2 (B cell lymphoma 2) and activates several apoptotic genes (62).

Alternatively, ER protein buildup may activate EOR (70;71). EOR involves the release of calcium from the ER into the cytoplasm and subsequent production of reactive oxygen species (ROS) mediates the activation of NFκB (nuclear factor kappa-light-chain-enhancer of activated B cells) (70;71). The existence of EOR is currently under scrutiny as NFκB can also be activated by PERK signaling (72), but others have shown UPR-independent NFκB activation (73). NFκB induces the transcription of many genes involved in pro- and anti-apoptotic pathways, inflammation, immunity, and proliferation (74).

Protein buildup in the cell may be cleared by activating ERAD or autophagy (75). ERAD involves targeting misfolded proteins to the ubiquitin-proteasome pathway by retro-translocation from the ER to the cytoplasm (75). Autophagy involves the degradation of large aggregates by membrane vesicles called autophagosomes that engulf the protein load and fuse with lysosomes (76). Autophagy has been linked to apoptosis, although its direct role is unclear (77).

Recently, Davies *et al.* demonstrated that neuroserpin polymers fail to activate the UPR, but found that S52R and G392E neuroserpin mutants can activate NFκB in the rat adrenal pheochromocytoma cell line, PC12, and mouse embryonic fibroblast (MEF) cells (73). Further, Kroeger *et al*. demonstrated that mammalian cells employ ERAD and, in MEF cells, autophagy, to clear polymeric mutant serpins (78).

2.1.2.5 Models of FENIB in lower organisms

To assess the effects of polymer accumulation in model organisms, transgenic *Drosophila melanogaster* expressing hNS S49P, S52R, H338R, or G392E mutants (61) and mice expressing hNS S49P, S52R, or G392E mutants (79;80) were generated. Intracellular accumulation is detected in both model organisms. Flies expressing mutant hNS suffer from locomotor dysfunction, but no differences in longevity are observed (61). Also, WT and mutant neuroserpin are cleared with equal efficiency from fly brains (78). The transgenic mice exhibit clinical features such as ataxia and tremors (79). Neuronal apoptosis, measureable by caspases and cytoplasmic cytochrome C, is not apparent (80). Dose-dependence of protein aggregate formation is demonstrated in transgenic hemizygous G392E mice, which do not form protein aggregates, and their homozygous counterparts, which do (80). Together, these results indicate that human mutant neuroserpin forms intracellular aggregates that can independently cause neurodegeneration.

Further, a rat model of FENIB was generated from the overexpression of human wild-type megsin (81), a serpin targeting plasmin *in vitro* (82). While homozygous transgenic megsin rats suffer from renal and pancreatic lesions (83), heterozygous transgenic rats fail to show any abnormities in those organs (81). Instead, the heterozygous transgenic rats display characteristic inclusions in neurons, express ER stress and apoptotic proteins (BiP, hypoxia upregulated 1 protein, caspase 12 and 3), have significant neuronal loss, but have the same life span as control non-transgenic rats (81).

2.1.2.6 Further questions and Spn4A

Within a decade of the discovery of FENIB, hNS mutants were identified and demonstrated to form polymers that led to disease. However, the details of the molecular and cellular events contributing to pathology are still unclear. Importantly, the signaling pathways that activate NFκB and its consequent pathways leading to cell survival, proliferation, or death (74) still needs to be elucidated. NFκB can control the transcription of over 150 genes depending on cell type and stimulus (84). Relevant genes in response to pathogenic polymers can be addressed using cDNA (complementary deoxyribonucleic acid) microarray technology.

Further, the effects of the modulated cellular pathways will need to be assessed in a model organism. *Drosophila* is an economical and genetically amenable model organism in which we could dissect the cellular mechanisms underlying FENIB. The current transgenic *Drosophila* FENIB models express human neuroserpin mutants and recapitulate some clinical symptoms of neurological disease, but not life span or neuronal loss (61). Further, they could clear hNS WT or mutants with equal efficiency (78). In comparison, the serpinopathy model of α_1-antitrypsin deficiency in *Drosophila* uses the endogenously-expressing serpin Necrotic, homologous to α_1-antitrypsin (85). Transgenic *Drosophila* expressing polymeric Necrotic mutants were observed to have a temperature-dependent lethality phenotype. The lack of a strong toxic phenotype in the FENIB *Drosophila* model may be due to the levels of expression, since higher levels of mutant hNS are associated with greater disease severity (Table 2.1), or the production of foreign human proteins in transgenic models. Increased expression of polymeric mutants or the use of endogenous serpins with homologous mutations may be advantageous.

To date, only Serpin 4 (Spn4) is known to be expressed in the *Drosophila* CNS (35). *Spn4* can be alternatively spliced to produce eight different protein isoforms, changing between four different reactive site loops (RSL) to bait different proteases, and omitting or including an N-terminal signal peptide, allowing different cellular localizations (32). Spn4A (isoform A) contains an N-terminal signal peptide and a 13 amino acid C-terminus extension, similar to hNS (86). Several studies have demonstrated that Spn4A is an inhibitor of human and *Drosophila* furin, as well as *Drosophila* PC2 (proprotein convertase 2) (33-36). Transgenic *Drosophila* generated from the native and neuron-localized serpin, Spn4A, may provide a good model system for studying FENIB. The ability of Spn4A mutants to form polymers like hNS would first have to be evaluated. The expression of Spn4A mutants in a mammalian cell line may be used to

study polymer formation. Further, this cellular expression system may be used to address the subsequent cellular responses to serpin polymers.

2.1.3 Hypothesis, aims, and experimental approach

The overall goal was to develop a cell-based and transgenic *Drosophila* model of FENIB to study the serpinopathy disease mechanisms, using Spn4A.

We hypothesized that mutant Spn4A could form polymers, modulate cellular stress pathways, and cause disease symptoms in transgenic *Drosophila*, similar to mutant hNS.

Specific Aim 1: Establish a cell-based system to evaluate polymer formation, retention, and non-inhibitory function of Spn4A mutants. First, we evaluated the phylogenetic relationship between Spn4A and hNS, and generated Spn4A mutants with amino acid substitutions equivalent to those found in FENIB-causing hNS residues. Next, we tested the ability of Spn4A mutants to form polymers and be retained in the ER, which are cellular signatures of hNS mutants. We used transfection and adenovirus infection systems to express Spn4A WT and mutants in an H4 mammalian neuroglioma cell line. We chose to use H4 cells, instead of macrophage-like *Drosophila* Schneider 2 cells, in order to investigate polymer formation and consequences in a neuronal cell context (specific aim 2). Further, tools such as antibodies and microarray chips are more readily available for human systems. Polymer formation and retention were assessed by SDS-PAGE (sodium dodecyl sulfate polyacrylamide gel electrophoresis), non-denaturating PAGE, and confocal microscopy. Lastly, the inhibitory activities toward furin were also studied.

Specific Aim 2: Determine transcriptome changes in response to Spn4A mutants. Polymer accumulation may lead to the activation of stress signaling cascades, which may affect cell health and eventually lead to cell death. To inspect the whole transcriptome for genes that were regulated in response to mutant Spn4A expression, we performed a microarray experiment using the Illumina HumanHT-12 v3 Beadchip.

Specific Aim 3: Generate transgenic *Drosophila* overexpressing Spn4A mutants. In collaboration with Dr. Carl Hashimoto (Yale University), we generated transgenic flies overexpressing Spn4A variants. I cloned the mutants and Dr. Hashimoto's lab generated transgenic flies. The model will be useful for further studies investigating the impact of Spn4A mutants on a whole organism.

2.2 Methods

2.2.1 Phylogenetic analysis

Serpin primary sequences were aligned using CLUSTALW2 (87) for construction of the phylogenetic tree. Two methods for building phylogenetic trees, maximum likelihood (ML) and Bayesian methods, are preferred because these algorithms take into account how the data evolves (model of evolution), which leads to more accurate trees. The Bayesian method used for this analysis is faster than ML since it combines the ML tree search and the bootstrapping steps into one. This saves time while producing trees that are comparable in accuracy. The tree was built using Mr. Bayes v3.1.2 (88;89). The amino acid substitution rates used were those derived from the Whelan and Goldman (WAG) matrix (90). The analysis was run twice for 1 million generations with sampling frequency of 1000 and the number of chains set to 4. The trees retained are those obtained after the convergence of the two runs. This set of trees was summarized into a majority rule consensus tree, with values on the branches reflecting clade credibility.

2.2.2 Cell lines

H4 neuroglioma cells, human embryonic kidney 293 cells (HEK293 or AD293) and HEK293-C4 furin-overexpressing cells (Dr. Richard Leduc, University of Sherbrooke) were maintained in DMEM (Dulbecco's Modified Eagle Medium) containing 10% fetal bovine serum and 100 units of penicillin and streptomycin per mL. Cells were incubated at 37°C in 5% CO_2.

2.2.3 Plasmid constructs

Plasmid cloning reagents include *pfu* polymerase (Fermentas), restriction enzymes (New England Biolabs), Dephosphorylation and Ligation kits (Roche), and DH5α competent cells. Plasmids were purified from DH5α using QIAprep Spin Miniprep Kit (Qiagen) or Nucleobond Xtra Midi kit (Macherey-Nagel). PCR (polymerase chain reaction) fragments were purified using the QIAquick PCR Purification kit (Qiagen). Plasmids used for transfection experiments were constructed in the mammalian expression vector pcDNA3.1 plus (Invitrogen). Primers are listed in Appendix 2, Supplemental Table A2.1.

His and FLAG-tagged (HF) Spn4A, with or without tagRFP (91) (red fluorescent protein), were localized to three different cellular compartments by deletion of the C-terminal

HDEL ER retention motif or the N-terminal SP (signal peptide) (Fig. 2.2). Martine Boutin (Jean lab) had cloned the HF Spn4A ER-retained (designated Spn4A WT-R) and secreted (HDEL deletion, designated Spn4A WT-S) variants into pGEM-T. I further sub-cloned Spn4A WT-S and WT-R into pcDNA3.1 using *KpnI* and *NotI* sites. The RFP-tagged Spn4A WT-R and WT-S variants were cloned by Martine Boutin in pcDNA3.1. For protein localization to the cytoplasm, I removed the SP. Spn4A fragments without the SP were amplified from either Spn4A WT-S (for non-RFP-tagged) or RFP Spn4A WT-R (for RFP-tagged) plasmids using *KpnI* or *NotI* flanking primers, then inserted into the empty vector pcDNA3.1 using the same sites. Mutations at S36P, S39R, H317R, and G374E were inserted using the Stratagene site directed mutagenesis method.

A plasmid containing full length hNS was a gift from Dr. Hashimoto (Yale University). I cloned the hNS cDNA into pcDNA3.1 using *BamHI* and *NotI* flanking primers. A FLAG tag (F) after the SP was inserted using phosphorylated primers carrying the tag (Fig. 2.2). The primers amplified the entire plasmid, which were ligated together after PCR to form a circular vector for transformation into DH5α competent cells. Site-directed mutagenesis was used to make point mutations to hNS at S49P and H338R. All cloned constructs were sequenced to verify integrity.

2.2.4 Recombinant adenovirus constructs and production

Martine Boutin had previously generated adenovirus without transgene (Ad. Empty) and recombinant adenovirus expressing RFP Spn4A WT-S or RFP Spn4A WT-R (Ad. RFP WT-S, Ad. RFP WT-R).

I cloned and produced adenovirus expressing the polymeric mutants RFP Spn4A S52-R or H338R-R following the AdEasy XL Adenoviral Vector System from Stratagene. Briefly, the two mutants were cloned into a pShuttle vector using *KpnI* and *NotI* digest sites, linearized with *PmeI*, and transformed into BJ5183-AD-1 competent cells (Stratagene), where *in vivo* recombination into the plasmid pAdEasy occurs (pAdEasy contains most of the adenovirus genome, but not genes for E1 and E3). Positive recombinants were selected based on the restriction digest pattern with *PacI* and amplified in DH5α competent cells. Plasmids were purified using the Nucleobond Midi kit from Clonetech, further digested with *PacI*, and phenol/chloroform extracted. Linearized plasmids were transfected into low-passage AD293 cells (Stratagene) using TransIT-LT1 (Mirus). AD293 cells carry the E1 gene, which is necessary for production of viral particles (Stratagene). Primary viral stocks were prepared by

harvesting and lysing transfected AD293 cells and used for large scale production of recombinant adenovirus, which was purified with the Adeno-X Maxi Purification kit (Clonetech).

I also cloned RFP Spn4A H338R-S and H338R-C into the pShuttle vector using *KpnI/NotI* sites for adenovirus production by ViraQuest Inc (North Liberty, IA). I titered all viruses used in this thesis with Adeno-X Rapid Titer kit (Clonetech) and titers are reported in Appendix 2, Supplemental Table A2.2.

2.2.5 Transfection and infection conditions

Two hundred thousand H4 or HEK293 cells were seeded per well the day before transfection into 6-well plates and transfected at 70% confluency following the manufacturer's protocol for TransIT-LT1 (Mirus). Specifically, transfections were performed using 1.5 μg DNA and 4.5 μL TransIT-LT1 transfection reagent. For immunofluorescence experiments, 40 000 H4 cells were seeded onto coverslips in 24-well plates the day before transfection and transfected with 0.3 μg DNA and 0.9 μL TransIT-LT1.

Adenovirus infection experiments were performed using the same number of cells per well as the transfections. Cells were counted, resuspended in growth media to the proper concentration, immediately infected with viruses, and seeded onto 6- or 24-well plates.

2.2.6 SDS-PAGE, native PAGE, and western blot

Media and cell samples were collected from both transfection and infection experiments for western blot analysis. Samples from transfections were prepared in the absence of SDS loading buffer to allow for loading onto native PAGE. Media and cell samples from infections were immediately mixed with SDS loading buffer to inactivate viruses and were not used on native gels.

After 48 hours of transfection, media and cell samples were collected. A total of 500 μL of media was collected from each well, centrifuged for 3 minutes at 3000 x g to pellet cell debris, and the top 300 μL kept. Cells were washed with PBS (phosphate buffered saline), scraped from the wells in PBS, and centrifuged for 3 minutes at 3000 x g. The supernatant was removed and cells were lysed in 100-120 μL of hypotonic buffer (20 mM Tris pH 7.4, 10 mM $MgCl_2$, 10 mM

$CaCl_2$) supplemented with fresh Complete, EDTA (ethylenediaminetetraacetic acid)-free protease inhibitor cocktail (Roche).

For SDS-PAGE, 24 μL of cell lysate or media were mixed with 5 x SDS loading buffer containing fresh β-mercaptoethanol and boiled at 95°C for 10 minutes. Samples were separated on 8%, 10%, or 15% SDS-PAGE gels depending on the protein of interest. To detect polymers, 24 μL of cell lysates or media were mixed with 5 x native loading buffer lacking SDS and β-mercaptoethanol, incubated for 30 minutes at 37°C, and loaded onto 8% native PAGE gels (57-60).

After 48 hours of infection, media and cells were harvested as described. To 120 μL of media samples, 30 μL of 5 x SDS loading buffer containing β-mercaptoethanol was added. Cells were lysed in 150-200 μL of hypotonic buffer pre-mixed with SDS loading buffer and β-mercaptoethanol. Samples were immediately boiled at 95°C for 10 minutes to inactivate viruses and used for SDS-PAGE analysis. Electrophoresis was performed at 100-110 V.

Protein on gels were transferred to nitrocellulose blotting membrane (Pall Corporation) using a BioRad Trans-Blot Semi-dry Transfer machine. Transfers were performed for 45 minutes at 25 V.

Blots were blocked using Li-Cor Odyssey Blocking Buffer diluted 1:1 in PBS for at least one hour. Primary and secondary antibodies were diluted in Odyssey Blocking Buffer diluted 1:1 in 0.1% Tween in PBS (PBS-T). Primary antibodies used include 1:1000 mouse anti-FLAG M2 (Sigma, F1804), 1:1000 rabbit anti-FLAG (ABR Affinity BioReagents, PA1-984B), 1:1000 rabbit anti-β tubulin (Abcam, ab6046), 1:1000 mouse anti-Hsp47 (Stressgen, SPA-470), 1:500 mouse anti-His (Applied Biological Materials, G020) and 1:500 rabbit anti-caspase3 (Epitomics, 1476-1). Secondary antibodies were all diluted at 1:12000 and include IRDye 800CW donkey anti-mouse IgG (LI-COR, 926-32212), IRDye 800CW donkey anti-rabbit IgG (LI-COR, 926-32213), IRDye 680CW donkey anti-mouse IgG (LI-COR, 926-32222), and IRDye 680CW donkey anti-rabbit IgG (LI-COR, 926-32223). Blots were scanned and quantified on an Odyssey Infrared Imaging System (Li-Cor Biosciences) using the Odyssey v2.0 and v3.0 software.

Western blot quantification of intracellular and extracellular levels of Spn4A was performed by normalizing the band intensities of Spn4A to that of Hsp47 (loading control), as detected by SDS-PAGE. Normalized intensities are expressed as a percentage compared to the

WT. Statistical significance was calculated based on two-tailed Student's t-test from three experiments performed in duplicates.

2.2.7 Immunofluorescence

After 48 hours of transfection or infection, H4 cells were fixed for 30 minutes in 3.7% formaldehyde. Cells were permeablized in 0.05% saponin in PBS (PBS-S) for 30 minutes. Primary labeling was performed using mouse anti-FLAG M2 (Sigma, F1804) or rabbit anti-FLAG (ABR Affinity BioReagents, PA1-984B) at 1:100 dilution, rabbit anti-β tubulin (Abcam, ab6046), rabbit anti-calnexin (Sigma, C4731), or mouse anti-GM130 (BD, 610823) at 1:200 in PBS-S with 3% BSA for at least one hour. Secondary labeling was performed using Alexa Fluor 488 donkey anti-mouse IgG (Invitrogen, A-21202), Alexa Fluor 488 donkey anti-rabbit IgG (Invitrogen, A-21206), Alexa Fluor 568 donkey anti-mouse IgG (Invitrogen, A10037), and Alexa Fluor 568 donkey anti-rabbit IgG (Invitrogen, A-10042) at 1:300 in PBS-S with 3% BSA for at least one hour. Lastly, the nuclei were stained for 25 minutes using Hoechst dye (Invitrogen) diluted in PBS to 5 μg/mL. Slides were mounted in mounting solution (2.5% DABCO in 90% glycerol, 20 mM Tris pH8.8). Fluorescence was visualized using an Olympus Fluoview FV1000 laser scanning confocal microscope.

2.2.8 Furin complex formation assay

Enzyme-inhibitor complex formation of furin and Spn4A was assessed by incubating cell lysates with recombinant furin and detecting the presence of a heat- and SDS-stable complex using SDS-PAGE. Per reaction, 100 ng of recombinant His-tagged human furin (R&D Systems, 1503-SE) was incubated with 15 μL of cell lysates in hypotonic buffer mixed with 15 μL of 2 x furin assay buffer (100 mM Hepes pH 7.5, 1 mM $CaCl_2$, 0.5% Triton-X100) (36). The reaction proceeded for 10 minutes at 30°C and was quenched with a final concentration of 50 mM EDTA. SDS loading buffer was added to the reaction and the samples were boiled for 10 minutes at 95°C and loaded onto an SDS-PAGE for western blot analysis.

Spn4A-furin complex formation was also assessed using HEK293-C4 cells that overexpress FLAG-tagged furin (92). Plasmids were transfected into HEK293-C4 cells and media were harvested after 48 hours for PAGE analysis, as described in sections 2.2.5 and 2.2.6.

2.2.9 MTS cell viability assay

Cell viability was assessed using the CellTiter 96 AQueous One Solution Cell Proliferation Assay (Promega) following the manufacture's protocol. Two thousand H4 cells were infected and seeded into clear 96-well plates (Sarstedt Tissue Culture Plate Flat Bottom). After 72 hours, 20 µL of MTS (3-(4,5-dimethylthiazol-2-yl)-5-(3-carboxymethoxyphenyl)-2-(4-sulfophenyl)-2H-tetrazolium inner salt) solution was added to each well, the plates incubated for 45 minutes at 37°C, and absorbance readings taken at 490 nm (SpectraMax 190, Molecular Devices).

2.2.10 Flow cytometry

RFP expression was quantified from infected cells using flow cytometry. Two hundred thousand H4 cells were infected and seeded into 6-well plates. After 48 hours of infection, cells were washed with PBS, trypsinized, and collected by centrifugation for 3 minutes at 3000 x g. The supernatant was removed and cells were resuspended in 900 µL of PBS. Cells were fixed by adding 100 µL of 37% formaldehyde and incubating at 37°C for 15 minutes. Cells were collected by centrifugation for 3 minutes at 3000 x g, washed in PBS, and resuspended in flow cytometry buffer (4% fetal bovine serum, 2 mM EDTA in PBS).

Flow experiments were performed on a BD FACScan Flow Cytometer. A total of 30 000 events were collected per sample using CellQuest and analyzed with FlowJo v4.0.2 (TreeStar). Events with very low forward scatter, which indicates degenerated cells, were excluded from the analysis.

2.2.11 RNA extraction and cDNA synthesis

RNA was extracted from infected cells for microarray experiments. H4 cells were infected and seeded into 6-well plates in duplicates. Cells were incubated for 48 hours, washed with PBS, lysed in RLT buffer containing β-mercaptoethanol, and passed through QiaShredder columns. RNA was extracted using the Qiagen RNeasy Mini kit with DNase on-column digest (Qiagen) or Qiagen RNeasy Plus Mini kit and eluted in 40 µL of RNase-free water. RNA purity was assessed with absorbance readings (A_{260}: A_{280} ratios between 1.9-2.1 and A_{260}:A_{230} ratios between 1.8-2.3) using a NanoDrop 1000 spectrophotometer (Thermo Scientific) and integrity tested on agarose 2.2 M formaldehyde RNA gels.

Complementary DNA synthesis was performed using TaqMan Reverse Transcription Reagent (Applied Biosystems) with 200 ng of RNA and oligo dT primers in a reaction volume of 12.5 μL. To ensure RNA preparations were not contaminated with genomic DNA, end-point PCR was performed on 0.5 μL of each cDNA reaction using intron-flanking β-actin primers.

2.2.12 Microarray and data analysis

Extracted RNA from three independent experiments was used on an Illumina HumanHT-12 v3 Expression BeadChip. Microarray experiments were carried out by Dr. Anne Haegart and data statistical analysis by Dr. Robert Bell at the Vancouver Prostate Centre Microarray Facility (Vancouver, Canada). Briefly, RNA quality was verified using an Agilent 2100 Bioanalyzer, and 200 ng of all RNA samples were biotin-labeled with the Ambion Illumina TotalPrep RNA Amplification Kit and hybridized onto the Illumina BeadChip, following the Whole-Genome Gene Expression Direct Hybridization Assay Guide. Arrays were scanned using an Illumina iScan scanner. The quantified data was loaded into Illumina GenomeStudio, where array quality control was assessed. Raw data were imported into Agilent GeneSpring v7.3.1, where data was normalized. Fold changes (FCs) were calculated between averages of each condition and t-tests were performed between the conditions.

Genes above the threshold cut-off of 1.7 fold ($p<0.05$), either up or downregulated, were considered significant and used for analysis. We used the Database for Annotation, Visualization and Integrated Discovery (DAVID v6.7) (93) for gene ontology and enrichment analysis. Briefly, gene lists were uploaded onto the DAVID online software, where various gene ontology terms are assigned to each gene. In a second step, genes are classified into functional annotation terms, and highly related/redundant annotation terms can be further grouped into annotation clusters. To examine the significance (p-value) of the functional annotation term, the probability of obtaining the number of genes in a term is compared to the total number of genes in that term from all the genes in the microarray, and is calculated by a modified Fisher's exact test (93). To examine the significance (enrichment score [ES]) of the annotation clusters, the geometric mean of all the enrichment p-values of each annotation term in the cluster is calculated. Because the geometric mean is a relative score, the negative log transformation is applied onto the mean, and reported as ES. ES above two are considered significant.

2.2.13 Real-time PCR

Quantitative real-time PCR (qPCR) was performed on an AB 7500 Fast Real-time PCR system with 7500 Software v2.0.1. Reaction components included 4 µL of 1:10 diluted cDNA, Brilliant II Fast qPCR Master Mix (Stratagene), probes from Roche Universal Probe Library, and primers from Integrated DNA Technologies in a 20 µL reaction. Roche probes and primer sets are listed in Appendix 2, Supplemental Table A2.3. Cycling conditions were 95°C for 5 minutes followed by 40 cycles of 95°C for 5 seconds and 60°C for 30 seconds. Differential gene expression was calculated by the $\Delta\Delta C_T$ (threshold cycle) method (94) using β-actin as the reference amplicon. For all real time assays, acceptable doubling efficiencies (86% - 110%) were ensured by calculating PCR efficiency from slopes of standard curves (C_T vs. serially diluted cDNA, slope between -3.1 to -3.7). FC averages were calculated from three independent experiments performed in duplicates and presented with the standard error of the mean (SEM). Statistical significance was calculated from two-tailed Student's t-tests.

2.3 Results

2.3.1 Phylogenetic analysis of Spn4A

Our goal was to use *Drosophila* Spn4A as a tool to study the serpinopathy associated with hNS. Thus, we assessed the relationship of *Drosophila* Spn4A with human serpins. Serpins are classified into 16 clades (A to P), with an additional ten unclassified orphan serpins, according to their amino acid sequence and secondary structure alignments (5). In general, clades A to I contain vertebrate serpins, while clades J to P contain serpins in nonvertebrate species (5). For comparative analysis, we selected one archetypal member from each vertebrate clade (A to I) representing serpins found in humans, *Triticum aestivum* (bread wheat) Serpin Z1A belonging to the plant clade P (5), and Spn4A which belongs to the insect clade K (5;95). We made an amino acid alignment of these sequences and built a phylogenetic tree using Serpin Z1A as the outgroup sequence. We summarized the trees resulting from a Bayesian tree search into a majority rule consensus tree to explore the relationship between Spn4A and other serpins. Fig. 2.3 showed that hNS and PAI-1 (plasminogen activator inhibitor 1) were highly related, while Spn4A was most closely related to both groups. In terms of sequence characteristics, Spn4A shared a higher amino acid alignment score with hNS compared to PAI-1 (Table 2.2). Further, Spn4A contains a 13 amino acid C-terminal targeting sequence, which is shared only between Spn4A, hNS, pancpin, and Hsp47 among more than 500 serpins tested (86).

Spn4A is expressed specifically in *Drosophila* neurons and like hNS, is directed to the secretory pathway (35). The overexpression of either Spn4A or hNS produces similar molting defects in *Drosophila* (35), despite their divergent protein functions. Further, the hNS amino acids related to disease are conserved in Spn4A (Fig. 2.4). Therefore, we predicted that Spn4A could be used as a tool to study serpinopathy associated with FENIB.

2.3.2 Development of Spn4A variants

In *Drosophila*, Spn4A possesses an N-terminal signal peptide and a C-terminal HDEL motif (Spn4A-R or WT-R), which suggests it may cycle between the ER and early Golgi compartments (34;36). Since hNS is a secreted serpin whose mutants are partially retained in the ER as polymers (61), we used a secreted Spn4A variant (Spn4A-S or WT-S) that lacked the HDEL signal (Fig. 2.2) to study the trafficking and possible intracellular polymer retention of Spn4A. To test if the polymer formation was an ER-specific phenomenon, we engineered a

cytoplasmic-localized Spn4A by deletion of the signal peptide, designated Spn4A-C or WT-C (Fig. 2.2). Notably, Spn4E is a naturally occurring splice variant of *Spn4* that contains the HDEL signal but not the N-terminal signal peptide, like Spn4A-C. All three constructs have been tagged with RFP (91), a monomeric red fluorescent protein, to facilitate immunofluorescence and *in vivo* experiments. The hNS constructs were cloned as positive controls for establishing methods.

Four mutations at sites S36P, S39R, H317R, and G374E (equivalent to human S49P, S52R, H338R, and G392E) were introduced to each WT construct (Fig. 2.2). We will use the hNS template for Spn4A amino acid numbering from here on to avoid confusion. We have cloned one negative control mutant, S49A, in order to verify that mutations linked to FENIB, and not any point mutation, formed serpinopathy specific polymers.

2.3.3 Polymer formation studies of Spn4A variants

Mutant polymeric hNS are retained in the ER as previously demonstrated through native PAGE and confocal imaging analysis (60). Following the same polymer detection techniques, we confirmed that Spn4A mutants also formed polymers and localized to the ER in human H4 neuroglioma cells.

First, we demonstrated that Spn4A mutants formed polymers similar to hNS mutants by native PAGE analysis. FLAG-tagged hNS WT as well as S49P and H338R mutants were cloned and transfected into H4 cells to validate our system. H4 cells were harvested and cultured media collected for both non-denaturating and SDS-PAGE analysis. Polymers were detected as ladders on a native PAGE only when hNS mutants were expressed (Fig. 2.5A). Also, hNS mutants had higher levels of protein in cell lysates and less in media samples compared to the WT, as seen on the SDS-PAGE (Fig. 2.5A). Accordingly, we performed the same experiments with Spn4A WT-S and mutants. We demonstrated that Spn4A mutants, with the exception of S49A, could also form polymers (Fig. 2.5B).

We used SDS-PAGE analysis to standardize protein expression to Hsp47 (heat shock protein 47 kDa) and to quantify intracellular and extracellular protein amounts. Spn4A variants, with the exception of S49A, were retained intracellularly to a significant extent and had an approximately 60% reduction extracellularly compared to the WT protein (Fig. 2.5C). Most likely, the mutants were secreted at a lower level or were more prone to extracellular proteolysis due to greater protein destabilization. Further, we tested RFP-tagged Spn4A-S, with similar

results to the non-tagged (Fig. 2.5D). We noted that Spn4A-R (retained) mutants, RFP-tagged and untagged, exhibited the same ladder formation in native PAGE analysis (data not shown). Additionally, cytoplasmic Spn4A mutants, both RFP-tagged and untagged, were capable of forming polymers as detected by native PAGE, unlike the WT-C (Fig. 2.5E). Spn4A-S had an approximately 4 kDa increase in molecular weight compared to Spn4A-C, presumably due to its glycosylation in the secretory pathway (Fig. 2.5B and E).

We then fixed transfected H4 cells and used cellular markers to visualize the localization and staining patterns of both WT and mutant hNS and Spn4A. The hNS mutants exhibit a specific punctate characteristic in transfected monkey kidney fibroblast COS-7 cells (60;61) and in stably transfected rat pheochromocytoma PC12 cells (61). The punctate phenotype of hNS mutants was reproduced in H4 cells (Fig. 2.6A). We further demonstrated similar staining patterns in Spn4A H338R-S but not WT-S (Fig. 2.6B and Appendix 3, Supplemental Fig. A3.1). Spn4A WT-R localized to the ER, but not the Golgi (Fig. 2.6C and D) and Spn4A WT-C stained the cytoplasm (Fig. 2.6E), while their mutant counterparts exhibited distinct dotted features (Fig. 2.6C to E). We noted that some cells expressing cytoplasmic mutants exhibited the dispersed cytoplasmic staining pattern like the WT (data not shown). Immunofluorescence experiments of H4 cells transfected with RFP Spn4A constructs were performed first with the non-RFP-tagged constructs to ensure similar staining patterns (data not shown for non-RFP-tagged constructs).

2.3.4 Spn4A mutants do not have inhibitory activities *in vitro* and *in cellulo*

WT Spn4A is an inhibitor of human furin and *Drosophila* PC2 (36). It forms complexes with furin with a K_i (inhibitory constant of the enzyme-inhibitor complex) of 13 pM and a 1:1 stoichiometry of inhibition (36). To assess the inhibitory activities of polymeric mutants, we performed complex formation assays using recombinant His-tagged furin or HEK293-C4 cells that overexpress FLAG-tagged furin (92).

Inhibition is achieved through a covalent complex between Spn4A and furin (Fig. 2.7A) that is heat- and SDS-stable, and therefore detectable by SDS-PAGE and western analysis. Incubation of furin with cell lysates transfected with Spn4A WT-R resulted in the detection of a high molecular weight band, but not with those expressing Spn4A H338R-R (Fig. 2.7B). Both WT-R and mutant H338R-R resulted in some cleaved product, suggesting that although Spn4A H338R-R does not have inhibitory activity against furin, its reactive center loop may be accessible to cleavage.

We also tested all of the Spn4A mutants for inhibitory activities in HEK293-C4 cells. Transfected cells were analyzed for polymer formation by native PAGE and complex formation by SDS-PAGE (Fig. 2.7C). We found that Spn4A mutants were able to form polymers in HEK293 cells as indicated by the ladder formation in native PAGE (Fig. 2.7C). Free furin was detected as doublet bands intracellularly and singlet bands extracellularly on SDS-PAGE, as previously reported (92). Enzyme-inhibitor (EI) complexes were observed intracellularly and extracellularly as high molecular weight bands in cells transfected with Spn4A WT-S, negative control mutant Spn4A S49A-S, and RFP Spn4A WT-S (Fig. 2.7C and D). Cells expressing serpinopathy-linked mutants did not form complexes intracellularly or extracellularly with furin, except those transfected with Spn4A S49P-S (Fig. 2.7C and D). A high molecular weight band was detected in the media samples of cells expressing Spn4A S49P-S, but not intracellularly. However, the amount of extracellular free furin was visibly greater in the media sample from cells transfected with S49P compared to the WT and S49A negative control mutant (Fig. 2.7C), which may bring into question the identity of the high molecular weight band (discussed below).

2.3.5 Cellular characterization of recombinant adenoviruses expressing Spn4A WT and mutants

Next, we established an infection system using recombinant adenoviruses in order to achieve higher and dose-dependent expression levels of Spn4A. We reasoned that very high expression levels of Spn4A (higher than can be achieved by transfection) might exacerbate the cellular effects of polymers. In addition, the adenovirus expression system might allow us to delineate how different doses of polymer formation affect cells by infecting with different multiplicity of infection (MOI).

We constructed recombinant adenoviruses containing two polymeric mutants that were ER-retained and one mutant that was secreted. Since the ER is the site of polymer localization, we reasoned that cellular stress signals would be amplified if all polymers were retained. On the other hand, if Golgi or extracellularly-localized polymers are affecting the cell, then a comparison of polymers that are retained to those that are trafficked through the secretory pathway could elucidate those specific effects. We chose to make recombinant adenovirus expressing S52R or H338R retained mutants (Ad. RFP S52R-R and Ad. RFP H338R-R) because they formed the most polymers indicated on native PAGE analysis. In their hNS counterpart, the H338R mutant causes an earlier onset of disease than S52R (45). We have also generated

secreted Ad. RFP H338R-S. We used adenoviruses without transgene (Ad. Emp [Empty]) as a negative control, Ad. RFP WT-R for comparison with the S52R-R and H338R-R mutants, and Ad. RFP WT-S for comparison with H338R-S. Ad. Emp, Ad. RFP WT-R, and Ad. RFP WT-S were previously generated by the Jean lab.

We used several methods to quantify the levels of expression at various MOIs. First, we infected H4 cells at MOI 1 and 5 and used western blot analysis to ensure a dose response with increasing MOI (Fig. 2.8A). Second, for cellular response analysis, we titrated for the MOI sufficient to express Spn4A in all cells using flow cytometry (Fig. 2.8B). We found that infections at MOI 50 were sufficient for 100% of cells to contain retained Spn4A-R and at least 95% of cells to contain secreted Spn4A-S. Third, the dose response was further examined using confocal experiments (Fig. 2.8C). Cells infected with MOI 1 compared to those at MOI 50 expressed less Spn4A. Fourth, consistent with flow cytometry data, cells infected at MOI 50 showed that all cells expressed Spn4A (Fig. 2.8D). Further, staining patterns of WT and polymer-forming Spn4A in adenovirus infected cells (Fig. 2.8D) were the same as those from transfection experiments (Fig. 2.6). Last, MTS cell viability assays ensured that transgene expression of the retained Spn4A-R (Fig. 2.8E) and secreted Spn4A-S (data not shown) by adenovirus was not cytotoxic in H4s.

2.3.6 Microarray strategy

We showed that Spn4A mutants had the same cellular signatures as hNS polymers in mammalian cells and predicted that Spn4A polymers would modulate the same cellular stress pathways as hNS. In order to address the cellular response to serpin polymers, we analyzed the transcriptome of H4 cells infected with Spn4A polymeric mutants.

H4 cells were infected with Ad. Emp, RFP WT-R, RFP S52R-R, RFP H338R-R, RFP WT-S, or RFP H338R-S. RNA was extracted and used on the Illumina HumanHT-12 v3 Expression BeadChip, targeting more than 25 000 annotated genes using 48 000 probes. Expression data from Ad. RFP WT-R, S52R-R, H338R-R, WT-S, and H338R-S were compared to Ad. Emp (Fig. 2.9).

Genes with altered expression levels due to mutant Spn4A polymers were compiled. Only FCs with a threshold cut-off of 1.7 fold ($p<0.05$) were considered significant and used for analysis. Using these criteria, 71 genes in S52R-R, 74 genes in H338R-R, and 45 genes in

H338R-S expressing cells reached significance. Next, these genes were compared to those significantly regulated by the WT Spn4A (Fig. 2.9). We found that a total of 18 genes were unique to the mutants while 76 genes overlapped with the WT (Fig. 2.9). These two different gene lists were separately analyzed (sections 2.3.7 and 2.3.8) and the altered genes from the expression of retained and secreted Spn4A WT will be discussed in Chapter 3.

2.3.7 Spn4A WT and mutant overexpression induces ER stress genes

The expression of Spn4A, regardless of inhibitory function or polymer formation, induced a response in 76 genes (Appendix 5, Supplemental Table A5.1). Gene ontology analysis was performed using DAVID. From 76 similarly regulated genes, 35 upregulated and 41 downregulated genes were separately submitted to DAVID Functional Annotation Clustering analysis. Genes were classified into gene ontology groups, enrichment for each annotation term was calculated, and annotation terms further grouped according to highly similar annotation terms. Notably, the most enriched cluster (ES = 4.3) from the upregulated genes was the response to ER stress (Table 2.3). Other enriched clusters with ES above two included annotations for heat shock proteins (ES = 2.5) and ER membranes (ES = 2.4), among others. The enrichment scores for the downregulated gene list were not as high as the upregulated, and are shown in Appendix 3, Supplemental Table A3.1.

Notably, seven ER stress genes (Table 2.4) were among the top 12 most upregulated genes in response to WT-R, S52R, and H338R-S expression, but not WT-S. These genes are common to the UPR and include chaperones, a transcription factor controlling ER stress and cell cycle genes, a component of the ER-associated degradation system, and a regulator of ER-induced apoptosis. All seven genes were similarly regulated by Spn4A WT-R, the two retained mutants, and Spn4A H338R-S, except for secreted Spn4A WT-S, which did not induce the upregulation of *DDIT3* (DNA-damage-inducible transcript 3, also known as CHOP) as all others had.

We tested the mRNA levels of the ERAD component *HERPUD1* (Homocysteine-inducible, ER stress-inducible, ubiquitin-like domain member 1), transcription factor *DDIT3*, and ER chaperone *HSPA5* (heat shock 70 kDa protein 5, also known as BiP) by qPCR. We confirmed that *DDIT3* and *HSPA5* were all significantly upregulated by Spn4A WT or mutant expression, and that *HERPUD1* is upregulated in cells expressing S52R-R (Fig. 2.10). Further, *HSP5A* was significantly more upregulated by H338R-R expression, compared to WT-R. We

could not validate the upregulation of *HERPUD1* in response to WT-R and H338R-R (Fig. 2.10), as suggested by the microarray. We predicted that our analysis method may have a false discovery rate of approximately 25%.

2.3.8 Retained and secreted non-inhibitory and polymeric Spn4A mutants affect few genes in the H4 transcriptome

Comparisons of Spn4A WT-R or WT-S with polymeric mutants identified 18 genes that were differentially expressed in the presence of secreted and retained mutants (Fig. 2.9). Unique gene expression changes in each mutant group were identified by comparisons against each other (Fig. 2.11, Table 2.5). We reasoned that the response to non-inhibitory and polymeric Spn4A buildup in the ER should be detected in both S52R-R and H338R-R mutants as well as the secreted H338R-S. Surprisingly, *KRT81* (keratin 81), which codes for fibrous structural proteins (96), was the only gene induced by all three mutants. Further, the H338R-S secreted mutant would reveal effects stemming from Golgi transit and extracellular polymer accumulation when compared with the retained mutants. We found that six genes were uniquely regulated by the secreted mutant (Table 2.5). Additionally, five genes were differentially regulated by both retained mutants (Fig. 2.11, Table 2.5).

Using DAVID functional annotation chart, we grouped all 18 genes according to their ontology (Table 2.6). Functional annotations included cell adhesion, aminotransferase activity, carbohydrate binding, cartilage development, and calcium binding. Also, polymorphisms existed for most genes. There was no clear trend in the regulation for each annotation and how they relate to the presence of polymers in a cell was unclear.

The most downregulated gene was *MGP* (matrix gla protein), which encodes for an extracellular matrix protein that binds calcium and may function in the migration of glioblastoma cells (97). The most upregulated gene was *SPRR2D* (small proline-rich protein 2D) in the retained mutants. SPRR2D is normally expressed in the cytosol of keratinocytes and becomes crosslinked to the membrane resulting in a protective barrier beneath the membrane (98). We have validated the *SPRR2D* upregulation in the mutants, but were unable to show that expression was unique to mutants (Fig. 2.13). As detected by microarray analysis, RFP WT-R upregulated *SPRR2D* by 2.00 fold, but was excluded from the analysis based on its p-value ($p = 0.07$), which did not reach the cut-off. By qPCR, *SPRR2D* had a FC of 30.31 ($p<0.01$) and was not significantly different from the mutants (Fig. 2.12).

2.4 Discussion

2.4.1 Molecular and cellular comparisons of *Drosophila* Spn4A and human neuroserpin mutants

Despite the divergent functions of *Drosophila* Spn4A and hNS, both proteins were closely related compared to other serpin clade prototypes by phylogenetic analysis and have brain-specific expression. Importantly, disease-linked amino acid residues are conserved in both serpins. Thus, we have evaluated the ability of Spn4A mutants to form polymers in order to study the cellular pathogenesis and organismal impacts of the serpinopathies.

Following the biochemical and cellular work on hNS mutants, we examined the ability of mutant Spn4A to form polymers. We used hNS WT and two mutants as positive controls. Under our experimental conditions, hNS mutants formed polymers intracellularly and extracellularly, detected by western blots and immunofluorescence, as previously reported (57-60). However, low levels of monomeric mutant hNS were detected intracellularly. This is in contrast to native PAGE results in COS7 cells (61), where hNS S49P monomers were detected extracellularly, but not intracellularly. The discrepancy may be due to differences in cell types or different cell lysis conditions. Nonetheless, we were successful in replicating ladder-like formations on native PAGE, punctate characteristics by confocal microscopy, and ER retention using SDS-PAGE and immunofluorescence.

Next, we asked if Spn4A mutants encoding amino acid substitutions equivalent to those found in hNS FENIB-causing mutants also formed polymers. As a negative control, we engineered the Spn4A S49A mutant, whose equivalent mutation in hNS has not been associated with disease. Our PAGE analysis confirmed that S49A failed to form polymers and was secreted, like WT Spn4A. In contrast, mutants with disease-associated residue substitutions formed polymers intracellularly and extracellularly, and were not secreted to WT levels. RFP tag and cytoplasmic localization did not affect the ability of mutants to form polymers.

We noticed that while immunofluorescence images were similar between Spn4A and hNS mutants, their oligomeric states may be different as detected by native PAGE. In the extracellular samples, Spn4A mutants formed low and high order oligomers while human neuroserpin mutants only formed high molecular weight species. Perhaps Spn4A mutants formed polymers slower compared to human neuroserpin so that we were able to capture different

oligomeric species. By incubating mutant Spn4A for a longer period of time before native PAGE loading, we can test if lower molecular weight oligomers are lost. If they can still be detected, we suggest that Spn4A mutants can form different intramolecular linkages. Precedence for different structural multimer formation is best exemplified by antithrombin, which exhibits self-terminating dimers as well as higher order polymers (99;100).

We also found that the Spn4A G392E mutants were barely detectable by native PAGE. However, intracellular and extracellular proteins levels were detected by SDS-PAGE at levels comparable to other Spn4A mutants. Further, punctate staining patterns were detected by immunofluorescence for Spn4A G392E mutants. The reason for the loss of visible bands on native PAGE is unclear, but may be due to a different polymer fold that concealed the FLAG tag, and was therefore undetectable with FLAG antibodies under native conditions. The use of antibodies directed at other epitopes may be useful in clarifying whether polymers of a different conformation are formed. Spn4A G392E may have different molecular properties to the hNS G392E mutant, which forms high order oligomers (61).

Lastly, we studied the inhibitory activities of the Spn4A mutants. Functional studies of hNS mutants have revealed that hNS S49P is partially active (57). The ability of Spn4A S49P to form an EI complex in the extracellular environment, unlike the other mutants, indicates that it may be similar to its human counterpart. It also suggests that the mutation did not compromise catalytic activity. The identity of the high molecular weight band is unclear. Unlike the media samples from WT-S and S49A-S expressing cells, the extracellular furin levels did not decrease in the presence of Spn4A S49P-S (Fig. 2.7C). It is possible that S49P-S inhibited and formed SDS-stable EI complexes with another extracellular protease. The use of furin antibodies may clarify the identity of the high molecular weight band. Further, the ability of Spn4A S49P mutants to complex with furin may be assessed using recombinant furin. We did not detect intracellular EI complexes in S49P-S expressing cells (Fig. 2.7C). The lack of complexes may be due to the retention of Spn4A polymers in the ER and the localization of target proteases to the Golgi and extracellular space. For example, since furin localizes mainly to the Golgi or is shed to the extracellular space (92;101), insufficient levels of Spn4A S49P may reside in the Golgi (due to ER retention) at the steady state for complexes to form and be detected.

2.4.2 Cellular model development

We have developed a new mammalian cell-based system to study serpinopathies using Spn4A mutants. Our model recapitulates the known features of mutant neuroserpin including polymer formation, ER retention, and lack of inhibitory activity.

Our cell-based system has three advantages over current cellular models. First, we have developed RFP fusions of serpins and demonstrated that the tag does not affect polymer formation. The RFP tag has facilitated imaging of serpins in cells and flies (Supplemental Fig. A3.3). Importantly, the tag will allow us to visualize Spn4A trafficking, formation of polymers, and/or interactions with cellular proteins over time in live cells. For many proteins associated with neurodegenerative diseases, FRAP (fluorescence recovery after photobleaching), FLIP (fluorescence loss in photobleaching), and time-lapse microscopy have been successfully applied to visualize the dynamic process of protein aggregate remodeling and defective intracellular transport mechanism (for example, monitoring rates of vesicle transport), among others (102).

Second, we have developed an adenovirus delivery system to allow titration of mutant serpin expression using different MOIs. Polymer expression levels are important for pathogenesis as demonstrated in hemizygous versus homozygous transgenic mice expressing the hNS G392E mutation (80). We now have the molecular tools to study the gene dosage-dependent accumulation of mutant serpin.

Third, we have localized polymers to different compartments of a cell. Spn4A is naturally ER-retained. We showed that deletion of C-terminal HDEL allowed secretion of Spn4A and removal of the N-terminus signal peptide targeted Spn4A to the cytoplasm. We demonstrated polymer formation in the cytoplasm, ER, and extracellular space. The current hypothesis is that polymer formation in the ER leads to ER stress-induced changes followed by cell dysfunction and death (103). In our model systems, we may address if mutant serpins in the Golgi and extracellular space have additional cellular effects compared to ER-retained Spn4 variants. Further, we showed that polymer formation is not exclusive to the secretory pathway and can occur regardless of the ER environment. Interestingly, cytoplasmic polymers were not observed at the same frequency or amount as secretory pathway polymers. We suggest that while polymerization is not the result of the ER environment, confinement of mutant serpins to a membrane enclosed space aggravates polymer formation.

2.4.3 Transcriptome profiling of retained and secreted Spn4A mutants

In order to better understand the cellular response to polymer accumulation, we used the adenovirus delivery system to express secreted and retained Spn4A WT and mutants in H4s for microarray analysis. Our assumption was that Spn4A polymers would regulate the same cellular stress pathways as human neuroserpin polymers in mammalian cells. Experimental conditions were chosen based on the expression of Spn4A in all cells and visible punctate inclusions as visualized by confocal microscopy.

We hypothesized that the expression of polymers would specifically activate cellular stress genes. However, a general response to the overexpression of Spn4A was ER stress, regardless of protein activity or polymer formation. Using a MOI of 50, more than one infectious virus particle was expected to enter one cell, and thus a very high Spn4A expression was expected. It is likely that proteins overwhelmed the ER by overexpression and induced ER-associated gene expression, masking possible stress responses to polymer formation. HSPA5 (also known as BiP) is a chaperone that regulates the UPR and was upregulated in response to retained Spn4A-R WT and mutants. Under our experimental conditions, we suggest that UPR was a general response to Spn4A overexpression, regardless of localization, function, or oligomerization.

From our qPCR assay, we detected upregulation of *HERPUD1* in response to the retained S52R-R mutant but not WT-R, in contradiction to the microarray data. We believe that qPCR, which can detect small amounts of DNA through amplification, may be a more sensitive detection method compared to hybridization on a microarray. Currently, we estimate a false discovery rate of 25% (we validated nine of 12 genes tested). *HERPUD1* codes for a regulator of ERAD, which promotes proteasome-mediated protein degradation. ERAD is implicated in the clearance of hNS polymeric mutants, as proteasome inhibition results in a buildup of mutant hNS but not WT hNS (78). Further investigation into the regulation of *HERPUD1* and proteasome-mediated degradation of Spn4A polymers is needed.

Microarray comparisons showed that *DDIT3* (also known as CHOP) was specifically upregulated in H338R-S, but not WT-S. Signaling from DDIT3 may induce apoptosis (63), and whether the gene regulation difference is significant needs to be validated by qPCR.

Last, we analyzed genes that were specifically regulated in response to Spn4A mutants. We did not observe specific changes in genes related to UPR, EOR, autophagy, or apoptosis. However, we did identify 18 significantly changed genes in response to polymer accumulation. Unfortunately, we could not validate by qPCR that *SPRR2D* was specifically upregulated in response to retained Spn4A polymers. The validation of the rest of the genes is of immediate interest.

2.4.4 Conclusions and future directions

FENIB is characterized by destabilizing mutations in neuroserpin leading to pathogenic polymer formation, decreased extracellular levels, and inclusion body formation. We showed that the *Drosophila* brain-specific serpin, Spn4A, has equivalent amino acids to its human homolog that when mutated, recapitulated the same cellular signatures. Further, we demonstrated that polymer formation is not an ER-specific event. We used this cellular model for transcriptome analysis of the cellular response to the accumulation of polymeric Spn4A. However, we found that ER stress was a general response to Spn4A overexpression and few genes were regulated specifically in response to Spn4A polymer-forming mutants.

We have performed qPCR experiments to test the expression levels of ER stress genes using retained Spn4A WT-R and mutants. We suggest that for future qPCR assays, comparisons between secreted WT-S and H338R-S will more clearly reveal differences in ER stress regulation, since WT-R already induced high ER stress levels. Of interest are *HERPUD1* and *DDIT3*, which may be upregulated in the presence of polymeric mutants but not the WT, as suggested by qPCR and microarray experiments. Functional assays will be necessary to evaluate the consequences. To test if ERAD is activated, we will compare the quantity of Spn4A WT and mutants with and without proteasome inhibition. A buildup of protein after inhibition would suggest that the proteasome is normally activated to degrade the proteins. Further, DDIT3 is a transcriptional regulator whose activity can be monitored using a promoter-luciferase reporter assay. However, it is unlikely that DDIT3 signaling leads to apoptosis in the neuroglioma cells as we have grown them for up to five days without toxic effects. Further, cells transiently transfected with Spn4A polymeric mutants did not activate caspase 3 after 48 hours (data not shown). The 17 changes in gene expression that were regulated in response to Spn4A polymers, but not the WT, will need to be validated by qPCR. Once true targets have been confirmed,

western blotting and functional assays can be designed to evaluate the cellular response to the polymers.

The transcriptome analysis did not reveal obvious toxic effects in response to the polymers. Indeed, previous studies performed in cell lines were unable to detect toxic effects (61). Perhaps H4 neuroglioma cells may tolerate serpin polymer expression due to their proliferative ability as a cancer cell line. It may be beneficial to use primary neuron cultures for further examination of the toxic effects of serpin polymers.

Lastly, transgenic *Drosophila* will help decipher the effects of Spn4A variants *in vivo*. In collaboration with Dr. Carl Hashimoto, we generated transgenic *Drosophila* overexpressing retained and cytoplasmic RFP Spn4A WT and RFP Spn4A H338R. The secreted counterparts will be generated for future studies. Currently, RFP expression in fly pupae has been confirmed (Supplemental Fig. A3.3), but no detectable phenotypic changes in the flies generated were found (personal communication). Further characterization of the transgenic *Drosophila* to ascertain the effects of Spn4A polymer-forming mutants *in vivo* is of great interest.

Figure 2.1. Unfolded protein response signaling pathways. The chaperone BiP binds IRE1, ATF6 and PERK under non-stressed conditions. Accumulation of unfolded proteins causes BiP to dissociate with the sensors leading to their activation. Activated IRE1 alternatively splices *XBP1* mRNA, ATF6 is activated by proteolysis, and PERK phosphorylates eIF2. Together, UPR signaling leads to upregulation of ERAD, chaperones, lipid synthesis, anti-oxidative stress response, amino acid metabolism, and/or apoptotic genes. Reprinted from Seminars in Cell & Developmental Biology, 18, Malhotra JD and Kaufman RJ , The endoplasmic reticulum and the unfolded protein response (62), 716-731, © 2007, with permission from Elsevier.

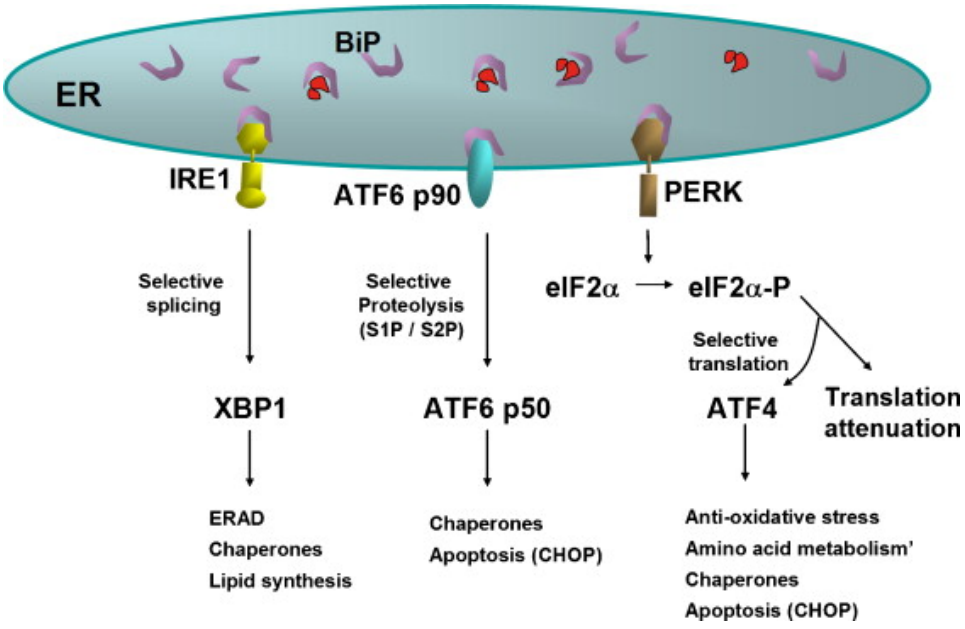

Figure 2.2. Serpin variants used in this study. We have three wild type Spn4A constructs with different predicted cellular localization, with and without tagged-RFP, and one human neuroserpin (hNS) construct, without RFP. Construct names for Spn4A indicate predicted localization (R for ER-retained, S for secreted, C for cytoplasmic) as indicated. Key characteristics of the constructs include SP (signal peptide) for targeting to the secretory pathway, HF (his and FLAG tag) or F (FLAG tag), RFP, RSL (reactive site loop), and HDEL ER-retention signal. From these wild type constructs, we have made single point mutations at sites S36, S39, H317, and G374 (triangles) in Spn4A, according to the human neuroserpin serpinopathy-associated residues (S49P, S52R, H338R, and G392E), and single point mutations in human neuroserpin at positions S49 and H338.

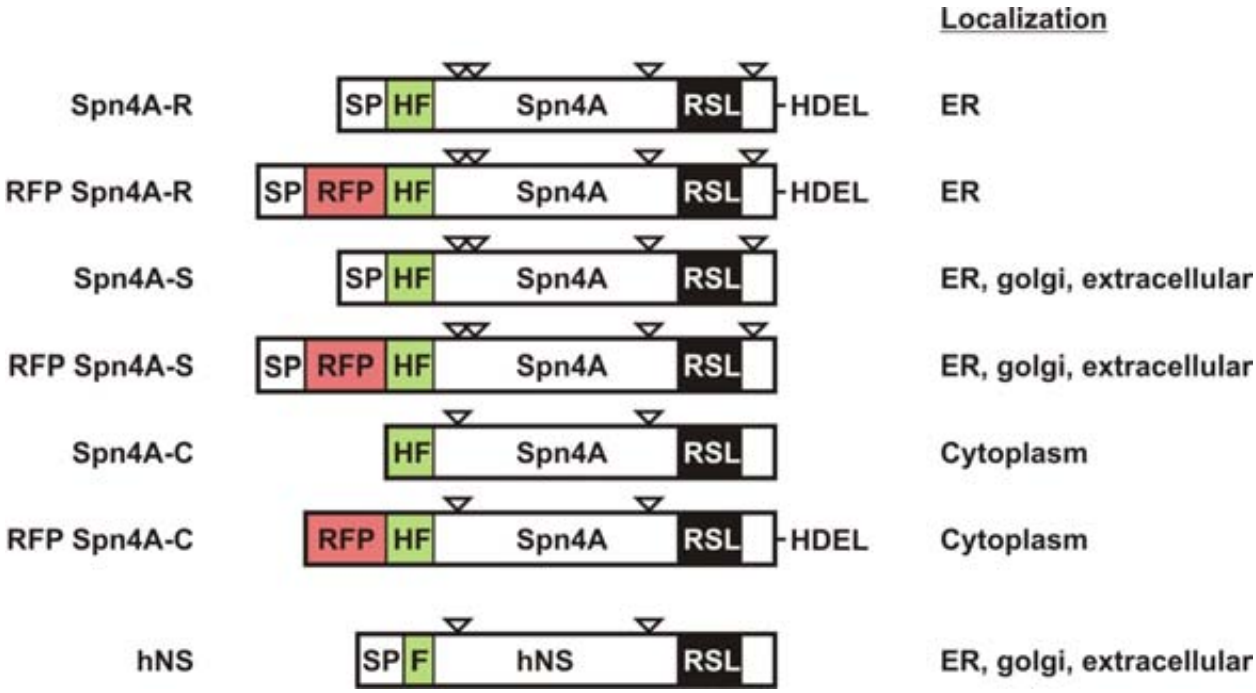

Figure 2.3. Phylogenetic relationship of *Drosophila* Spn4A to one archetypal member of each serpin clade (A-I) that contains human serpins. The tree is a majority rule consensus of the set of trees resulting from a Bayesian search method. *Triticum aestivum* Serpin Z1A was used as an outgroup. The values on the internal nodes reflect group support. Label prefixes "Hs", "Dm", and "Ta" were used for genes of human, *Drosophila*, and wheat, respectively. The bracketed letter is the clade for which the serpin belongs to. The lineage leading to Spn4A is bolded. The scale bar represents the number of substitutions per site.

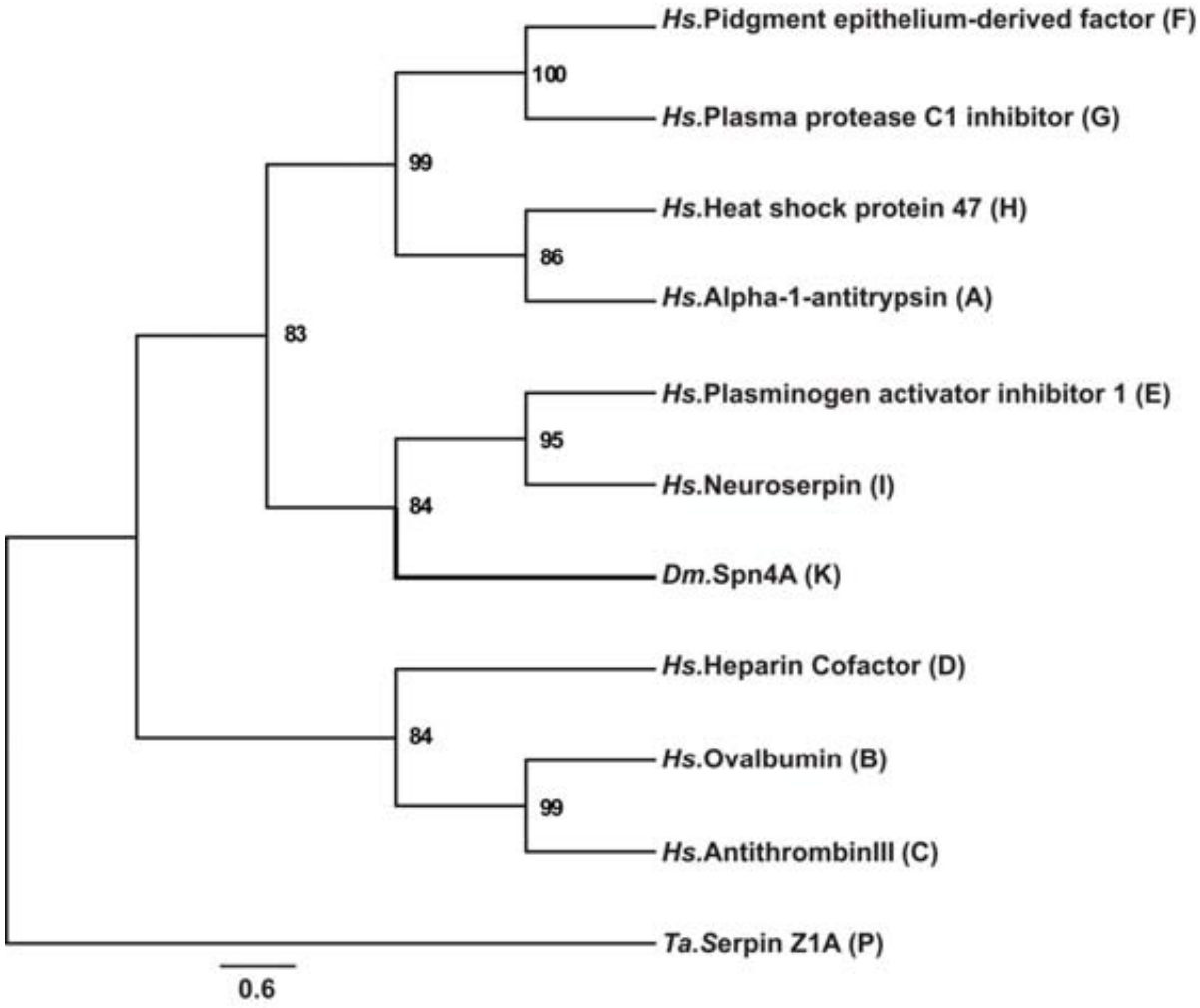

Figure 2.4. Sequence alignment between human nueroserpin and Spn4A. Residues are fully conserved (highlighted), have high identity similarities (red text), or are not conserved (black text). Serpinopathy-associated residues (S49P, S52R, H338R, and G392E) are asterisked. Sequences were aligned using Espript 2.2 (104).

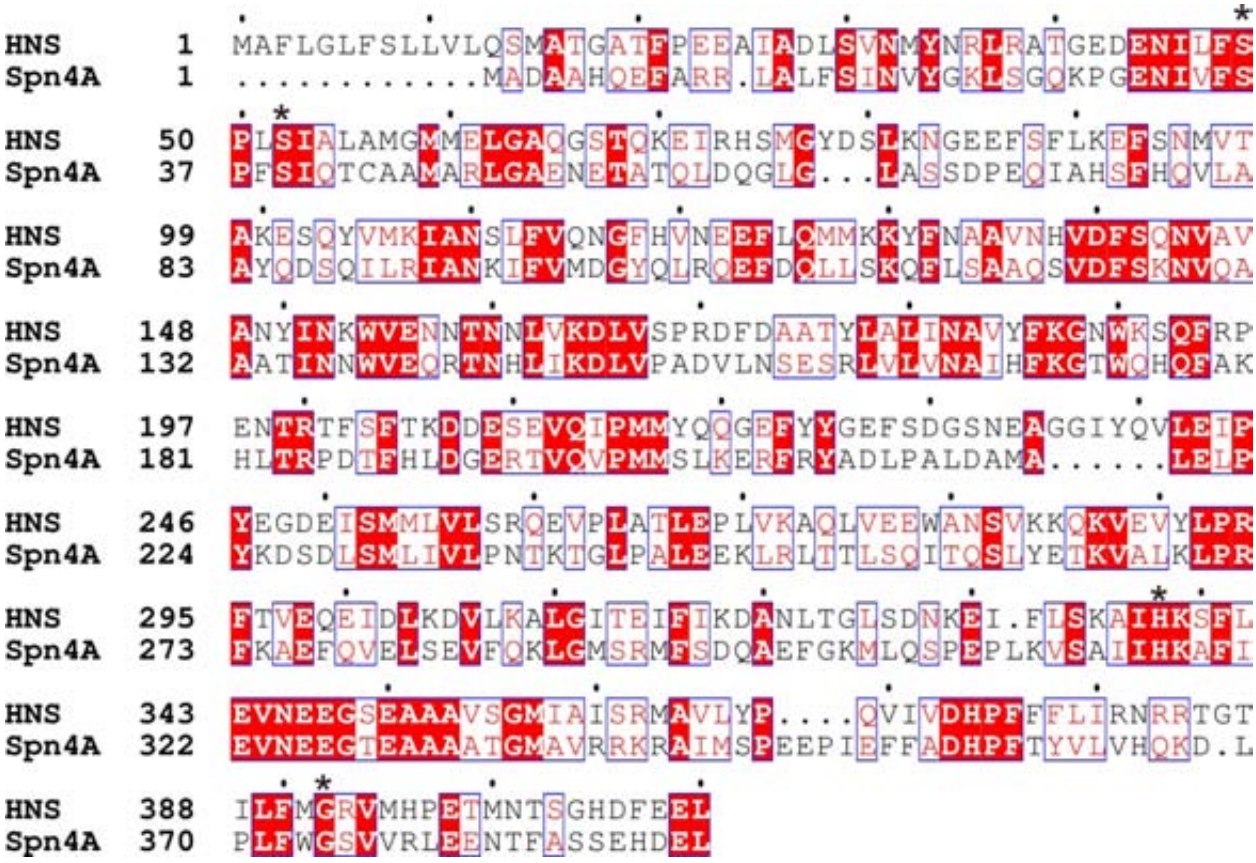

Figure 2.5. Polymer formation studies of human nueroserpin and Spn4A WT and mutants and quantification of intracellular and extracellular levels of Spn4A WT and mutants. A) Native PAGE and SDS-PAGE analysis of hNS WT and mutants. Human neuroserpin, empty vector, and wildtype are abbreviated as hNS, EV, and WT respectively. H4 cells were transfected as labeled. Cultured media were collected (extracellular samples) and cells were lysed (intracellular samples) after 48 hours, ran on a native PAGE to detect polymer formation and SDS-PAGE to quantify total amounts. Western blot analysis was performed using anti-FLAG antibodies for Spn4A (green) and anti-Hsp47 antibodies for Hsp47 (red) as a loading control. B) Native PAGE and SDS-PAGE analysis of secreted Spn4A WT-S and mutants, as described above. C) Quantification of intracellular and extracellular amounts of secreted Spn4A WT-S and mutants. Using SDS-PAGE such as in (B), we normalized the band intensities of Spn4A to Hsp47, and calculate the percent expressed compared to the WT. Percentages are averages ± SEM (standard error of the mean), and p-values have been calculated with a two-tailed student t-test from three experiments performed in duplicates. With the exception of the S49A mutant, the other four mutants had significantly increased amounts of intracellular protein ($p<0.05$*) and decreased amounts of extracellular protein ($p<0.0001$**) compared to the WT. D) and E) Native PAGE and SDS-PAGE analysis of secreted RFP Spn4A WT-S and mutants (D) and cytoplasmic Spn4A WT-C and mutants, with and without RFP (E), as described in (A).

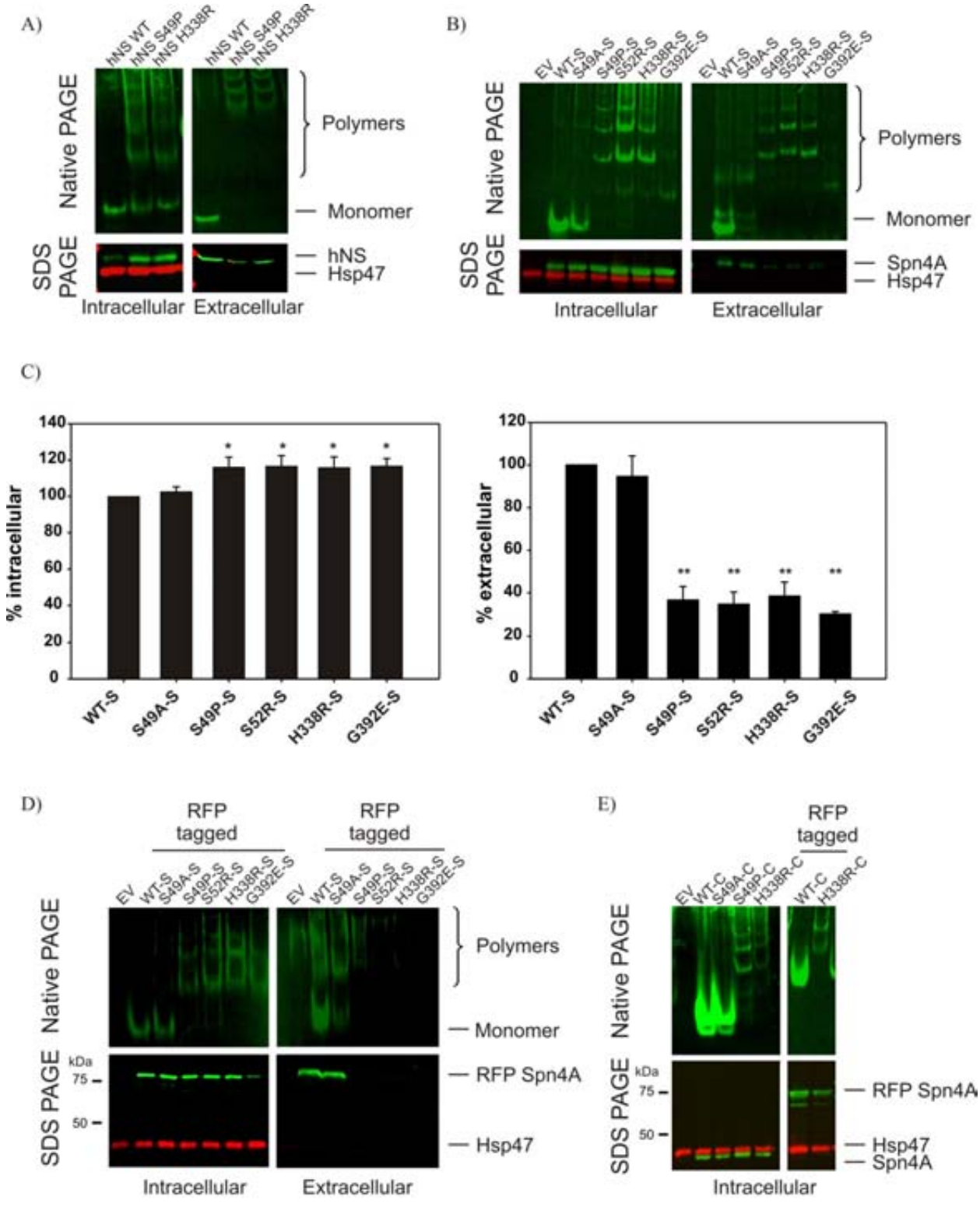
A)
hNS WT
hNS S49P
hNS H338R
Native PAGE
Polymers
Monomer
SDS PAGE
hNS
Hsp47
Intracellular
Extracellular
B)
EV
WT-S
S49A-S
S49P-S
S52R-S
H338R-S
G392E-S
Native PAGE
Polymers
Monomer
SDS PAGE
Spn4A
Hsp47
Intracellular
Extracellular
C)
% intracellular
% extracellular
WT-S
S49A-S
S49P-S
S52R-S
H338R-S
G392E-S
D)
RFP tagged
Native PAGE
Polymers
Monomer
SDS PAGE
kDa
75
50
RFP Spn4A
Hsp47
Intracellular
Extracellular
E)
RFP tagged
EV
WT-C
S49A-C
S49P-C
H338R-C
Native PAGE
SDS PAGE
RFP Spn4A
Hsp47
Spn4A
Intracellular

Figure 2.6. Localization and staining patterns of human neuroserpin and Spn4A WT and mutants. H4 cells were transfected with the WT or mutants of A) FLAG-tagged hNS, B) RFP Spn4A-S, C) and D) RFP Spn4A-R, or E) RFP Spn4A-C, as labeled. After 48 hours, they were fixed and probed for hNS (red) with anti-FLAG antibodies, ER (green) with anti-calnexin antibodies, Golgi (green) with anti-Gm130, or tubulin (green) with anti-tubulin, and stained for nuclei (blue) with Hoechst dye. See Appendix 3, Supplemental Fig. A3.1 for enlarged figures.

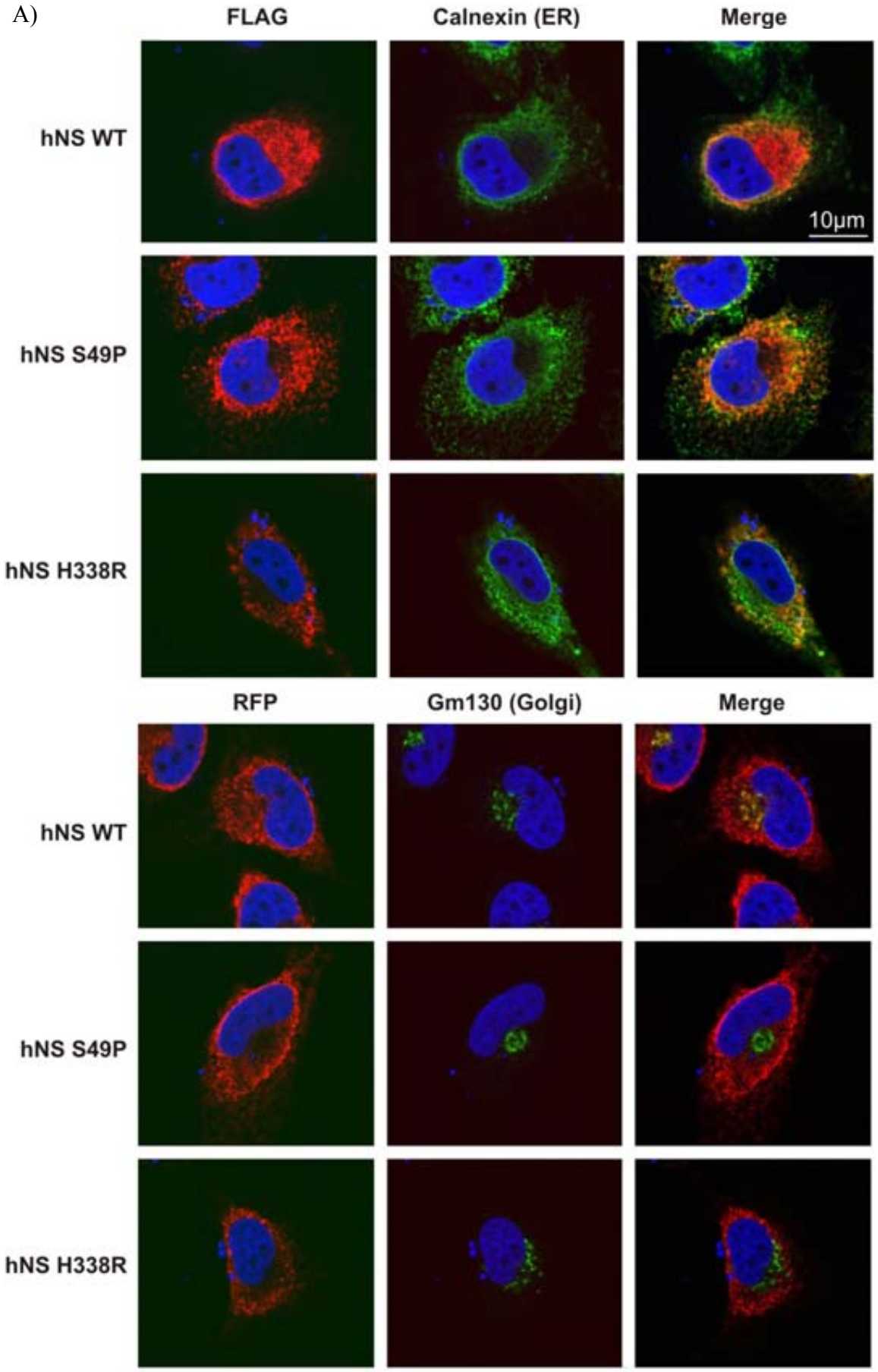
A)
FLAG
Calnexin (ER)
Merge
hNS WT
hNS S49P
hNS H338R
10μm
RFP
Gm130 (Golgi)
Merge
hNS WT
hNS S49P
hNS H338R

B)

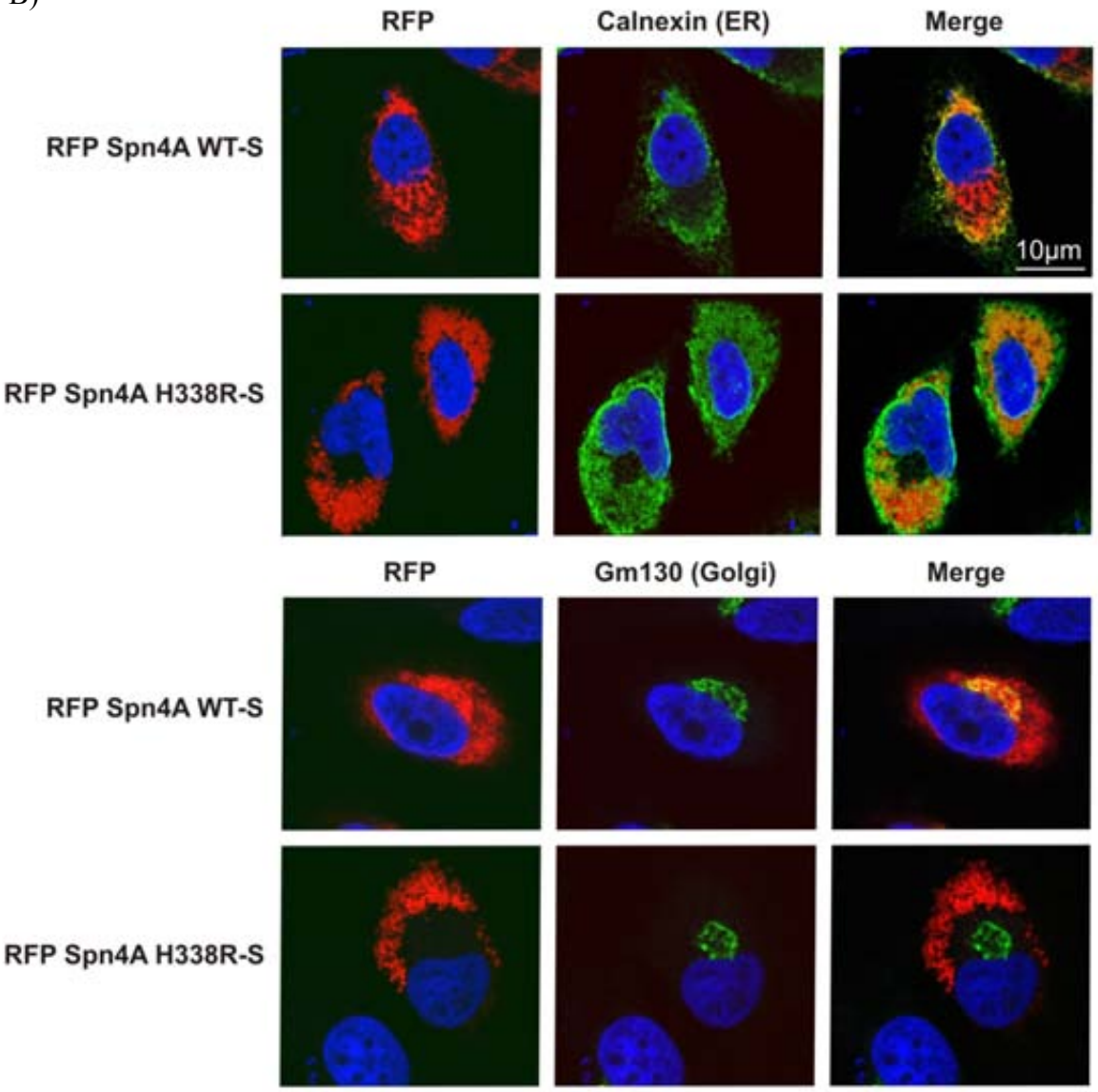
RFP
Calnexin (ER)
Merge
RFP Spn4A WT-S
10μm
RFP Spn4A H338R-S
RFP
Gm130 (Golgi)
Merge
RFP Spn4A WT-S
RFP Spn4A H338R-S

C)

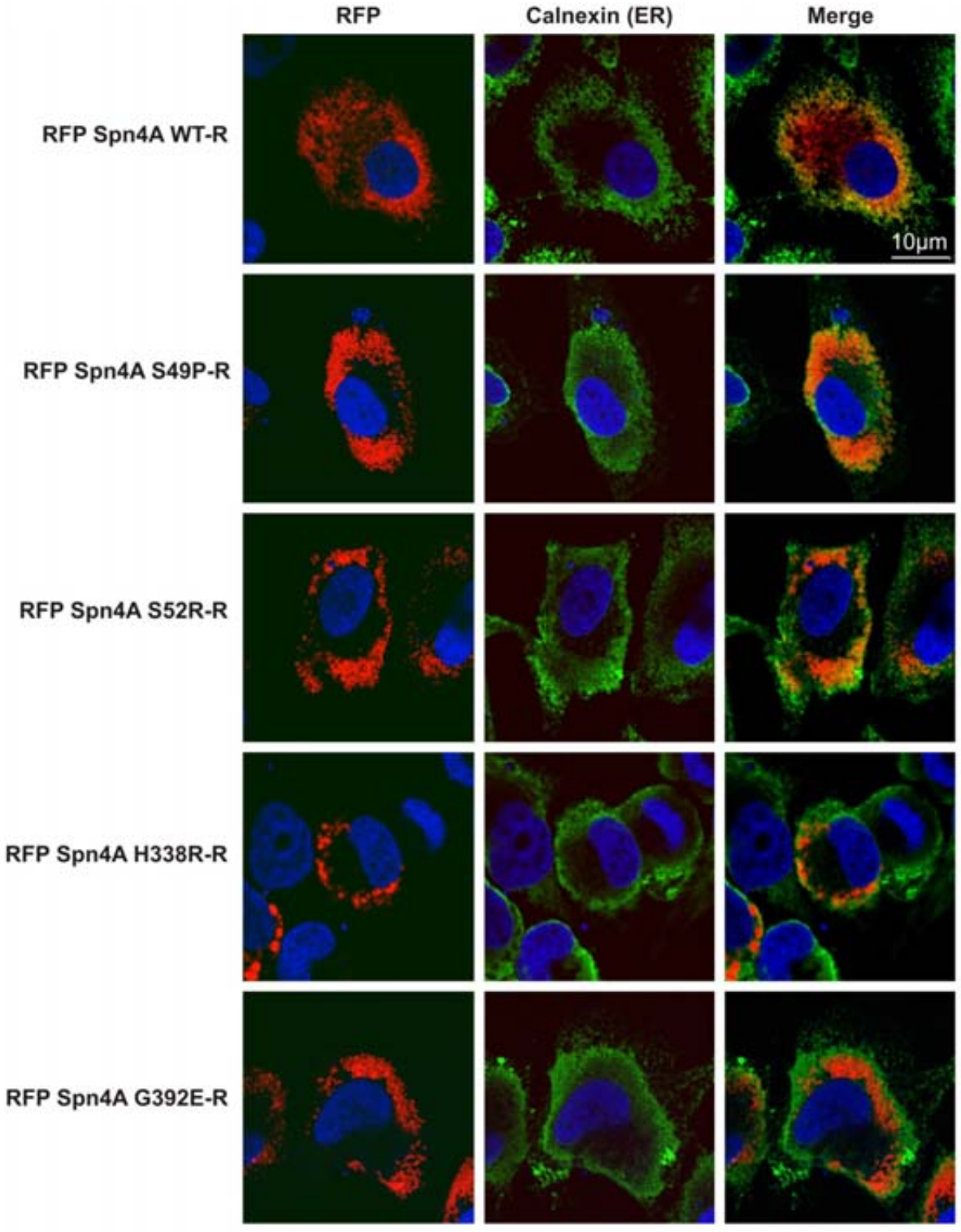
RFP
Calnexin (ER)
Merge
RFP Spn4A WT-R
RFP Spn4A S49P-R
RFP Spn4A S52R-R
RFP Spn4A H338R-R
RFP Spn4A G392E-R
10μm

D)

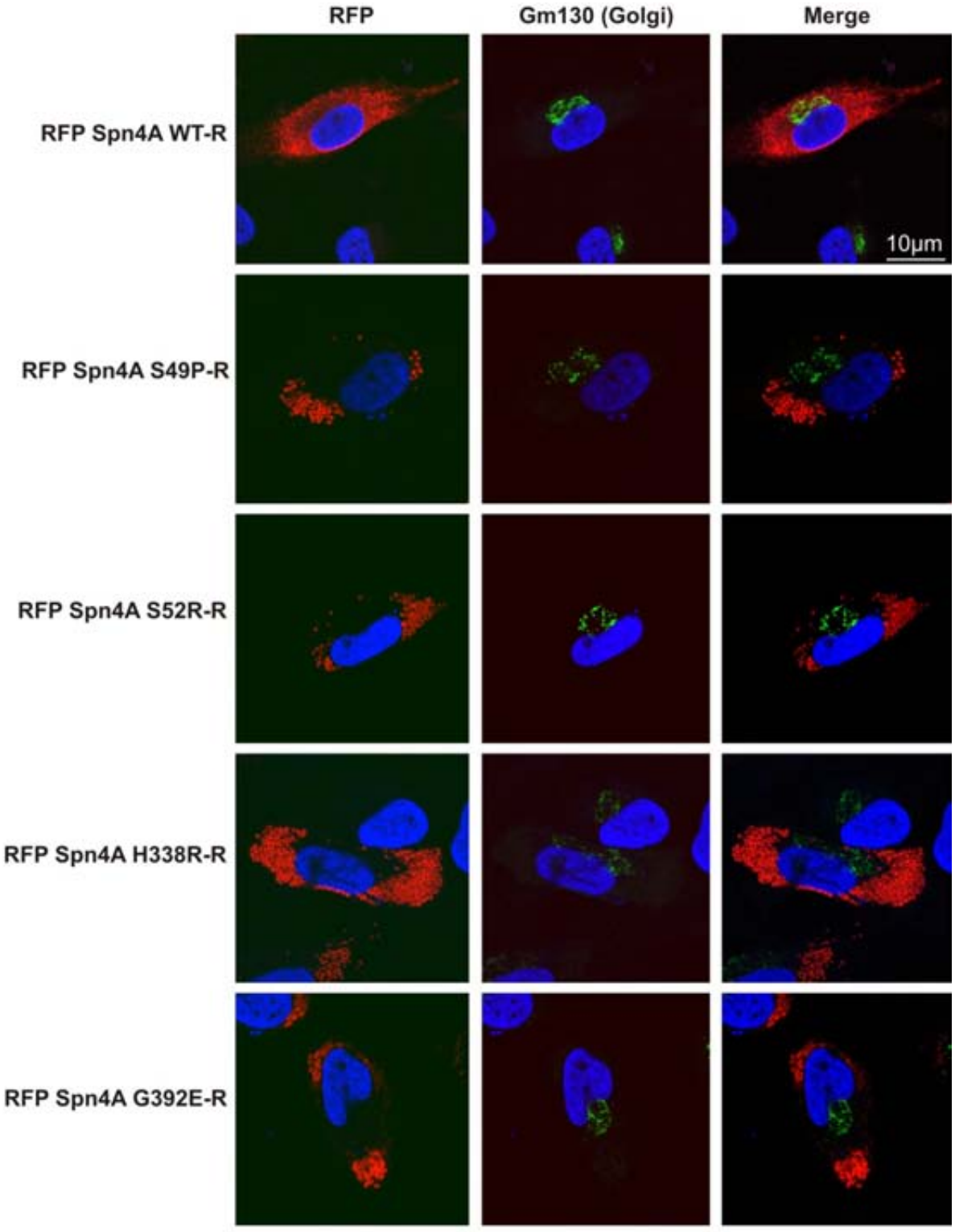
RFP
Gm130 (Golgi)
Merge
RFP Spn4A WT-R
RFP Spn4A S49P-R
RFP Spn4A S52R-R
RFP Spn4A H338R-R
RFP Spn4A G392E-R
10μm

E)

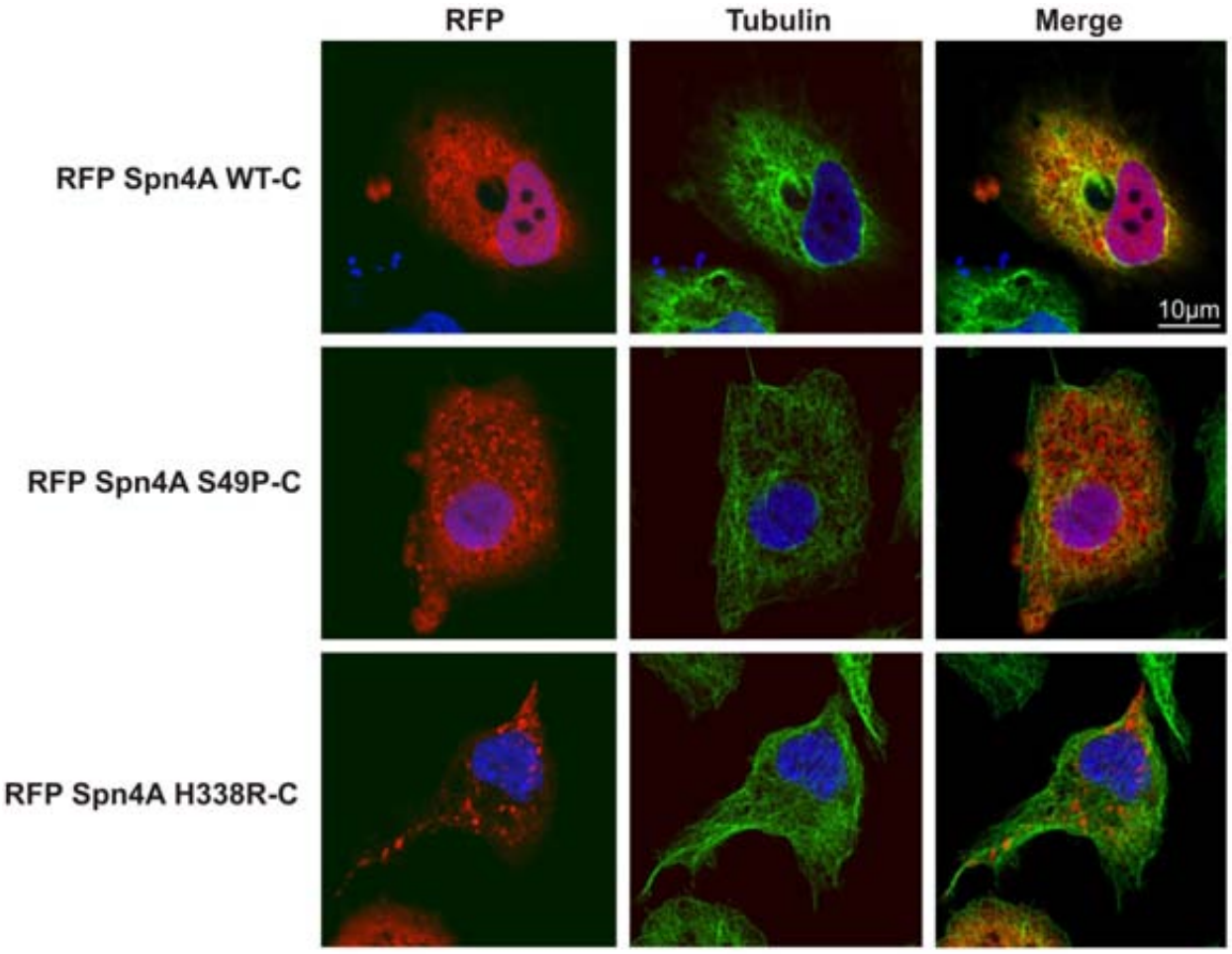
RFP
Tubulin
Merge
RFP Spn4A WT-C
RFP Spn4A S49P-C
RFP Spn4A H338R-C
10μm

Figure 2.7. Heat and SDS-stable complex formation assay between furin and Spn4A WT and mutants. A) Branched pathway mechanism of serpins. Serpins (I) encounter protease (E) and form a reversible complex, EI. Cleavage of the serpin leads to the short-lived enzyme intermediate [EI']. Either the inhibitory pathway proceeds to a stable EI* complex or the substrate pathway continues with proteolysis of the serpins. B) *In vitro* EI* complex formation assay. H4 cells were transfected with Spn4A WT-R or H338R-R for 48 hours. Cells were harvested, lysed, and incubated for 10 minutes with His-tagged recombinant furin at 30°C. The reaction was quenched with 50 mM EDTA, ran on an SDS-PAGE, and probed with anti-His antibodies for Spn4A and furin (green) and anti-tubulin antibodies (red), as a loading control, for western blot analysis. C) *In cellulo* EI* complex formation assay of secreted Spn4A WT-S and mutants. FLAG-tagged furin overexpressing HEK293-C4 cells were transfected as labeled for 48 hours. Empty vector and wildtype are abbreviated as EV and WT, respectively. Media was collected (extracellular), cells were lysed (intracellular), and loaded onto a native PAGE or boiled for 10 minutes in SDS loading buffer for SDS-PAGE. Western blot analysis was performed using anti-FLAG antibodies for Spn4A and furin (green) and anti-Hsp47 antibodies for Hsp47 (red) as a loading control. D) *In cellulo* EI* complex formation assay for secreted RFP Spn4A WT-S and H338R-S, as described in (C).

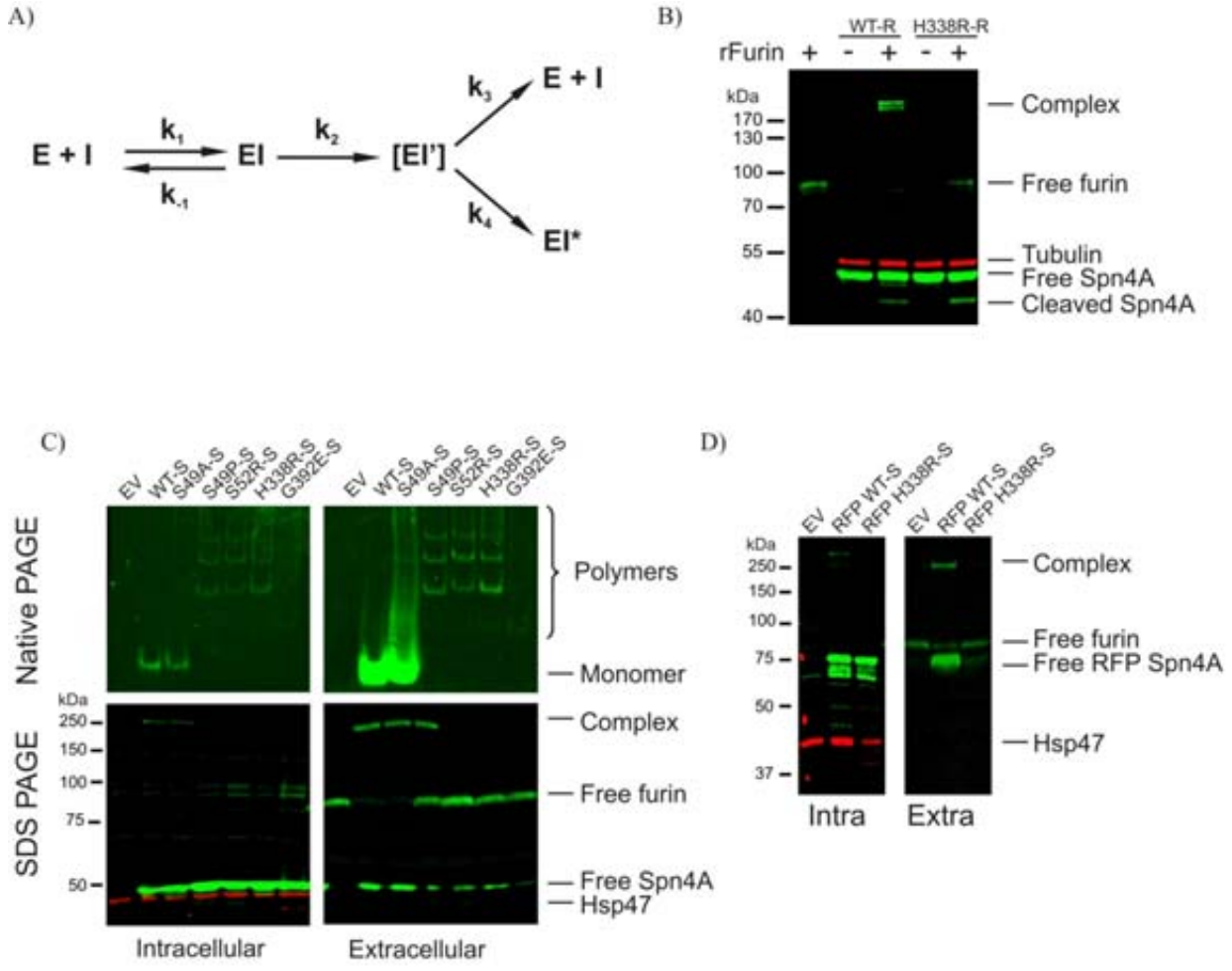

Figure 2.8. Qualitative and quantitative measurements of Spn4A expression levels as delivered by recombinant adenoviruses and cell viability measurements of virus-induced toxicity. A) Western blot analysis of H4s infected at MOI 1 or 5. Cells were infected for 48 hours, lysed in SDS buffer, and loaded onto an 8% SDS-PAGE. For western blotting, anti-FLAG for Spn4A (green) and anti-Hsp47 (red) were used. B) Flow cytometry quantitation of RFP expressing H4s. Cells were infected for 48 hours with Ad. RFP WT-R or WT-S at different MOIs, or Spn4A mutants at MOI 50. Cells were fixed in 2% formaldehyde and RFP expressing cells were quantified on a flow cytometer. The number in the label represents MOI. Example raw data are shown in Appendix 3, Supplemental Fig. A3.2. C) Confocal analysis of infected cells expressing Spn4A H338R-S at MOI 1 and MOI 50. H4 cells were infected for 48 hours, fixed, labeled using anti-calnexin for ER (green), and stained for the nuclei (blue) using Hoechst dye. D) Confocal analysis of infected cells at MOI 50. H4 cells were infected as labeled and fixed after 48 hours. Cells were labeled using anti-calnexin for ER (green) or anti-Gm130 for the Golgi (green), and stained for the nuclei (blue) using Hoechst dye. E) MTS cell viability assay of non-infected cells (NI), infected cells, and STS (staurosporine) treated cells. Cells were treated with 500nM of STS for 16 hours before MTS was added. After 72 hours of infection, MTS was added, cells were incubated for 45 minutes at 37°C, and absorbance at 490 nm measured. Experiments were performed in triplicates in three independent experiments and one representative experiment is shown. Absorbance was normalized to the NI and standard deviations of the triplicates are shown.

A)

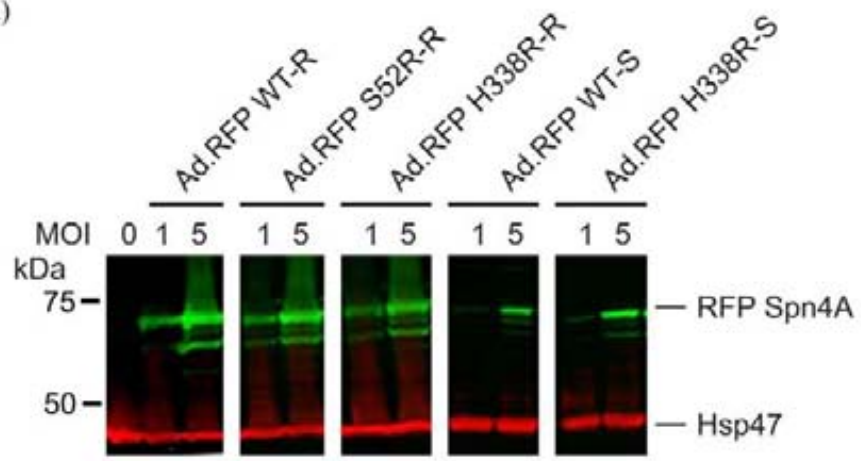
Ad.RFP WT-R
Ad.RFP S52R-R
Ad.RFP H338R-R
Ad.RFP WT-S
Ad.RFP H338R-S
MOI 0 1 5 1 5 1 5 1 5 1 5
kDa
75
50
RFP Spn4A
Hsp47

B)

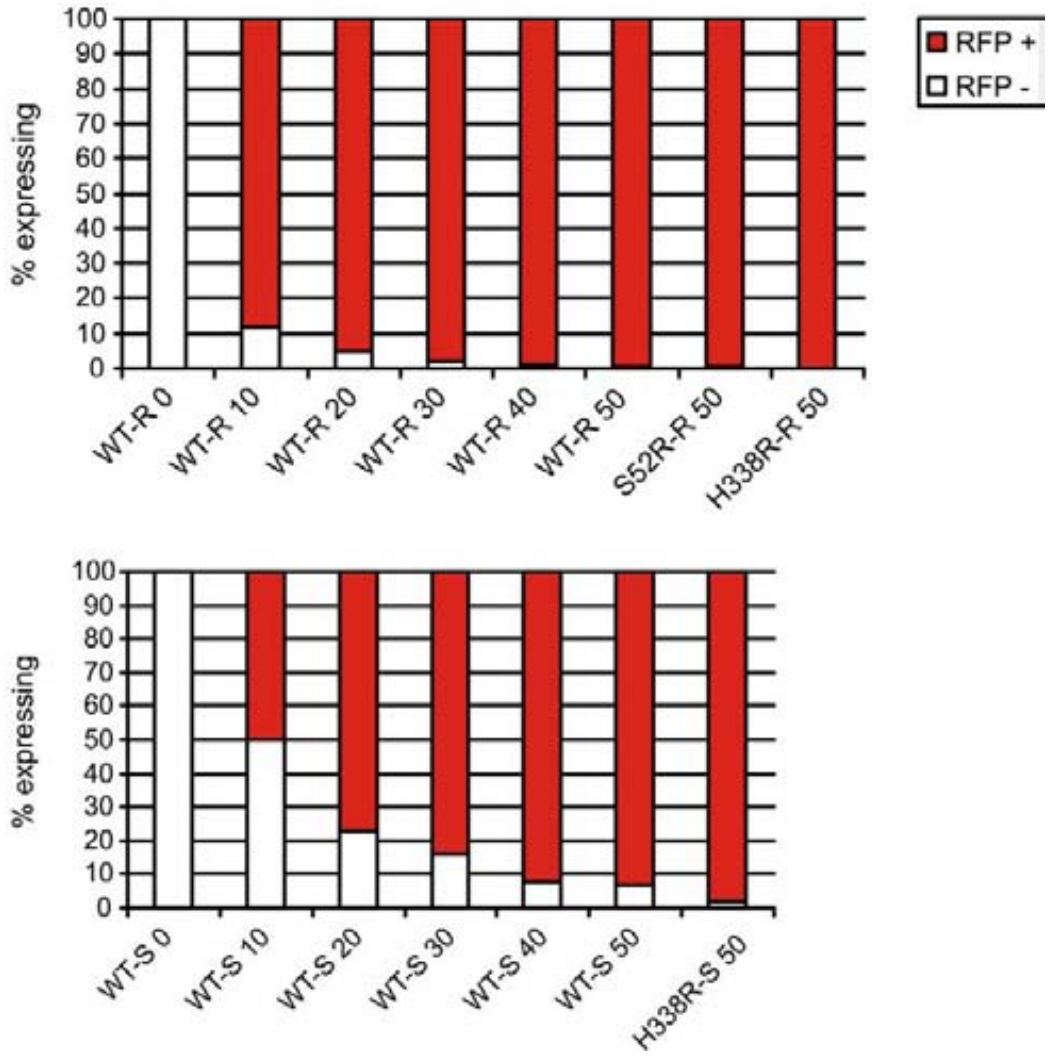
RFP +
RFP -
% expressing
100
90
80
70
60
50
40
30
20
10
0
WT-R 0
WT-R 10
WT-R 20
WT-R 30
WT-R 40
WT-R 50
S52R-R 50
H338R-R 50
% expressing
WT-S 0
WT-S 10
WT-S 20
WT-S 30
WT-S 40
WT-S 50
H338R-S 50

C)

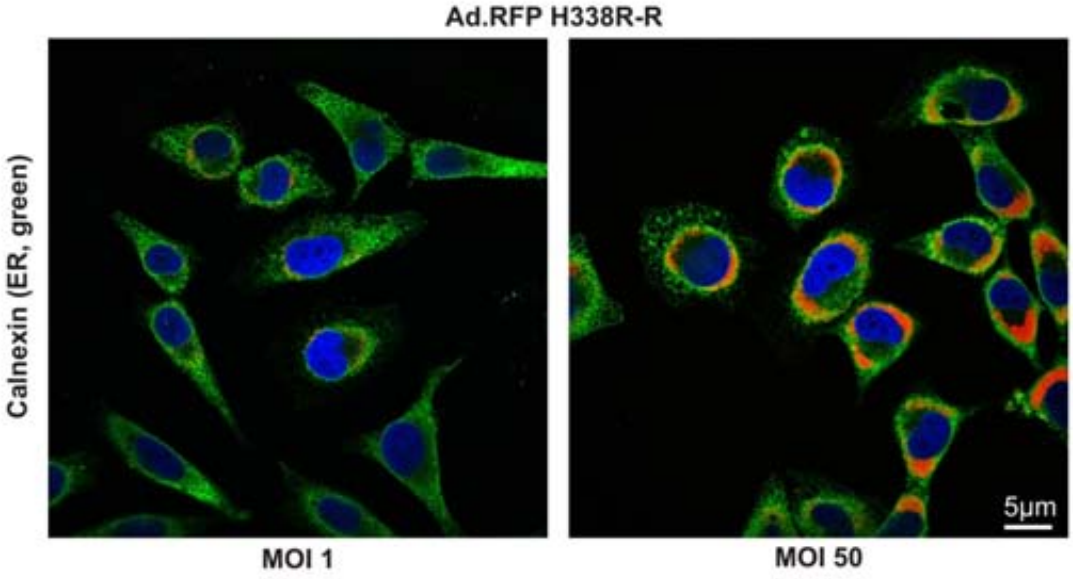
Ad.RFP H338R-R
Calnexin (ER, green)
5μm
MOI 1
MOI 50

D)

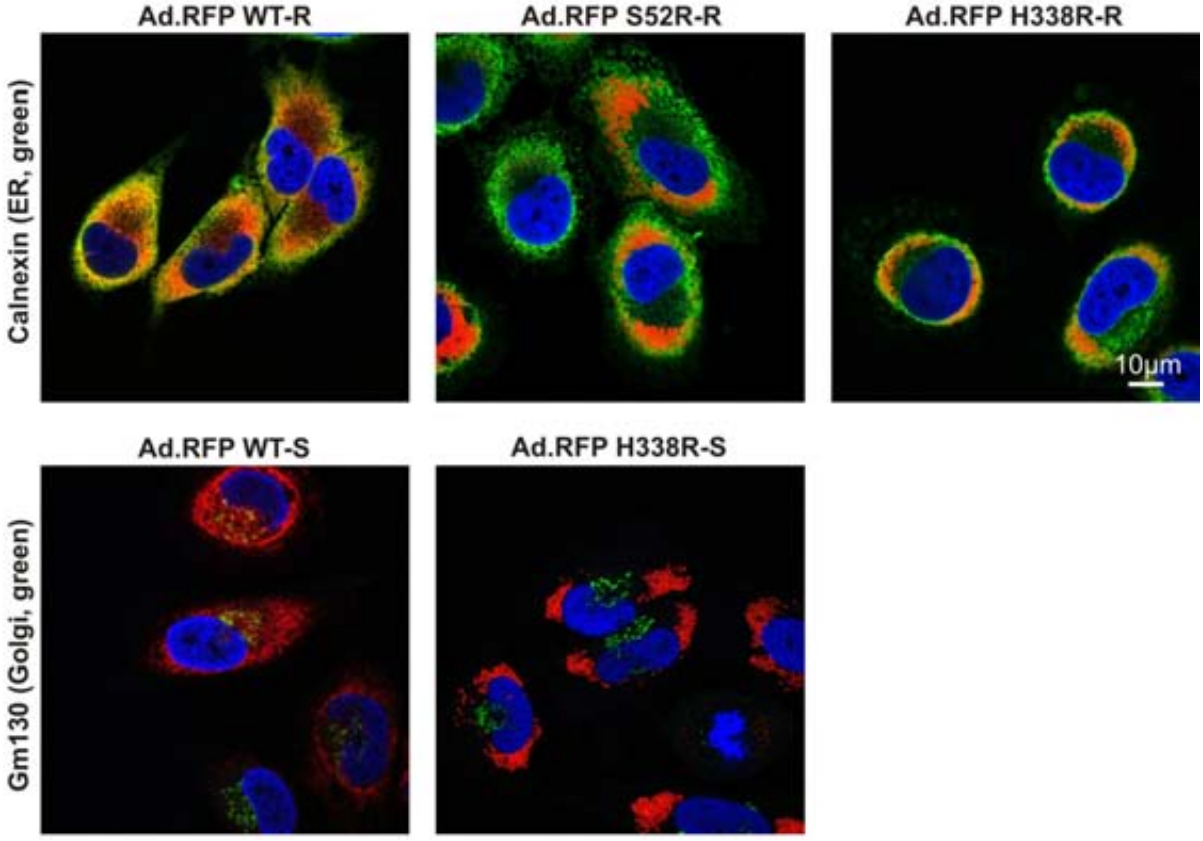
Ad.RFP WT-R
Ad.RFP S52R-R
Ad.RFP H338R-R
Calnexin (ER, green)
10μm
Ad.RFP WT-S
Ad.RFP H338R-S
Gm130 (Golgi, green)

E)

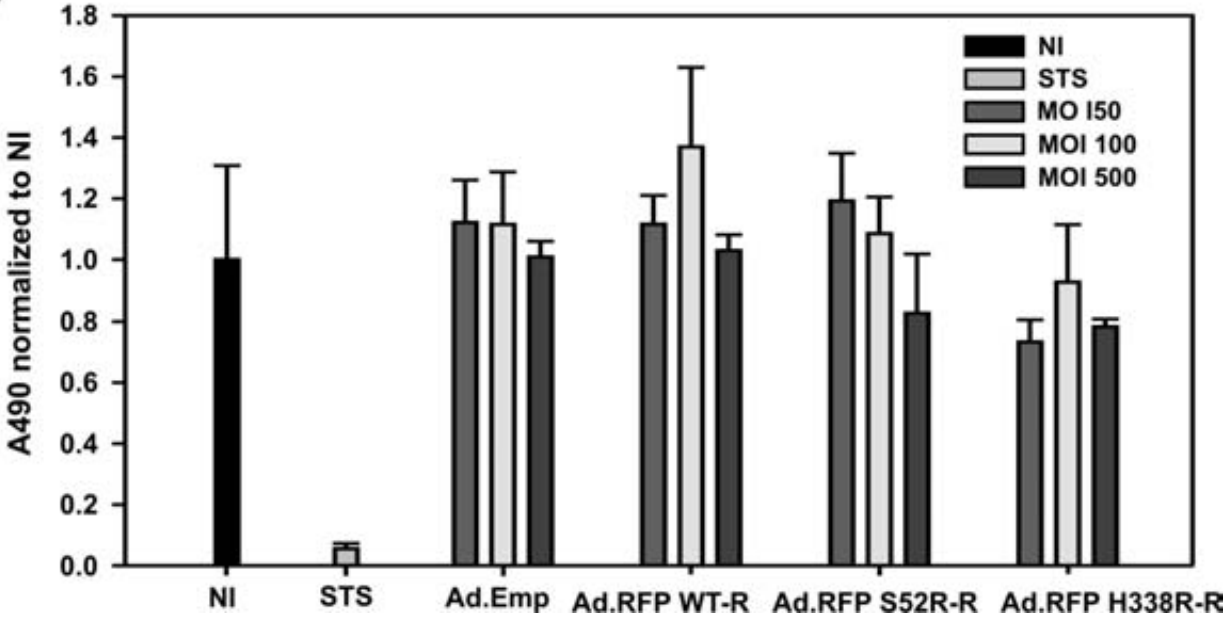
A490 normalized to NI
1.8
1.6
1.4
1.2
1.0
0.8
0.6
0.4
0.2
0.0
NI
STS
MO I50
MOI 100
MOI 500
NI
STS
Ad.Emp
Ad.RFP WT-R
Ad.RFP S52R-R
Ad.RFP H338R-R

Figure 2.9. Strategy for microarray analysis of H4 neuroglioma cells infected with recombinant adenovirus. H4 cells were infected with Ad. Emp, Ad. RFP WT-R, Ad. RFP S52R-R, Ad. RFP H338-R, Ad. RFP WT-S, or Ad. RFP H338R-S at MOI 50 and incubated for 48 hours before RNA extraction and analysis using the Illumina HumanHT-12 v3 Expression BeadChip. Adenovirus expressing Spn4A were compared to Ad. Emp and expression values with a 1.7 fold difference ($p<0.05$) were considered for analysis. The distribution of overlapping and unique genes over the threshold is shown in the venn diagram.

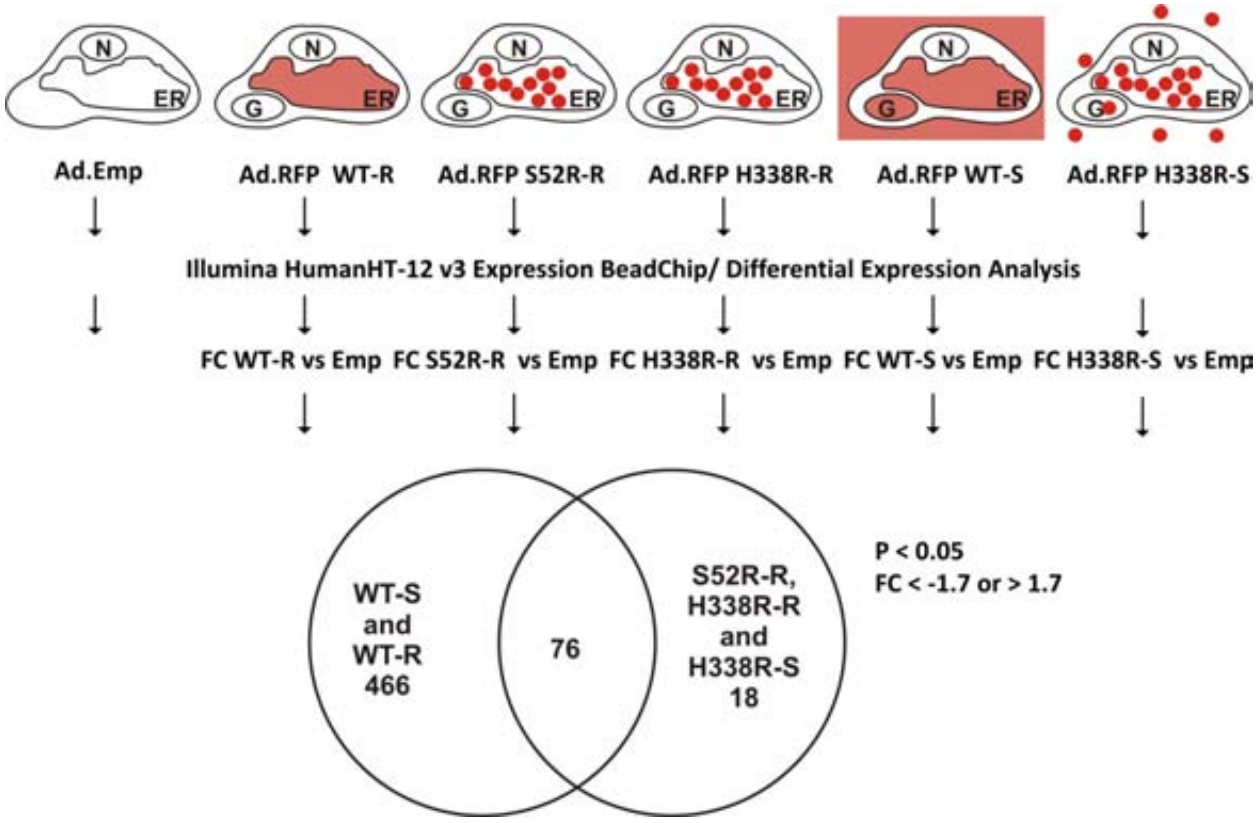

Figure 2.10. The mRNA levels of three ER stress genes in response to RFP Spn4A WT-R, S52R-R, or H338R-R determined by qPCR. RNA was collected from infected H4 neuroglioma cells, reverse transcribed to cDNA, and used for real-time PCR. FC represent comparisons of Ad. RFP WT-R, Ad. RFP S52R-R or Ad. RFP H338R-R to Ad. Emp. Significance ($p<0.05$*) was calculated from two-tailed Student's t-test from three experiments performed in duplicates. Error bars represent SEM.

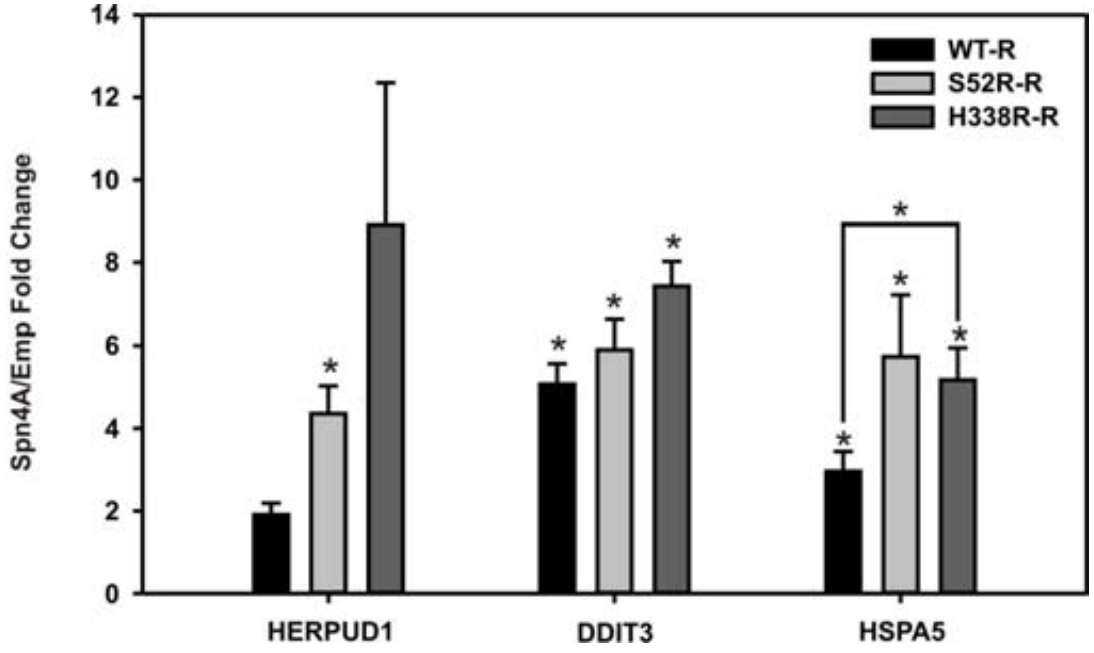

Figure 2.11. Distribution of genes differentially regulated in response to polymeric Spn4A mutants. The numbers are the number of genes up or down regulated.

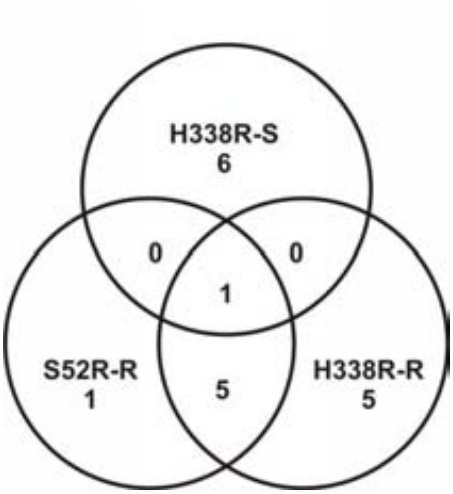

Figure 2.12. The mRNA levels of small proline-rich protein 2D in response to RFP Spn4A WT-R, S52R-R, or H338R-R determined by qPCR. RNA was collected from infected H4 neuroglioma cells, reverse transcribed to cDNA, and used for real-time PCR. FC represent comparisons of Ad. RFP WT-R, Ad. RFP S52R-R or Ad. RFP H338R-R to Ad. Emp. Significance ($p<0.05$*) was calculated from two-tailed Student's t-test from three experiments performed in duplicates. Error bars represent SEM.

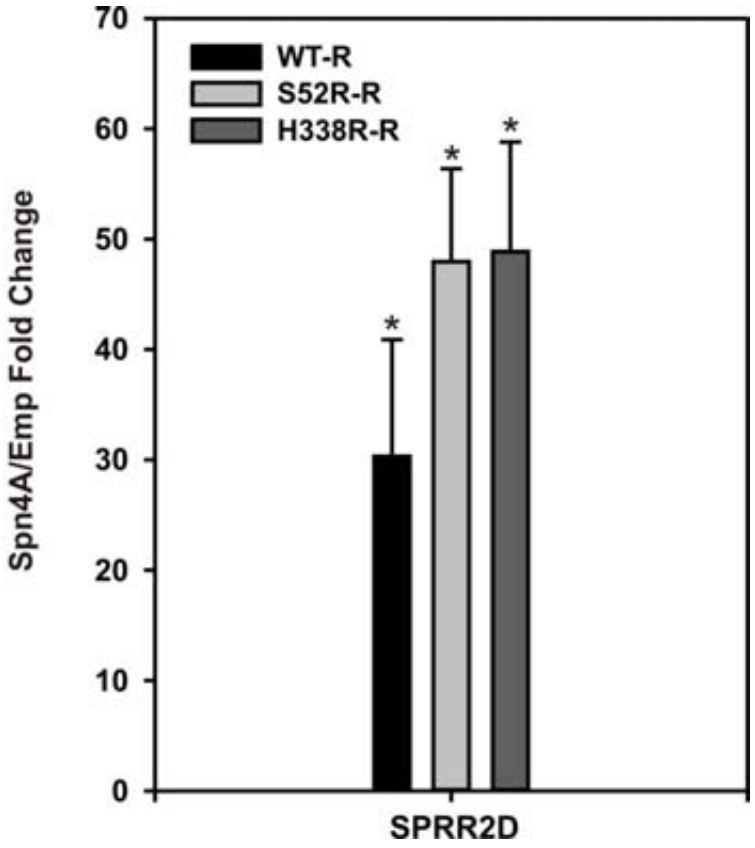

Table 2.1. Serpin rate of polymer formation correlates with severity of disease. Mutants of neuroserpin are each associated with a rate of polymer formation, as demonstrated by *in vitro* biochemical polymer formation assays. Increased polymer formation and inclusion body deposition (evident in cross sections of cerebral cortex stained for inclusions) are associated with a decreased age of disease onset and increased disease severity. Reprinted from The International Journal of Biochemistry & Cell Biology, 40, Davies MJ and Lomas DA, The molecular aetiology of the serpinopathies (105), 1273-1286, © 2008, with permission from Elsevier.

Mutation	Rate of Polymerisation	Number of Inclusions	Disease Onset (yrs)	Clinical Features
S49P	+	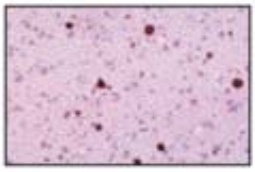	45-63	dementia, seizures
S52R	++	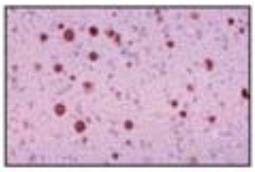	20-40	dementia, myoclonus
H338R	+++	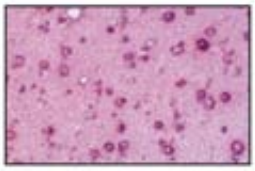	15	progressive myoclonus epilepsy
G392E	++++	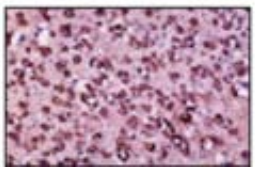	13	progressive myoclonus epilepsy, chorea

Table 2.2. Serpin clades A to I, prototypical serpins belonging to the clades, and their amino acid sequence identity to Spn4A. Amino acid sequences were compared using CLUSTALW2 (87).

Clade letter	Clade name (5)	Example	% amino acids identical to Spn4A
A	Antitrypsin-like	Alpha-1-antitrypsin	27
B	Intracellular, ovalbumin-like	Ovalbumin	32
C	Antithrombin	Antithrombin-III	25
D	Heparin cofactor II	Heparin cofactor	21
E	Plasminogen activator inhibitor	Plasminogen activator inhibitor 1	28
F	Pigment epithelium-derived factor	Pigment epithelium-derived factor	22
G	C1 inhibitor	Plasma protease C1 inhibitor	25
H	Heat shock protein 47	Heat shock protein 47	18
I	Neuroserpin	Neuroserpin	31

Table 2.3. Functional annotation clusters for genes upregulated by secreted or retained RFP Spn4A WT and mutants expression. DAVID functional annotation clustering was carried out using only the non unique upregulated genes and high stringency filter. Term represent annotation term, count is the number of genes involved in the individual term, p-value is calculated using a modified Fisher's exact test and represent the significance of gene-term enrichment, fold enrichment measures the magnitude of enrichment against the complete array background, and annotation cluster enrichment score is the negative log transformation of the geometric mean of the p-values in the group.

Term	Count	p-value	Fold Enrichment	Genes
Annotation Cluster 1: Enrichment Score = 4.3				
GO:0034976~response to endoplasmic reticulum stress	5	3.21E-07	80.41	HERPUD1,HSPA5,FAM129A,AC023024.2,DDIT3
GO:0006984~ER-nuclear signaling pathway	4	2.97E-05	62.49	HERPUD1,HSPA5,AC023024.2,DDIT3
GO:0033554~cellular response to stress	5	1.52E-02	4.88	HERPUD1,HSPA5,FAM129A,AC023024.2,DDIT3
Annotation Cluster 2: Enrichment Score = 2.5				
SM00271:DnaJ	3	2.18E-03	39.39	DNAJB9,DNAJB11,DNAJC3
IPR015609:Molecular chaperone, heat shock protein, Hsp40, DnaJ	3	2.18E-03	41.70	DNAJB9,DNAJB11,DNAJC3
domain:J	3	3.06E-03	35.30	DNAJB9,DNAJB11,DNAJC3
IPR001623:Heat shock protein DnaJ, N-terminal	3	3.12E-03	34.75	DNAJB9,DNAJB11,DNAJC3
IPR018253:Heat shock protein DnaJ, conserved site	3	3.25E-03	34.04	DNAJB9,DNAJB11,DNAJC3
GO:0031072~heat shock protein binding	3	7.95E-03	21.29	DNAJB9,DNAJB11,DNAJC3
Annotation Cluster 3: Enrichment Score = 2.4				
GO:0042175~nuclear envelope-endoplasmic reticulum network	6	1.78E-04	10.52	HERPUD1,HSP90B1,SEC11C,NUCB2,HSPA5,AC023024.2
GO:0005789~endoplasmic reticulum membrane	5	1.61E-03	9.26	HERPUD1,HSP90B1,SEC11C,HSPA5,AC023024.2
GO:0012505~endomembrane system	6	1.52E-02	3.82	HERPUD1,HSP90B1,SEC11C,NUCB2,HSPA5,AC023024.2
GO:0031090~organelle membrane	6	5.13E-02	2.77	HERPUD1,HSP90B1,SEC11C,NUCB2,HSPA5,AC023024.2
Annotation Cluster 4: Enrichment Score = 2.3				
IPR000886:Endoplasmic reticulum, targeting sequence	5	9.41E-07	63.19	HSP90B1,SDF2L1,PDIA6,PDIA4,HSPA5
GO:0042470~melanosome	4	6.34E-04	22.47	HSP90B1,PDIA6,PDIA4,HSPA5
GO:0048770~pigment granule	4	6.34E-04	22.47	HSP90B1,PDIA6,PDIA4,HSPA5
GO:0016023~cytoplasmic membrane-bounded vesicle	4	8.69E-02	3.63	HSP90B1,PDIA6,PDIA4,HSPA5
GO:0031988~membrane-bounded vesicle	4	9.37E-02	3.51	HSP90B1,PDIA6,PDIA4,HSPA5
GO:0031410~cytoplasmic vesicle	4	1.24E-01	3.10	HSP90B1,PDIA6,PDIA4,HSPA5
GO:0031982~vesicle	4	1.36E-01	2.97	HSP90B1,PDIA6,PDIA4,HSPA5
Annotation Cluster 5: Enrichment Score = 2.3				
GO:0070013~intracellular organelle lumen	10	4.15E-03	2.80	HYOU1,HSP90B1,DNAJB9,DNAJB11,ANG,SDF2L1,RP5-1103G7.7,PDIA6,PDIA4,HSPA5
GO:0043233~organelle lumen	10	4.86E-03	2.74	HYOU1,HSP90B1,DNAJB9,DNAJB11,ANG,SDF2L1,RP5-1103G7.7,PDIA6,PDIA4,HSPA5

Term	Count	p-value	Fold Enrichment	Genes
GO:0031974~membrane-enclosed lumen	10	5.52E-03	2.69	HYOU1,HSP90B1,DNAJB9,DNAJB11,ANG,SDF2L1,RP5-1103G7.7,PDIA6,PDIA4,HSPA5
Annotation Cluster 6: Enrichment Score = 2.1				
GO:0006984~ER-nuclear signaling pathway	4	2.97E-05	62.49	HERPUD1,HSPA5,AC023024.2,DDIT3
GO:0042981~regulation of apoptosis	5	4.83E-02	3.41	HERPUD1,HSP90B1,HSPA5,AC023024.2,DDIT3
GO:0043067~regulation of programmed cell death	5	4.98E-02	3.38	HERPUD1,HSP90B1,HSPA5,AC023024.2,DDIT3
GO:0010941~regulation of cell death	5	5.03E-02	3.37	HERPUD1,HSP90B1,HSPA5,AC023024.2,DDIT3

Table 2.4. ER stress genes, gene descriptions, and fold changes for WT-R, S52R-R, H338R-R, WT-S, and H338R-S. These seven genes were within the top 11 most upregulated in response to RFP WT-R expressing, top 10 for retained mutants, and top 12 for the secreted H338R-S mutant. None of the genes listed were within the top 15 genes upregulated in response to WT-S. NS is not significant. All FCs reported had $p<0.05$.

Gene	Gene name and description	WT-R	S52R-R	H338R-R	WT-S	H338R-S
HERPUD 1	Homocysteine-inducible, endoplasmic reticulum stress-inducible, ubiquitin-like domain member 1 – upregulated during UPR, participates in ERAD	3.79	3.73	3.78	1.94	2.41
HYOU1	Hypoxia upregulated 1 – upregulated during hypoxic stress, functions in protein folding and ER secretion	3.50	3.54	3.75	2.63	2.88
PDIA4	Protein disulfide isomerase family A, member 4 – ER chaperone	3.45	3.50	3.28	2.52	3.14
SDF2L1	Stromal cell-derived factor 2-like 1 – ER chaperone	3.23	3.76	3.45	1.80	2.46
DDIT3	DNA-damage-inducible transcript 3 (also known as CHOP) – transcription factor upregulated during ER stress or DNA damage, leading to in ER stress response and cell cycle arrest among others; may induce apoptosis	3.19	2.69	3.01	NS	2.05
CRELD2	Cysteine-rich with EGF-like domains 2 – upregulated during ER stress, functions in protein folding and trafficking	3.13	3.30	2.99	2.92	3.03
HSPA5	Heat shock 70 kDa protein 5 (also known as BiP) – ER chaperone	2.91	3.16	3.19	2.30	2.68

Table 2.5. Genes differentially regulated in response to polymeric serpins. The gene symbol, gene name, and fold changes (FC) for 18 genes differentially regulated in response to RFP S52R-R, RFP H338R-R, or RFP H338R-S are listed. Some genes were not significant (NS).

Gene Symbol	Gene name	FC RFP S52R-R	FC RFP H338R-R	FC RFP H338R-S
Downregulated				
MGP	Homo sapiens matrix Gla protein	**-2.99**	**-3.23**	NS
VWA5A	Homo sapiens von Willebrand factor A domain containing 5A	NS	NS	**-1.94**
KIAA0363	PREDICTED: Homo sapiens KIAA0363 protein	NS	**-1.91**	NS
INDO	Homo sapiens indoleamine-pyrrole 2,3 dioxygenase	NS	NS	**-1.82**
CDH6	Homo sapiens cadherin 6, type 2, K-cadherin (fetal kidney)	**-1.80**	**-1.86**	NS
SIPA1	Homo sapiens signal-induced proliferation-associated gene 1	**-1.75**	**-1.95**	NS
DPYSL3	Homo sapiens dihydropyrimidinase-like 3	NS	**-1.73**	NS
SIDT2	Homo sapiens SID1 transmembrane family, member 2	NS	**-1.70**	NS
Upregulated				
PSAT1	Homo sapiens phosphoserine aminotransferase 1	NS	**1.73**	NS
INHBE	Homo sapiens inhibin, beta E	NS	NS	**1.74**
GFPT1	Homo sapiens glutamine-fructose-6-phosphate transaminase 1	NS	**1.76**	NS
LOC643031	PREDICTED: Homo sapiens similar to NADH dehydrogenase subunit 5	NS	NS	**1.77**
CD34	Homo sapiens CD34 antigen	NS	NS	**1.78**
WDR69	Homo sapiens WD repeat domain 69	NS	NS	**1.78**
CALR	Homo sapiens calreticulin	**1.80**	NS	NS
SLC35B1	Homo sapiens solute carrier family 35, member B1	**1.71**	**1.85**	NS
KRT81	Homo sapiens keratin 81	**1.99**	**1.74**	**1.79**
SPRR2D	Homo sapiens small proline-rich protein 2D	**2.67**	**2.81**	NS

Table 2.6. Functional annotations for genes differentially regulated by polymeric serpins expression. DAVID functional annotation chart was carried out using genes unique to the mutants. Red coloured genes are upregulated and green, downregulated.

Term	Genes
cell-cell adhesion	CD34, MGP, CDH6
aminotransferase	GFPT1, PSAT1
carbohydrate binding	CD34, GFPT1, CALR
cartilage development	GFPT1, MGP
polymorphism	VWA5A, SIPA1, MGP, DPYSL3, INDO, SIDT2, KIAA0363, KRT81, SLC35B1, INHBE, SPRR2D, CD34, WDR69, PSAT1
calcium binding	MGP, CALR

Chapter 3: Transcriptome profiling of human neuroglioma cells expressing the proprotein convertase inhibitor, Spn4A

3.1 Introduction

3.1.1 Proprotein convertases

The concept of enzyme maturation by proteolysis was first described in 1967 for sheep β-lipotrophic hormone (106) and human insulin (107). However, the responsible protease would remain unidentified for nearly another two decades until the discovery of the precursor processing endoprotease, Kex2, in yeast (108). Shortly afterwards, in 1989, the mammalian homolog of Kex2, furin, was discovered (109). Within a year, furin was shown to convert a glycoprotein (110) and growth factor (111) to their mature forms.

Today, nine structurally similar proprotein convertases (PCs) have been discovered in humans including furin, PC1/3, PC2, PC4, PACE4, PC5/6 (two isoforms), PC7 (also known as lymphoma PC [LPC]), SKI-1 (subtilisin/kexin-like isozyme-1, also known as site-1 protease [S1P]) and PCSK9 (proprotein convertase subtilisin kexin 9, also known as neural apoptosis regulated convertase-1 [NARC-1]). Furin, SKI-1, and PC7 are ubiquitously expressed (112), while tissue-specific PCs include PC1/3 and PC2 in neuroendocrine cells (113;114), PC4 in germ cells (115), and PCSK9 in brain, liver, and intestinal cells (116). Their physiological roles as enzyme regulators and aberrant expression in disease are of great biological and clinical significance (discussed in 3.1.2).

3.1.1.1 Structural features

Several structural features are important for the targeting, activation, and localization of PCs (Fig. 3.1). An N-terminal signal peptide targets PCs to the endoplasmic reticulum (ER). A prodomain follows the signal peptide cleavage site and acts as an intramolecular chaperone that facilitates folding in the ER, transport, and activation (117;118). Immediately downstream is a set of basic amino acids that make up the autoproteolytic cleavage site for excision of the propeptide, a catalytic domain containing the catalytic triad, and lastly, a P domain which regulates the pH and calcium dependence of the protein (101;119). Additionally, furin, PC7, the isoform PC5/6B, and SKI-1 have transmembrane domains and C-terminal cytoplasmic domains for localization and sorting to the TGN (trans-Golgi network), endosomal system, and cell surface (120;121). While these four PCs exist as membrane bound proteins, additional cleavage

sequences near the C-terminus of furin and SKI-1 allow truncation of the PCs and generation of soluble and secreted forms (92;120). Other PCs are found in dense core granules or are constitutively secreted (112;122).

3.1.1.2 Activation and subcellular localization

The activation of PCs is spatially regulated (Fig. 3.2). The first step is the autocatalytic cleavage of the prodomain in the ER for all convertases except PC2, which is processed in immature secretory granules (122). The propeptide remains associated with, and inhibits, the active site until the PC-propeptide heterodimer exits the ER to the Golgi, where a decrease in pH and increase in calcium promote the cleavage and release of the inhibitory propeptide (101). The exception is PCSK9, which is secreted as the inactive heterodimer (116;123). Specifically, furin, PC5/6, PACE4, and PC7 are activated in the TGN (118;124;125), PC1/3 and PC2 in secretory granules (126), and SKI-1 in the cis/medial-Golgi compartments (127). Once activated, functional PCs cycle between different cellular compartments (Fig. 3.3). Furin activation in the TGN has been recently contested with two papers, which report furin-mediated degradation of an ER-localized misfolded insulin proreceptor (128) and furin-mediated cleavage of the chimeric ER-retained hemojuvelin, and suggest that furin can be functional in the ERGIC (ER-Golgi Intermediate Compartment) pathway (129).

3.1.1.3 Substrate specificity and physiological substrates

The family of PCs can be separated into two groups based on their substrate specificity. The first group consists of furin, PC1/3, PC2, PC4, PACE4, PC5/6, and PC7, which recognize basic amino acids and have the general consensus sequence (K/R)-$(X)_n$-(K/R)↓, where n = 0, 2, 4, or 6, X is any amino acid, and the down arrow denotes cleavage (122). Other substrate characteristics may form more favorable cleavage conditions specific for a PC. For example, the most efficient processing site for furin is R-X-(K/R)-R↓ with basic residues at P3, P5, and P6 sites, while the minimal is R-X-X-R (130-132). The first group differs from SKI-1 and PCSK9 which have the consensus motif (R/K)-X-(hydrophobic)-X↓ (133) and VFAQ↓ (123), respectively.

Various protein precursors such as hormones, neuropeptides, growth factors and their receptors, cell surface receptors, enzymes, as well as bacterial and viral products have been identified as substrates for PCs, with the exception of PCSK9. The only substrate identified for

PCSK9 is the autocatalytic cleavage of its own prodomain. While substrates could be predicted from amino acid sequences and demonstrated *in vitro*, the discovery of bona fide endogenous substrates for each PC has been complicated by their similar specificity, which allows processing of some precursors by multiple convertases, and the spatial and temporal expression of PCs and predicted substrates.

The most convincing evidence of their physiological roles comes from knockout mice studies. A wide range of phenotypes are detected with the knockout of each PC, and include embryonic lethality (furin (134), PC5/6 (135), or SKI-1 (136)), craniofacial abnormalities and some death (PACE4 (137)), hormonal and/or neuroendocrine deficiency (PC1/3 (138) or PC2 (139)), reduced fertility (PC4 (140)), and enhanced cholesterol uptake by the liver (PCSK9 (141)). Only PC7 knockout mice fail to show any abnormal phenotype (142). The phenotype from the loss of PC function would mimic that of the loss of matured substrate. Accordingly, substrates can be inferred. For example, the phenotypes of TGFβ1 (transforming growth factor beta 1), bone morphogenetic proteins, or α4-integrin deficient embryos mimic furin null embryos and are suggested as substrates (143;144). Different from null mice, conditional furin knockout in the liver is not lethal and predicted precursors are still processed, albeit with reduced efficiency (145). Likely, hepatocytes express convertases with redundant functions. The full list of substrates for furin and other PCs will not be discussed here, but included throughout the chapter as needed.

3.1.2 Furin as a therapeutic target

PCs activate several bacterial toxin and viral glycoproteins and their aberrant expression is associated with diseases such as cancer, atherosclerosis, neurodegenerative disorders, and dyslipidemia (146). We will focus our discussion on pathologies related to the ubiquitously expressed furin and for which furin-targeted intervention may be beneficial.

3.1.2.1 Bacterial and viral infections requiring furin-like enzymes

Bacteria and viruses have hijacked the spatial and temporal regulation of protein maturation for their own protoxins or proproteins. These include cell surface activation of anthrax toxin protective antigen (PA) (147), *Aeromonas hydrophila* aerolysin toxin (148), and *Clostridium septicum* α-toxin (149). Proteolytically activated toxins form pores in cell membranes, allowing entry of the bacteria, and causing cell toxicity. Additionally, endocytosed

toxins such as *Pseudomonas* exotoxin A (PEA), diphtheria toxin, and shiga toxin are processed by furin in the endosome to enable translocation to the cytosol (101). Last, many pathogenic viruses including Ebola, highly pathogenic avian influenza virus, human immunodeficiency virus 1 (HIV-1), human cytomegalovirus (hCMV), Dengue virus, West Nile virus, and tick-borne encephalitis virus require furin or furin-like protease processing of viral glycoproteins (150-156).

3.1.2.2 Cancers associated with increased furin-like activity

Aberrant expression of convertases is detected in many cancers. Furin is upregulated in head and neck (157), breast (158), and lung (159) cancers, as well as in a number of tumor cell lines such as glioblastomas (160) and gonadal cancer lines (161). Further, critical proteins upregulated in malignancy are either directly processed by PCs or are indirectly controlled by PC substrates. Consequently, inhibition of PCs can attenuate the malignancy phenotype *in vivo* (162-165) (discussed in section 3.1.3).

Tumorigenesis and metastasis are driven by multiple complex mechanisms, the details of which will not be covered here. Simply, uncontrolled growth of cells due to misregulation of the cell cycle, formation of blood vessels for attaining nutrients and oxygen, as well as invasion and migration of tumor cells by remodeling of the extracellular matrix (ECM) contribute to cancer pathology (166). We will discuss specific examples of PC-processed proteins that promote tumor malignancy: TGFβ, PDGF (platelet-derived growth factor), IGF1 (insulin growth factor 1), IGFR (IGF receptor), and MT1-MMP (membrane type 1 matrix metalloprotease).

TGFβ is a cytokine that controls multiple cellular functions, including cell proliferation, differentiation, migration, and apoptosis, among others (167). TGFβ is a potent cell growth inhibitor in most cells. It is processed by furin intracellularly and secreted into the extracellular matrix as a latent protein. Once activated by proteases or integrins, TGFβ signals through TGFβR (TGFβ receptor) and primarily through Smad transcription factors (167). Downstream cell growth inhibition effects are mediated by upregulation of cell cycle inhibitors, the action of retinoblastoma protein (Rb) and E2F transcription factors to suppress the G1/S transition (Gap1/Synthesis), and downregulation of the proto-oncogene, c-myc (168-170). However, in mesenchymal cells, TGFβ can promote proliferation through upregulation of the growth factor PDGF (171).

Many tumor cells can escape the tumor-suppressive activities of TGFβ through various pathways such as increasing expression of oncoproteins or inactivation of TGFβ signaling pathways (170). Once they are resistant to the TGFβ tumor suppressor effects, TGFβ is upregulated in many cancers to confer proliferative, invasive and angiogenic ability by increasing the production of mitogenic growth factors PDGF (172;173) and fibroblast growth factor (FGF) (174), extracellular matrix-degrading enzymes for motility (175), and VEGF (176) (vascular endothelial growth factor) for angiogenesis. Maturation of both TGFβ and PDGF are mostly mediated by furin (177).

IGF1 and its receptor IGFR are also highly expressed in cancer cells to stimulate cell proliferation and inhibit apoptosis (178). Through regulation of MMPs (matrix metalloproteases) expression (179;180), they can further mediate tumor invasion. Furin, and to a lesser extent PC6A and PC7, are responsible for processing IGF and IGFR (181;182).

Last, furin processes many ECM proteins important for tumor invasion and metastasis. The ECM is composed of glycosaminoglycans and fibrous proteins such as proteoglycans, collagen, elastin, fibronectin, and laminin to mediate cell adhesion and support (175). One of the earliest MMPs that acts on the basement membrane is the collagenase MT1-MMP, which also cleaves and activates the gelatinase MMP2 (166;183). Many members of the MMP family have furin consensus sites and furin activation of MT1-MMP has been demonstrated (184;185).

3.1.3 Furin-targeted inhibitors

The molecular targets of furin have spurred the development of inhibitors to treat microbial diseases and cancer. Several lines of evidence suggest that furin knockdown would be a viable strategy. First, no obvious phenotype is seen in liver-specific furin knockouts, which suggest that related PCs could compensate for the loss of furin in specific cell types. Second, furin inhibitors protect against furin-mediated *Pseudomonas* toxicity in mice without adverse physiological effects (186). Last, double transgenic mice with salivary gland heterozygous furin knockout and PLAG-1 (pleiomorphic-adenoma gene 1) proto-oncogene overexpression show delayed salivary gland tumorigenesis (162). However, mice with homozygous furin knockdown in the salivary gland exhibit poor health.

Much progress has been made on the design of furin inhibitors. We will focus on small molecule, prodomain-based, peptide-based, and protein-based inhibitors, which are best characterized and show the most promise.

3.1.3.1 Small molecule inhibitors

Small molecule inhibitors are attractive therapeutic strategies because they are easily produced through synthetic routes, may be metabolically and proteolytically stable, and can be administered easily. They are the newest inhibitors being developed for furin and only two have been recently discovered. From a small molecule screen, guanidinylated aryl 2,5-dideoxystreptamine derivatives (GADDs) are found to potently and relatively specifically inhibit furin (K_i = 6nM) and protect RAW264.7 macrophage cells from anthrax PA by inhibiting its processing (187). Further, GADDs preferentially recognize furin and PC5/6B compared to PACE4 and PC7 (187). Another high-throughput screen identified B3, a cell permeable compound, which exhibits a K_i of 12 μM. B3 can inhibit furin-mediated processing of pro-MT1-MMP, which leads to a reduction in cancer cell motility and invasiveness (188). The authors report that B3 may also inhibit other PCs. While small molecule inhibitors may have a promising future, prodomain-, peptide-, or protein-based inhibitors are much better characterized and importantly, are effective *in vivo*.

3.1.3.2 Prodomain-based inhibitors

The next class of inhibitors is based on the PC natural prodomain, which tightly binds and inhibits the catalytic domain of PCs. Purified prodomain, vectors carrying the prodomain, or smaller synthetic prodomain peptides can inhibit PCs in the low nanomolar to high picomolar range (189-191). Tumor cells transfected with the furin prodomain and transplanted onto SCID (Severe Combined Immunodeficiency) mice display less proliferation and invasiveness compared to controls (163). However, the furin prodomain can inhibit PC5/6 ten-fold more potently than furin and thus, the selectivity of prodomain inhibitors would have to be improved to be useful (189).

3.1.3.3 Peptide-based inhibitors

Many peptide inhibitors are substrate analogs (192-196). The most promising inhibitors are polyarginine peptides (192) and the TPRARRRKKRX peptide (195) for their potency and characterization in cell culture and mice. Specifically, D-hexa-arginine (K_i = 106 nM) protects

cultured cells and mice from PEA toxicity without side effects (186) and the TPRARRRKKRT peptide (K_i = 23 nM) protects mice from inhaled anthrax and injected PEA (195). These peptides are broad PC inhibitors. D-hexa-arginine also inhibits PACE4 and PC1 in the high nanomolar and low micromolar range (192) and TPRARRRKKRT inhibits PACE4, PC4, PC5/6, and PC7, in the high nanomolar range (195).

3.1.3.4 Protein-based inhibitors

Bioengineered proteins and natural endogenous proteins constitute the last group of inhibitors. Several protein-based inhibitors have been designed by mutating the reactive sites of protease inhibitors to target furin, such as turkey ovomucoid third domain (197), α_2-macroglobulin (198), eglin C (199), and α_1-antitrypsin (200).

The α_1-antitrypsin variant, known as α_1-PDX (α_1 antitrypsin Portland), has been studied extensively because of its potency, selectivity, and demonstrated application under pathological circumstances. *In vitro*, α_1-PDX inhibits furin (K_i = 0.6 nM) and PC5/6B (K_i = 2.3 nM) (201), but *in cellulo*, it may target additional PCs in a cell-type specific manner (202). Application of α_1-PDX to cells confers protection from furin-mediated activation of pore-forming proaerolysin (148), HIV-1 glycoprotein 160 (gp160) (200), PEA (201), and hCMV pro-glycoprotein B (gB) (203). Further, it is a powerful tool for tumorigenesis inhibition in cell culture and *in vivo* (204;205). Nude mice that are injected with colon carcinoma HT29 cells expressing α_1-PDX showed decreased tumor size and incidence and delayed tumor development in comparison to control mice injected with HT29 cells (205). Further *in vivo* studies using transplantation of astrocytoma cells (164) or colon carcinoma CT26 cells (165) have shown that α_1-PDX expressing cancer cells are less proliferative, invasive, and metastatic. Cancer cell lines treated with α_1-PDX have unprocessed IGFR, TGFβ, and MT1-MMP (164;165;205). However, the effects of α_1-PDX on cancer cells may be cell-type specific as breast cancer cells transfected with α_1-PDX have increased cell motility, migration, and invasion due to increased MMP9 activity (206).

Lastly, two naturally occurring serpins, the human proteinase inhibitor 8 (PI8) (207) and *Drosophila* Spn4A (34-36), inhibit furin. Human PI8 has a K_i of 54 pM, but its lack of an N-terminal signal peptide means its cytoplasmic localization prohibits interactions with furin. Furthermore, PI8 can also inhibit other types of proteases, such as trypsin and chymotrypsin (208). In comparison to all other furin inhibitors, Spn4A is the most potent (K_i = 13pM) (36).

Also, Spn4A has been shown to inhibit *Drosophila* PC2 (K_i = 3.5 nM) (36), which suggests it may have a broad specificity for PCs.

Spn4A naturally has a C-terminal HDEL ER retention signal, whose deletion leads to Spn4A secretion to the extracellular milieu. Our lab has demonstrated the effectiveness of secreted Spn4A (Spn4A-S) in blocking furin-mediated processing of HIV-1 gp160, influenza A hemagglutinin (HA), and hCMV gB (unpublished data). Further, the ER-retained Spn4A (Spn4A-R) also inhibited maturation of hCMV gB, implying that furin may be actively processing enzymes in the ERGIC pathway and can be inhibited.

3.1.4 Project rationale, hypothesis, and experimental approach

The involvement of furin in a myriad of pathologies underlies the intense development of furin inhibitors. However, many issues have to be resolved before they are used in a clinical setting. Most fundamentally, the cellular effects of furin inhibition need to be comprehensively studied, including those that ameliorate the disorders as well as unwanted side effects.

As a first step, we profiled the transcriptome of neuroglioma cells expressing the most potent furin inhibitor, Spn4A. In the United States, approximately 25 000 people are diagnosed with malignant brain tumors annually, two thirds of which are high grade gliomas (HGG) (209). There are currently no effective therapies to treat HGG and it is associated with poor prognosis. Five year survival rates are as low as 10% (210). Hallmarks of the disease are local invasion, angiogenesis, and a lack of metastasis (211). While furin expression levels have not been investigated in primary brain tumors, it is upregulated in many glioblastoma cell lines (160). Further, α_1-PDX expression in astrocytoma (164) and glioma cells (160) inhibit furin-mediated substrate processing and reduce cancer cell proliferation and invasion. Since furin may be considered a target for glioblastoma therapy, a complete and unbiased study of the cellular response to PC inhibition on glioma cells is essential.

The compartments in which furin is active have come under scrutiny (section 3.1.1.2). Since Spn4A is naturally ER-retained, and the deletion of the ER retention motif results in a secreted variant, we were able to assess how compartmentalization of the inhibitor affects furin activity.

Lastly, the possibility of using Spn4A as a therapeutic agent will ultimately need to be assessed *in vivo*. As fusion fluorescent proteins can facilitate animal studies, we examined if

Spn4A tagged with RFP (91), a monomeric red fluorescent protein, can inhibit furin and regulate the same pathways in neuroglioma cells.

In summary, we addressed the questions: How does Spn4A affect the transcriptome of neuroglioma cells? Is the cellular response to Spn4A specific on its compartmentalization? Can fluorescently-tagged Spn4A inhibit furin and regulate the same pathways? Our approach was to express Spn4A-S, RFP Spn4A-S, and RFP Spn4A-R in H4 human neuroglioma cells and profile the transcriptome via microarray.

We hypothesized that we could identify the downstream effects of the loss of functional PCs such as furin and their substrates. Specifically, the loss of growth factor processing may lead to changes in genes related to cell proliferation, invasion, and angiogenesis. Additionally, the microarray data would reveal if expression of Spn4A had stress or apoptotic effects on mammalian cells. Since active furin is usually localized to the TGN and cell surface, we predicted that ER localized Spn4A would still inhibit furin, but to a lesser extent than secreted Spn4A. Last, we hoped the addition of a RFP tag would not affect inhibitory activity.

3.2 Methods

Methods were performed as described in Chapter 2: Transfection and infection conditions (2.2.5), SDS-PAGE, native PAGE, and western blot (2.2.6), Furin complex formation assay (2.2.8), RNA extraction and cDNA synthesis (2.2.11), Microarray and data analysis (2.2.12), and Real-time PCR (2.2.13).

The microarray was performed using Ad. Emp, Ad. RFP WT-S and Ad. RFP WT-R as described in Chapter 2. In addition, H4 neuroglioma cells were infected with adenovirus expressing Spn4A-S (Ad. WT-S, no RFP tag) and RNA extracted for microarray experiments. Ad. WT-S was generated previously by the Jean lab.

Microarray data analysis was performed using DAVID v6.7 (93) and Ingenuity Pathway Analysis (IPA v8.5, Ingenuity® Systems, www.ingenuity.com). DAVID analysis was performed as described (2.2.12). Further, differentially regulated genes (threshold cut-off of 1.7 fold, $p<0.05$) were uploaded into IPA for functional analysis, network generation, and canonical pathway analysis. The functional analysis identified the molecular and cellular functions that were most significant to the data set. Right-tailed Fisher's exact test was used to calculate a p-value determining the probability that each biological function and/or disease assigned to that data set is due to chance alone. For network generation, genes were overlaid onto a global molecular network developed from information contained in Ingenuity's Knowledge Base. Networks were then algorithmically generated based on their connectivity and biological functions and/or diseases that were most significant to the genes in the network identified. Right-tailed Fisher's exact test was used to calculate a p-value determining the probability that the identified biological function assigned to the network is due to chance. Last, canonical pathway analysis identified pathways from the IPA library of canonical pathways that were most significant to the uploaded data set. Fisher's exact test was used to calculate a p-value.

3.3 Results and discussion

3.3.1 RFP Spn4A inhibitory activities

In order to use RFP-tagged Spn4A in future transgenic animal studies, we addressed if RFP-tagged Spn4A could still inhibit furin. Normally, for inhibition to occur, a heat- and SDS-stable complex needs to form between the serpin and protease. We performed complex formation assays using HEK293-C4 cells, a human embryonic kidney cell line overexpressing FLAG-tagged furin (92) and confirmed that the enzyme-inhibitor complex still formed (Fig. 3.4).

3.3.2 Experimental procedures and microarray strategy

To study the response of neuroglioma cells to Spn4A, we used an adenovirus delivery system to overexpress Spn4A in human H4 neuroglioma cells. Development of the expression system is described in section 2.3.5. Briefly, infections performed at MOI 50 resulted in infections of nearly 100% of the cells, as detected through flow cytometry and confocal microscopy. Viral infections were not toxic. Since furin is localized to the Golgi and endosomal compartments, we used Ad. WT-S for inhibition of PCs in the secretory pathway. Further, RFP-tagged Spn4A would be useful for live cell imaging or transgenic animal studies. Therefore, we also studied the gene expression profile of Ad. RFP WT-S. Last, we addressed the compartmental specificity of Spn4A function by comparing the profile of secreted RFP WT-S to ER-retained RFP WT-R. Experimentally, H4 cells were infected with Ad. Emp, Ad. WT-S, Ad. RFP WT-S, and Ad. RFP WT-R. After 48 hours, RNA was extracted and used on the Illumina HumanHT-12 v3 Expression BeadChip, which targets more than 25 000 annotated genes using 48 000 probes. Expression data from Ad. WT-S, Ad. RFP WT-S, or Ad. RFP WT-R were compared to Ad. Emp for fold change and p-value calculation.

Genes with altered expression levels due to the presence of inhibitory Spn4A were compiled. Only fold changes with a threshold cut-off of 1.7 fold ($p<0.05$) were considered significant and used for analysis. Further, off-target effects were excluded by a comparison of non-inhibitory Spn4A mutants (Chapter 2). Using these criteria, 643 genes in Ad. WT-S, 383 genes in Ad. RFP WT-S, and 214 genes in Ad. RFP WT-R infected cells reached significance. To identify over-represented biological themes and affected pathways and networks from the gene list, we used DAVID Functional Annotation Clustering analysis and IPA. Annotations or

pathways were considered significant if their enrichment scores (ES) or the negative log of the p-values were greater than two.

3.3.3 Ontological, pathway, and network analysis of genes regulated by Spn4A in the secretory pathway

In response to the expression of Spn4A-S, 643 genes were differentially regulated using the described criteria. Gene ontology and enrichment analysis was performed by separately submitting the 468 downregulated and 175 upregulated genes to the DAVID Functional Annotation Clustering software. Genes were classified into gene ontology groups, enrichment for each annotation term calculated, and annotation terms further grouped according to highly similar annotation terms. Gene ontology and enrichment analysis revealed 20 significant annotation clusters (Table 3.1, genes in Supplemental Table A5.2), with the highest cluster annotating cell division, cell cycle process, and nuclear division (ES = 23.6). Of the top ten clusters, eight were directly related to cell cycle progression including annotations for kinetochore and centromere structural proteins (ES = 13.3), different groups of DNA binding proteins (ES = 7.3, 4.7, 4.3, 3.6), motor proteins for mitosis (ES = 3.7), and cyclins (ES = 3.4). Other categories with significant changes included sprouty development genes (ES = 4.0), regulation of phosphorylation (ES = 3.3), response to nutrient (ES = 2.2), and coagulation (ES = 2.1). Through a gene ontology search of the upregulated genes, five significant gene ontology clusters were identified (Table 3.2, genes in Supplemental Table A5.2). All clusters annotated to extracellular matrix components (ES = 6.7) such as collagen (ES = 2.7), glycosaminoglycans (ES = 2.3), cysteine-rich secretory proteins (ES = 2.3), and leucine-rich proteoglycans (ES = 2.1). Molecular and cellular function analysis from IPA largely agreed with the biological themes identified by DAVID. Top functions included those described above as well as cell death, cellular movement, cellular compromise, cell morphology, and amino acid metabolism (Fig. 3.5, genes in Supplemental Tables A5.3 and A5.4).

To identify well-characterized cell signaling pathways that were the most relevant to these 643 genes, Canonical Pathway Analysis from IPA was used. Notably, seven of the eight statistically enriched pathways identified affected cell cycle progression and cancer signaling (Fig. 3.6, genes listed in Supplemental table A5.5). Five pathways affecting cell cycle included two cell cycle checkpoint regulation pathways, two DNA damage response pathways, and one mitosis transition pathway. Additionally, several genes associated with breast and pancreatic

cancer signaling pathways were identified. Last, aryl hydrocarbon receptor (AhR) signaling, which is a response to xenobiotics (212), was also identified as an affected pathway.

To further explore the relationships between the regulated genes, we used IPA network analysis to visualize the interactions between molecules. The list of significant networks and the functions associated with molecules of the network are summarized in Table 3.3. The top two networks were similarly annotated with cell cycle, cellular assembly and organization, DNA replication, recombination, and repair, and gene expression (Table 3.3, Fig. 3.7). The most powerful network contained 33 focus genes out of a maximum of 35. The network converged on *MYC* (v-myc myelocytomatosis viral oncogene homolog), an oncogene coding for a transcription factor that regulates cell cycle progression, apoptosis, and cellular transformation (213) (Fig. 3.7A). Further, several downregulated genes were connected to MIR124 (Fig 3.7A). The overexpression of the microRNA MIR124 depresses the expression of those target genes (214) in Fig. 3.7A, and promotes differentiation and inhibits proliferation in glioma cells (215). Similarly, most genes were downregulated in the second most powerful network, which converged on *E2F2* (E2F transcription factor 2), a regulator of S-phase entry in cell cycle (216) (Fig. 3.7B). The downregulation of *MYC* and *E2F2*, and expression of MIR124 could play a crucial role in the control of cell proliferation.

The global profiling of the transcriptome revealed several biological themes that were affected in response to Spn4A WT-S. To investigate how PC inhibition may affect tumor malignancy, we focused on the regulation of specific genes implicated in cell proliferation, cell movement, and angiogenesis.

3.3.4 Regulation of specific genes implicated in cell proliferation

Previous studies have demonstrated an inhibition of cell proliferation in the presence of furin inhibitors (160;164). Our global analysis now provides the genetic basis for inhibition. Approximately 160 genes annotating to cellular proliferation were differentially regulated (Supplemental Table A5.3). As visualized in the network analysis, MYC, MIR124, and E2F2 are likely some key regulators of cell growth and proliferation. Further, we summarized genes whose products directly affected cell proliferation in Fig. 3.8 (FCs in Supplemental Table A4.1). First, we scanned the list of genes annotated with cell cycle from DAVID (Supplemental Table A5.2) and IPA (Supplemental Table A5.3) for kinases, cyclins, and their regulators that control the phases of the cell cycle. Notably, many were downregulated, with the exception of *CDKN1C*

(cyclin-dependent kinase inhibitor 1C), which codes for an inhibitor of CDK2 (cyclin-dependent kinase 2)/cyclinE complexes, and *CDKN2C*, an inhibitor of G1 kinases CDK4 and CDK6 (217). CDC25A (cell division cycle 25) is an enzyme that removes phosphates from CDK2/cyclinE, which activates the complex and allows for G1 to S transition (218). We observed downregulation of *CDC25A*, *CDK2*, *CCNE2* (cyclin E2), *CDC2*, *CCND1*, and *CCNB1*, important for G1/S and G2/M (Gap2/Mitosis) transitions (Fig. 3.8).

Next, we mapped genes important for proliferation and growth, such as those coding for DNA replication and mitosis proteins onto Fig. 3.8 (FCs in Supplemental Table A4.1). ORCs (origin of replication complex) and MCMs (mini chromosome maintenance) for formation of the pre-initiation replication complex (219), as well as DNA polymerase components were all downregulated, suggesting the inhibition of chromosome duplication. We also identified the differential regulation of several genes coding for components or regulators of mitotic progression and chromosome segregation. SMCs (structural maintenance of chromosome) for chromosome condensation and sister chromatid cohesion (220), centromere proteins that function in sister chromatid adhesion and kinetochore formation, and several kinases (NEK2 [never in mitosis gene A-related kinase 2], AURKA [aurora kinase A], AURKB) regulating mitotic processes (221;222) were downregulated (Fig. 3.8, Supplemental Table A4.1).

These genes represented the most proximal causes for cell proliferation inhibition observed in glioma cells expressing PC inhibitors (160;164). Notably, many of these gene, such as CDKs, CDC25, and the aurora kinases, are overexpressed in cancer cells and are targets for therapy (218;222;223).

3.3.5 Regulation of specific genes implicated in cell movement

Tumor cells invade surrounding tissues by a dynamic process of detachment and adhesion to the ECM and degradation of the ECM (224). The loss of invasive ability was reported in glioma cells expressing PC inhibitors (160;164). The invasiveness of H4 neuroglioma cells has not been tested and the expression levels of adhesion proteins and ECM proteases are unknown. Nonetheless, cell movement was a significant theme identified in IPA function analysis (Fig. 3.5). To assess motility and ECM remodeling, we analyzed the top ten most downregulated and upregulated genes annotated with cell movement (Table 3.4, full list in Supplemental Table A5.4). Among the downregulated were the chemokine IL8 (Interleukin-8), adhesion proteins ITGA2 (integrin alpha 2), AJAP1 (adherens junctions associated protein 1),

and ITGA6, transcription factor ETV5 (ets variant 5), growth factors TGFα and GDF15, the ECM protein SPP1 (secreted phosphoprotein 1, also known as osteopotin), and signaling molecules ERRFI1 (ERBB receptor feedback inhibitor 1) and RGS1 (regulator of G-protein signaling 1). Among the upregulated were regulators of the cytoskeleton C5ORF13 (chromosome 5 open reading frame 13, also known as P311) and S100A4 (S100 calcium binding protein A4), signaling molecule SOCS2 (suppressor of cytokine signaling 2) and GUCY1A3 (guanylate cyclase 1, soluble, alpha 3), phosphatases ALPP (alkaline phosphatase, placental [regan isozyme]) and PPAP2A (phosphatidic acid phosphatase type 2A), adhesion molecules CD24 (CD24 molecule), CD36 (CD36 molecule, thrombospondin receptor), and OLR1 (oxidized low density lipoprotein [lectin-like] receptor 1), and the ECM protein DCN (decorin). We focused on cell adhesion molecules, ECM proteins, and regulators of the cytoskeleton, which have immediate implications in tumor cell invasion.

Integrins, osteopotin, and AJAP1 (downregulated) can mediate adhesion (Table 3.4). First, integrins, which are transmembrane heterodimers composed of α and β chains, bind ECM ligands to induce cytoskeletal reorganization and cell motility signaling cascades (224). While several integrins are overexpressed in tumor cells to assist invasion (224), IGTA2 and IGTA6 have not yet been reported as such. Second, osteopotin is an ECM ligand for integrins and CD44 (downregulated by 1.8 fold, Supplemental Table A5.4) and is highly expressed in several malignancies to induce inhibition of apoptosis and activation of various ECM proteases (225). Last, the transmembrane adhesion protein, AJAP1, can also modulate tumor cell migration and invasion, although contradictory roles are reported (226;227). Invasiveness is attenuated in glioma cells (227) but enhanced in epithelial and mesenchymal cells (226) that overexpress AJAP1.

Six upregulated genes can affect the regulation of growth factors, adhesion, angiogenesis, and cytoskeletal organization. The most upregulated gene was decorin, an ECM component that may enhance cellular structural stability (228) as well as inhibit TGFβ activity and EGFR (epidermal growth factor receptor) activation (229;230). Its overexpression inhibits malignancy *in vivo* (229;230). Next, two adhesion molecules *OLR1* and *CD24* were upregulated (231;232). While OLR1 has thus far not been directly implicated in cancer, CD24 was shown to promote invasion in glioma cells *in vivo* when overexpressed (232). CD36 is a receptor that negatively regulates angiogenesis in human endothelial cells (233). Its function in human neurons is unclear, but it plays a role in detecting pheromones in insects and responding to fatty acids in

rodents when expressed in sensory neurons (233). Last, two regulators of the cytoskeleton, P311 and S100A4, are highly implicated in glioma cell invasion. P311 is overexpressed in invading glioma cells and its interaction with Filamin A is hypothesized to promote cytoskeletal re-organization (234). S100A4, also overexpressed in glioma cells (235), bind to myosin IIA at the leading edge to promote protrusions (236). Further, S100A4 also promotes expression of MMPs (237;238) for degradation of the ECM.

Notably, we did not observe genes coding for ECM proteases and protease inhibitors within the top ten most down or upregulated genes (Table 3.4). Scanning for these genes in the full list (Supplemental Table A5.4) revealed that only MMP3 was differentially regulated (downregulated by -2.2 fold). MMP3 (also called stromelysin-1) can degrade many ECM substrates, including collagens, laminins, fibronectin, and proteoglycans as well as release cell surface molecules, such as heparin-binding EGF-like growth factor, and activate other MMPs (239). Its overexpression in mammary epithelial cells promotes tumorigenesis (239). Further, MMP3 has a furin consensus site and was demonstrated to be an *in vitro* substrate (240); thus post-translational MMP3 activity may also be modulated through inhibition of furin. Plasmin is another extracellular protease that is activated by tissue plasminogen activator (tPA) or urokinase plasminogen activator (uPA). Plasmin, the activated form, can degrade ECM components as well as activate MMPs (241). PLAT (tissue type plasminogen activator) and PLAUR (urokinase plasminogen activator receptor), whose gene product activates tPA and localizes uPA, were downregulated by -1.8 and -2.1 fold, respectively (Supplemental Table A5.4).

We have reported the differential regulation of several genes that may affect invasive ability. As current data suggest that PC inhibitors block invasiveness in neuroglioma cells, the downregulation of integrins, osteopotin, MMP3, PLAT, and PLAUR as well as the upregulation of DCN may be additional mechanisms important in the loss of invasive ability in furin-inhibited cancer cells. Conflictingly, the downregulation of AJAP1 and upregulation of CD24, P311, and S100A4 could promote invasion. Functional assays (discussed later) will need to be performed to study the invasive ability of neuroglioma cells expressing Spn4A. The phenotype can then be related to these gene products to determine which more readily influences invasive ability.

3.3.6 Regulation of specific genes implicated in angiogenesis

Although no confirmatory data has been reported, our microarray profiling suggested that PC inhibitors may also indirectly affect tumor-induced angiogenesis. The ability to form new

blood vessels requires growth signaling. We found that two key angiogenic factors, VEGFA and IL8 (209), were downregulated by -2.5 and -5.3 fold, respectively. Other angiogenic factors PDGF and FGF (209) were not differentially regulated. Notably, furin, and other PCs, cleave and activate PDGF (177). It is possible that PC inhibitors can directly inhibit processing of PDGF and indirectly affect expression levels of VEGFA and IL8 to block angiogenic signaling to endothelial cells.

3.3.7 Regulation of specific genes implicated in stress and apoptotic responses

To evaluate if Spn4A expression would be pathogenic, we looked for induction of cellular stress and apoptosis. Unfortunately, overexpression of Spn4A, regardless of function, upregulated ER stress responses (Chapter 2). IPA and DAVID GO analysis did not identify enrichment for genes in response to stress specifically induced by inhibitory Spn4A WT.

Cell death was a significant cellular function identified by IPA (Fig 3.2). However, most genes that were annotated with cell death overlapped with those of cell cycle and proliferation. Therefore, we specifically looked for the differential regulation of genes from three major players of apoptosis: the caspases, TNF (tumor necrosis factor) superfamily, and BCL2 (B cell lymphoma) superfamily. All apoptotic signaling pathways converge on caspases, a family of cysteine proteases, which were not differentially regulated transcriptionally. However, they are made as zymogens and activated by cleavage or dimerization (242). Therefore, apoptosis mediated by caspases may not be apparent in microarray analysis. We further investigated apoptotic genes mediated through transmembrane death receptors of the TNF receptor superfamily. Only one gene, *TNFRSF10B*, was affected (downregulated by -1.77 fold). Last, we asked if members of the BCL2 families were differentially regulated. The BCL2 superfamily of proteins has both pro-apoptotic and anti-apoptotic members. We observed differential gene regulation of *BCL6* (downregulated by -1.75 fold), *BCL11A* (upregulated by 1.97 fold), and *BMF* (BCL2 modifying factor, upregulated by 2.76 fold). The role of BCL11A in apoptosis is unclear, but it regulates axonal branching in glial cells (243). Notably, BCL6 is anti-apoptotic (244) and BMF is pro-apoptotic (245). Normally, BMF is sequestered by association with myosin, and apoptosis can only be activated if BMF is released and binds BCL2 (245). Whether or not it is activated in the presence of Spn4A will have to be examined. We have grown infected cells expressing Spn4A for up to five days and have not detected cell death (data not shown). Further,

cells transiently transfected with Spn4A did not exhibit activated caspase 3 after 48 hours (data not shown).

3.3.8 Ontological, pathway, and network analysis of genes regulated by RFP-tagged Spn4A in the secretory pathway

To investigate if an RFP tag may affect the function of Spn4A, we analyzed the global transcriptional changes for secreted RFP-tagged Spn4A-S. Notably, fewer genes were regulated compared to Spn4A without RFP. From a total of 383 differentially regulated genes, 236 were downregulated and 147 upregulated. Gene ontology and enrichment analysis of the downregulated genes revealed nine significant clusters including sprouty assisted development (ES = 5.1), cell cycle progression (several clusters), regulation of phosphorylation (two clusters), blood vessel development (ES = 2.9), and coagulation (ES = 2.4) as listed in Appendix 4, Supplementary Table A4.2. Compared to non-RFP-tagged Spn4A, these clusters had lower enrichment scores but shared the same annotations. Gene ontology of the upregulated genes annotated to extracellular matrix components (Supplemental Table A4.3). In addition, molecular and cellular functional analysis for genes regulated in the presence of RFP Spn4A was performed using IPA. Gene functions largely agreed with the DAVID analysis, and were very similar to the functional annotations for Spn4A (Supplemental Fig. A4.1).

Pathway analysis performed using Ingenuity revealed ten significant canonical pathways (Supplemental Fig. A4.2). Cell cycle progression pathways as well as metabolism of xenobiotics, coagulation, hepatic fibrosis/hepatic stellate cell activation, and arginine and proline metabolism were recognized. Several networks were found to be significant (Supplemental Table A4.4). Most genes of the top two networks mapped to cancer, cardiovascular system development and function, embryonic development, dermatological disease and conditions, and cell cycle functions. We noted that *MYC*, identified as a key regulator in response to Spn4A-S, was not differentially regulated in cells expressing RFP Spn4A-S. Further, not as many genes associated with DNA replication and mitosis components were differentially regulated (Supplemental Table A4.1).

To evaluate the gene ontology similarities and differences in response to RFP-tagged or non-tagged Spn4A, each unique or overlapped gene list was separately analyzed by DAVID and summarized in Figure 3.9. Full cluster annotations are reported in Supplemental Tables A4.5 to A4.9. In general, cell cycle and extracellular matrix annotations were found in the genes unique

to WT-S and in the overlapping region, which suggested that while WT-S and RFP WT-S regulated many similar pathways, WT-S induced transcriptional changes in many more genes of that pathway. No gene annotations reached significance from the unique and downregulated RFP WT-S gene list. One cluster reached significance using the list unique for RFP WT-S upregulated genes, and involved chloride ion binding (ES = 2.1). However, only three molecules were associated with the annotation, which may call its significance into question.

The decrease in differentially regulated genes may be due to the reduced ability of RFP-tagged Spn4A-S to inhibit furin. Although we were able to detect a complex between RFP Spn4A and furin (Fig. 3.1), it is probable that the tag slowed down the kinetics of binding, which may have allowed some furin to escape the complex. Alternatively, the tag may have destabilized the final complex and allowed faster hydrolysis and release of the protease.

3.3.9 Ontological, pathway, and network analysis of genes regulated by RFP-tagged Spn4A retained in the ER

Last, we asked whether or not the effects of Spn4A function are compartment-specific by profiling the transcriptome of ER-localized RFP Spn4A-R and comparing the profile to that of RFP WT-S and WT-S. We found that pathways and functions altered by expression of RFP WT-R were very similar, but with a lower number of gene expression changes. Of 214 differentially regulated genes, 158 were downregulated and 56 upregulated. DAVID gene ontology analysis of down and upregulated genes (Supplemental Tables A4.10 and A4.11), IPA molecular and cellular functional analysis (Supplemental Fig. A4.3), and IPA network analysis (Supplemental A4.12) pointed to cellular proliferation as the most significantly altered gene function and network.

In comparison to RFP WT-S, 83 genes were uniquely regulated by RFP WT-R (58 downregulated, 25 upregulated) and 131 were shared (100 downregulated, 31 upregulated) (Fig. 3.10, full annotation in Supplemental Table A4.13 to A4.16). All enriched clusters of downregulated genes for either unique or overlapped groups showed that DNA replication and cell cycle were affected. Analysis of the unique and upregulated genes demonstrated a difference between secreted and retained Spn4A. The response to RFP WT-R expression did not involve upregulation of genes coding for extracellular matrix proteins, which was an annotation enriched in RFP WT-S (ES = 3.2).

With the exception of ECM related genes, ER-retained Spn4A-R affected similar genes compared to secreted Spn4A-S, suggesting that their cellular mechanism of action may be the same. Furin activity is believed to be inhibited in the ER and early Golgi compartments due to its association with its pro-peptide, which is cleaved and released in the Golgi due to the acidic environment (101). We suggest that in the slightly acidic environments of the ERGIC and cis-Golgi compartments, activated furin may encounter ER-retained Spn4A-R. Spn4A-R may move by anterograde transport to the ERGIC and cis-Golgi compartments, where some could inhibit furin, while others move by retrograde transport back to the ER. Precedence of ER-retained proteins that cycle in the ERGIC and cis-Golgi compartments is demonstrated by the KDEL (Lys-Asp-Glu-Leu) receptor, which transport ligands with KDEL motifs back to the ER. Optimal binding of receptor to ligand is at pH 5.5 *in vitro*, suggesting that binding of ligands occur in the ERGIC and cis-Golgi compartments (246). Spn4A-R may inhibit the same PCs as secretory pathway Spn4A-S, but its usual ER localization would hamper the extent of inhibition. Thus, fewer cell cycle genes and ECM related genes would be regulated in response to Spn4A-R expression.

To visualize the differences between the regulation of genes in the presence of WT-S, RFP WT-S, or RFP WT-R, we compared the absolute number of genes differentially regulated in cell growth and proliferation as well as cell movement (Fig. 3.11). These two functions were among the most significant in all three analyses and represented two themes especially important in tumorigenesis and metastasis. Cells differentially regulated the most number of genes in response to WT-S and the fewest number to RFP WT-R. The RFP tag and compartmentalization affected Spn4A function, although neither could totally abolish its function.

3.3.10 Real-time PCR validation

We measured the mRNA levels of three cell cycle genes, *CDK2*, *CDC2*, and *PCNA*, and the chemokine *IL8*, using qPCR (real-time PCR) for cells infected with Ad. RFP WT-R compared to those infected with Ad. Emp (Fig. 3.12). We validated *PCNA*, *CDK2*, and *IL8* downregulation. These genes were not significantly and differentially regulated in cells expressing non-inhibitory Spn4A mutants (Chapter 2), RFP S52R-R and RFP H338R-R (data not shown).

3.4 Conclusions and future directions

We and others have hypothesized that PCs represent a novel class of therapeutic targets for bacterial and viral diseases as well as cancer (40;112;196;247;248). Here, we evaluate the applicability of Spn4A as a PC inhibitor in neuroglioma cells. We used gene expression analysis to evaluate potential effects on tumor progression and invasion as well as to uncover stress or apoptotic pathways.

Previously, two studies featuring furin inhibition in glioma cells demonstrated decreased tumor proliferation and invasive ability due to the loss of matured IGF-1R, TGFβ, MT1-MMP, and MMP-2 (160;164). Results presented here corroborate those findings and uncover additional genes that could explain the loss of the malignancy phenotype. First, we suggest that the loss of cell proliferative ability is likely due to upregulation of G1 kinase/cyclin inhibitors and downregulation of kinases, cyclins, DNA replication machinery, and mitosis components. Second, we report changes in the regulation of genes implicated in cell adhesion and migration and ECM degradation, which may contribute to the loss of malignancy. However, we have also uncovered genes that promote invasion, which are regulated by Spn4A expression. Third, our results demonstrated a new potential antiangiogenic role for PC inhibitors in their ability to downregulate *VEGFA* and *IL8*. Further, our microarray data did not reveal specific induction of cellular stress and apoptosis by Spn4A. Last, the results demonstrate that an RFP tag as well as ER compartmentalization will affect the role of Spn4A in mediating the above effects. Kinetic studies will have to be performed to evaluate if the RFP tag slows the serpin inhibitory mechanism.

We have demonstrated the ability of Spn4A to change the transcriptome of neuroglioma cells. We will first validate more genes by qPCR to measure the robustness of the data. Of interest are the cell proliferation, cell movement, and angiogenesis genes discussed. Next, we will validate the results with functional assays targeting changes in cell cycle and invasive ability. We predict that Spn4A would induce cell cycle arrest, which we will test through CFSE (carboxyfluorescein succinimidyl ester) staining. CFSE is a dye that enters the cytoplasm of cells and is passed to daughter cells following division. Therefore, cell proliferation can be visualized using flow cytometry analysis. Next, the ability of Spn4A to affect cell adhesion and ECM remodeling will be assessed. As the invasiveness of H4 neuroglioma cells has not been tested, we will use an already established invasive glioma cell line such as U87MG in parallel. Invasive

ability may be tested by monitoring a scratch wound on a cell monolayer or in a Matrigel invasion assay, in which cells are plated in an invasion chamber coated with Matrigel and allowed to invade. Last, we will use antibodies and western blotting to evaluate if the angiogenic factors *VEGFA* and *IL8* are downregulated on the protein level. As a negative control, we have constructed non-inhibitory Spn4A hinge-mutants (Appendix 1), which are fully processed by furin.

Further, a better understanding of how Spn4A exerts its biological influence is needed. Primarily, its physiological targets need to be clarified. Spn4A is highly specific for furin, but has not been tested against other PCs. To detect Spn4A targets, we will immunoprecipitate Spn4A and use antibodies specific for the PCs to identify the co-immunoprecipitated complexes on western blots. Alternatively, we may target furin with siRNA and test if the same mRNAs are differentially regulated. If Spn4A does primarily inhibit furin, we hypothesize that inhibition of furin-mediated processing of TGFβ, IGFR, and PDGF may lead to the changes observed. Western blots to test for processing of furin targets and the ability of recombinant processed substrates to restore malignancy will be necessary to show the mechanism underlying Spn4A cellular effects.

Although the inhibition of PCs by Spn4A is the most likely cause for the transcriptome changes, we cannot rule out other functional domains of serpins, beyond its inhibitory domain, that may contribute to the described effects. For example, non-inhibitory serpins, such as ovine uterine serpin and maspin, have blocked cell cycle progression through unknown mechanisms when exogenously supplied or expressed (22;249;250). Further, the serpins' cleaved C-terminal tails, which are released upon serpin-protease complex formation, may have activity. Exogenously synthesized peptides corresponding to the 26 residue C-terminus of α_1-antitrypsin has been shown to increase the proliferation of hepatoma and breast cancer cells, but not kidney or skin cells (251). Other functional domains of Spn4A, beyond its inhibitory activity, have not been reported. Non-inhibitory Spn4A (Appendix 1) and synthesized peptides corresponding to the C-terminal tail of Spn4A are important controls to understand the contribution of additional domains to transcriptome changes.

In summary, we have expressed a furin inhibitor, Spn4A, in a neuroglioma cell line and conducted a transcriptome analysis. We found several patterns of gene expression suggesting changes in cell proliferation and cell mobility, which collectively support previous studies

demonstrating loss of tumor growth and invasive ability (160;164). Further, we provide new mechanistic hypotheses as to how treatment with furin inhibitors may lead to the loss of invasive ability and angiogenesis.

Figure 3.1. Structural features of PCs. The structural features of human furin and six other PCs, yeast Kex2p, and bacterial subtilisin E are shown. PC5/6 is expressed as two isoforms, which are generated by alternative splicing. The diagonally dashed line links two halves of the PC5/6B isoform. The bold labels D, H, S highlight the active site residues while N and D highlight the oxyanion hole residues. Reprinted by permission from Macmillan Publishers Ltd: Nature Reviews Molecular Cell Biology, Thomas G, Furin at the cutting edge: From protein traffic to embryogenesis and disease (101), © 2002.

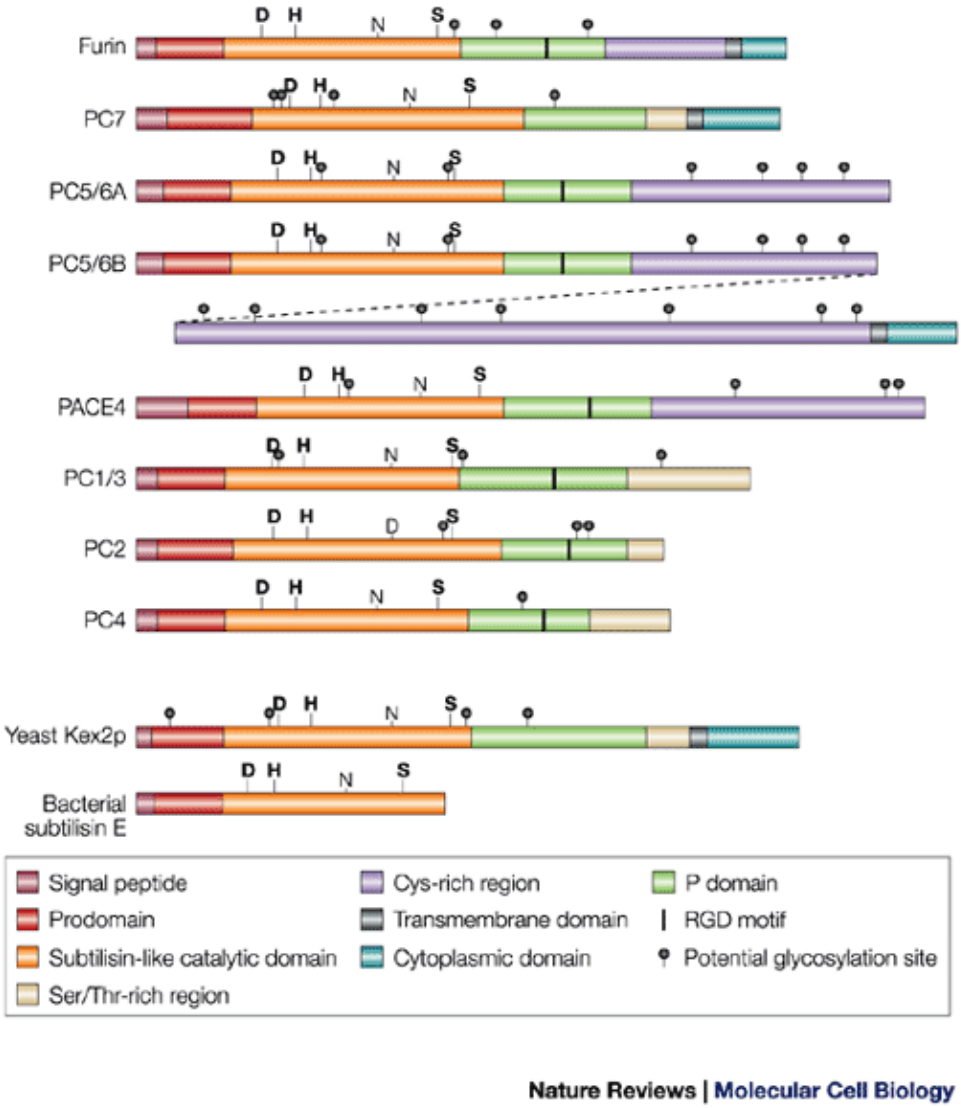

Figure 3.2. Activation of furin is spatially regulated. In the ER, the furin prodomain acts as an intramolecular chaperone (IMC) to facilitate folding of the inactive catalytic domain (pink) into the active conformation (red oval). Furin undergoes autoproteolytic intramolecular excision of the propeptide at Arg107 (blue). However, the propeptide still remains associated with the mature domain as a potent inhibitor during transport to the Golgi. The acidic pH of the trans-Golgi network promotes the autoproteolytic intramolecular cleavage of the propeptide at Arg75 (blue) and subsequent disassociation of the fragments from furin. Adapted with permission from Anderson E, Molloy SS, Jean F, Fei H, Shimamura S, and Thomas G (117), © 2002 American Society for Biochemistry and Molecular Biology. Reprinted by permission from Macmillan Publishers Ltd: Nature Reviews Molecular Cell Biology, Thomas G, Furin at the cutting edge: From protein traffic to embryogenesis and disease (101), © 2002.

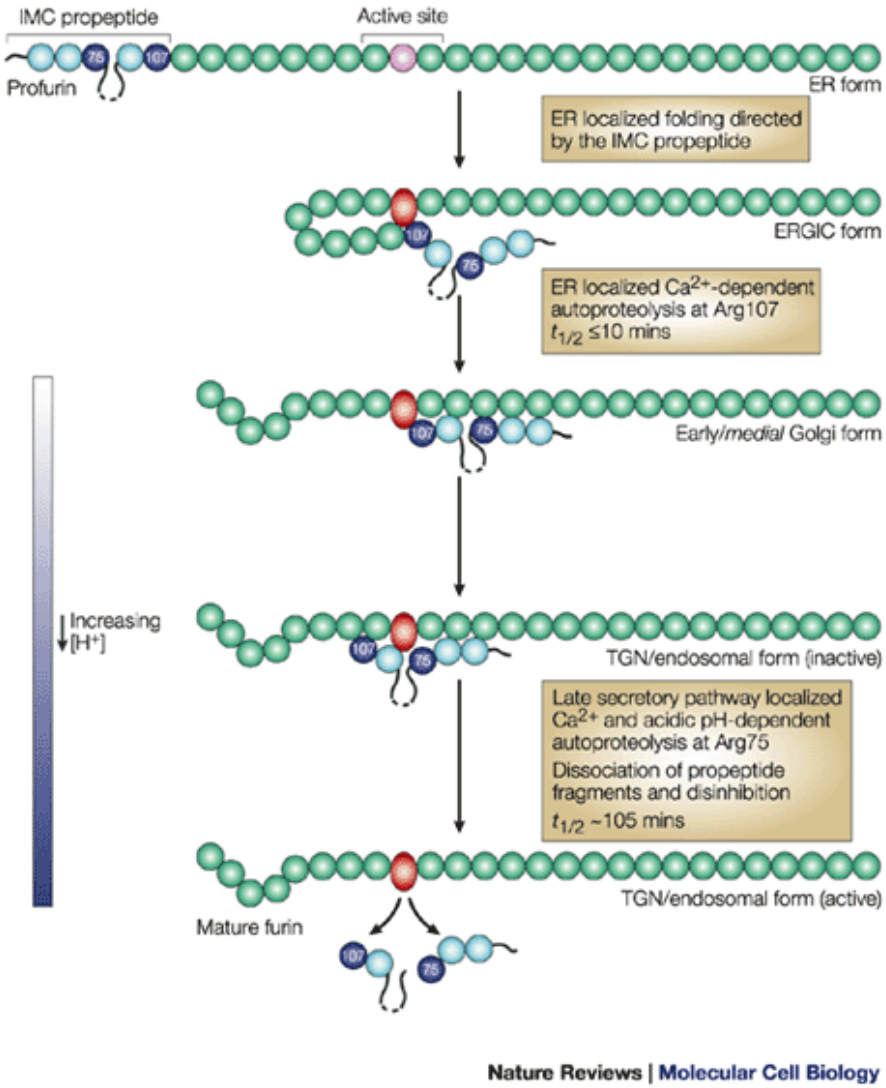

Figure 3.3. Cellular localization of the PCs. PCs can be found in the Golgi, the trans-Golgi network (TGN), secretory granules (SG), endosomes (END), at the plasma membrane (PM) as integral membrane proteins, in the extracellular matrix (ECM) and at the cell surface (CS), and/or in the extracellular space (ECS). Reprinted by permission from Informa UK Ltd: Expert Opinion, Chretien M, Seidah NG, Basak A and Mbikay M, Proprotein convertases as therapeutic targets (40), © 2008.

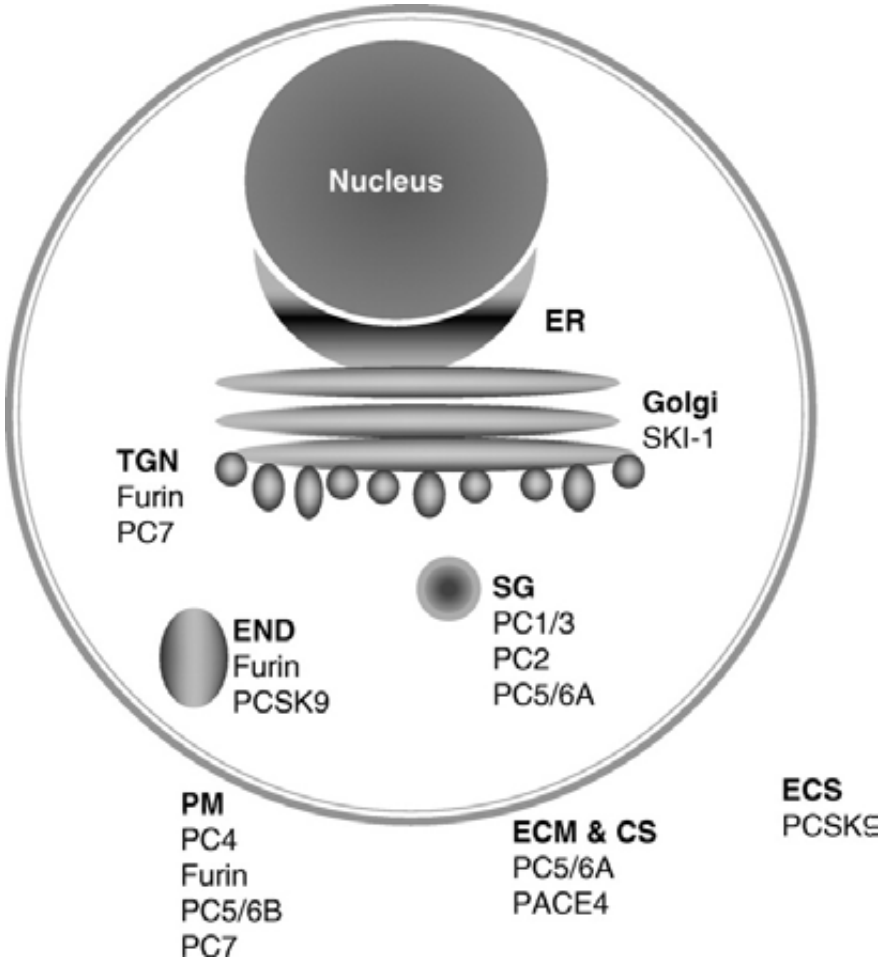

Figure 3.4. Spn4A and furin EI complex formation assay. HEK293-C4 cells overexpressing FLAG-tagged furin were transfected as labeled for 48 hours. Cells (C) were lysed and media (M) was collected, boiled for 10 minutes in SDS loading buffer, and proteins separated on a SDS-PAGE. Western blot analysis was performed using anti-FLAG antibodies for Spn4A and furin (green) and anti-Hsp47 (red) as a loading control.

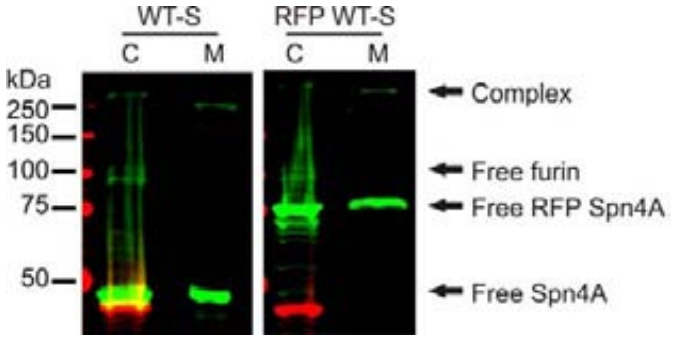

Figure 3.5. Top 10 most significant cellular and molecular functions for genes differentially regulated by Spn4A WT-S expression identified by Ingenuity Pathway Analysis. Ingenuity Pathway Analysis software was used to associate cellular and molecular functions to differentially regulated genes in response to Spn4A WT-S. Significance was calculated from Fisher's exact test. Genes associated with cellular growth and proliferation and cellular movement are in Appendix 5, Supplemental Tables A5.3 and A5.4.

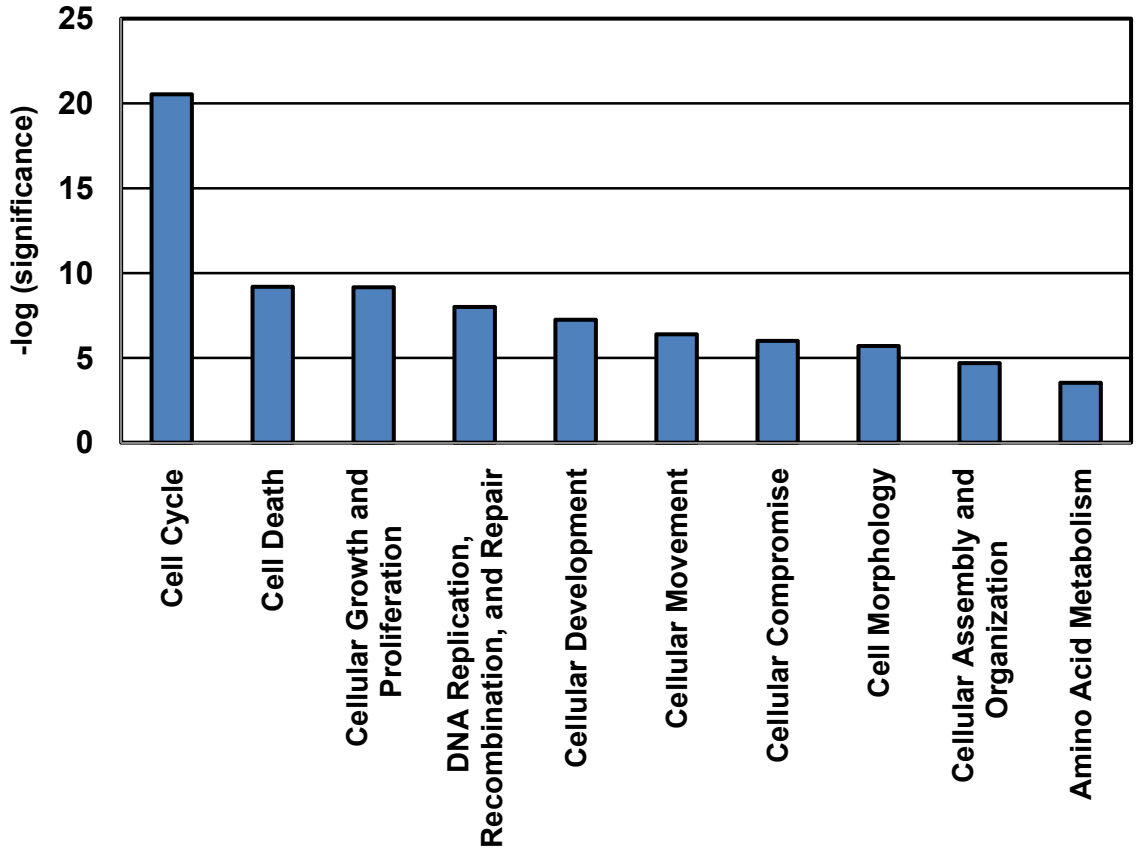

Figure 3.6. The most significant canonical pathways deduced from genes differentially regulated by Spn4A WT-S expression. Ingenuity Pathway Analysis software was used to generate canonical pathways regulated in response to Spn4A WT-S. Significance was calculated from Fisher's exact test ($p<0.01$). Genes associated with each canonical pathway are listed in Supplemental Table A5.5.

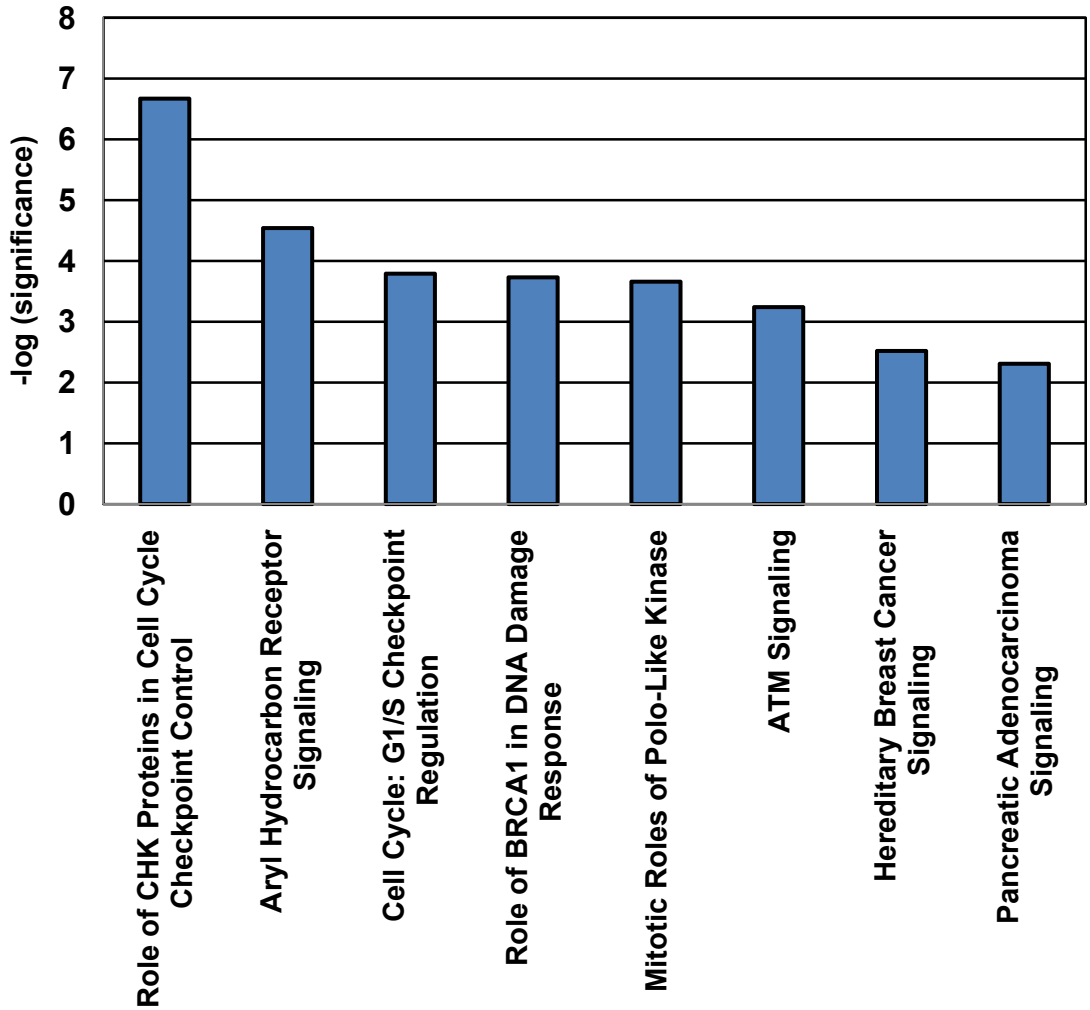

Figure 3.7. The top two most significant networks of genes regulated by Spn4A WT-S expression. A) and B) Networks were identified by Ingenuity Pathway Analysis. Different shapes identify with different types of molecular classes and the lines connecting the molecules indicate their relationships. The fold changes of upregulated genes (red) and downregulated genes (green) are labeled underneath the molecule. Colour denotes intensity of regulation.

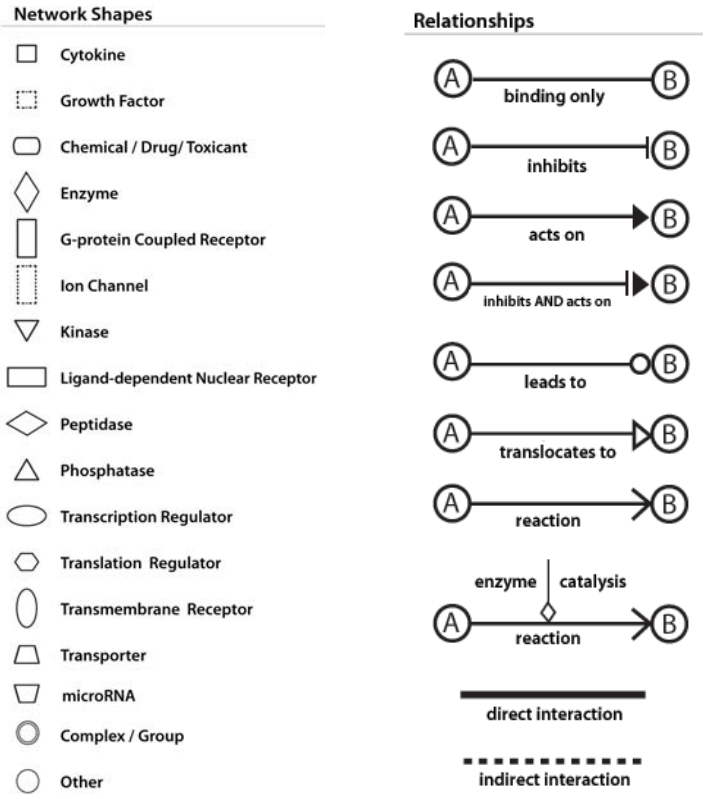

A)

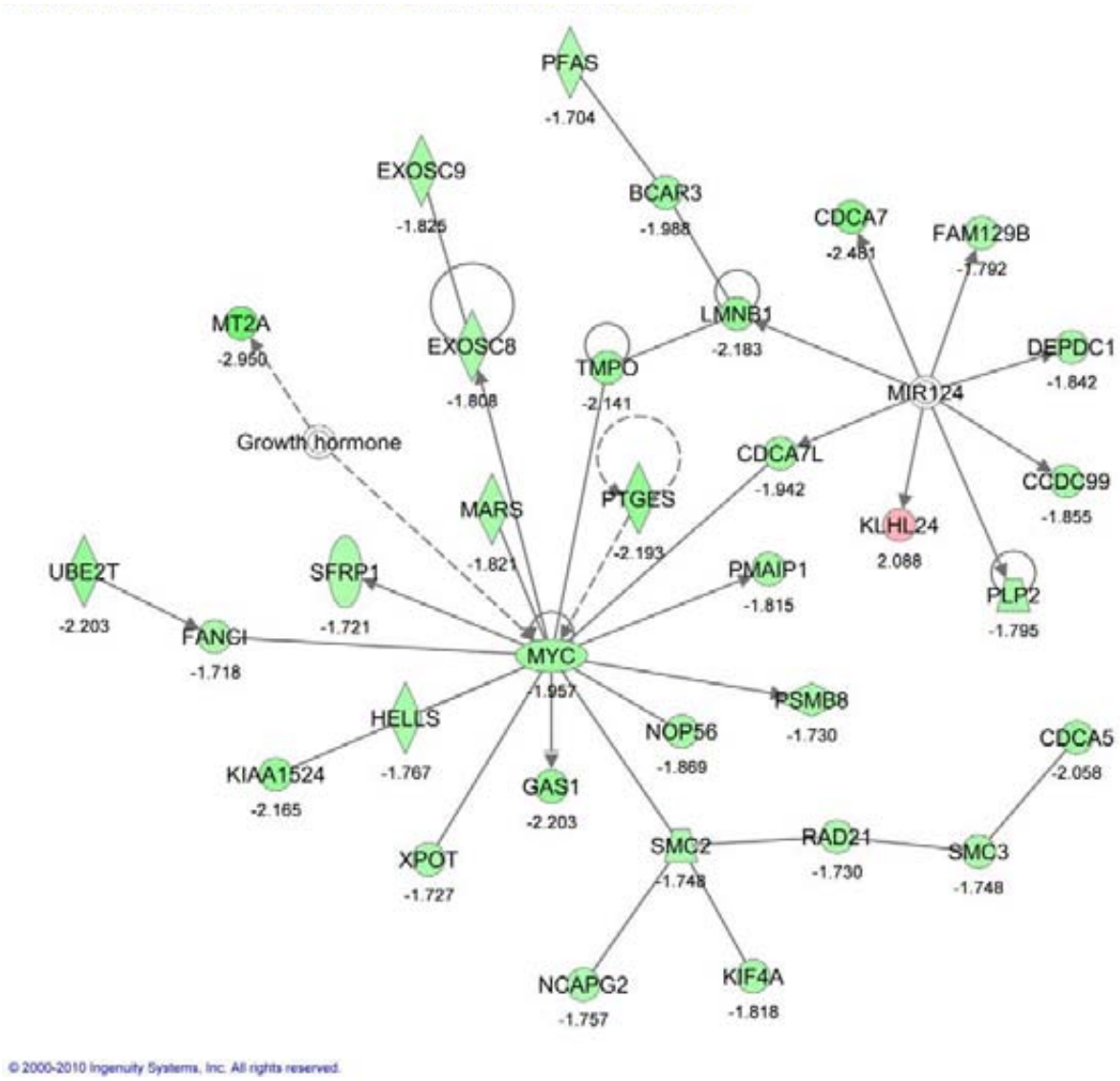

B)

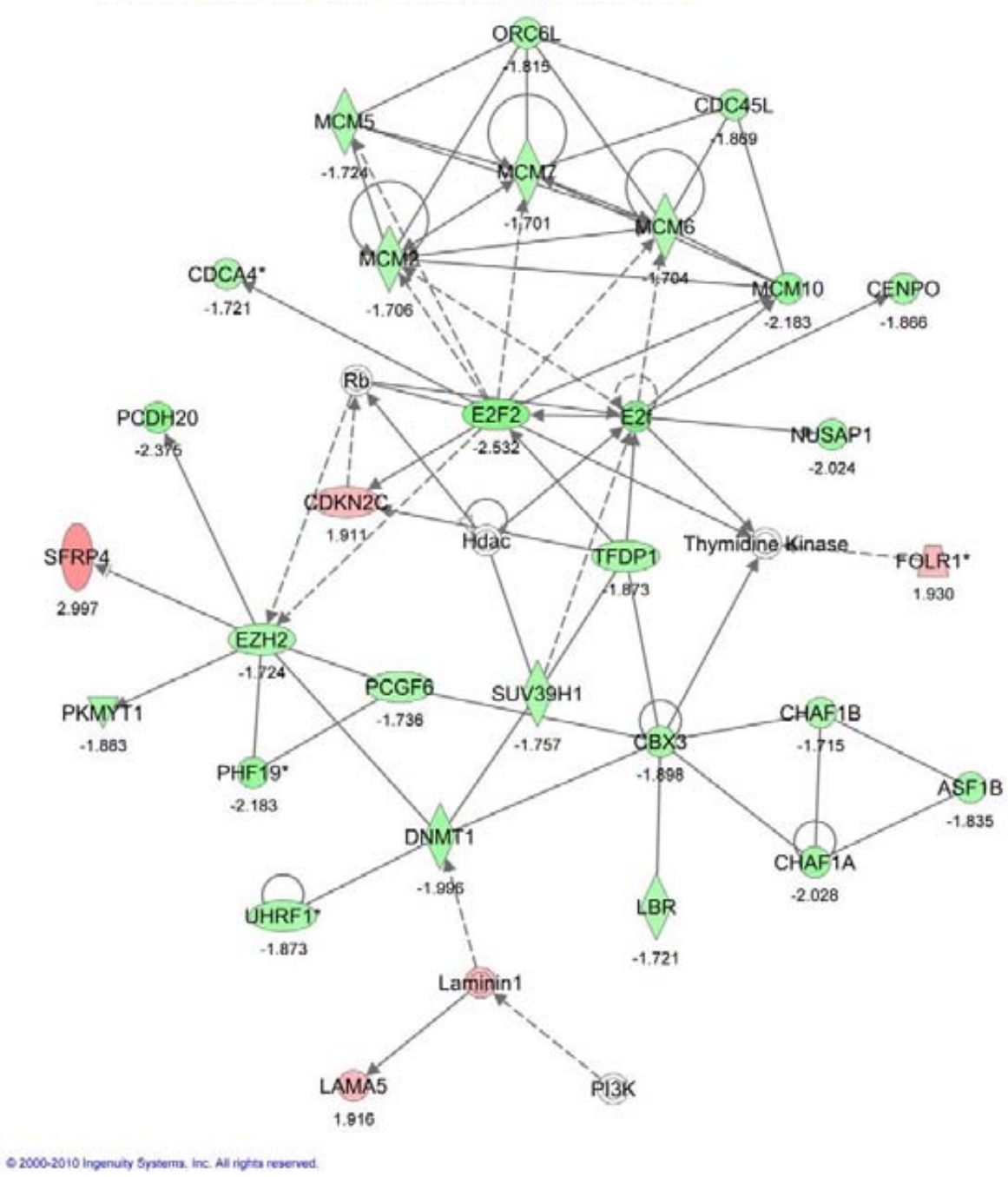

Figure 3.8. Points of the cell cycle where genes are differentially regulated in response to Spn4A-S expression. The cell cycle consists of G1 (Gap 1), S (synthesis), G2 (Gap 2), and M (mitosis). The amount of DNA (coloured lines) and size of cell are illustrated in each stage. Differentially regulated genes that act on transitions or at stages of the cell cycle are labelled. Full gene names and fold changes are in Supplemental Table A4.1.

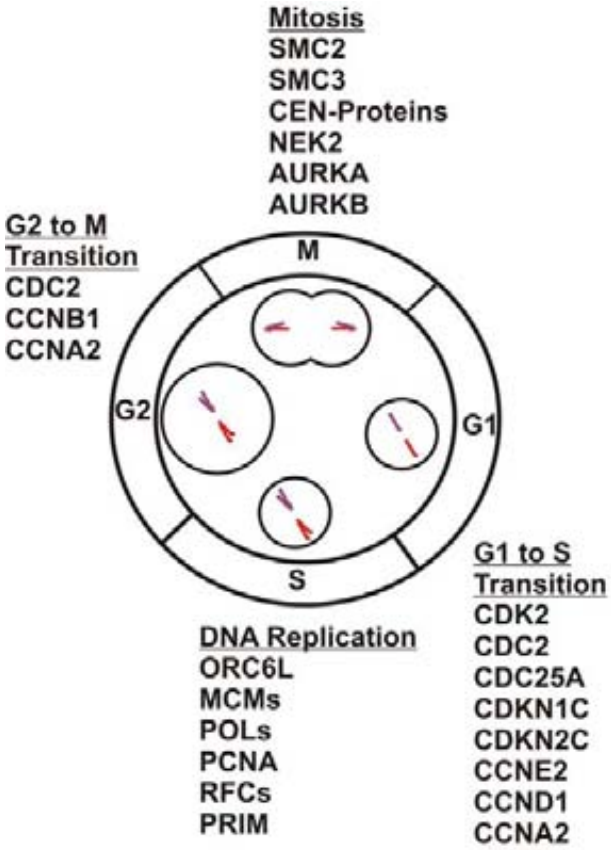

Figure 3.9. Summary of DAVID gene ontology analysis for each list of regulated genes unique to or shared between WT-S and RFP WT-S. The list of differentially regulated genes in response to WT-S expression were compared to those of RFP WT-S and summarized into a venn diagram. Downregulated (green circles) or upregulated (red circles) genes for each unique or shared list were separately analyzed on DAVID functional annotation clustering and one representative term from each cluster is shown. The numbers in brackets are enrichment scores for the clusters. Only significant clusters (enrichment score > 2) are shown, up to ten clusters. Full gene annotations are in Appendix 4, Supplemental Tables A4.5 to A4.9.

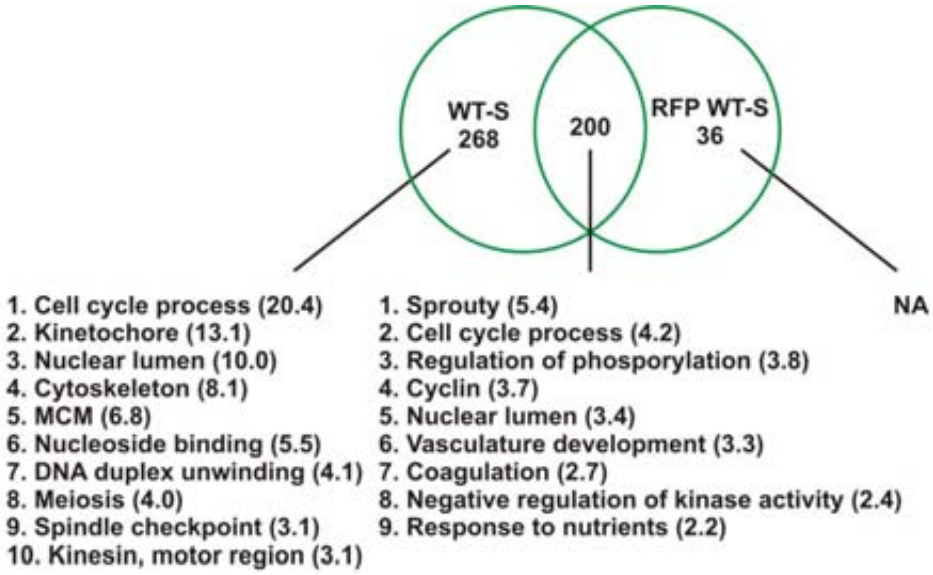

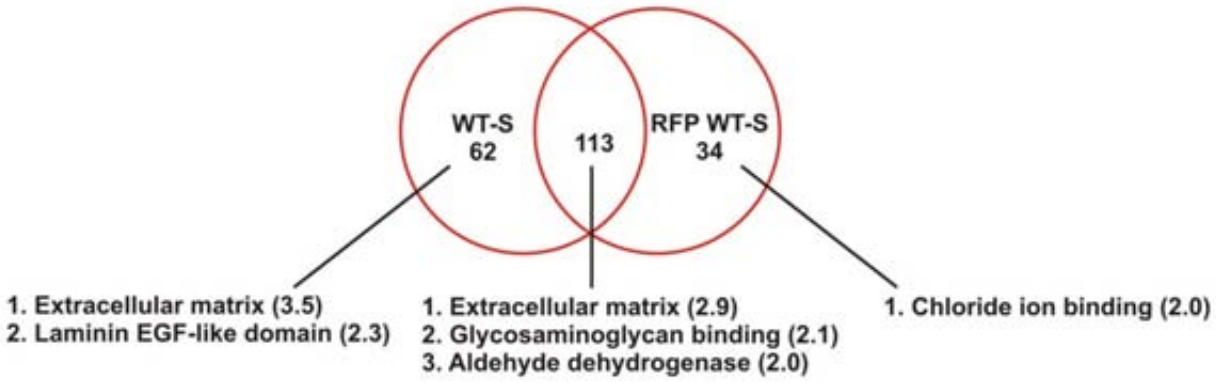

Figure 3.10. Summary of DAVID gene ontology analysis for each list of regulated genes unique to or shared between RFP WT-S and RFP WT-R. The list of differentially regulated genes in response to RFP WT-S expression were compared to those of RFP WT-R and summarized into a venn diagram. Downregulated (green circles) or upregulated (red circles) genes for each unique or shared list were separately analyzed on DAVID functional annotation clustering and one representative term from each cluster is shown. The numbers in brackets represent enrichment score for the cluster. Only significant clusters (enrichment score > 2) are shown. Full gene annotations are in Appendix 4, Supplemental Tables A4.13 to A4.16.

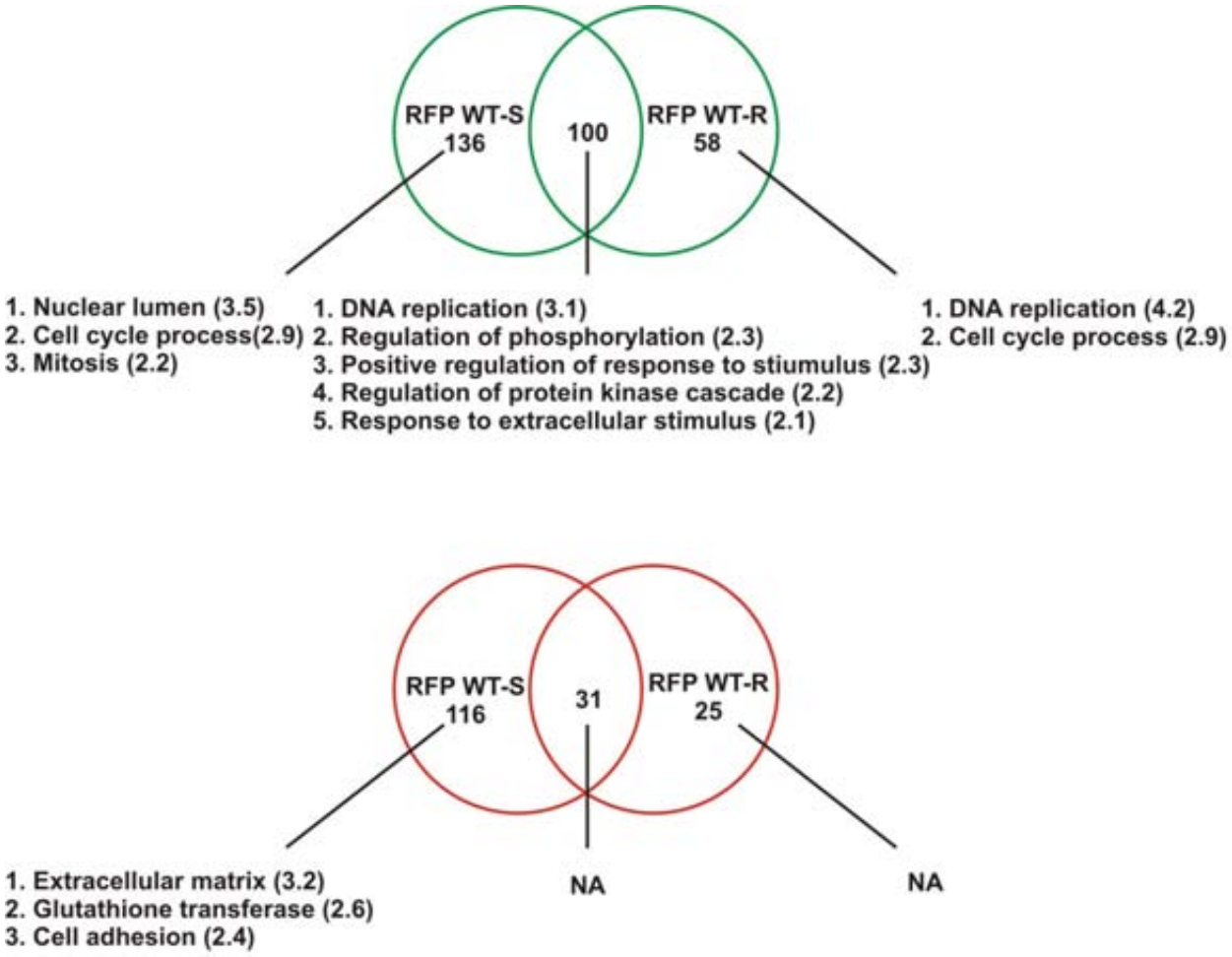

Figure 3.11. Comparison of the number of genes annotated with cell growth and proliferation or cell movement that are regulated in response to WT-S, RFP WT-S, and RFP WT-R. Genes annotated by Ingenuity Pathway Analysis as cell growth and proliferation or cell movement were counted and summarised.

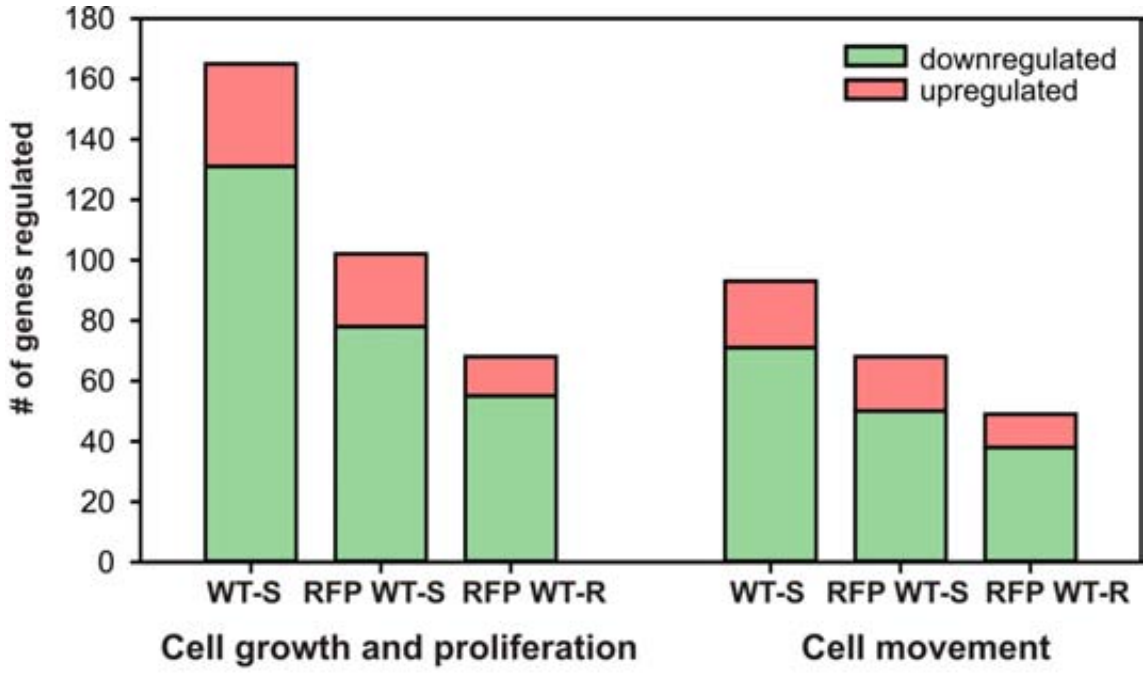

Figure 3.12. The mRNA levels of three cell cycle genes and *IL8* in response to RFP WT-R determined by microarray and qPCR. RNA was collected from H4 neuroglioma cells infected with Ad. Emp or Ad. RFP WT-R, reverse transcribed to cDNA, and used for real-time PCR. FC represent comparisons of Ad. RFP WT-R to Ad. Emp. Significant values ($p<0.05$*) are as denoted (two-tailed Student's t-test). Error bars represent SEM (standard error of the mean).

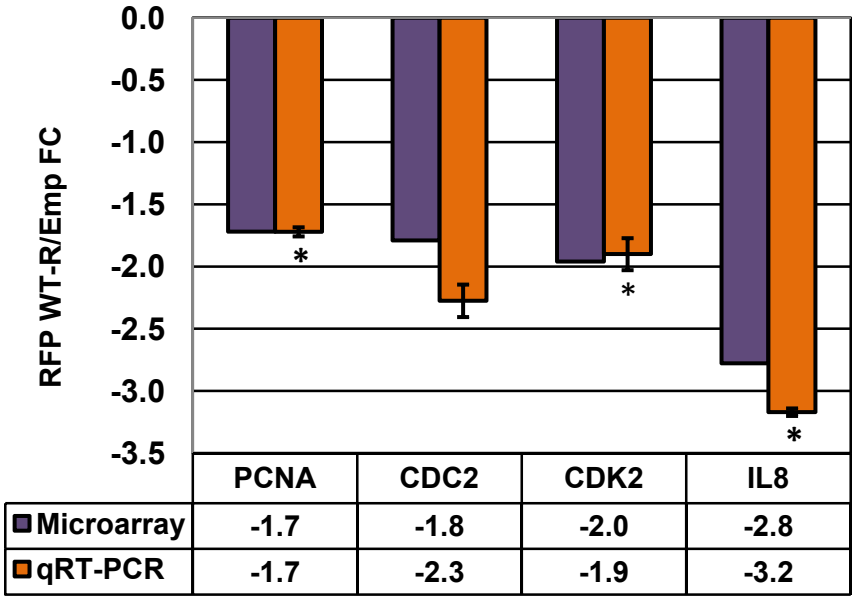

	PCNA	CDC2	CDK2	IL8
Microarray	-1.7	-1.8	-2.0	-2.8
qRT-PCR	-1.7	-2.3	-1.9	-3.2

Table 3.1. DAVID GO functional annotation clusters for genes downregulated by Spn4A WT-S expression. DAVID functional annotation clustering was carried out using high stringency for clustering. Term represent annotation term, count is the number of genes involved in the individual term, p-value is calculated using a modified Fisher's exact test and represent the significance of gene-term enrichment, fold enrichment measures the magnitude of enrichment against the complete array background, and annotation cluster enrichment score is the negative log transformation of the geometric mean of the p-values in the group. Genes from one annotation for each cluster, up to ten clusters, are listed in Supplemental Table A5.2.

Term	Count	p-value	Fold Enrichment
Annotation Cluster 1: Enrichment Score = 23.6			
cell division	45	2.13E-25	7.42
GO:0022402~cell cycle process	66	7.44E-25	4.47
GO:0000278~mitotic cell cycle	54	8.53E-25	5.58
GO:0007067~mitosis	43	1.02E-24	7.46
GO:0000280~nuclear division	43	1.02E-24	7.46
mitosis	38	1.53E-24	9.02
GO:0000087~M phase of mitotic cell cycle	43	2.15E-24	7.33
GO:0022403~cell cycle phase	56	3.65E-24	5.19
GO:0048285~organelle fission	43	5.37E-24	7.16
GO:0000279~M phase	50	9.50E-24	5.82
GO:0051301~cell division	46	3.40E-22	5.94
Annotation Cluster 2: Enrichment Score = 13.3			
kinetochore	20	1.23E-16	13.72
GO:0000779~condensed chromosome, centromeric region	20	1.53E-15	11.97
GO:0000777~condensed chromosome kinetochore	17	5.70E-13	11.57
GO:0000776~kinetochore	17	5.12E-11	8.83
Annotation Cluster 3: Enrichment Score 11.9			
GO:0031981~nuclear lumen	85	4.43E-14	2.34
GO:0031974~membrane-enclosed lumen	96	1.16E-12	2.06
GO:0043233~organelle lumen	94	2.61E-12	2.06
GO:0070013~intracellular organelle lumen	91	1.20E-11	2.04
Annotation Cluster 4: Enrichment Score = 7.3			
IPR018525:DNA-dependent ATPase MCM, conserved site	7	3.54E-09	38.45
domain:MCM	7	3.83E-09	37.99
IPR001208:DNA-dependent ATPase MCM	7	1.04E-08	34.17
SM00350:MCM	7	1.54E-08	31.77
IPR012340:Nucleic acid-binding, OB-fold	8	1.63E-04	6.76

Term	Count	p-value	Fold Enrichment
Annotation Cluster 5: Enrichment Score = 4.7			
nucleotide phosphate-binding region:ATP	49	3.09E-07	2.23
GO:0005524~ATP binding	65	1.14E-06	1.84
GO:0001882~nucleoside binding	69	1.28E-06	1.79
GO:0032559~adenyl ribonucleotide binding	65	1.83E-06	1.82
GO:0030554~adenyl nucleotide binding	67	2.52E-06	1.78
atp-binding	58	3.09E-06	1.91
GO:0001883~purine nucleoside binding	67	4.25E-06	1.75
GO:0032555~purine ribonucleotide binding	66	4.92E-04	1.51
GO:0032553~ribonucleotide binding	66	4.92E-04	1.51
GO:0017076~purine nucleotide binding	68	5.72E-04	1.49
nucleotide-binding	59	1.07E-03	1.53
GO:0000166~nucleotide binding	73	3.43E-03	1.37
Annotation Cluster 6: Enrichment Score: 4.3			
GO:0006268~DNA unwinding during replication	6	2.04E-05	16.21
GO:0032392~DNA geometric change	6	7.99E-05	12.61
GO:0032508~DNA duplex unwinding	6	7.99E-05	12.61
Annotation Cluster 7: Enrichment Score = 4.0			
IPR007875:Sprouty	5	8.66E-06	31.38
domain:SPR	5	9.11E-06	31.01
GO:0043407~negative regulation of MAP kinase activity	5	1.44E-02	5.25
Annotation Cluster 8: Enrichment Score = 3.7			
domain:Kinesin-motor	9	4.33E-06	9.30
IPR001752:Kinesin, motor region	8	3.39E-05	8.57
IPR019821:Kinesin, motor region, conserved site	8	3.39E-05	8.57
SM00129:KISc	8	5.14E-05	7.97
GO:0003777~microtubule motor activity	10	8.27E-05	5.45
GO:0003774~motor activity	11	2.15E-03	3.23
motor protein	10	3.39E-03	3.30
Annotation Cluster 9: Enrichment Score = 3.6			
GO:0005663~DNA replication factor C complex	5	5.74E-06	32.90
PIRSF004274:phage T4 DNA polymerase accessory protein 44	4	5.65E-05	40.65
GO:0003689~DNA clamp loader activity	4	1.33E-04	33.16
GO:0033170~protein-DNA loading ATPase activity	4	1.33E-04	33.16
IPR013748:Replication factor C	3	1.52E-03	43.94
GO:0008094~DNA-dependent ATPase activity	5	4.79E-02	3.64

Term	Count	p-value	Fold Enrichment
Annotation Cluster 10: Enrichment Score = 3.4			
IPR004367:Cyclin, C-terminal	6	9.91E-06	18.83
PIRSF001771:cyclin, A/B/D/E types	5	9.98E-05	18.48
IPR014400:Cyclin, A/B/D/E	5	1.12E-04	18.31
PIRSF001771:Cyclin_A_B_D_E	5	1.47E-04	16.94
IPR006671:Cyclin, N-terminal	6	8.24E-04	7.99
cyclin	7	9.83E-04	6.05
IPR013763:Cyclin-related	6	1.41E-03	7.12
IPR006670:Cyclin	6	2.01E-03	6.59
SM00385:CYCLIN	6	2.69E-03	6.13
Annotation Cluster 11: Enrichment Score = 3.3			
GO:0005663~DNA replication factor C complex	5	5.74E-06	32.90
GO:0006297~nucleotide-excision repair, DNA gap filling	6	5.90E-05	13.35
hsa03420:Nucleotide excision repair	6	9.30E-03	4.55
GO:0006289~nucleotide-excision repair	6	1.36E-02	4.20
Annotation Cluster 12: Enrichment Score = 3.3			
GO:0019220~regulation of phosphate metabolic process	28	1.77E-04	2.21
GO:0051174~regulation of phosphorus metabolic process	28	1.77E-04	2.21
GO:0042325~regulation of phosphorylation	27	2.33E-04	2.21
GO:0045859~regulation of protein kinase activity	21	8.34E-04	2.30
GO:0043549~regulation of kinase activity	21	1.28E-03	2.22
GO:0051338~regulation of transferase activity	21	2.08E-03	2.13
Annotation Cluster 13: Enrichment Score = 3.1			
GO:0051303~establishment of chromosome localization	5	5.15E-04	12.61
GO:0050000~chromosome localization	5	5.15E-04	12.61
GO:0051310~metaphase plate congression	4	2.56E-03	13.75
Annotation Cluster 14: Enrichment Score = 3.0			
GO:0007126~meiosis	10	9.58E-04	3.94
GO:0051327~M phase of meiotic cell cycle	10	9.58E-04	3.94
GO:0051321~meiotic cell cycle	10	1.11E-03	3.86
Annotation Cluster 15: Enrichment Score = 2.6			
GO:0031577~spindle checkpoint	5	1.99E-04	15.76
GO:0045841~negative regulation of mitotic metaphase/anaphase transition	4	2.56E-03	13.75
GO:0007094~mitotic cell cycle spindle assembly checkpoint	4	2.56E-03	13.75
GO:0045839~negative regulation of mitosis	4	3.35E-03	12.61
GO:0051784~negative regulation of nuclear division	4	3.35E-03	12.61
GO:0030071~regulation of mitotic metaphase/anaphase transition	4	1.93E-02	6.88

Term	Count	p-value	Fold Enrichment
Annotation Cluster 16: Enrichment Score = 2.3			
GO:0048754~branching morphogenesis of a tube	8	1.56E-03	4.65
GO:0001763~morphogenesis of a branching structure	8	3.30E-03	4.09
GO:0035239~tube morphogenesis	9	1.92E-02	2.68
Annotation Cluster 17: Enrichment Score = 2.2			
GO:0005658~alpha DNA polymerase:primase complex	4	3.01E-04	26.32
GO:0030894~replisome	4	4.72E-03	11.28
GO:0043601~nuclear replisome	4	4.72E-03	11.28
GO:0043596~nuclear replication fork	4	5.79E-03	10.53
GO:0032993~protein-DNA complex	5	1.62E-01	2.35
Annotation Cluster 18: Enrichment Score = 2.2			
domain:BRCT 1	4	2.27E-03	14.47
domain:BRCT 2	4	2.27E-03	14.47
IPR001357:BRCT	4	1.65E-02	7.32
SM00292:BRCT	4	1.98E-02	6.81
Annotation Cluster 19: Enrichment Score = 2.2			
GO:0007584~response to nutrient	11	3.96E-03	2.97
GO:0009991~response to extracellular stimulus	14	5.55E-03	2.41
GO:0031667~response to nutrient levels	12	1.50E-02	2.30
Annotation Cluster 20: Enrichment Score = 2.1			
GO:0007596~blood coagulation	9	4.89E-03	3.40
GO:0050817~coagulation	9	4.89E-03	3.40
GO:0007599~hemostasis	9	6.92E-03	3.21
GO:0050878~regulation of body fluid levels	9	2.97E-02	2.47

Table 3.2. DAVID GO functional annotation clusters for genes upregulated by Spn4A WT-S expression. Parameters are as described in Table 3.1.

Term	Count	p-value	Fold Enrichment
Annotation Cluster 1: Enrichment Score = 6.7			
GO:0031012~extracellular matrix	17	1.03E-08	6.20
GO:0005578~proteinaceous extracellular matrix	16	2.67E-08	6.30
extracellular matrix	14	2.85E-08	7.80
GO:0044421~extracellular region part	20	1.57E-04	2.61
Annotation Cluster 2: Enrichment Score = 2.7			
GO:0005581~collagen	5	1.68E-04	17.66
trimer	4	9.31E-04	20.48
hydroxylysine	4	1.57E-03	17.17
triple helix	4	1.57E-03	17.17
GO:0030934~anchoring collagen	3	2.20E-03	41.20
hydroxyproline	4	2.62E-03	14.39
collagen	5	5.18E-03	7.16
IPR008160:Collagen triple helix repeat	4	2.61E-02	6.22
Annotation Cluster 3: Enrichment Score = 2.3			
GO:0005539~glycosaminoglycan binding	6	3.80E-03	5.73
GO:0030247~polysaccharide binding	6	5.55E-03	5.24
GO:0001871~pattern binding	6	5.55E-03	5.24
Annotation Cluster 4: Enrichment Score = 2.3			
IPR018244:Allergen V5/Tpx-1 related, conserved site	3	3.08E-03	35.18
IPR001283:Allergen V5/Tpx-1 related	3	5.77E-03	25.80
IPR014044:SCP-like extracellular	3	5.77E-03	25.80
SM00198:SCP	3	7.71E-03	22.06
Annotation Cluster 5: Enrichment Score = 2.1			
IPR000372:Leucine-rich repeat, cysteine-rich flanking region, N-terminal	6	8.27E-04	8.15
SM00013:LRRNT	6	1.56E-03	6.97
repeat:LRR 6	7	4.36E-03	4.55
IPR001611:Leucine-rich repeat	7	5.31E-03	4.36
repeat:LRR 5	7	6.97E-03	4.13
repeat:LRR 7	6	9.30E-03	4.66
repeat:LRR 4	7	1.06E-02	3.78
repeat:LRR 3	7	2.10E-02	3.24
repeat:LRR 1	7	2.69E-02	3.06
repeat:LRR 2	7	2.73E-02	3.05
leucine-rich repeat	7	2.81E-02	3.02

Table 3.3. Top 10 networks generated from genes differentially regulated by Spn4A WT-S expression as identified by Ingenuity Pathway Analysis. Networks were generated using Ingenuity Pathway Analysis. Score is the negative log of the significance, which is based on number of focus molecules and size of network. The most annotated functions from molecules in the network are listed.

ID	Score	Focus Molecules	Top Functions
1	49	33	Cell Cycle, Cellular Assembly and Organization, DNA Replication, Recombination, and Repair
2	39	29	Cellular Assembly and Organization, DNA Replication, Recombination, and Repair, Gene Expression
3	37	28	DNA Replication, Recombination, and Repair, Infection Mechanism, Gene Expression
4	31	25	Cardiovascular System Development and Function, Embryonic Development, Tissue Development
5	31	26	Cell Cycle, Embryonic Development, Small Molecule Biochemistry
6	29	24	Cell Cycle, Cellular Assembly and Organization, DNA Replication, Recombination, and Repair
7	29	24	Connective Tissue Disorders, Organismal Injury and Abnormalities, Cardiovascular System Development and Function
8	23	21	Cell-To-Cell Signaling and Interaction, Reproductive System Development and Function, Cardiovascular Disease
9	23	24	Nervous System Development and Function, Organ Development, Gene Expression
10	22	20	Dermatological Diseases and Conditions, Genetic Disorder, Immunological Disease

Table 3.4. Top 10 downregulated or upregulated genes associated with cell movement as annotated by Ingenuity Pathway Analysis molecular functions in response to Spn4A WT-S expression. Gene symbol, gene names, and fold changes are listed. The full list is in Supplemental Table A5.4.

Gene Symbol	Gene Name	Fold Change
Downregulated		
IL8	interleukin 8	-5.319
ITGA2	integrin, alpha 2 (CD49B, alpha 2 subunit of VLA-2 receptor)	-4.695
ETV5	ets variant 5	-4.348
TGFA	transforming growth factor, alpha	-3.846
GDF15	growth differentiation factor 15	-3.236
SPP1	secreted phosphoprotein 1	-2.959
ERRFI1	ERBB receptor feedback inhibitor 1	-2.933
AJAP1	adherens junctions associated protein 1	-2.924
ITGA6	integrin, alpha 6	-2.857
RGS1	regulator of G-protein signaling 1	-2.710
Upregulated		
C5ORF13	chromosome 5 open reading frame 13, also known as P311	2.203
ALPP	alkaline phosphatase, placental (Regan isozyme)	2.206
CD24	CD24 molecule	2.283
S100A4	S100 calcium binding protein A4	2.364
SOCS2	suppressor of cytokine signaling 2	2.643
PPAP2A	phosphatidic acid phosphatase type 2A	2.717
GUCY1A3	guanylate cyclase 1, soluble, alpha 3	3.054
CD36	CD36 molecule (thrombospondin receptor)	3.329
OLR1	oxidized low density lipoprotein (lectin-like) receptor 1	3.630
DCN	decorin	4.215

Chapter 4: Conclusion

The goals of this thesis were to study the cellular response to both the disease-causing and therapeutic roles of serpins using *Drosophila* Spn4A. Accordingly, we developed polymer-forming Spn4A mutants and expressed Spn4A WT and mutants in H4 neuroglioma cells to simultaneously address their cellular effects via microarray. Fig. 4.1 summarizes the key findings and future work.

4.1 Implications for cellular and animal models of serpinopathies

Current cellular models expressing hNS mutants reveal that polymers induce an EOR response (73). However, pathways activating EOR and its downstream effects leading to disease are not clear. To address the cellular pathways leading to pathology, we expressed Spn4A polymer-forming mutants in H4 neuroglioma cells and identified genes, via microarray, that are differentially regulated in their presence. The validation of the 17 differentially regulated genes is of immediate interest. Further, the question of whether or not human neuroserpin mutants regulate the same genes will need to be addressed. These genes that are specifically regulated in the presence of polymers may provide insight into mutant serpin pathogenesis. Identification and characterization of the proteins regulated by serpin polymers may serve as potential targets for effective therapy.

It is possible that none of the genes identified can be validated or their gene products linked to cytotoxicity. In fact, we and others have not observed or reported toxic effects of serpin polymers in cell culture systems, suggesting that studies performed in cancer cells may not be appropriate. Non-cancerous neuronal cells or transgenic animals may be more appropriate models. Such systems would allow us to address, for example, if apoptosis may result from NFκB activation that drives proliferation (74) of post-mitotic neurons. The adenovirus constructs that we have developed can be applied to most cell systems efficiently, which will aid the transition for future studies.

Last, in collaboration with Dr. Carl Hashimoto, we are making transgenic *Drosophila* overexpressing Spn4A WT and mutants. Our future studies will include characterization of the transgenic flies. Using the *Drosophila* model, we will evaluate if Spn4A polymers may mediate disease like hNS mutants. If the transgenic flies recapitulate the neurological dysfunction associated with FENIB, we will characterize disease pathways *in vivo*. Alternatively, if the

polymers do not cause neurological disorders, we will examine the mechanisms underlying how polymers are cleared or pathways leading to restoration of neuronal function.

4.2 Implications for the use of PCs as therapeutic targets

We and others have hypothesized that PCs may represent therapeutic targets for cancer and infectious diseases (40;112;196;247;248). It was previously shown that PC inhibitors ameliorate the malignancy phenotype in glioma cells (160;164), as well as several other cancer cell lines (163;165;206). Now, we have profiled the transcriptome of neuroglioma cells expressing Spn4A, a potent inhibitor of furin and identified additional genes that may mediate tumor proliferation and invasion, as well as angiogenesis.

Our data suggest that Spn4A expression can, on the transcriptome level, modulate multiple pathways contributing to malignancy and therefore, may represent a good therapeutic agent. Spn4A directly inhibits the maturation (160;164) and may indirectly affect the expression of several proteins currently being evaluated as therapeutic targets. For example, inhibitors for MMPs (252), VEGFA (253), and Aurora kinases (254) are currently in clinical trials. However, targeted inhibition of several MMPs and MT1-MMP in phase II or III clinical trials were ineffective (255) and resistance to VEGFA inhibitors by upregulation of other angiogenic factors (IL8, FGF, PDFG) or recruitment of vascular progenitors inevitably occurs (209). We propose that using a PC inhibitor such as Spn4A may be advantageous as it simultaneously disrupts multiple genes and proteins involved in tumorigenesis and metastasis (Fig. 4.2).

The microarray results will be valuable for researchers proposing to use PC inhibitors for proliferative diseases. Although the microarray was performed on neuroglioma cells, similar pathways may be regulated in other types of cancer cells. Others have demonstrated that furin inhibition can suppress the metastatic potential in multiple cell types such as colon carcinoma (165), breast cancer cells (206), and head and neck squamous carcinoma cells (163). However, regulation is dependent on the inhibitor used. For example, in breast cancer cells, α_1-PDX promotes invasiveness while the prosegment of furin inhibits the process (206). Therefore, the ability of Spn4A to reduce the malignancy phenotype will need to be assessed in a cell specific manner.

The applicability of Spn4A in fighting infectious disease in normal cells will have to be evaluated based on our new data. Since Spn4A expression may affect cellular proliferation,

motility, and cardiovascular systems, systematic treatment using furin inhibitors would not be possible, at least in the long term. We did not observe induction of cellular stress and apoptosis specific to Spn4A WT, but we detected differential regulation of genes of the BCL2 family. While no apparent apoptosis was observed under our experimental conditions, we cannot rule out that the cells may be sensitized to stress. The use of Spn4A in short term therapy for acute diseases in non-proliferating cells may be possible with minimal effects.

4.3 Closing remarks

We have developed a cell-based system expressing Spn4A WT and polymer-forming mutants to assess their effects on the cellular transcriptome. Importantly, we identified genes that may reflect the downstream effects of the loss of functional PC substrates or of polymer buildup. The proposed future experiments are targeted at elucidating the underlying mechanisms and/or consequences of Spn4A WT and mutants. Defining the mechanism underlying the cellular changes in response to Spn4A WT will be essential in the development of PC inhibitors as therapeutic agents. Further, understanding the genes modulated by polymers may provide important insight into disease mechanisms. Taken together, our study lays the foundation for future studies aimed at elucidating the serpins' roles as a therapeutic and in disease.

Figure 4.1. Flow chart of key findings and future directions in this thesis project.

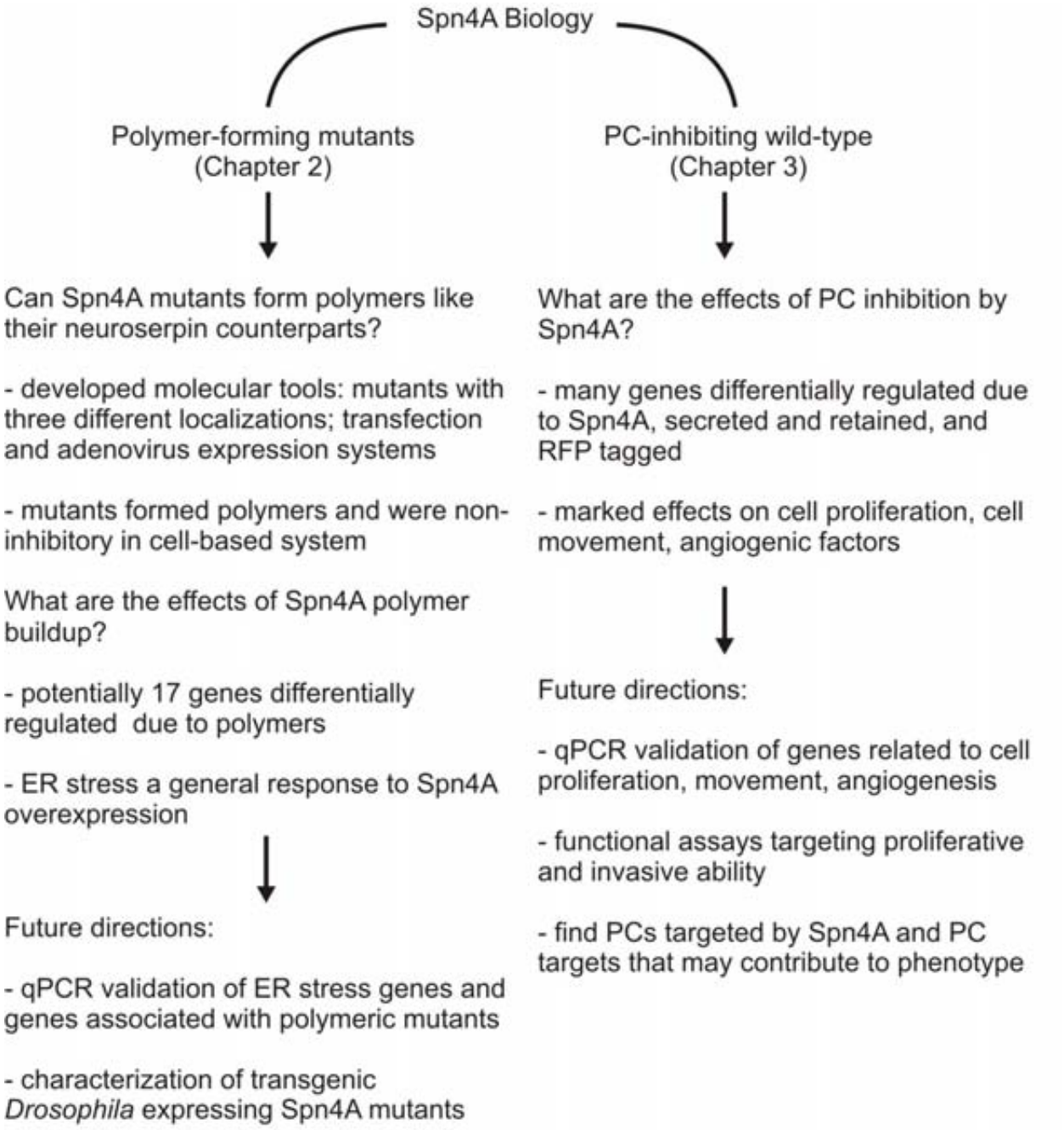

Figure 4.2. PCs as anti-cancer treatment targets. Inhibition of PCs may mediate multiple aspects of the malignant phenotype, including proliferation, cell cycle, invasion and metastasis, and angiogenesis through regulation of protein processing and gene expression.

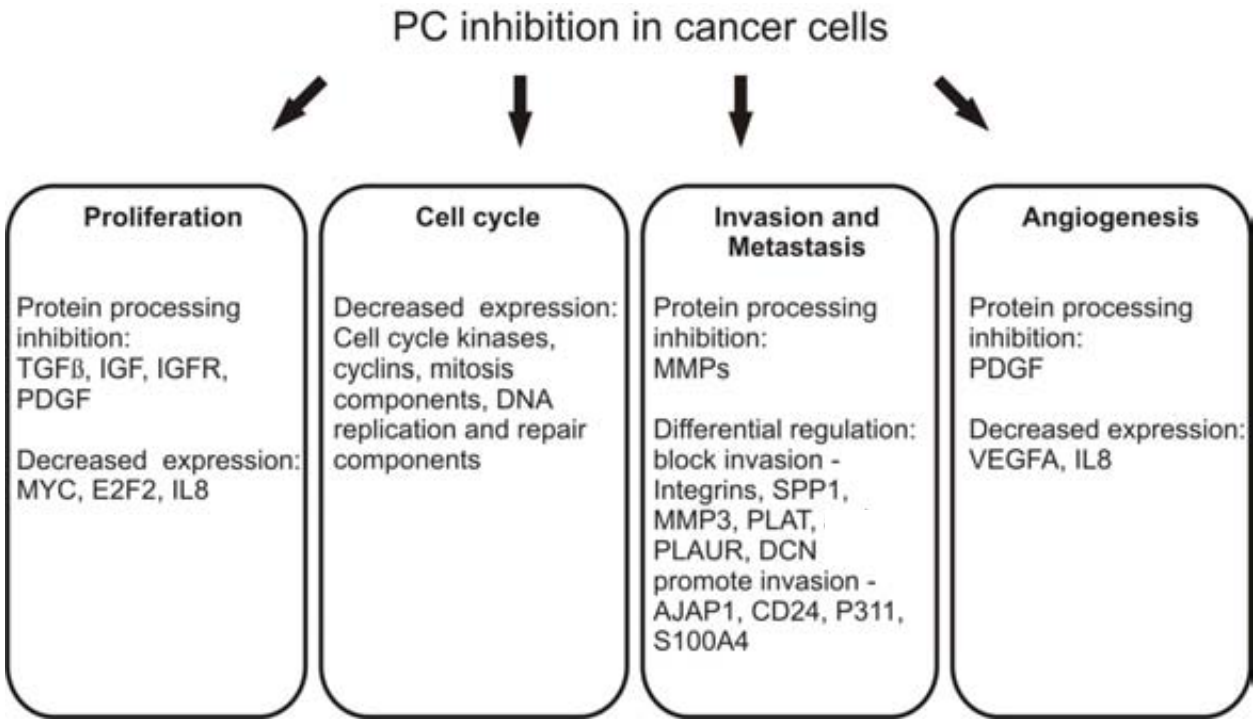

References

(1) Irving JA, Steenbakkers PJM, Lesk AM, Op den Camp HJM, Pike RN, Whisstock JC. Serpins in Prokaryotes. Mol Biol Evol 2002 Nov 1;19(11):1881-90.

(2) Law R, Zhang Q, McGowan S, Buckle A, Silverman G, Wong W, et al. An overview of the serpin superfamily. Genome Biology 2006;7(5):216.

(3) Garrett M, Fullaondo A, Troxler L, Micklem G, Gubb D. Identification and analysis of serpin-family genes by homology and synteny across the 12 sequenced Drosophilid genomes. BMC Genomics 2009;10:489.

(4) Steenbakkers PJM, Irving JA, Harhangi HR, Swinkels WJC, Akhmanova A, Dijkerman R, et al. A serpin in the cellulosome of the anaerobic fungus Piromyces sp. strain E2. Mycological Research 2008 Aug;112(8):999-1006.

(5) Irving JA, Pike RN, Lesk AM, Whisstock JC. Phylogeny of the serpin superfamily: implications of patterns of amino acid conservation for structure and function. Genome Res 2000 Dec;10(12):1845-64.

(6) Gettins PG. Serpin structure, mechanism, and function. Chem Rev 2002 Dec;102(12):4751-804.

(7) Elliott PR, Lomas DA, Carrell RW, Abrahams JP. Inhibitory conformation of the reactive loop of [alpha]1-antitrypsin. Nat Struct Mol Biol 1996 Aug;3(8):676-81.

(8) Carrell RW, Owen MC. Plakalbumin, [alpha]1-antitrypsin, antithrombin and the mechanism of inflammatory thrombosis. Nature 1985 Oct 24;317(6039):730-2.

(9) Huntington JA, Read RJ, Carrell RW. Structure of a serpin-protease complex shows inhibition by deformation. Nature 2000 Oct 19;407(6806):923-6.

(10) Patston PA, Gettins P, Beechem J, Schapira M. Mechanism of serpin action: evidence that C1 inhibitor functions as a suicide substrate. Biochemistry 1991 Sep 1;30(36):8876-82.

(11) Lawrence DA, Olson ST, Palaniappan S, Ginsburg D. Serpin reactive center loop mobility is required for inhibitor function but not for enzyme recognition. Journal of Biological Chemistry 1994 Nov 4;269(44):27657-62.

(12) Lawrence DA, Olson ST, Muhammad S, Day DE, Kvassman JO, Ginsburg D, et al. Partitioning of serpin-proteinase reactions between stable inhibition and substrate cleavage is regulated by the rate of serpin reactive center loop insertion into beta-sheet A. J Biol Chem 2000 Feb 25;275(8):5839-44.

(13) Lawless MW, Mankan AK, Gray SG, Norris S. Endoplasmic reticulum stress--a double edged sword for Z alpha-1 antitrypsin deficiency hepatoxicity. Int J Biochem Cell Biol 2008;40(8):1403-14.

(14) Cicardi M, Zingale L, Zanichelli A, Pappalardo E, Cicardi B. C1 inhibitor: molecular and clinical aspects. Springer Seminars in Immunopathology 2005 Nov 1;27(3):286-98.

(15) Perry DJ, Carrell RW. Molecular genetics of human antithrombin deficiency. Hum Mutat 1996;7(1):7-22.

(16) Osterwalder T, Contartese J, Stoeckli ET, Kuhn TB, Sonderegger P. Neuroserpin, an axonally secreted serine protease inhibitor. EMBO J 1996 Jun 17;15(12):2944-53.

(17) Bird PI. Regulation of pro-apoptotic leucocyte granule serine proteinases by intracellular serpins. Immunol Cell Biol 1999 Feb;77(1):47-57.

(18) Bird CH, Sutton VR, Sun J, Hirst CE, Novak A, Kumar S, et al. Selective Regulation of Apoptosis: the Cytotoxic Lymphocyte Serpin Proteinase Inhibitor 9áProtects against Granzyme B-Mediated Apoptosis without Perturbing the Fas Cell Death Pathway. Mol Cell Biol 1998 Nov 1;18(11):6387-98.

(19) Campbell DJ. The renin-angiotensin and the kallikrein-kinin systems. The International Journal of Biochemistry & Cell Biology 2003 Jun;35(6):784-91.

(20) Zhou A, Wei Z, Read RJ, Carrell RW. Structural mechanism for the carriage and release of thyroxine in the blood. Proceedings of the National Academy of Sciences 2006 Sep 5;103(36):13321-6.

(21) Nagata K. Expression and function of heat shock protein 47: A collagen-specific molecular chaperone in the endoplasmic reticulum. Matrix Biology 1998 Feb;16(7):379-86.

(22) Zou Z, Anisowicz A, Hendrix MJ, Thor A, Neveu M, Sheng S, et al. Maspin, a serpin with tumor-suppressing activity in human mammary epithelial cells. Science 1994 Jan 28;263(5146):526-9.

(23) Yamasaki M, Li W, Johnson DJ, Huntington JA. Crystal structure of a stable dimer reveals the molecular basis of serpin polymerization. Nature 2008 Oct 30;455(7217):1255-8.

(24) Whisstock JC, Bottomley SP. Structural biology: Serpins' mystery solved. Nature 2008 Oct 30;455(7217):1189-90.

(25) Carrell RW, Lomas DA. Alpha1-antitrypsin deficiency--a model for conformational diseases. N Engl J Med 2002 Jan 3;346(1):45-53.

(26) Lomas DA, Carrell RW. Serpinopathies and the conformational dementias. Nat Rev Genet 2002 Oct;3(10):759-68.

(27) Sveger T. Liver disease in alpha1-antitrypsin deficiency detected by screening of 200,000 infants. N Engl J Med 1976 Jun 10;294(24):1316-21.

(28) Eriksson S, Carlson J, Velez R. Risk of cirrhosis and primary liver cancer in alpha 1-antitrypsin deficiency. N Engl J Med 1986 Mar 20;314(12):736-9.

(29) Hastings GA, Coleman TA, Haudenschild CC, Stefansson S, Smith EP, Barthlow R, et al. Neuroserpin, a Brain-associated Inhibitor of Tissue Plasminogen Activator Is Localized Primarily in Neurons. Journal of Biological Chemistry 1997 Dec 26;272(52):33062-7.

(30) Coutelier M, Andries S, Ghariani S, Dan B, Duyckaerts C, van RK, et al. Neuroserpin mutation causes electrical status epilepticus of slow-wave sleep. Neurology 2008 Jul 1;71(1):64-6.

(31) Davis RL, Shrimpton AE, Carrell RW, Lomas DA, Gerhard L, Baumann B, et al. Association between conformational mutations in neuroserpin and onset and severity of dementia. Lancet 2002 Jun 29;359(9325):2242-7.

(32) Kruger O, Ladewig J, Koster K, Ragg H. Widespread occurrence of serpin genes with multiple reactive centre-containing exon cassettes in insects and nematodes. Gene 2002 Jun 26;293(1-2):97-105.

(33) Bruning M, Lummer M, Bentele C, Smolenaars MM, Rodenburg KW, Ragg H. The Spn4 gene from Drosophila melanogaster is a multipurpose defence tool directed against proteases from three different peptidase families. Biochem J 2007 Jan 1;401(1):325-31.

(34) Oley M, Letzel MC, Ragg H. Inhibition of furin by serpin Spn4A from Drosophila melanogaster. FEBS Lett 2004 Nov 5;577(1-2):165-9.

(35) Osterwalder T, Kuhnen A, Leiserson WM, Kim YS, Keshishian H. Drosophila serpin 4 functions as a neuroserpin-like inhibitor of subtilisin-like proprotein convertases. J Neurosci 2004 Jun 16;24(24):5482-91.

(36) Richer MJ, Keays CA, Waterhouse J, Minhas J, Hashimoto C, Jean F. The Spn4 gene of Drosophila encodes a potent furin-directed secretory pathway serpin. Proc Natl Acad Sci U S A 2004 Jul 20;101(29):10560-5.

(37) Rayburn LYM, Gooding HC, Choksi SP, Maloney D, Kidd AR, III, Siekhaus DE, et al. amontillado, the Drosophila Homolog of the Prohormone Processing Protease PC2, Is Required During Embryogenesis and Early Larval Development. Genetics 2003 Jan 1;163(1):227-37.

(38) Park Y, Filippov V, Gill SS, Adams ME. Deletion of the ecdysis-triggering hormone gene leads to lethal ecdysis deficiency. Development 2002 Jan 15;129(2):493-503.

(39) Bentele C, Kruger O, Todtmann U, Oley M, Ragg H. A proprotein convertase-inhibiting serpin with an endoplasmic reticulum targeting signal from Branchiostoma lanceolatum, a close relative of vertebrates. Biochem J 2006 May 1;395(3):449-56.

(40) Chretien M, Seidah NG, Basak A, Mbikay M. Proprotein convertases as therapeutic targets. Expert Opin Ther Targets 2008 Oct;12(10):1289-300.

(41) Fulton KF, Buckle AM, Cabrita LD, Irving JA, Butcher RE, Smith I, et al. The high resolution crystal structure of a native thermostable serpin reveals the complex mechanism underpinning the stressed to relaxed transition. J Biol Chem 2005 Mar 4;280(9):8435-42.

(42) Dementiev A, Simonovic M, Volz K, Gettins PG. Canonical inhibitor-like interactions explain reactivity of alpha1-proteinase inhibitor Pittsburgh and antithrombin with proteinases. J Biol Chem 2003 Sep 26;278(39):37881-7.

(43) Loebermann H, Tokuoka R, Deisenhofer J, Huber R. Human alpha 1-proteinase inhibitor. Crystal structure analysis of two crystal modifications, molecular model and preliminary analysis of the implications for function. J Mol Biol 1984 Aug 15;177(3):531-57.

(44) Osterwalder T, Cinelli P, Baici A, Pennella A, Krueger SR, Schrimpf SP, et al. The axonally secreted serine proteinase inhibitor, neuroserpin, inhibits plasminogen activators and plasmin but not thrombin. J Biol Chem 1998 Jan 23;273(4):2312-21.

(45) Gooptu B, Lomas DA. Conformational Pathology of the Serpins: Themes, Variations, and Therapeutic Strategies. Annu Rev Biochem 2009 Feb 26.

(46) Davis RL, Shrimpton AE, Holohan PD, Bradshaw C, Feiglin D, Collins GH, et al. Familial dementia caused by polymerization of mutant neuroserpin. Nature 1999 Sep 23;401(6751):376-9.

(47) Takehara S, Onda M, Zhang J, Nishiyama M, Yang X, Mikami B, et al. The 2.1-A crystal structure of native neuroserpin reveals unique structural elements that contribute to conformational instability. J Mol Biol 2009 Apr 24;388(1):11-20.

(48) Kopito RR, Ron D. Conformational disease. Nat Cell Biol 2000 Nov;2(11):E207-E209.

(49) Hill RM, Parmar PK, Coates LC, Mezey E, Pearson JF, Birch NP. Neuroserpin is expressed in the pituitary and adrenal glands and induces the extension of neurite-like processes in AtT-20 cells. Biochem J 2000 Feb 1;345(3):595-601.

(50) Miranda E, Lomas DA. Neuroserpin: a serpin to think about. Cell Mol Life Sci 2006 Mar;63(6):709-22.

(51) Yepes M, Sandkvist M, Coleman TA, Moore E, Wu JY, Mitola D, et al. Regulation of seizure spreading by neuroserpin and tissue-type plasminogen activator is plasminogen-independent. J Clin Invest 2002 Jun;109(12):1571-8.

(52) Yepes M, Sandkvist M, Wong MK, Coleman TA, Smith E, Cohan SL, et al. Neuroserpin reduces cerebral infarct volume and protects neurons from ischemia-induced apoptosis. Blood 2000 Jul 15;96(2):569-76.

(53) Cinelli P, Madani R, Tsuzuki N, Vallet P, Arras M, Zhao CN, et al. Neuroserpin, a Neuroprotective Factor in Focal Ischemic Stroke. Molecular and Cellular Neuroscience 2001 Nov;18(5):443-57.

(54) Bradshaw CB, Davis RL, Shrimpton AE, Holohan PD, Rea CB, Fieglin D, et al. Cognitive deficits associated with a recently reported familial neurodegenerative disease: familial encephalopathy with neuroserpin inclusion bodies. Arch Neurol 2001 Sep;58(9):1429-34.

(55) Takao M, Benson MD, Murrell JR, Yazaki M, Piccardo P, Unverzagt FW, et al. Neuroserpin mutation S52R causes neuroserpin accumulation in neurons and is

associated with progressive myoclonus epilepsy. J Neuropathol Exp Neurol 2000 Dec;59(12):1070-86.

(56) Yazaki M, Liepnieks JJ, Murrell JR, Takao M, Guenther B, Piccardo P, et al. Biochemical characterization of a neuroserpin variant associated with hereditary dementia. Am J Pathol 2001 Jan;158(1):227-33.

(57) Belorgey D, Crowther DC, Mahadeva R, Lomas DA. Mutant Neuroserpin (S49P) that causes familial encephalopathy with neuroserpin inclusion bodies is a poor proteinase inhibitor and readily forms polymers in vitro. J Biol Chem 2002 May 10;277(19):17367-73.

(58) Belorgey D, Sharp LK, Crowther DC, Onda M, Johansson J, Lomas DA. Neuroserpin Portland (Ser52Arg) is trapped as an inactive intermediate that rapidly forms polymers: implications for the epilepsy seen in the dementia FENIB. Eur J Biochem 2004 Aug;271(16):3360-7.

(59) Onda M, Belorgey D, Sharp LK, Lomas DA. Latent S49P neuroserpin forms polymers in the dementia familial encephalopathy with neuroserpin inclusion bodies. J Biol Chem 2005 Apr 8;280(14):13735-41.

(60) Miranda E, Romisch K, Lomas DA. Mutants of neuroserpin that cause dementia accumulate as polymers within the endoplasmic reticulum. J Biol Chem 2004 Jul 2;279(27):28283-91.

(61) Miranda E, MacLeod I, Davies MJ, Perez J, Romisch K, Crowther DC, et al. The intracellular accumulation of polymeric neuroserpin explains the severity of the dementia FENIB. Hum Mol Genet 2008 Jun 1;17(11):1527-39.

(62) Malhotra JD, Kaufman RJ. The endoplasmic reticulum and the unfolded protein response. Seminars in Cell & Developmental Biology 2007 Dec;18(6):716-31.

(63) Oyadomari S, Mori M. Roles of CHOP//GADD153 in endoplasmic reticulum stress. Cell Death Differ 2003 Dec 19;11(4):381-9.

(64) Bertolotti A, Zhang Y, Hendershot LM, Harding HP, Ron D. Dynamic interaction of BiP and ER stress transducers in the unfolded-protein response. Nat Cell Biol 2000 Jun;2(6):326-32.

(65) Morl K, Ma W, Gething MJ, Sambrook J. A transmembrane protein with a cdc2+/CDC28-related kinase activity is required for signaling from the ER to the nucleus. Cell 1993 Aug 27;74(4):743-56.

(66) Cox JS, Walter P. A Novel Mechanism for Regulating Activity of a Transcription Factor That Controls the Unfolded Protein Response. Cell 1996 Nov 1;87(3):391-404.

(67) Haze K, Yoshida H, Yanagi H, Yura T, Mori K. Mammalian Transcription Factor ATF6 Is Synthesized as a Transmembrane Protein and Activated by Proteolysis in Response to Endoplasmic Reticulum Stress. Mol Biol Cell 1999 Nov 1;10(11):3787-99.

(68) Harding HP, Zhang Y, Bertolotti A, Zeng H, Ron D. Perk is essential for translational regulation and cell survival during the unfolded protein response. Mol Cell 2000 May;5(5):897-904.

(69) Harding HP, Novoa I, Zhang Y, Zeng H, Wek R, Schapira M, et al. Regulated Translation Initiation Controls Stress-Induced Gene Expression in Mammalian Cells. Molecular Cell 2000 Nov;6(5):1099-108.

(70) Pahl HL, Sester M, Burgert HG, Baeuerle PA. Activation of transcription factor NF-kappaB by the adenovirus E3/19K protein requires its ER retention. J Cell Biol 1996 Feb;132(4):511-22.

(71) Pahl HL. Signal transduction from the endoplasmic reticulum to the cell nucleus. Physiol Rev 1999 Jul;79(3):683-701.

(72) Deng J, Lu PD, Zhang Y, Scheuner D, Kaufman RJ, Sonenberg N, et al. Translational Repression Mediates Activation of Nuclear Factor Kappa B by Phosphorylated Translation Initiation Factor 2. Mol Cell Biol 2004 Dec 1;24(23):10161-8.

(73) Davies MJ, Miranda E, Roussel BD, Kaufman RJ, Marciniak SJ, Lomas DA. Neuroserpin polymers activate NF-kappaB by a calcium signalling pathway that is independent of the unfolded protein response. J Biol Chem 2009 May 7.

(74) Mattson MP, Meffert MK. Roles for NF-kappaB in nerve cell survival, plasticity, and disease. Cell Death Differ 2006 May;13(5):852-60.

(75) Vembar SS, Brodsky JL. One step at a time: endoplasmic reticulum-associated degradation. Nat Rev Mol Cell Biol 2008 Dec;9(12):944-57.

(76) Klionsky DJ, Ohsumi Y. Vacuolar import of proteins and organelles from the cytoplasm. Annual Review of Cell and Developmental Biology 1999 Nov 1;15(1):1-32.

(77) Maiuri MC, Zalckvar E, Kimchi A, Kroemer G. Self-eating and self-killing: crosstalk between autophagy and apoptosis. Nat Rev Mol Cell Biol 2007 Sep;8(9):741-52.

(78) Kroeger H, Miranda E, MacLeod I, Perez J, Crowther DC, Marciniak SJ, et al. Endoplasmic reticulum-associated degradation (ERAD) and autophagy cooperate to degrade polymerogenic mutant serpins. J Biol Chem 2009 Aug 21;284(34):22793-802.

(79) Galliciotti G, Glatzel M, Kinter J, Kozlov SV, Cinelli P, Rulicke T, et al. Accumulation of mutant neuroserpin precedes development of clinical symptoms in familial encephalopathy with neuroserpin inclusion bodies. Am J Pathol 2007 Apr;170(4):1305-13.

(80) Takasawa A, Kato I, Takasawa K, Ishii Y, Yoshida T, Shehata MH, et al. Mutation-, aging-, and gene dosage-dependent accumulation of neuroserpin (G392E) in endoplasmic reticula and lysosomes of neurons in transgenic mice. J Biol Chem 2008 Dec 19;283(51):35606-13.

(81) Takano K, Kitao Y, Inagi R, Momoi T, Matsuyama T, Miyata T, et al. A rat model of human FENIB (familial encephalopathy with neuroserpin inclusion bodies). Biochemical and Biophysical Research Communications 2006 Aug 4;346(3):1040-7.

(82) Ohtomo S, Nangaku M, Izuhara Y, Yamada N, Dan T, Mori T, et al. The role of megsin, a serine protease inhibitor, in diabetic mesangial matrix accumulation. Kidney Int 2008 Sep;74(6):768-74.

(83) Inagi R, Nangaku M, Usuda N, Shimizu A, Onogi H, Izuhara Y, et al. Novel Serpinopathy in Rat Kidney and Pancreas Induced by Overexpression of Megsin. J Am Soc Nephrol 2005 May 1;16(5):1339-49.

(84) Pahl HL. Activators and target genes of Rel/NF-kappaB transcription factors. Oncogene 1999 Nov 22;18(49):6853-66.

(85) Green C, Brown G, Dafforn TR, Reichhart JM, Morley T, Lomas DA, et al. Drosophila necrotic mutations mirror disease-associated variants of human serpins. Development 2003 Apr;130(7):1473-8.

(86) Ishigami S, Sandkvist M, Tsui F, Moore E, Coleman TA, Lawrence DA. Identification of a novel targeting sequence for regulated secretion in the serine protease inhibitor neuroserpin. Biochem J 2007 Feb 15;402(1):25-34.

(87) Larkin MA, Blackshields G, Brown NP, Chenna R, McGettigan PA, McWilliam H, et al. Clustal W and Clustal X version 2.0. Bioinformatics 2007 Nov 1;23(21):2947-8.

(88) Huelsenbeck JP, Ronquist F, Nielsen R, Bollback JP. Bayesian Inference of Phylogeny and Its Impact on Evolutionary Biology. Science 2001 Dec 14;294(5550):2310-4.

(89) Ronquist F, Huelsenbeck JP. MrBayes 3: Bayesian phylogenetic inference under mixed models. Bioinformatics 2003 Aug 12;19(12):1572-4.

(90) Whelan S, Goldman N. A general empirical model of protein evolution derived from multiple protein families using a maximum-likelihood approach. Mol Biol Evol 2001 May;18(5):691-9.

(91) Merzlyak EM, Goedhart J, Shcherbo D, Bulina ME, Shcheglov AS, Fradkov AF, et al. Bright monomeric red fluorescent protein with an extended fluorescence lifetime. Nat Methods 2007 Jul;4(7):555-7.

(92) Denault JB, Bissonnette L, Longprθ JM, Charest G, Lavigne P, Leduc R. Ectodomain shedding of furin: kinetics and role of the cysteine-rich region. FEBS Letters 2002 Sep 11;527(1-3):309-14.

(93) Huang DW, Sherman BT, Lempicki RA. Systematic and integrative analysis of large gene lists using DAVID bioinformatics resources. Nat Protocols 2008 Dec;4(1):44-57.

(94) Schmittgen TD, Livak KJ. Analyzing real-time PCR data by the comparative C(T) method. Nat Protoc 2008;3(6):1101-8.

(95) Reichhart JM. Tip of another iceberg: Drosophila serpins. Trends in Cell Biology 2005 Dec;15(12):659-65.

(96) Schweizer J, Bowden PE, Coulombe PA, Langbein L, Lane EB, Magin TM, et al. New consensus nomenclature for mammalian keratins. The Journal of Cell Biology 2006 Jul 17;174(2):169-74.

(97) Mertsch S, Schurgers L, Weber K, Paulus W, Senner V. Matrix gla protein (MGP): an overexpressed and migration-promoting mesenchymal component in glioblastoma. BMC Cancer 2009;9(1):302.

(98) Cabral A, Voskamp P, Cleton-Jansen AM, South A, Nizetic D, Backendorf C. Structural Organization and Regulation of the Small Proline-rich Family of Cornified Envelope Precursors Suggest a Role in Adaptive Barrier Function. Journal of Biological Chemistry 2001 Jun 1;276(22):19231-7.

(99) Corral J, Huntington JA, Gonzalez-Conejero R, Mushunje A, Navarro M, Marco P, et al. Mutations in the shutter region of antithrombin result in formation of disulfide-linked dimers and severe venous thrombosis. J Thromb Haemost 2004 Jun;2(6):931-9.

(100) Jin L, Abrahams JP, Skinner R, Petitou M, Pike RN, Carrell RW. The anticoagulant activation of antithrombin by heparin. Proc Natl Acad Sci U S A 1997 Dec 23;94(26):14683-8.

(101) Thomas G. Furin at the cutting edge: From protein traffic to embryogenesis and disease. Nat Rev Mol Cell Biol 2002 Oct;3(10):753-66.

(102) Weissmann C, Brandt R. Mechanisms of neurodegenerative diseases: insights from live cell imaging. J Neurosci Res 2008 Feb 15;86(3):504-11.

(103) Carrell RW. Cell toxicity and conformational disease. Trends Cell Biol 2005 Nov;15(11):574-80.

(104) Gouet P, Courcelle E, Stuart DI, Metoz F. ESPript: analysis of multiple sequence alignments in PostScript. Bioinformatics 1999 Apr;15(4):305-8.

(105) Davies MJ, Lomas DA. The molecular aetiology of the serpinopathies. Int J Biochem Cell Biol 2008;40(6-7):1273-86.

(106) Chretien M, Li CH. Isolation, purification, and characterization of gamma-lipotropic hormone from sheep pituitary glands. Can J Biochem 1967 Jul;45(7):1163-74.

(107) Steiner DF, Cunningham D, Spigelman L, Aten B. Insulin biosynthesis: evidence for a precursor. Science 1967 Aug 11;157(789):697-700.

(108) Julius D, Brake A, Blair L, Kunisawa R, Thorner J. Isolation of the putative structural gene for the lysine-arginine-cleaving endopeptidase required for processing of yeast prepro-alpha-factor. Cell 1984 Jul;37(3):1075-89.

(109) Fuller RS, Brake AJ, Thorner J. Intracellular targeting and structural conservation of a prohormone-processing endoprotease. Science 1989 Oct 27;246(4929):482-6.

(110) Ven WJM, Voorberg J, Fontijn R, Pannekoek H, Ouweland AMW, Duijnhoven HLP, et al. Furin is a subtilisin-like proprotein processing enzyme in higher eukaryotes. Molecular Biology Reports 1990 Nov 1;14(4):265-75.

(111) Bresnahan PA, Leduc R, Thomas L, Thorner J, Gibson HL, Brake AJ, et al. Human fur gene encodes a yeast KEX2-like endoprotease that cleaves pro-beta-NGF in vivo. The Journal of Cell Biology 1990 Dec;111(6):2851-9.

(112) Taylor NA, Van de Ben WJ, Creemers J. Curbing activation: proprotein convertases in homeostasis and pathology. FASEB J 2003 Jul 1;17(10):1215-27.

(113) Zheng M, Streck RD, Scott RE, Seidah NG, Pintar JE. The developmental expression in rat of proteases furin, PC1, PC2, and carboxypeptidase E: implications for early maturation of proteolytic processing capacity. J Neurosci 1994 Aug 1;14(8):4656-73.

(114) Schafer MK, Day R, Cullinan WE, Chretien M, Seidah NG, Watson SJ. Gene expression of prohormone and proprotein convertases in the rat CNS: a comparative in situ hybridization analysis. J Neurosci 1993 Mar 1;13(3):1258-79.

(115) Seidah NG, Day R, Hamelin J, Gaspar A, Collard MW, Chretien M. Testicular expression of PC4 in the rat: molecular diversity of a novel germ cell-specific Kex2/subtilisin-like proprotein convertase. Mol Endocrinol 1992 Oct 1;6(10):1559-70.

(116) Seidah NG, Benjannet S, Wickham L, Marcinkiewicz J, Jasmin SpBl, Stifani S, et al. The secretory proprotein convertase neural apoptosis-regulated convertase 1 (NARC-1): Liver regeneration and neuronal differentiation. Proceedings of the National Academy of Sciences of the United States of America 2003 Feb 4;100(3):928-33.

(117) Anderson ED, Molloy SS, Jean F, Fei H, Shimamura S, Thomas G. The Ordered and Compartment-specific Autoproteolytic Removal of the Furin Intramolecular Chaperone Is Required for Enzyme Activation. Journal of Biological Chemistry 2002 Apr 12;277(15):12879-90.

(118) Creemers J, Vey M, Sch+ñfer W, Ayoubi TAY, Roebroek AJM, Klenk HD, et al. Endoproteolytic Cleavage of Its Propeptide Is a Prerequisite for Efficient Transport of Furin Out of the Endoplasmic Reticulum. Journal of Biological Chemistry 1995 Feb 10;270(6):2695-702.

(119) Zhou A, Martin S, Lipkind G, LaMendola J, Steiner DF. Regulatory Roles of the P Domain of the Subtilisin-like Prohormone Convertases. Journal of Biological Chemistry 1998 May 1;273(18):11107-14.

(120) Elagoz A, Benjannet S, Mammarbassi A, Wickham L, Seidah NG. Biosynthesis and Cellular Trafficking of the Convertase SKI-1/S1P. Journal of Biological Chemistry 2002 Mar 29;277(13):11265-75.

(121) Molloy SS, Anderson ED, Jean F, Thomas G. Bi-cycling the furin pathway: from TGN localization to pathogen activation and embryogenesis. Trends in Cell Biology 1999 Jan 1;9(1):28-35.

(122) Seidah NG, Mayer G, Zaid A, Rousselet E, Nassoury N, Poirier S, et al. The activation and physiological functions of the proprotein convertases. The International Journal of Biochemistry & Cell Biology 8 A.D. Jul;40(6-7):1111-25.

(123) Benjannet S, Rhainds D, Essalmani R, Mayne J, Wickham L, Jin W, et al. NARC-1/PCSK9 and Its Natural Mutants. Journal of Biological Chemistry 2004 Nov 19;279(47):48865-75.

(124) Seidah NG, Hamelin J, Mamarbachi M, Dong W, Tardos H, Mbikay M, et al. cDNA structure, tissue distribution, and chromosomal localization of rat PC7, a novel mammalian proprotein convertase closest to yeast kexin-like proteinases. Proceedings of the National Academy of Sciences of the United States of America 1996 Apr 16;93(8):3388-93.

(125) Nour N, Mayer G, Mort JS, Salvas A, Mbikay M, Morrison CJ, et al. The Cysteine-rich Domain of the Secreted Proprotein Convertases PC5A and PACE4 Functions as a Cell Surface Anchor and Interacts with Tissue Inhibitors of Metalloproteinases. Mol Biol Cell 2005 Nov 1;16(11):5215-26.

(126) Benjannet S, Rondeau N, Paquet L, Boudreault A, Lazure C, Chretien M, et al. Comparative biosynthesis, covalent post-translational modifications and efficiency of prosegment cleavage of the prohormone convertases PC1 and PC2: glycosylation, sulphation and identification of the intracellular site of prosegment cleavage of PC1 and PC2. Biochem J 1993 Sep 15;294 (Pt 3):735-43.

(127) Pullikotil P, Benjannet S, Mayne J, Seidah NG. The Proprotein Convertase SKI-1/S1P. Journal of Biological Chemistry 2007 Sep 14;282(37):27402-13.

(128) Bass J, Turck C, Rouard M, Steiner DF. Furin-mediated processing in the early secretory pathway: sequential cleavage and degradation of misfolded insulin receptors. Proc Natl Acad Sci U S A 2000 Oct 24;97(22):11905-9.

(129) Silvestri L, Pagani A, Camaschella C. Furin-mediated release of soluble hemojuvelin: a new link between hypoxia and iron homeostasis. Blood 2008 Jan 15;111(2):924-31.

(130) Walker JA, Molloy SS, Thomas G, Sakaguchi T, Yoshida T, Chambers TM, et al. Sequence specificity of furin, a proprotein-processing endoprotease, for the hemagglutinin of a virulent avian influenza virus. J Virol 1994 Feb 1;68(2):1213-8.

(131) Jean F, Boudreault A, Basak A, Seidah NG, Lazure C. Fluorescent peptidyl substrates as an aid in studying the substrate specificity of human prohormone convertase PC1 and human furin and designing a potent irreversible inhibitor. J Biol Chem 1995 Aug 18;270(33):19225-31.

(132) Molloy SS, Bresnahan PA, Leppla SH, Klimpel KR, Thomas G. Human furin is a calcium-dependent serine endoprotease that recognizes the sequence Arg-X-X-Arg and efficiently cleaves anthrax toxin protective antigen. Journal of Biological Chemistry 1992 Aug 15;267(23):16396-402.

(133) Pasquato A, Pullikotil P, Asselin MC, Vacatello M, Paolillo L, Ghezzo F, et al. The proprotein convertase SKI-1/S1P. In vitro analysis of Lassa virus glycoprotein-derived

substrates and ex vivo validation of irreversible peptide inhibitors. J Biol Chem 2006 Aug 18;281(33):23471-81.

(134) Roebroek AJ, Umans L, Pauli IG, Robertson EJ, van Leuven F, Van de Ven WJ, et al. Failure of ventral closure and axial rotation in embryos lacking the proprotein convertase Furin. Development 1998 Dec 15;125(24):4863-76.

(135) Essalmani R, Hamelin J, Marcinkiewicz J, Chamberland A, Mbikay M, Chretien M, et al. Deletion of the Gene Encoding Proprotein Convertase 5/6 Causes Early Embryonic Lethality in the Mouse. Mol Cell Biol 2006 Jan 1;26(1):354-61.

(136) Yang J, Goldstein JL, Hammer RE, Moon YA, Brown MS, Horton JD. Decreased lipid synthesis in livers of mice with disrupted Site-1 protease gene. Proceedings of the National Academy of Sciences of the United States of America 2001 Nov 20;98(24):13607-12.

(137) Constam DB, Robertson EJ. SPC4/PACE4 regulates a TGFb signaling network during axis formation. Genes & Development 2000 May 1;14(9):1146-55.

(138) Zhu X, Zhou A, Dey A, Norrbom C, Carroll R, Zhang C, et al. Disruption of PC1/3 expression in mice causes dwarfism and multiple neuroendocrine peptide processing defects. Proceedings of the National Academy of Sciences of the United States of America 2002 Aug 6;99(16):10293-8.

(139) Furuta M, Yano H, Zhou A, Rouill+® Y, Holst JJ, Carroll R, et al. Defective prohormone processing and altered pancreatic islet morphology in mice lacking active SPC2. Proceedings of the National Academy of Sciences of the United States of America 1997 Jun 24;94(13):6646-51.

(140) Mbikay M, Tadros H, Ishida N, Lerner CP, De Lamirande E, Chen A, et al. Impaired fertility in mice deficient for the testicular germ-cell protease PC4. Proceedings of the National Academy of Sciences of the United States of America 1997 Jun 24;94(13):6842-6.

(141) Rashid S, Curtis DE, Garuti R, Anderson NN, Bashmakov Y, Ho YK, et al. Decreased plasma cholesterol and hypersensitivity to statins in mice lacking Pcsk9. Proceedings of the National Academy of Sciences of the United States of America 2005 Apr 12;102(15):5374-9.

(142) Constam DB, Calfon M, Robertson EJ. SPC4, SPC6, and the novel protease SPC7 are coexpressed with bone morphogenetic proteins at distinct sites during embryogenesis. The Journal of Cell Biology 1996 Jul;134(1):181-91.

(143) Dunker N, Krieglstein K. Targeted mutations of transforming growth factor-beta genes reveal important roles in mouse development and adult homeostasis. Eur J Biochem 2000 Dec;267(24):6982-8.

(144) Cross JC, Simmons DG, Watson ED. Chorioallantoic morphogenesis and formation of the placental villous tree. Ann N Y Acad Sci 2003 May;995:84-93.

(145) Roebroek AJM, TAYLOR NA, Louagie E, Pauli I, Smeijers L, Snellinx A, et al. Limited Redundancy of the Proprotein Convertase Furin in Mouse Liver. Journal of Biological Chemistry 2004 Dec 17;279(51):53442-50.

(146) Scamuffa N, Calvo F, Chretien M, Seidah NG, Khatib AM. Proprotein convertases: lessons from knockouts. FASEB J 2006 Oct 1;20(12):1954-63.

(147) Klimpel KR, Molloy SS, Thomas G, Leppla SH. Anthrax toxin protective antigen is activated by a cell surface protease with the sequence specificity and catalytic properties of furin. Proceedings of the National Academy of Sciences of the United States of America 1992 Nov 1;89(21):10277-81.

(148) Abrami L, Fivaz M, Decroly E, Seidah NG, Jean F, Thomas G, et al. The Pore-forming Toxin Proaerolysin Is Activated by Furin. Journal of Biological Chemistry 1998 Dec 4;273(49):32656-61.

(149) Gordon VM, Benz R, Fujii K, Leppla SH, Tweten RK. Clostridium septicum alpha-toxin is proteolytically activated by furin. Infect Immun 1997 Oct 1;65(10):4130-4.

(150) Moulard M, Hallenberger S, Garten W, Klenk HD. Processing and routage of HIV glycoproteins by furin to the cell surface. Virus Research 1999 Mar;60(1):55-65.

(151) Basak A, Zhong M, Munzer JS, Chretien M, Seidah NG. Implication of the proprotein convertases furin, PC5 and PC7 in the cleavage of surface glycoproteins of Hong Kong, Ebola and respiratory syncytial viruses: a comparative analysis with fluorogenic peptides. Biochem J 2001 Feb 1;353(3):537-45.

(152) Nakayama K. Furin: a mammalian subtilisin/Kex2p-like endoprotease involved in processing of a wide variety of precursor proteins. Biochem J 1997 Nov 1;327(3):625-35.

(153) Stadler K, Allison SL, Schalich J, Heinz FX. Proteolytic activation of tick-borne encephalitis virus by furin. J Virol 1997 Nov 1;71(11):8475-81.

(154) Horimoto T, Nakayama K, Smeekens SP, Kawaoka Y. Proprotein-processing endoproteases PC6 and furin both activate hemagglutinin of virulent avian influenza viruses. J Virol 1994 Sep 1;68(9):6074-8.

(155) Zybert IA, van der Ende-Metselaar H, Wilschut J, Smit JM. Functional importance of dengue virus maturation: infectious properties of immature virions. J Gen Virol 2008 Dec 1;89(12):3047-51.

(156) Moesker B, Rodenhuis-Zybert IA, Meijerhof T, Wilschut J, Smit JM. Characterization of the functional requirements of West Nile virus membrane fusion. J Gen Virol 2010 Feb 1;91(2):389-93.

(157) Bassi DE, Mahloogi H, Al-Saleem L, Lopez De CR, Ridge JA, Klein-Szanto AJ. Elevated furin expression in aggressive human head and neck tumors and tumor cell lines. Mol Carcinog 2001 Aug;31(4):224-32.

(158) Cheng M, Watson PH, Paterson JA, Seidah N, Chretien M, Shiu RP. Pro-protein convertase gene expression in human breast cancer. Int J Cancer 1997 Jun 11;71(6):966-71.

(159) Mbikay M, Sirois F, Yao J, Seidah NG, Chretien M. Comparative analysis of expression of the proprotein convertases furin, PACE4, PC1 and PC2 in human lung tumours. Br J Cancer 1997;75(10):1509-14.

(160) Leitlein J, Aulwurm S, Waltereit R, Naumann U, Wagenknecht B, Garten W, et al. Processing of Immunosuppressive Pro-TGF-{{beta}}1,2 by Human Glioblastoma Cells Involves Cytoplasmic and Secreted Furin-Like Proteases. J Immunol 2001 Jun 15;166(12):7238-43.

(161) Liu B, Amizuka N, Goltzman D, Rabbani SA. Inhibition of processing of parathyroid hormone-related peptide by anti-sense furin: effect in vitro and in vivo on rat Leydig (H-500) tumor cells. Int J Cancer 1995 Oct 9;63(2):276-81.

(162) De VL, Declercq J, Rosas GG, Van DB, Roebroek A, Vermorken F, et al. MMTV-cre-mediated fur inactivation concomitant with PLAG1 proto-oncogene activation delays salivary gland tumorigenesis in mice. Int J Oncol 2008 May;32(5):1073-83.

(163) Lopez De Cicco R, Bassi DE, Zucker S, Seidah NG, Klein-Szanto AJP. Human Carcinoma Cell Growth and Invasiveness Is Impaired by the Propeptide of the Ubiquitous Proprotein Convertase Furin. Cancer Res 2005 May 15;65(10):4162-71.

(164) Mercapide J, Lopez De CR, Bassi DE, Castresana JS, Thomas G, Klein-Szanto AJ. Inhibition of furin-mediated processing results in suppression of astrocytoma cell growth and invasiveness. Clin Cancer Res 2002 Jun;8(6):1740-6.

(165) Scamuffa N, Siegfried G, Bontemps Y, Ma L, Basak A, Cherel G, et al. Selective inhibition of proprotein convertases represses the metastatic potential of human colorectal tumor cells. J Clin Invest 2008 Jan 2;118(1):352-63.

(166) Bacac M, Stamenkovic I. Metastatic Cancer Cell. Annual Review of Pathology: Mechanisms of Disease 2008 Feb 1;3(1):221-47.

(167) Derynck R, Akhurst RJ, Balmain A. TGF-[beta] signaling in tumor suppression and cancer progression. Nat Genet 2001 Oct;29(2):117-29.

(168) Scandura JM, Boccuni P, Massague J, Nimer SD. Transforming growth factor b induced cell cycle arrest of human hematopoietic cells requires p57KIP2 up-regulation. Proceedings of the National Academy of Sciences of the United States of America 2004 Oct 19;101(42):15231-6.

(169) Yagi K, Furuhashi M, Aoki H, Goto D, Kuwano H, Sugamura K, et al. c-myc Is a Downstream Target of the Smad Pathway . Journal of Biological Chemistry 2002 Jan 4;277(1):854-61.

(170) Jakowlew SB. Transforming growth factor-beta in cancer and metastasis. Cancer Metastasis Rev 2006 Sep;25(3):435-57.

(171) Battegay EJ, Raines EW, Seifert RA, Bowen-Pope DF, Ross R. TGF-[beta] induces bimodal proliferation of connective tissue cells via complex control of an autocrine PDGF loop. Cell 1990 Nov 2;63(3):515-24.

(172) Seifert RA, Coats SA, Raines EW, Ross R, Bowen-Pope DF. Platelet-derived growth factor (PDGF) receptor alpha-subunit mutant and reconstituted cell lines demonstrate that transforming growth factor-beta can be mitogenic through PDGF A-chain-dependent and -independent pathways. Journal of Biological Chemistry 1994 May 13;269(19):13951-5.

(173) Bruna A, Darken RS, Rojo F, Oca±a A, Pe±uelas S, Arias A, et al. High TGF[beta]-Smad Activity Confers Poor Prognosis in Glioma Patients and Promotes Cell Proliferation Depending on the Methylation of the PDGF-B Gene. Cancer Cell 2007 Feb 13;11(2):147-60.

(174) Strutz F, Zeisberg M, Renziehausen A, Raschke B, Becker V, Van Kooten C, et al. TGF-[b]1 induces proliferation in human renal fibroblasts via induction of basic fibroblast growth factor (FGF-2). Kidney Int 2001 Feb;59(2):579-92.

(175) Sehgal I, Thompson TC. Novel regulation of type IV collagenase (matrix metalloproteinase-9 and -2) activities by transforming growth factor-beta1 in human prostate cancer cell lines. Mol Biol Cell 1999 Feb;10(2):407-16.

(176) Sanchez-Elsner T, Botella LM, Velasco B, Corb-¦¦ü A, Attisano L, Bernab+®u C. Synergistic Cooperation between Hypoxia and Transforming Growth Factor b Pathways on Human Vascular Endothelial Growth Factor Gene Expression. Journal of Biological Chemistry 2001 Oct 19;276(42):38527-35.

(177) Siegfried G, Khatib AM, Benjannet S, Chretien M, Seidah NG. The Proteolytic Processing of Pro-Platelet-derived Growth Factor-A at RRKR86 by Members of the Proprotein Convertase Family Is Functionally Correlated to Platelet-derived Growth Factor-A-induced Functions and Tumorigenicity. Cancer Res 2003 Apr 1;63(7):1458-63.

(178) Pollak M. Insulin and insulin-like growth factor signalling in neoplasia. Nat Rev Cancer 2008 Dec;8(12):915-28.

(179) Long L, Navab R, Brodt P. Regulation of the Mr 72,000 type IV collagenase by the type I insulin-like growth factor receptor. Cancer Res 1998 Aug 1;58(15):3243-7.

(180) Zhang D, Brodt P. Type 1 insulin-like growth factor regulates MT1-MMP synthesis and tumor invasion via PI 3-kinase//Akt signaling. Oncogene 0 AD;22(7):974-82.

(181) Lehmann M, Andre F, Bellan C, Remacle-Bonnet M, Garrouste F, Parat F, et al. Deficient Processing and Activity of Type I Insulin-Like Growth Factor Receptor in the Furin-Deficient LoVo-C5 Cells. Endocrinology 1998 Sep 1;139(9):3763-71.

(182) Duguay SJ, Milewski WM, Young BD, Nakayama K, Steiner DF. Processing of Wild-type and Mutant Proinsulin-like Growth Factor-IA by Subtilisin-related Proprotein Convertases. Journal of Biological Chemistry 1997 Mar 7;272(10):6663-70.

(183) Murakami K, Sakukawa R, Ikeda T, Matsuura T, Hasumura S, Nagamori S, et al. Invasiveness of hepatocellular carcinoma cell lines: contribution of membrane-type 1 matrix metalloproteinase. Neoplasia 1999 Nov;1(5):424-30.

(184) Sato H, Kinoshita T, Takino T, Nakayama K, Seiki M. Activation of a recombinant membrane type 1-matrix metalloproteinase (MT1-MMP) by furin and its interaction with tissue inhibitor of metalloproteinases (TIMP)-2. FEBS Letters 1996 Sep 9;393(1):101-4.

(185) Pei D, Weiss SJ. Transmembrane-deletion Mutants of the Membrane-type Matrix Metalloproteinase-1 Process Progelatinase A and Express Intrinsic Matrix-degrading Activity. Journal of Biological Chemistry 1996 Apr 12;271(15):9135-40.

(186) Sarac MS, Cameron A, Lindberg I. The Furin Inhibitor Hexa-D-Arginine Blocks the Activation of Pseudomonas aeruginosa Exotoxin A In Vivo. Infect Immun 2002 Dec 1;70(12):7136-9.

(187) Jiao GS, Cregar L, Wang J, Millis SZ, Tang C, O'Malley S, et al. Synthetic small molecule furin inhibitors derived from 2,5-dideoxystreptamine. Proc Natl Acad Sci U S A 2006 Dec 26;103(52):19707-12.

(188) Coppola JM, Bhojani MS, Ross BD, Rehemtulla A. A small-molecule furin inhibitor inhibits cancer cell motility and invasiveness. Neoplasia 2008 Apr;10(4):363-70.

(189) Zhong M, Munzer JS, Basak A, Benjannet S, Mowla SJ, Decroly E, et al. The Prosegments of Furin and PC7 as Potent Inhibitors of Proprotein Convertases. Journal of Biological Chemistry 1999 Nov 26;274(48):33913-20.

(190) Basak A, Lazure C. Synthetic peptides derived from the prosegments of proprotein convertase 1/3 and furin are potent inhibitors of both enzymes. Biochem J 2003 Jul 1;373(Pt 1):231-9.

(191) Boudreault A, Gauthier D, Lazure C. Proprotein Convertase PC1/3-related Peptides Are Potent Slow Tight-binding Inhibitors of Murine PC1/3 and Hfurin. Journal of Biological Chemistry 1998 Nov 20;273(47):31574-80.

(192) Cameron A, Appel J, Houghten RA, Lindberg I. Polyarginines Are Potent Furin Inhibitors. Journal of Biological Chemistry 2000 Nov 24;275(47):36741-9.

(193) Angliker H. Synthesis of Tight Binding Inhibitors and Their Action on the Proprotein-Processing Enzyme Furin. Journal of Medicinal Chemistry 1995 Sep 1;38(20):4014-8.

(194) Villemure M, Fournier A, Gauthier D, Rabah N, Wilkes BC, Lazure C. Barley Serine Proteinase Inhibitor 2-Derived Cyclic Peptides as Potent and Selective Inhibitors of Convertases PC1/3 and Furin. Biochemistry 2003 Jul 23;42(32):9659-68.

(195) Shiryaev SA, Remacle AG, Ratnikov BI, Nelson NA, Savinov AY, Wei G, et al. Targeting host cell furin proprotein convertases as a therapeutic strategy against bacterial toxins and viral pathogens. J Biol Chem 2007 Jul 20;282(29):20847-53.

(196) Basak A. Inhibitors of proprotein convertases. J Mol Med 2005 Nov;83(11):844-55.

(197) Lu W, Zhang W, Molloy SS, Thomas G, Ryan K, Chiang Y, et al. Arg15-Lys17-Arg18 turkey ovomucoid third domain inhibits human furin. Journal of Biological Chemistry 1993 Jul 15;268(20):14583-5.

(198) Van Rompaey L, Ayoubi T, Van De Ven W, Marynen P. Inhibition of intracellular proteolytic processing of soluble proproteins by an engineered alpha 2-macroglobulin containing a furin recognition sequence in the bait region. Biochem J 1997 Sep 1;326(2):507-14.

(199) Komiyama T, Fuller RS. Engineered Eglin c Variants Inhibit Yeast and Human Proprotein Processing Proteases, Kex2 and Furin. Biochemistry 2000 Nov 10;39(49):15156-65.

(200) Anderson ED, Thomas L, Hayflick JS, Thomas G. Inhibition of HIV-1 gp160-dependent membrane fusion by a furin-directed alpha 1-antitrypsin variant. Journal of Biological Chemistry 1993 Nov 25;268(33):24887-91.

(201) Jean F, Stella K, Thomas L, Liu G, Xiang Y, Reason AJ, et al. alpha1-Antitrypsin Portland, a bioengineered serpin highly selective for furin: application as an antipathogenic agent. Proc Natl Acad Sci U S A 1998 Jun 23;95(13):7293-8.

(202) Benjannet S, Savaria D, Laslop A, Munzer JS, Chretien M, Marcinkiewicz M, et al. A1-Antitrypsin Portland Inhibits Processing of Precursors Mediated by Proprotein Convertases Primarily within the Constitutive Secretory Pathway. Journal of Biological Chemistry 1997 Oct 17;272(42):26210-8.

(203) Jean F, Thomas L, Molloy SS, Liu G, Jarvis MA, Nelson JA, et al. A protein-based therapeutic for human cytomegalovirus infection. Proc Natl Acad Sci U S A 2000 Mar 14;97(6):2864-9.

(204) Bassi DE, Lopez De Cicco R, Mahloogi H, Zucker S, Thomas G, Klein-Szanto AJP. Furin inhibition results in absent or decreased invasiveness and tumorigenicity of human cancer cells. Proceedings of the National Academy of Sciences of the United States of America 2001 Aug 28;98(18):10326-31.

(205) Khatib AM, Siegfried G+, Prat A, Luis J, Chr+®tien M, Metrakos P, et al. Inhibition of Proprotein Convertases Is Associated with Loss of Growth and Tumorigenicity of HT-29 Human Colon Carcinoma Cells. Journal of Biological Chemistry 2001 Aug 17;276(33):30686-93.

(206) Lapierre M, Siegfried G, Scamuffa N, Bontemps Y, Calvo F, Seidah NG, et al. Opposing Function of the Proprotein Convertases Furin and PACE4 on Breast Cancer Cells' Malignant Phenotypes: Role of Tissue Inhibitors of Metalloproteinase-1. Cancer Res 2007 Oct 1;67(19):9030-4.

(207) Dahlen JR, Jean F, Thomas G, Foster DC, Kisiel W. Inhibition of Soluble Recombinant Furin by Human Proteinase Inhibitor 8. Journal of Biological Chemistry 1998 Jan 23;273(4):1851-4.

(208) Dahlen JR, Foster DC, Kisiel W. The Inhibitory Specificity of Human Proteinase Inhibitor 8 Is Expanded through the Use of Multiple Reactive Site Residues. Biochemical and Biophysical Research Communications 1998 Mar 6;244(1):172-7.

(209) Norden AD, Drappatz J, Wen PY. Antiangiogenic therapies for high-grade glioma. Nat Rev Neurol 2009 Nov;5(11):610-20.

(210) Stupp R, Hegi ME, Mason WP, van den Bent MJ, Taphoorn MJ, Janzer RC, et al. Effects of radiotherapy with concomitant and adjuvant temozolomide versus radiotherapy alone on survival in glioblastoma in a randomised phase III study: 5-year analysis of the EORTC-NCIC trial. Lancet Oncol 2009 May;10(5):459-66.

(211) Tate MC, Aghi MK. Biology of Angiogenesis and Invasion in Glioma. Neurotherapeutics 2009 Jul;6(3):447-57.

(212) Denison MS, Nagy SR. Activation of the aryl hydrocarbon receptor by structurally diverse exogenous and endogenous chemicals. Annual Review of Pharmacology and Toxicology 2003 Apr 1;43(1):309-34.

(213) Grandori C, Cowley SM, James LP, Eisenman RN. The Myc/Max/Mad network and the transcriptional control of cell behavior. Annual Review of Cell and Developmental Biology 2000 Nov 1;16(1):653-99.

(214) Lim LP, Lau NC, Garrett-Engele P, Grimson A, Schelter JM, Castle J, et al. Microarray analysis shows that some microRNAs downregulate large numbers of target mRNAs. Nature 2005 Feb 17;433(7027):769-73.

(215) Silber J, Lim D, Petritsch C, Persson A, Maunakea A, Yu M, et al. miR-124 and miR-137 inhibit proliferation of glioblastoma multiforme cells and induce differentiation of brain tumor stem cells. BMC Medicine 2008;6(1):14.

(216) Dyson N. The regulation of E2F by pRB-family proteins. Genes & Development 1998 Aug 1;12(15):2245-62.

(217) Komata T, Kanzawa T, Takeuchi H, Germano IM, Schreiber M, Kondo Y, et al. Antitumour effect of cyclin-dependent kinase inhibitors (p16INK4A, p18INK4C, p19INK4D, p21WAF1//CIP1 and p27KIP1) on malignant glioma cells. Br J Cancer 0 AD;88(8):1277-80.

(218) Kristjansdottirk K, Rudolph J. Cdc25 Phosphatases and Cancer. Chemistry & Biology 2004 Aug;11(8):1043-51.

(219) Lei M, Tye BK. Initiating DNA synthesis: from recruiting to activating the MCM complex. J Cell Sci 2001 Apr;114(Pt 8):1447-54.

(220) Strunnikov AV, Jessberger R. Structural maintenance of chromosomes (SMC) proteins: conserved molecular properties for multiple biological functions. Eur J Biochem 1999 Jul;263(1):6-13.

(221) Hayward DG, Fry AM. Nek2 kinase in chromosome instability and cancer. Cancer Letters 2006 Jun 18;237(2):155-66.

(222) Zeng WF, Navaratne K, Prayson RA, Weil RJ. Aurora B expression correlates with aggressive behaviour in glioblastoma multiforme. J Clin Pathol 2007 Feb;60(2):218-21.

(223) Dickson MA, Schwartz GK. Development of cell-cycle inhibitors for cancer therapy. Curr Oncol 2009 Mar;16(2):36-43.

(224) Friedl P, Wolf K. Tumour-cell invasion and migration: diversity and escape mechanisms. Nat Rev Cancer 2003 May;3(5):362-74.

(225) Rangaswami H, Bulbule A, Kundu GC. Osteopontin: role in cell signaling and cancer progression. Trends in Cell Biology 2006 Feb;16(2):79-87.

(226) Schreiner A, Ruonala M, Jakob V, Suthaus J, Boles E, Wouters F, et al. Junction Protein Shrew-1 Influences Cell Invasion and Interacts with Invasion-promoting Protein CD147. Mol Biol Cell 2007 Apr 1;18(4):1272-81.

(227) McDonald JM, Dunlap S, Cogdell D, Dunmire V, Wei Q, Starzinski-Powitz A, et al. The SHREW1 gene, frequently deleted in oligodendrogliomas, functions to inhibit cell adhesion and migration. Cancer Biol Ther 2006 Mar;5(3):300-4.

(228) Geng Y, McQuillan D, Roughley PJ. SLRP interaction can protect collagen fibrils from cleavage by collagenases. Matrix Biology 2006 Oct;25(8):484-91.

(229) Stander M, Naumann U, Dumitrescu L, Heneka M, Loschmann P, Gulbins E, et al. Decorin gene transfer-mediated suppression of TGF-beta synthesis abrogates experimental malignant glioma growth in vivo. Gene Ther 1998 Sep;5(9):1187-94.

(230) Reed CC, Gauldie J, Iozzo RV. Suppression of tumorigenicity by adenovirus-mediated gene transfer of decorin. Oncogene 2002 May 23;21(23):3688-95.

(231) Sawamura T, Kume N, Aoyama T, Moriwaki H, Hoshikawa H, Aiba Y, et al. An endothelial receptor for oxidized low-density lipoprotein. Nature 1997 Mar 6;386(6620):73-7.

(232) Senner V, Sturm A, Baur I, Schrell UHM, Distel L, Paulus W. CD24 Promotes Invasion of Glioma Cells In Vivo. Journal of Neuropathology & Experimental Neurology 1999;58(8).

(233) Silverstein RL, Febbraio M. CD36, a Scavenger Receptor Involved in Immunity, Metabolism, Angiogenesis, and Behavior. Sci Signal 2009 May 26;2(72):re3.

(234) McDonough WS, Tran NL, Berens ME. Regulation of glioma cell migration by serine-phosphorylated P311. Neoplasia 2005 Sep;7(9):862-72.

(235) Camby I, Nagy N, Lopes MB, Schafer BW, Maurage CA, Ruchoux MM, et al. Supratentorial pilocytic astrocytomas, astrocytomas, anaplastic astrocytomas and glioblastomas are characterized by a differential expression of S100 proteins. Brain Pathol 1999 Jan;9(1):1-19.

(236) Li ZH, Bresnick AR. The S100A4 Metastasis Factor Regulates Cellular Motility via a Direct Interaction with Myosin-IIA. Cancer Res 2006 May 15;66(10):5173-80.

(237) Schmidt-Hansen B, Ornas D, Grigorian M, Klingelhofer J, Tulchinsky E, Lukanidin E, et al. Extracellular S100A4(mts1) stimulates invasive growth of mouse endothelial cells and modulates MMP-13 matrix metalloproteinase activity. Oncogene 2004 May 3;23(32):5487-95.

(238) Bjornland K, Winberg JO, Odegaard OT, Hovig E, Loennechen T, Aasen AO, et al. S100A4 Involvement in Metastasis. Cancer Res 1999 Sep 15;59(18):4702-8.

(239) Sternlicht MD, Lochter A, Sympson CJ, Huey B, Rougier JP, Gray JW, et al. The Stromal Proteinase MMP3/Stromelysin-1 Promotes Mammary Carcinogenesis. Cell 1999 Jul 23;98(2):137-46.

(240) Cao J, Rehemtulla A, Pavlaki M, Kozarekar P, Chiarelli C. Furin Directly Cleaves proMMP-2 in the trans-Golgi Network Resulting in a Nonfunctioning Proteinase. Journal of Biological Chemistry 2005 Mar 25;280(12):10974-80.

(241) Reith A, Rucklidge GJ. Invasion of brain tissue by primary glioma: Evidence for the involvement of urokinase-type plasminogen activator as an activator of type iv collagenase. Biochemical and Biophysical Research Communications 1992 Jul 15;186(1):348-54.

(242) Boatright KM, Salvesen GS. Mechanisms of caspase activation. Current Opinion in Cell Biology 2003 Dec;15(6):725-31.

(243) Kuo TY, Hong CJ, Hsueh YP. Bcl11A/CTIP1 regulates expression of DCC and MAP1b in control of axon branching and dendrite outgrowth. Molecular and Cellular Neuroscience 2009 Oct;42(3):195-207.

(244) Kurosu T, Fukuda T, Miki T, Miura O. BCL6 overexpression prevents increase in reactive oxygen species and inhibits apoptosis induced by chemotherapeutic reagents in B-cell lymphoma cells. Oncogene 0 AD;22(29):4459-68.

(245) Puthalakath H, Villunger A, O'Reilly LA, Beaumont JG, Coultas L, Cheney RE, et al. Bmf: A Proapoptotic BH3-Only Protein Regulated by Interaction with the Myosin V Actin Motor Complex, Activated by Anoikis. Science 2001 Sep 7;293(5536):1829-32.

(246) Wilson DW, Lewis MJ, Pelham HR. pH-dependent binding of KDEL to its receptor in vitro. Journal of Biological Chemistry 1993 Apr 5;268(10):7465-8.

(247) Bassi DE, Fu J, Lopez De CR, Klein-Szanto AJ. Proprotein convertases: "master switches" in the regulation of tumor growth and progression. Mol Carcinog 2005 Nov;44(3):151-61.

(248) Khatib AM, Siegfried G, Chretien M, Metrakos P, Seidah NG. Proprotein Convertases in Tumor Progression and Malignancy : Novel Targets in Cancer Therapy. Am J Pathol 2002 Jun 1;160(6):1921-35.

(249) Padua MB, Hansen PJ. Regulation of DNA synthesis and the cell cycle in human prostate cancer cells and lymphocytes by ovine uterine serpin. BMC Cell Biol 2008;9:5.

(250) Padua MB, Hansen PJ. Changes in expression of cell-cycle-related genes in PC-3 prostate cancer cells caused by ovine uterine serpin. J Cell Biochem 2009 Aug 15;107(6):1182-8.

(251) Congote LF, Temmel N. The C-terminal 26-residue peptide of serpin A1 stimulates proliferation of breast and liver cancer cells: role of protein kinase C and CD47. FEBS Lett 2004 Oct 22;576(3):343-7.

(252) Rasmussen HS, McCann PP. Matrix Metalloproteinase Inhibition as a Novel Anticancer Strategy: A Review with Special Focus on Batimastat and Marimastat. Pharmacology & Therapeutics 1997 Jul;75(1):69-75.

(253) Norden AD, Young GS, Setayesh K, Muzikansky A, Klufas R, Ross GL, et al. Bevacizumab for recurrent malignant gliomas: Efficacy, toxicity, and patterns of recurrence. Neurology 2008 Mar 4;70(10):779-87.

(254) Cheung CHA, Coumar MS, Hsieh HP, Chang JY. Aurora kinase inhibitors in preclinical and clinical testing. Expert Opinion on Investigational Drugs 2009 Apr 1;18(4):379-98.

(255) Zucker S, Cao J, Chen WT. Critical appraisal of the use of matrix metalloproteinase inhibitors in cancer treatment. Oncogene 2000 Dec 27;19(56):6642-50.

Appendix 1: Spn4A hinge mutant inhibitory studies

Rationale

To address the specific function of PC inhibition, we constructed a non-inhibitory Spn4A negative control. The inhibitory action of serpins relies on the end-to-end translocation of the protease and the insertion of the cleaved RCL into the β-sheet network. The hinge motion requires a small and non-polar moiety at position P14, which is amino acid T328 in Spn4A (Supplemental Fig. A1.1). To disrupt the loop insertion, we engineered three different point mutations to T328, changing to a negatively charged aspartic acid, a small non-polar glycine, or a positively charged lysine. We hypothesized that glycine may disrupt the inhibitory action of serpins because glycine is found in non-inhibitory maspin (Supplemental Fig. A1.1).

Methods were as described in Chapter 2: Cell lines (2.2.2), Plasmid constructs (2.2.3) and primers (Appendix 2), Recombinant adenovirus constructs and production (2.2.4), Transfection and infection conditions (2.2.5), SDS-PAGE, native PAGE, and western blot (2.2.6), Immunofluorescence (2.2.7), and Furin complex formation assay (2.2.8).

Results and Discussion

We first substituted mutations at Spn4A T328D, T328G, and T328K into Spn4A-R (Supplemental Fig. A1.2A) and transfected them into H4 neuroglioma cells for *in vitro* complex formation assays with furin. H4 cell lysates containing Spn4A WT-R or the T328G variant could form a heat and SDS-stable complex with recombinant human furin (Supplemental Fig. A1.3A). However, the amount of SDS-stable complex formed by Spn4A T328G-R is clearly less than the WT and a large buildup of cleaved Spn4A T328G-R was observed. This suggests that P14 glycine affects the inhibitory mechanism, but does not completely abolish inhibitory function. Aspartic or lysine substitutions at T328 rendered Spn4A completely non-inhibitory, as no SDS-stable complex was detected (Supplemental Fig. A1.3A). The hinge mutants likely slowed down the rate of loop insertion so the serpin follows the substrate pathway. Using immunofluorescence, we ensured that the single point mutations did not affect protein folding or cause aggregation (Supplemental Fig. A1.3B).

We further engineered the T328D mutation into the secreted Spn4A-S and both secreted and retained RFP-tagged Spn4A (Supplemental Fig. A1.2A) and tested their activities *in cellulo* using HEK293-C4 cells that overexpress FLAG-tagged furin. Transfected cells were analyzed

for complex formation by SDS-PAGE. We found that intracellularly, secreted Spn4A WT-S were found as free serpins or as complexes while T328D mutants were mostly cleaved by furin and formed no inhibitory complexes (Supplemental Fig. A1.4A). In the media, complexes were detected in both WT-S and T328D-S, and not ER-retained T328D-R. The T328D-R should not be trafficked to the extracellular space. The presence of extracellular cleavage products suggests that some Spn4A-R may have escaped the ER retention because of the loss of the C-terminus from furin cleavage. Complex and cleavage product were both detected in the secreted T328D-S variant, suggesting that uncleaved Spn4A T328D-S are trafficked to the extracellular space where it can undergo both inhibitory and substrate pathways. In comparison, the lack of intracellular EI complexes suggests that the rate of loop insertion has been compromised, but could still occur in specific environments.

We confirmed that secreted and retained RFP Spn4A T328D variants do not form intracellular complexes and has increased cleavage product (Fig. A1.4B). Cleaved Spn4A T328D-R was not observed in the media, suggesting that the RFP tag may play a role in the retention, trafficking, or degradation of cleaved products. The RFP tag does not affect the secretion of Spn4A T328D-S, as extracellular EI complex and cleavage product were both observed in the T328D-S mutant, similar to the non-tagged Spn4A. Further, RFP tag Spn4A mutants exhibited similar staining to those without the RFP, as detected through confocal microscopy (data not shown).

Last, adenoviruses of furin-directed hinge mutants Spn4A T328D-R and T328D-S, and SKI-1 directed (RSL changed from RRKR to RRLL to inhibit SKI-1) hinge mutant Spn4A T328D RRLL-S and T328D RRLL-R (Supplemental Fig. A1.2B), were produced. These variants were used as negative controls for my own resesearch as well as others who study furin and SKI-1 processing of viral proteins during infections. The adenovirus expression of the hinge mutants were tested in HEK293-C4 cells (Supplemental Fig. A1.5). Spn4A T328D-R and T328D-S did not form an EI complex *in cellulo* unlike the WT forms (Supplemental Fig. A1.5). No EI complexes were detected with SKI-1 directed Spn4A RRLL WT or hinge mutant, as expected. Further work from Vanessa Silva (Jean Lab, technician) demonstrated that unlike Spn4A WT-S, the hinge mutant Spn4A T328D-S was not effective at blocking furin-processing of influenza HA. Andrea Olmstead (Jean Lab, phD student) confirmed that Ad. Spn4A T328D RRLL-S did not form a heat- and SDS-stable complex with SKI-1 and was not effective at blocking SKI-1 activation of sterol regulatory element-binding proteins.

Supplemental Figure A1.1. Sequence alignment of the hinge and reactive site loop region of *Drosophila* Spn4A and human maspin. The P14 amino acid from the RSL (reactive site loop) is in blue text.

Supplemental Figure A1.2. Serpin hinge mutant constructs. The mutations T328D (blue triangles) were engineered into A) furin-directed Spn4A-R, RFP Spn4A-R, Spn4A-S, and RFP Spn4A-S, and B) SKI-1 directed Spn4A RRLL-R and Spn4A RRLL-S. RRKR and RRLL are the amino acid pseudo-substrate sequences targeting furin and SKI-1, respectively. Other key characteristics of the constructs include SP (signal peptide) for targeting to the secretory pathway, HF (His and FLAG tag), RFP (Red fluorescent protein), and HDEL ER retention signal.

A)

B)

Supplemental Figure A1.3. *In vitro* EI complex formation assay and immunofluorescence of Spn4A hinge mutants. A) H4 cells were transfected with Spn4A WT-R and H338R-R for 48 hours. Cells were harvested, lysed, and incubated for 10 minutes with His-tagged recombinant furin at 30°C. The reaction was quenched with 50 mM EDTA, ran on an SDS-PAGE, and probed with anti-His antibodies for Spn4A and furin (green) and anti-tubulin antibodies (red), as a loading control, for western blot analysis. B) H4 cells were transfected as labeled. After 48 hours, they were fixed and probed for Spn4A (red) with anti-FLAG antibodies and ER (green) with anti-calnexin antibodies, and stained for nuclei (blue) with Hoechst dye.

A)

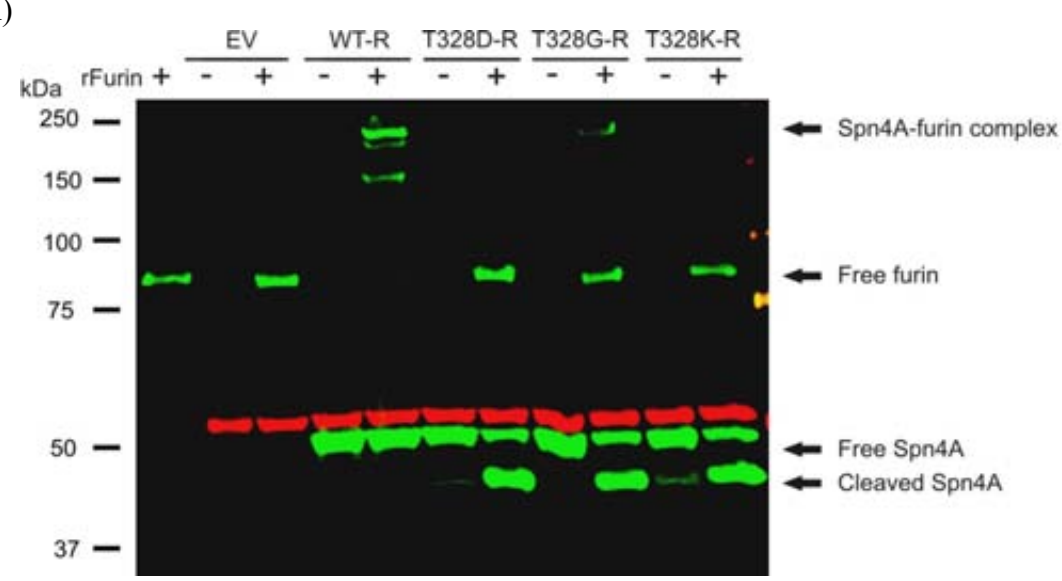
EV
WT-R
T328D-R
T328G-R
T328K-R
kDa
rFurin + - + - + - + - + - +
250
150
100
75
50
37
Spn4A-furin complex
Free furin
Free Spn4A
Cleaved Spn4A

B)

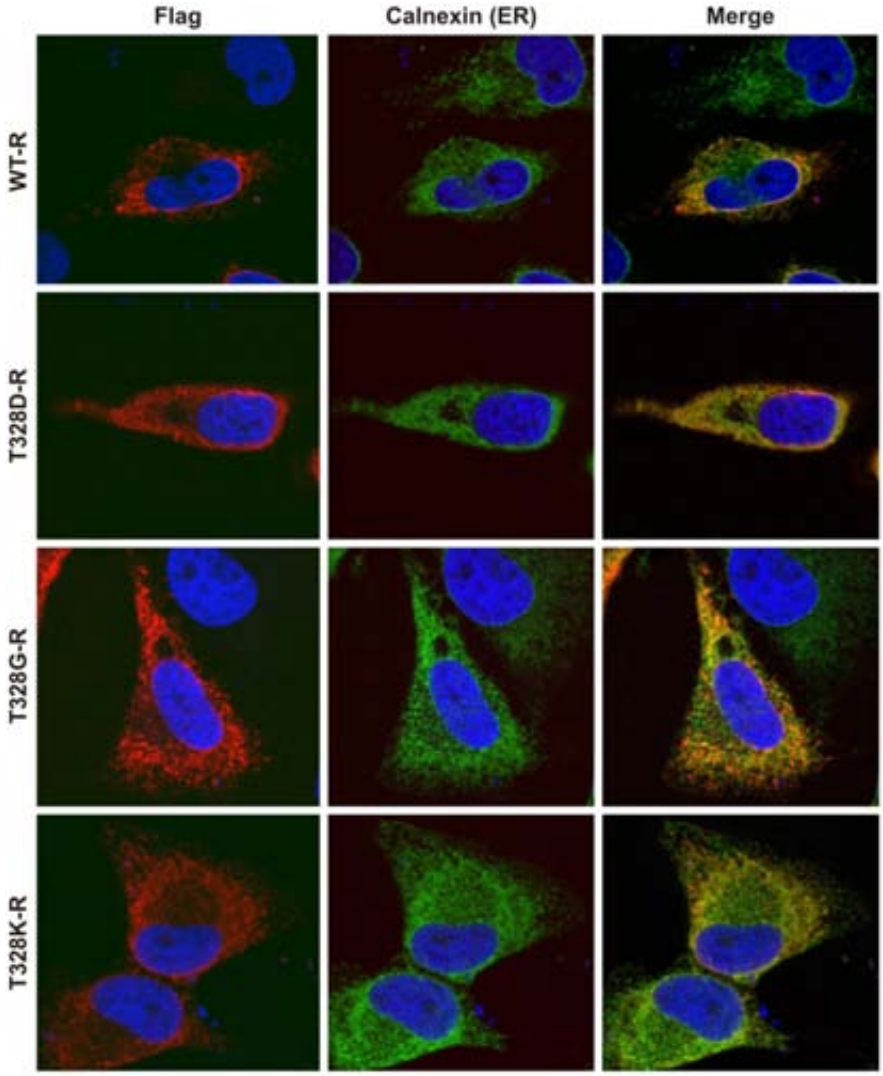
Flag
Calnexin (ER)
Merge
WT-R
T328D-R
T328G-R
T328K-R

Supplemental Figure A1.4. *In cellulo* EI complex formation assay with Spn4A hinge mutants. A) and B) HEK293-C4 cells that overexpress FLAG-tagged furin were transfected as labeled. After 48 hours, media (M) was collected, cells (C) were lysed, boiled for 10 minutes in SDS loading buffer, and proteins separated on a SDS-PAGE. Western blot analysis was performed using anti-FLAG antibodies for Spn4A and furin (green) and anti-Hsp47 (red) as a loading control.

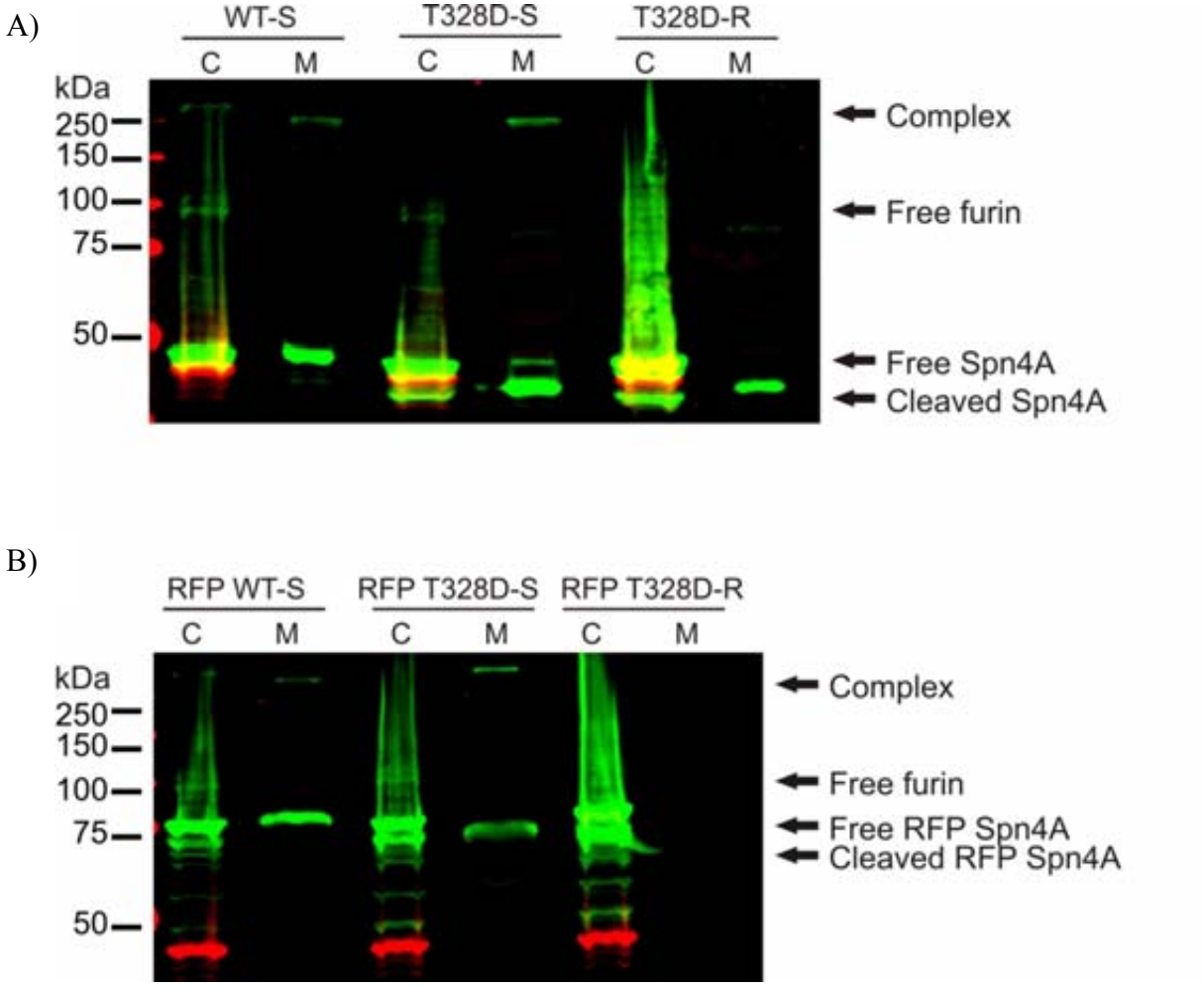

Supplemental Figure A1.5. *In cellulo* EI complex formation assay with adenovirus expressing Spn4A hinge mutants. HEK293-C4 cells that overexpress FLAG-tagged furin were infected as labeled at MOI 5 as labeled for 48 hours. Cells (C) were lysed, boiled for 10 minutes in SDS loading buffer, and proteins separated on a SDS-PAGE. Western blot analysis was performed using anti-FLAG antibodies for Spn4A and furin (green) and anti-Hsp47 (red) as a loading control.

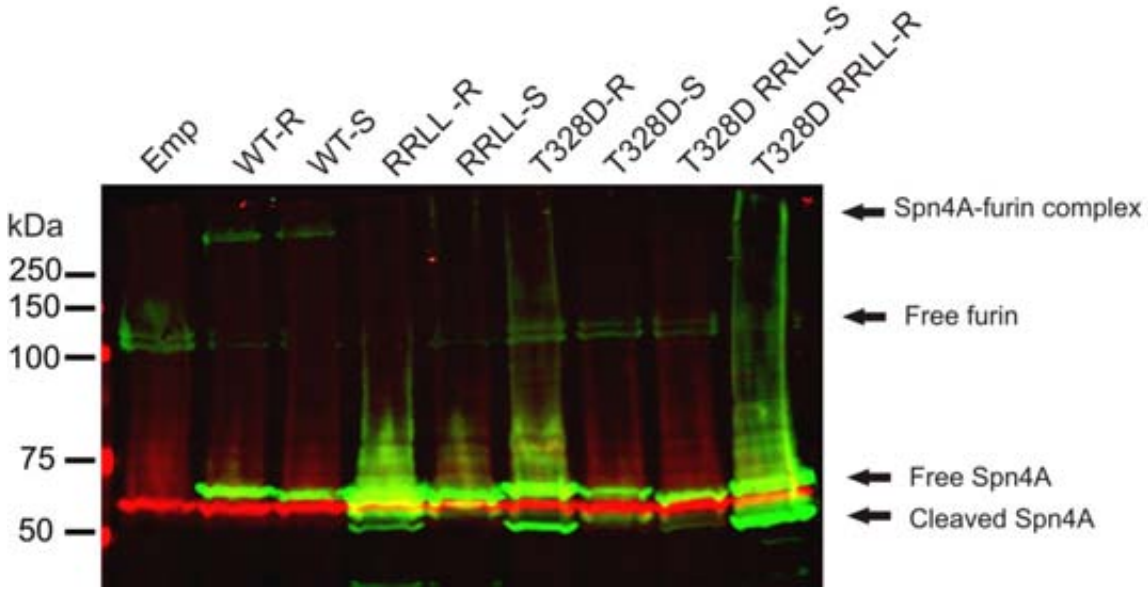

Appendix 2: Supplemental methods and materials

Supplemental Table A2.1. Primer names and sequences used for cloning. For mutagenesis primers, only the forward primer sequences are provided as the reverse primer is just the reverse complement of the forward.

Primer Name	Primer Sequence
Primers for cloning cytoplasmic Spn4A	
F-KpnI-HF Spn4A	ATCGGGTACC ATG CAC CAC CAC CAC CAC CAC GAC
R-Not1-Spn4A-S	ATCG GCGGCCGC TCACTCGCTGGAGGCGAAGGTATTTTC
F-EcoR1-tagRFP	ATCG GAATTC ATG GTG TCT AAG GGC GAA GAG
Sp4s.AS	GCGGCCGCTCACTCGCTGGAGGCGAAGG
Mutagenesis primers for Spn4A	
Spn4A S49A-F	GAGAACATCGTCTTCGCGCCCTTTTCCATCC
Spn4A S49P-F	GAGAACTCGTCTTCCCGCCCTTTTCCATCC
Spn4A S52R F	CGTCTTCTCGCCCTTTCGCATCCAGACTTGTGC
Spn4A H338R- F	GTGTCAGCCATCATACGCAAGGCCTTCATTGAAG
Spn4A G392E-F	CTGCCATTGTTTTGGGAGTCAGTTGTGCGGCTCG
F-Spn4A T328G	CAACGAGGAGGGAGGGGAGGCTGCGGCC
F-Spn4A-T328K	CAACGAGGAGGGAAAGGAGGCTGCGGCC
F-Spn4A-T328D	GTCAACGAGGAGGGAGACGAGGCTGCGGCCACG
Primers for cloning hNS	
F-BamH1- hNS	ATCGGGATCCATGGACTACAAAGATGACGATGACAAGATGGCTT TCCTTGGACTCTTCT
R-Not1-hNS	ATCG GCGGCCGC TTAAAGTTCTTCGAAATCATGTCCAC
F-QC-FhNS1	GTACCGAGCTCGGATCGTTGGACTACAAAGATGACG
F-QC-FhNS2	GGACTACAAAGATGACGTTGACAAGATGGCTTTCC
F-QC-FhNS3	GTTGGACTACAAAGTTGACGTTGACAAGATGGCTTTCC
F-SP-F-hNS	/5PHOS/GACGATGACAAGTTCCCTGAGGAAGCCATTG
R-SP-F-hNS	/5PHOS/ATCTTTGTAGTCAGTGGCCCCTGTAGCCATACT
hNS S49P-F	GATGAAAATATTCTCTTCCCTCCATTGAGTATTGCTCTTGC
hNS H338R-F	GATTTTTCTTTCCAAAGCAATTCGCAAGTCCTTCCTAGAGG

Supplemental Table A2.2. Titers of Adenovirus constructs.

Adenovirus construct	Titer
Empty	2.90E+06
RFP WT-R	5.10E+07
RFP S52R - R	8.10E+05
RFP H338R - R	6.80E+05
RFP WT-S	8.72E+07
RFP H338R-S	1.34E+08
WT-S	5.45E+07
RFP T328D-S*	1.20E+08
RFP H338R-C*	1.64E+08

* RFP T328D-S and RFP H338R-C constructs were made and titered for use in the future.

Supplemental Table A2.3. Primers and probes for qPCR.

Primer name	Sequence	Roche probe #
F-HERPUD1	AGGGACTTGCTTCCAAAGGT	82
R-HERPUD1	CTGTCCCCGATTAGAACCAG	82
F-DDIT3	CAGAGCTGGAACCTGAGGAG	9
R-DDIT3	TGGATCAGTCTGGAAAAGCA	9
F-Hspa5	CAGCCTGGCGACAAGAGT	39
R-Hspa5	CCTTGGGCAGTATTGGATTC	39
F-SPRR2D	GGTACTCTAGCACCGATCTGCT	18
R-SPRR2D	TGCACTGCTGCTGTTGATAA	18
F-CDK2	CCTCCTGGGCTGCAAATA	50
R-CDK2	CAGAATCTCCAGGGAATAGGG	50
F-PCNA	TGGAGAACTTGGAAATGGAAA	69
R-PCNA	GAACTGGTTCATTCATCTCTATGG	69
F-CDC2	TGGATCTGAAGAAATACTTGGATTCTA	79
R-CDC2	CAATCCCCTGTAGGATTTGG	79
F-bAct425	CCAACCGCGAGAAGATGA	64
R-bAct502	CCAGAGGCGTACAGGGATAG	64

Appendix 3: Chapter 2 supplemental figures and tables

Supplemental Figure A3.1. Enlarged figures of RFP Spn4A WT-S and H338R-S.
Experiments were as described in Fig. 2.6.

RFP Spn4A WT-S

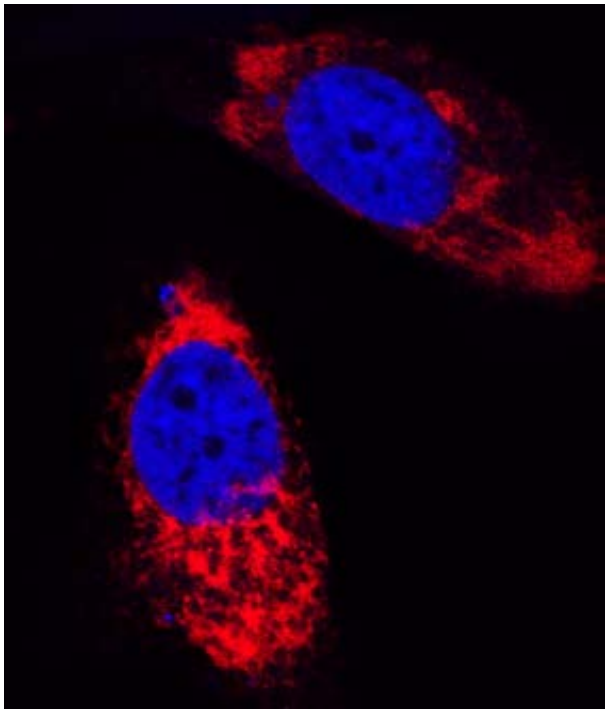

RFP Spn4A H338R-S

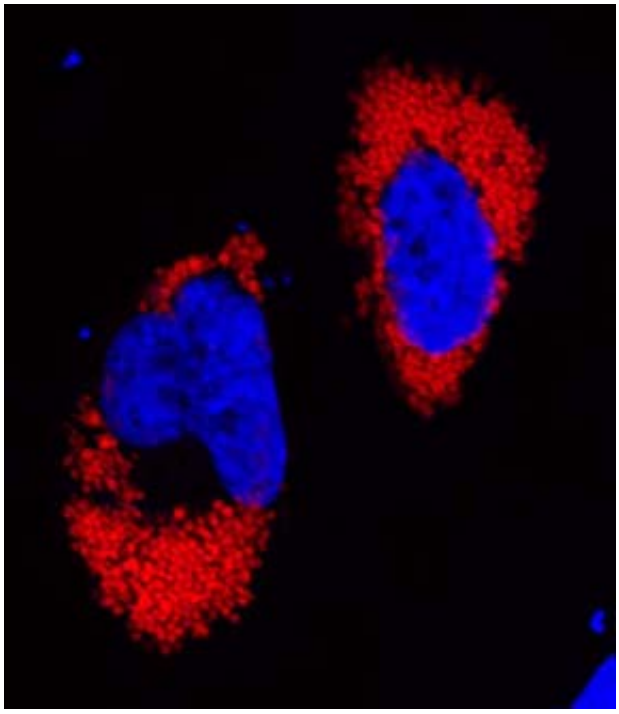

Supplemental Figure A3.2. Example flow cytometry graphs used to calculate percentage of cells expressing RFP Spn4A. Experiments were as described in Fig. 2.8.

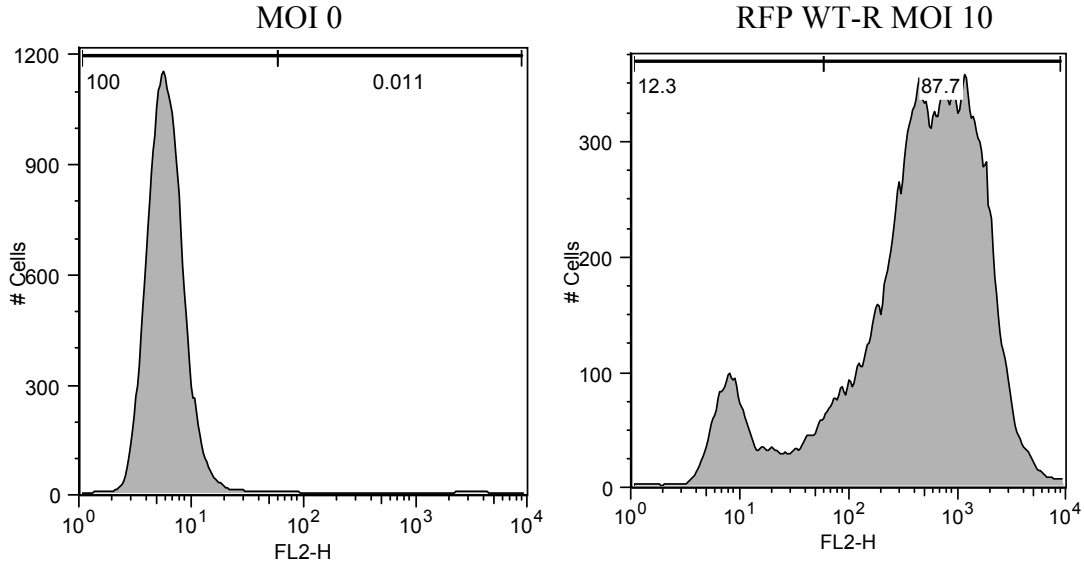

Supplemental Figure A3.3. Immunofluorescent images of transgenic *Drosophila* pupae expressing RFP Spn4A WT-R, RFP Spn4A T328D-R, and RFP Spn4A H338R-R. UAS (upstream activating sequence) transgenic *Drosophila* expressing RFP Spn4A WT-R, T328D-R, or H338R-R were generated and salivary gland expression was driven by Ptc-Gal4. Sample names start with YCL, and a and b denote two different transgenic lines. The non-inhibitory and monomeric Spn4A T328D-R mutant is described in Appendix 1. *Drosophila* images were from Dr. Carl Hashimoto (Yale University).

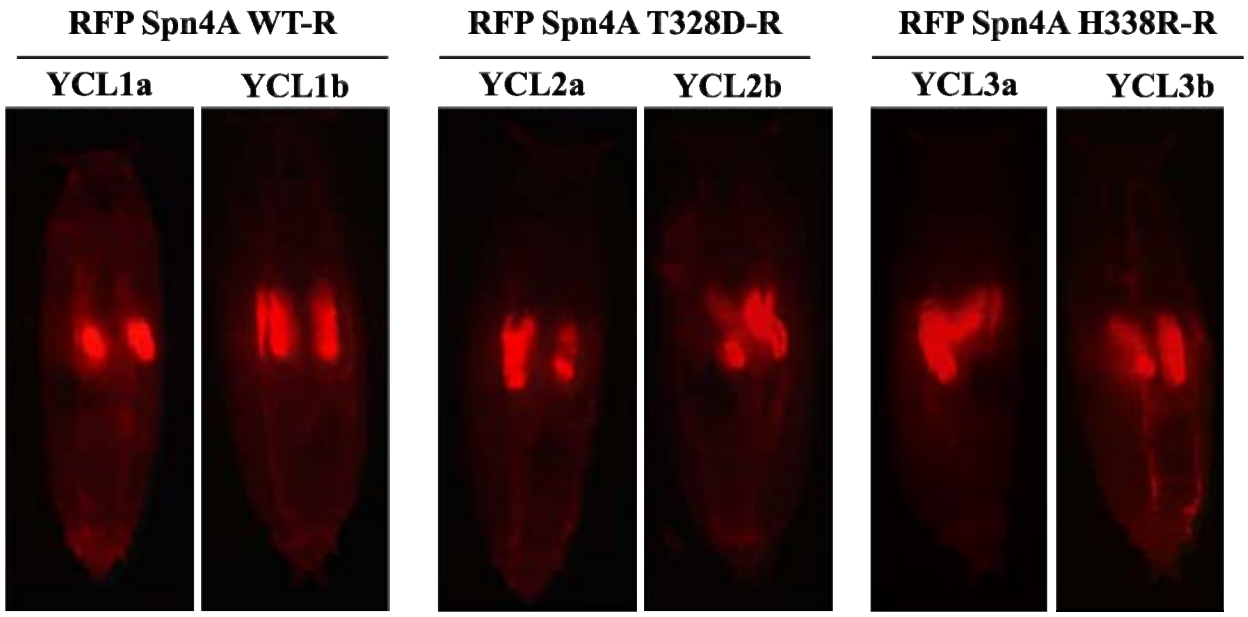

Supplemental Table A3.1. Functional annotation clusters for genes downregulated by secreted or retained RFP Spn4A WT and mutants expression. DAVID functional annotation clustering was carried out using only the non unique downregulated genes and high stringency filter. Term represent annotation term, count is the number of genes involved in the individual term, p-value is calculated using a modified Fisher's exact test and represent the significance of gene-term enrichment, fold enrichment measures the magnitude of enrichment against the complete array background, and annotation cluster enrichment score is the negative log transformation of the geometric mean of the p-values in the group.

Term	Count	p-value	Fold Enrichment
Annotation Cluster 1: Enrichment Score = 2.4			
GO:0009725~response to hormone stimulus	6	2.35E-03	6.15
GO:0009719~response to endogenous stimulus	6	3.59E-03	5.57
GO:0010033~response to organic substance	7	9.50E-03	3.66
Annotation Cluster 2: Enrichment Score = 2.1			
GO:0042493~response to drug	5	2.17E-03	8.76
GO:0007584~response to nutrient	4	5.58E-03	10.71
GO:0048545~response to steroid hormone stimulus	4	1.32E-02	7.81
GO:0031667~response to nutrient levels	4	1.42E-02	7.61
GO:0009991~response to extracellular stimulus	4	1.90E-02	6.82

Appendix 4: Chapter 3 supplemental figures and tables

Supplemental Figure A4.1. Top 10 most significant cellular and molecular functions for genes differentially regulated by RFP Spn4A WT-S expression identified by Ingenuity Pathway Analysis. Ingenuity Pathway Analysis software was used to associate cellular and molecular functions to differentially regulated genes. Significance was calculated from Fisher's exact test.

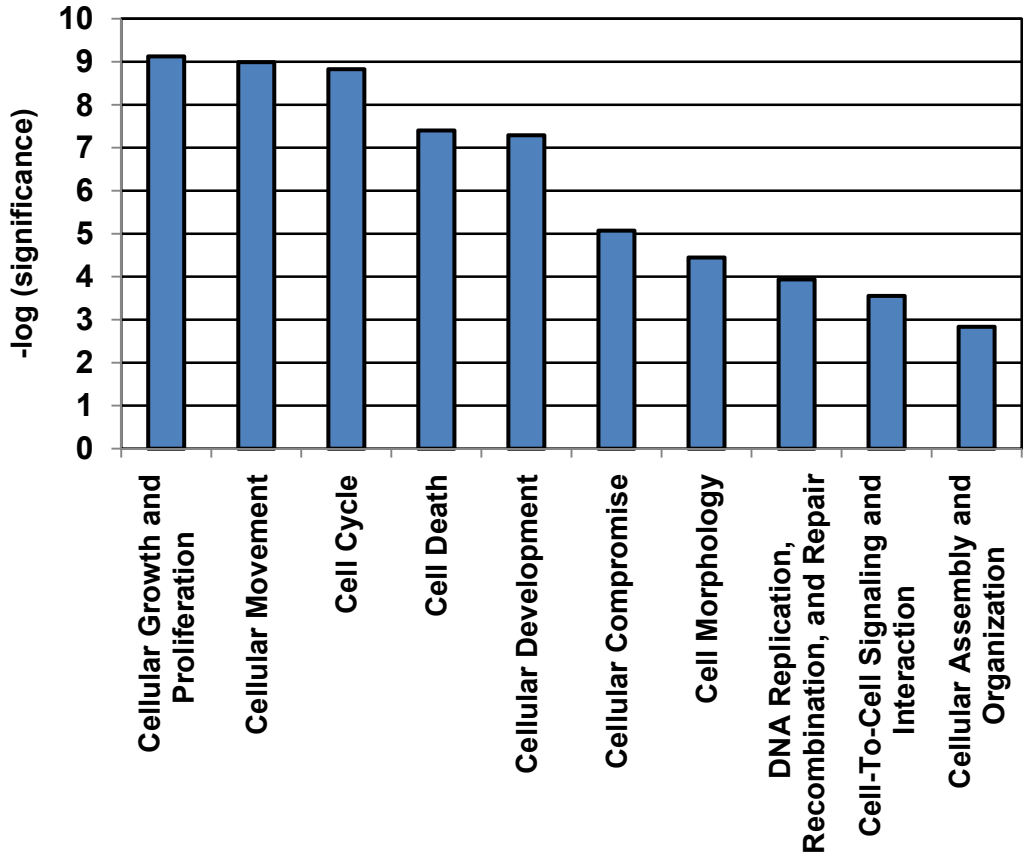

Supplemental Figure A4.2. The most significant canonical pathways deduced from differentially regulated genes in response to RFP Spn4A WT-S. Ingenuity Pathway Analysis software was used to generate canonical pathways regulated in response to RFP Spn4A WT-S. Significance was calculated from Fisher's exact test ($p<0.01$).

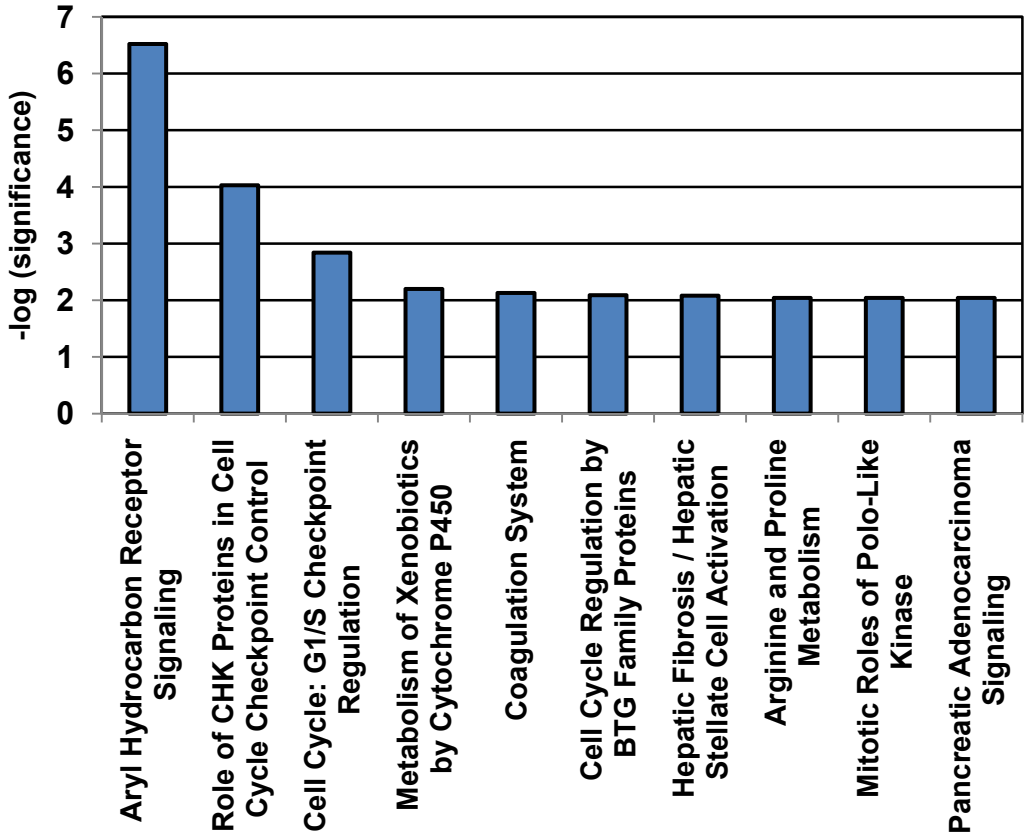

Supplemental Figure A4.3. Top 10 most significant cellular and molecular functions for genes differentially regulated by RFP Spn4A WT-R expression identified by Ingenuity Pathway Analysis. Ingenuity Pathway Analysis software was used to associate cellular and molecular functions to differentially regulated genes. Significance was calculated from Fisher's exact test.

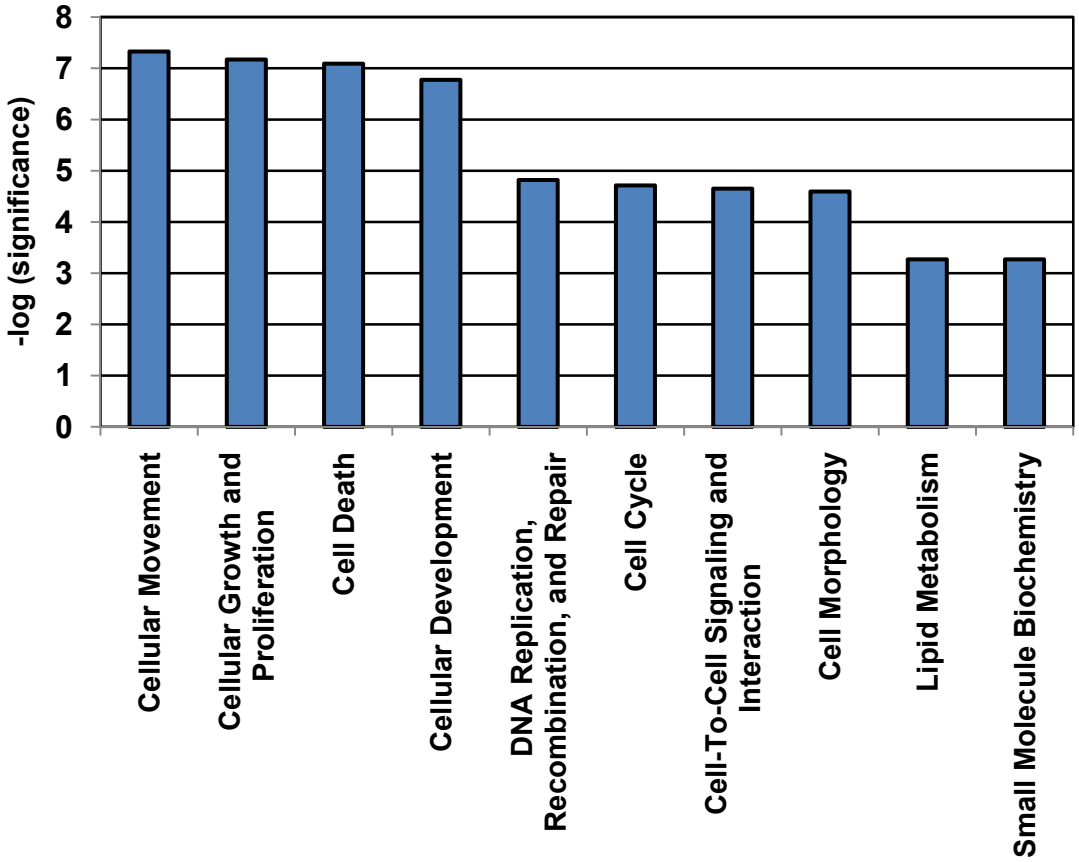

Supplemental Table A4.1. Fold changes of genes discussed in Figure 3.8. Genes symbols, gene names, and fold changes (FC) are listed. NS is not significant.

Gene symbol	Gene name	FC WT-S	FC RFP WT-S	FC RFP WT-R
CELL CYCLE REGULATOR				
CDK2	Homo sapiens cyclin-dependent kinase 2	NS	NS	-1.96
CDC2	Homo sapiens cell division cycle 2, G1 to S and G2 to M	-2.02	-1.81	NS
CDC25A	Homo sapiens cell division cycle 25 homolog A (S. pombe)	-1.82	-1.99	NS
CCNE2	Homo sapiens cyclin E2	-2.81	-2.07	-1.87
CCND1	Homo sapiens cyclin D1	-2.52	-2.51	-2.50
CCNB1	Homo sapiens cyclin B1	-1.92	NS	NS
CDKN1C	Homo sapiens cyclin-dependent kinase inhibitor 1C	2.58	2.66	NS
CDKN2C	Homo sapiens cyclin-dependent kinase inhibitor 2C (p18, inhibits CDK4)	1.91	NS	NS
E2F2	Homo sapiens E2F transcription factor 2	-2.53	-2.43	NS
MYC	Homo sapiens v-myc myelocytomatosis viral oncogene homolog	-1.96	NS	NS
DNA REPLICATION				
ORC6L	Homo sapiens origin recognition complex, subunit 6 like (yeast)	-1.81	NS	NS
MCM4	Homo sapiens minichromosome maintenance complex component 4	-2.10	-1.71	NS
MCM3	Homo sapiens minichromosome maintenance complex component 3	-2.15	-1.95	-1.83
MCM7	Homo sapiens minichromosome maintenance complex component 7	-1.70	NS	NS
MCM6	Homo sapiens minichromosome maintenance complex component 6	-1.70	NS	NS
MCM8	Homo sapiens minichromosome maintenance complex component 8	-1.71	NS	NS
MCM2	Homo sapiens minichromosome maintenance complex component 2	-1.71	NS	-1.70
MCM5	Homo sapiens minichromosome maintenance complex component 5	-1.72	NS	NS
MCM10	Homo sapiens minichromosome maintenance complex component 10	-2.18	-1.82	NS
POLA1	Homo sapiens polymerase (DNA directed), alpha 1, catalytic subunit	-1.71	NS	NS
POLA2	Homo sapiens polymerase (DNA directed), alpha 2 (70kD subunit)	-2.00	NS	NS
POLE2	Homo sapiens polymerase (DNA directed), epsilon 2 (p59 subunit)	-2.18	-2.21	NS
RFC4	Homo sapiens replication factor C (activator 1) 4, 37kDa	-2.16	NS	-1.77
RFC2	Homo sapiens replication factor C (activator 1) 2, 40kDa	-1.93	-2.06	NS
RFC5	Homo sapiens replication factor C (activator 1) 5, 36.5kDa	-2.11	NS	-1.79
RFC3	Homo sapiens replication factor C (activator 1) 3, 38kDa	-2.41	-1.95	-1.80
PRIM1	Homo sapiens primase, DNA, polypeptide 1 (49kDa)	-2.04	NS	-1.80

Genes	Gene name	FC WT-S	FC RFP WT-S	FC RFP WT-R
MITOSIS				
CENPO	Homo sapiens centromere protein O	-1.87	NS	NS
CENPK	Homo sapiens centromere protein K	-1.83	NS	-1.71
CENPE	Homo sapiens centromere protein E, 312kDa	-1.91	NS	NS
CENPA	Homo sapiens centromere protein A	-2.03	NS	NS
MLF1IP	Homo sapiens MLF1 interacting protein	-1.74	NS	NS
RAD21	Homo sapiens RAD21 homolog (S. pombe)	-1.73	NS	NS
NEK2	Homo sapiens NIMA (never in mitosis gene a)-related kinase 2	-1.89	NS	NS
AURKA	Homo sapiens aurora kinase A (AURKA), transcript variant 3, mRNA.	-2.04	-1.89	-2.18
AURKB	Homo sapiens aurora kinase B	NS	-2.11	-1.74
SMC2	Homo sapiens structural maintenance of chromosomes 2	-1.75	NS	NS
SMC3	Homo sapiens structural maintenance of chromosomes 3	-1.75	NS	NS

Supplemental Table A4.2. DAVID GO functional annotation clusters for genes downregulated by RFP Spn4A WT-S expression. DAVID functional annotation clustering was carried using high stringency filter. Term represent annotation term, count is the number of genes involved in the individual term, p-value is calculated using a modified Fisher's exact test and represent the significance of gene-term enrichment, fold enrichment measures the magnitude of enrichment against the complete array background, and annotation cluster enrichment score is the negative log transformation of the geometric mean of the p-values in the group.

Term	Count	p-value	Fold Enrichment
Annotation Cluster 1: Enrichment Score = 5.1			
IPR007875:Sprouty	5	5.59E-07	62.26
domain:SPR	5	5.88E-07	61.59
GO:0043407~negative regulation of MAP kinase activity	5	1.37E-03	10.18
Annotation Cluster 2: Enrichment Score = 4.3			
GO:0000278~mitotic cell cycle	17	3.85E-05	3.41
GO:0022403~cell cycle phase	18	4.01E-05	3.23
GO:0007067~mitosis	13	4.19E-05	4.37
GO:0000280~nuclear division	13	4.19E-05	4.37
GO:0000087~M phase of mitotic cell cycle	13	5.01E-05	4.29
mitosis	11	5.08E-05	5.22
GO:0048285~organelle fission	13	6.19E-05	4.20
GO:0022402~cell cycle process	21	7.11E-05	2.75
GO:0000279~M phase	15	1.39E-04	3.38
Annotation Cluster 3: Enrichment Score = 3.4			
GO:0045859~regulation of protein kinase activity	15	2.58E-04	3.19
GO:0019220~regulation of phosphate metabolic process	18	2.86E-04	2.75
GO:0051174~regulation of phosphorus metabolic process	18	2.86E-04	2.75
GO:0043549~regulation of kinase activity	15	3.64E-04	3.08
GO:0051338~regulation of transferase activity	15	5.49E-04	2.96
GO:0042325~regulation of phosphorylation	17	5.53E-04	2.70
Annotation Cluster 4: Enrichment Score = 3.4			
GO:0031974~membrane-enclosed lumen	42	1.61E-04	1.79
GO:0031981~nuclear lumen	35	2.21E-04	1.91
GO:0043233~organelle lumen	40	4.67E-04	1.73
GO:0070013~intracellular organelle lumen	38	1.19E-03	1.69
Annotation Cluster 5: Enrichment Score = 3.4			
IPR004367:Cyclin, C-terminal	5	1.50E-05	31.13
cyclin	6	2.68E-04	10.37
IPR014400:Cyclin, A/B/D/E	4	2.98E-04	29.05
PIRSF001771:cyclin, A/B/D/E types	4	4.08E-04	25.65
IPR006671:Cyclin, N-terminal	5	5.18E-04	13.21
PIRSF001771:Cyclin_A_B_D_E	4	5.39E-04	23.51
IPR013763:Cyclin-related	5	8.07E-04	11.78

Term	Count	p-value	Fold Enrichment
IPR006670:Cyclin	5	1.09E-03	10.90
SM00385:CYCLIN	5	1.74E-03	9.51
Annotation Cluster 6: Enrichment Score = 2.9			
GO:0001944~vasculature development	12	6.11E-04	3.52
GO:0001568~blood vessel development	11	1.83E-03	3.31
GO:0048514~blood vessel morphogenesis	10	2.27E-03	3.49
Annotation Cluster 7: Enrichment Score = 2.4			
GO:0050817~coagulation	7	2.38E-03	5.13
GO:0007596~blood coagulation	7	2.38E-03	5.13
GO:0007599~hemostasis	7	3.19E-03	4.84
GO:0050878~regulation of body fluid levels	7	1.13E-02	3.72
Annotation Cluster 8: Enrichment Score = 2.2			
GO:0006270~DNA replication initiation	4	1.21E-03	18.33
IPR018525:DNA-dependent ATPase MCM, conserved site	3	3.47E-03	32.69
domain:MCM	3	3.55E-03	32.33
IPR001208:DNA-dependent ATPase MCM	3	4.42E-03	29.05
SM00350:MCM	3	5.71E-03	25.36
IPR012340:Nucleic acid-binding, OB-fold	3	1.19E-01	5.03
Annotation Cluster 9: Enrichment Score = 2.1			
GO:0006469~negative regulation of protein kinase activity	7	1.17E-03	5.90
GO:0033673~negative regulation of kinase activity	7	1.39E-03	5.70
GO:0051348~negative regulation of transferase activity	7	1.94E-03	5.35
GO:0043086~negative regulation of catalytic activity	8	8.21E-02	2.13
GO:0044092~negative regulation of molecular function	9	8.39E-02	1.98

Supplemental Table A4.3. DAVID GO functional annotation clusters for genes upregulated by RFP Spn4A WT-S expression. Parameters are as described in Supplemental Table A4.2.

Term	Count	p-value	Fold Enrichment
Annotation Cluster 1: Enrichment Score = 3.2			
GO:0005578~proteinaceous extracellular matrix	10	3.54E-04	4.47
GO:0031012~extracellular matrix	10	6.18E-04	4.14
extracellular matrix	8	1.32E-03	4.84
Annotation Cluster 2: Enrichment Score = 2.4			
domain:GST N-terminal	4	3.87E-04	27.46
IPR004045:Glutathione S-transferase, N-terminal	4	4.93E-04	25.27
IPR010987:Glutathione S-transferase, C-terminal-like	4	1.13E-03	19.17
IPR017933:Glutathione S-transferase/chloride channel, C-terminal	4	1.25E-03	18.53
domain:GST C-terminal	4	1.49E-03	17.47
PIRSF000503:glutathione transferase	3	5.36E-03	26.36
IPR012335:Thioredoxin fold	5	5.69E-03	6.95
GO:0004364~glutathione transferase activity	3	9.58E-03	19.90
IPR004046:Glutathione S-transferase, C-terminal	3	9.69E-03	19.86
GO:0016765~transferase activity, transferring alkyl or aryl (other than methyl) groups	3	4.98E-02	8.29
hsa00480:Glutathione metabolism	3	5.15E-02	7.96
Annotation Cluster 3: Enrichment Score = 2.0			
GO:0030247~polysaccharide binding	6	5.55E-03	5.24
GO:0001871~pattern binding	6	5.55E-03	5.24
GO:0030246~carbohydrate binding	8	1.58E-02	3.02
GO:0005539~glycosaminoglycan binding	5	2.01E-02	4.77

Supplemental Table A4.4. Top 10 networks generated from genes differentially regulated by RFP Spn4A WT-S expression as identified by Ingenuity Pathway Analysis. Networks were generated using Ingenuity Pathway Analysis. Score is the negative log of the significance, which is based on number of focus molecules and size of network. The most annotated functions from molecules in the network are listed.

ID	Score	Focus Molecules	Top Functions
1	40	27	Cancer, Cardiovascular System Development and Function, Embryonic Development
2	39	26	Cancer, Dermatological Diseases and Conditions, Cell Cycle
3	31	23	Cancer, Gastrointestinal Disease, Hematological System Development and Function
4	29	21	Cancer, Cardiovascular System Development and Function, Cell Morphology
5	27	20	Cellular Growth and Proliferation, Hematological System Development and Function, Cell Death
6	27	20	Connective Tissue Disorders, Organismal Injury and Abnormalities, Cardiovascular System Development and Function
7	23	18	Cell Morphology, Cellular Development, Cellular Movement
8	18	16	Cellular Movement, Hepatic System Disease, Tissue Development
9	18	16	Embryonic Development, Tissue Development, Gene Expression
10	18	15	Genetic Disorder, Neurological Disease, DNA Replication, Recombination, and Repair

Supplemental Table A4.5. DAVID GO functional annotation clusters of unique and downregulated genes in response to Spn4A WT-S compared to RFP Spn4A WT-S. Parameters are as described in Supplemental Table A4.2.

Term	Count	p-value	Fold Enrichment
Annotation Cluster 1: Enrichment Score = 20.4			
GO:0022402~cell cycle process	48	4.59E-23	5.78
GO:0007067~mitosis	32	5.72E-22	9.88
GO:0000280~nuclear division	32	5.72E-22	9.88
GO:0000278~mitotic cell cycle	39	7.72E-22	7.17
GO:0000087~M phase of mitotic cell cycle	32	9.97E-22	9.70
GO:0000279~M phase	37	1.17E-21	7.66
GO:0048285~organelle fission	32	1.96E-21	9.49
GO:0022403~cell cycle phase	40	4.16E-21	6.60
mitosis	28	1.91E-20	11.25
cell division	31	2.55E-19	8.65
GO:0051301~cell division	32	3.81E-18	7.35
Annotation Cluster 2: Enrichment Score = 13.1			
Term	Count	PValue	Fold Enrichment
kinetochore	17	1.74E-16	19.73
GO:0000779~condensed chromosome, centromeric region	17	1.29E-15	17.21
GO:0000777~condensed chromosome kinetochore	14	2.03E-12	16.13
GO:0000776~kinetochore	14	7.78E-11	12.31
Annotation Cluster 3: Enrichment Score = 10.0			
GO:0031981~nuclear lumen	56	1.45E-11	2.61
GO:0043233~organelle lumen	62	1.48E-10	2.29
GO:0070013~intracellular organelle lumen	61	1.74E-10	2.31
GO:0031974~membrane-enclosed lumen	62	3.19E-10	2.25
Annotation Cluster 4: Enrichment Score = 8.1			
GO:0015630~microtubule cytoskeleton	34	3.26E-12	4.21
GO:0044430~cytoskeletal part	37	7.81E-08	2.67
GO:0005856~cytoskeleton	43	2.49E-06	2.12
Annotation Cluster 5: Enrichment Score =6.8			
IPR018525:DNA-dependent ATPase MCM, conserved site	6	2.03E-08	56.78
domain:MCM	6	2.33E-08	55.35
IPR001208:DNA-dependent ATPase MCM	6	4.52E-08	50.47
SM00350:MCM	6	5.16E-08	48.62
IPR012340:Nucleic acid-binding, OB-fold	7	5.92E-05	10.19
Annotation Cluster 6: Enrichment Score =5.54			
GO:0001882~nucleoside binding	48	7.55E-08	2.24
GO:0005524~ATP binding	45	1.22E-07	2.30
GO:0032559~adenyl ribonucleotide binding	45	1.81E-07	2.26
GO:0030554~adenyl nucleotide binding	46	2.94E-07	2.20
GO:0001883~purine nucleoside binding	46	4.55E-07	2.16

Term	Count	p-value	Fold Enrichment
nucleotide phosphate-binding region:ATP	34	6.98E-07	2.62
atp-binding	41	1.38E-06	2.28
GO:0032553~ribonucleotide binding	45	3.90E-05	1.85
GO:0032555~purine ribonucleotide binding	45	3.90E-05	1.85
GO:0017076~purine nucleotide binding	46	5.23E-05	1.81
GO:0000166~nucleotide binding	51	6.51E-05	1.72
nucleotide-binding	41	3.07E-04	1.80
Annotation Cluster 7: Enrichment Score = 4.1			
GO:0006268~DNA unwinding during replication	5	4.13E-05	24.03
GO:0032508~DNA duplex unwinding	5	1.20E-04	18.69
GO:0032392~DNA geometric change	5	1.20E-04	18.69
Annotation Cluster 8: Enrichment Score = 4.0			
GO:0007126~meiosis	9	8.62E-05	6.31
GO:0051327~M phase of meiotic cell cycle	9	8.62E-05	6.31
GO:0051321~meiotic cell cycle	9	9.97E-05	6.18
Annotation Cluster 9: Enrichment Score = 3.1			
GO:0031577~spindle checkpoint	5	2.09E-05	28.04
GO:0045841~negative regulation of mitotic metaphase/anaphase transition	4	4.81E-04	24.47
GO:0007094~mitotic cell cycle spindle assembly checkpoint	4	4.81E-04	24.47
GO:0045839~negative regulation of mitosis	4	6.34E-04	22.43
GO:0051784~negative regulation of nuclear division	4	6.34E-04	22.43
GO:0030071~regulation of mitotic metaphase/anaphase transition	4	3.98E-03	12.24
GO:0010639~negative regulation of organelle organization	5	3.19E-02	4.15
Annotation Cluster 10: Enrichment Score = 3.0			
IPR001752:Kinesin, motor region	6	1.91E-04	11.08
IPR019821:Kinesin, motor region, conserved site	6	1.91E-04	11.08
SM00129:KISc	6	2.17E-04	10.67
domain:Kinesin-motor	6	2.43E-04	10.54
GO:0003777~microtubule motor activity	7	5.19E-04	6.87
GO:0003774~motor activity	8	2.80E-03	4.23
motor protein	7	9.15E-03	3.91
GO:0007018~microtubule-based movement	6	2.36E-02	3.67
Annotation Cluster 11: Enrichment Score = 2.6			
GO:0050000~chromosome localization	4	1.27E-03	17.95
GO:0051303~establishment of chromosome localization	4	1.27E-03	17.95
GO:0051310~metaphase plate congression	3	1.10E-02	18.35
Annotation Cluster 12: Enrichment Score = 2.2			
GO:0032886~regulation of microtubule-based process	6	7.54E-04	8.24
GO:0070507~regulation of microtubule cytoskeleton organization	5	3.34E-03	8.01
GO:0051493~regulation of cytoskeleton organization	5	1.37E-01	2.51

Supplemental Table A4.6. DAVID GO functional annotation clusters of unique and upregulated genes in response to Spn4A WT-S compared to RFP Spn4A WT-S. Parameters are as described in Supplemental Table A4.2.

Term	Count	p-value	Fold Enrichment
Annotation Cluster 1: Enrichment Score = 3.6			
GO:0031012~extracellular matrix	8	3.12E-05	8.33
GO:0005578~proteinaceous extracellular matrix	7	1.89E-04	7.87
GO:0044421~extracellular region part	9	3.46E-03	3.36
Annotation Cluster 2: Enrichment Score: 2.3			
domain:Laminin EGF-like 1	3	1.90E-03	45.30
domain:Laminin EGF-like 2	3	2.05E-03	43.62
laminin egf-like domain	3	2.52E-03	39.36
IPR002049:EGF-like, laminin	3	4.63E-03	28.79
SM00180:EGF_Lam	3	7.53E-03	22.06
IPR013032:EGF-like region, conserved site	4	3.59E-02	5.37

Supplemental Table A4.7. DAVID GO functional annotation cluster of unique and downregulated genes in response to RFP Spn4A WT-S compared to Spn4A WT-S. Parameters are as described in Supplemental Table A4.2.

Term	Count	p-value	Fold Enrichment
Annotation Cluster 1: Enrichment Score = 2.0			
chloride	3	6.39E-03	24.19
GO:0031404~chloride ion binding	3	9.84E-03	19.13
GO:0043168~anion binding	3	1.39E-02	15.98

Supplemental Table A4.8. DAVID GO functional annotation clusters of shared and downregulated genes in response to RFP Spn4A WT-S and Spn4A WT-S. Parameters are as described in Supplemental Table A4.2.

Term	Count	p-value	Fold Enrichment
Annotation Cluster 1: Enrichment Score = 5.4			
IPR007875:Sprouty	5	3.04E-07	72.44
domain:SPR	5	3.13E-07	72.02
GO:0043407~negative regulation of MAP kinase activity	5	8.42E-04	11.61
Annotation Cluster 2: Enrichment Score = 4.2			
GO:0022403~cell cycle phase	17	2.82E-05	3.48
GO:0000278~mitotic cell cycle	16	3.06E-05	3.65
GO:0022402~cell cycle process	20	3.55E-05	2.99
GO:0007067~mitosis	12	5.84E-05	4.60
GO:0000280~nuclear division	12	5.84E-05	4.60
GO:0000087~M phase of mitotic cell cycle	12	6.88E-05	4.52
mitosis	10	8.14E-05	5.55
GO:0048285~organelle fission	12	8.41E-05	4.42
GO:0000279~M phase	14	1.34E-04	3.60
Annotation Cluster 3: Enrichment Score = 3.8			
GO:0045859~regulation of protein kinase activity	15	6.33E-05	3.63
GO:0043549~regulation of kinase activity	15	9.12E-05	3.51
GO:0051338~regulation of transferase activity	15	1.41E-04	3.37
GO:0019220~regulation of phosphate metabolic process	17	1.90E-04	2.96
GO:0051174~regulation of phosphorus metabolic process	17	1.90E-04	2.96
GO:0042325~regulation of phosphorylation	16	4.02E-04	2.89
Annotation Cluster 4: Enrichment Score = 3.6			
IPR004367:Cyclin, C-terminal	5	8.23E-06	36.22
cyclin	6	1.29E-04	12.13
IPR014400:Cyclin, A/B/D/E	4	1.90E-04	33.81
PIRSF001771:cyclin, A/B/D/E types	4	2.72E-04	29.40
IPR006671:Cyclin, N-terminal	5	2.91E-04	15.37
PIRSF001771:Cyclin_A_B_D_E	4	3.59E-04	26.95
IPR013763:Cyclin-related	5	4.56E-04	13.70
IPR006670:Cyclin	5	6.16E-04	12.68
SM00385:CYCLIN	5	9.62E-04	11.14
Annotation Cluster 5: Enrichment Score = 3.37			
GO:0005654~nucleoplasm	25	2.11E-05	2.61
GO:0031981~nuclear lumen	31	2.77E-04	1.98
GO:0031974~membrane-enclosed lumen	36	4.68E-04	1.79
GO:0043233~organelle lumen	34	1.44E-03	1.72
GO:0070013~intracellular organelle lumen	32	3.84E-03	1.66

Term	Count	p-value	Fold Enrichment
Annotation Cluster 6: Enrichment Score = 3.3			
GO:0001944~vasculature development	12	1.97E-04	4.01
GO:0001568~blood vessel development	11	6.71E-04	3.77
GO:0048514~blood vessel morphogenesis	10	9.09E-04	3.98
Annotation Cluster 7: Enrichment Score = 2.7			
GO:0050817~coagulation	7	1.22E-03	5.85
GO:0007596~blood coagulation	7	1.22E-03	5.85
GO:0007599~hemostasis	7	1.65E-03	5.52
GO:0050878~regulation of body fluid levels	7	6.08E-03	4.24
Annotation Cluster 8: Enrichment Score = 2.4			
GO:0006469~negative regulation of protein kinase activity	7	5.86E-04	6.73
GO:0033673~negative regulation of kinase activity	7	7.01E-04	6.50
GO:0051348~negative regulation of transferase activity	7	9.85E-04	6.09
GO:0044092~negative regulation of molecular function	9	4.54E-02	2.26
GO:0043086~negative regulation of catalytic activity	8	4.68E-02	2.42
Annotation Cluster 9: Enrichment Score = 2.2			
GO:0033273~response to vitamin	6	1.11E-03	7.60
GO:0009991~response to extracellular stimulus	9	4.78E-03	3.42
GO:0007584~response to nutrient	7	6.52E-03	4.18
GO:0031667~response to nutrient levels	7	3.03E-02	2.97

Supplemental Table A4.9. DAVID GO functional annotation clusters of shared and upregulated genes in response to RFP Spn4A WT-S and Spn4A WT-S. Parameters are as described in Supplemental Table A4.2.

Term	Count	p-value	Fold Enrichment
Annotation Cluster 1: Enrichment Score = 2.9			
extracellular matrix	8	2.47E-04	6.38
GO:0005578~proteinaceous extracellular matrix	9	3.45E-04	5.06
GO:0031012~extracellular matrix	9	5.74E-04	4.69
GO:0044421~extracellular region part	11	3.63E-02	2.05
Annotation Cluster 1: Enrichment Score = 2.1			
GO:0005539~glycosaminoglycan binding	5	6.69E-03	6.57
GO:0001871~pattern binding	5	9.12E-03	6.01
GO:0030247~polysaccharide binding	5	9.12E-03	6.01
Annotation Cluster 1: Enrichment Score = 2.0			
IPR015590:Aldehyde dehydrogenase	3	4.16E-03	30.54
IPR016162:Aldehyde dehydrogenase, N-terminal	3	4.64E-03	28.93
GO:0016620~oxidoreductase activity, acting on the aldehyde or oxo group of donors, NAD or NADP as acceptor	3	6.75E-03	23.82
IPR016160:Aldehyde dehydrogenase, conserved site	3	9.93E-03	19.63
GO:0006081~cellular aldehyde metabolic process	3	1.05E-02	19.00
nucleotide phosphate-binding region:NAD	3	5.96E-02	7.51

Supplemental Table A4.10. DAVID GO functional annotation clusters of genes downregulated by RFP Spn4A WT-R expression. Parameters are as described in Supplemental Table A4.2.

Term	Count	p-value	Fold Enrichment
Annotation Cluster 1: Enrichment Score = 3.8			
cell division	12	8.61E-06	5.69
GO:0000279~M phase	13	9.87E-05	3.98
mitosis	9	1.09E-04	6.14
GO:0022402~cell cycle process	17	1.40E-04	3.02
GO:0051301~cell division	12	1.68E-04	4.07
GO:0022403~cell cycle phase	14	2.19E-04	3.41
GO:0000278~mitotic cell cycle	13	2.98E-04	3.53
GO:0000280~nuclear division	10	3.35E-04	4.56
GO:0007067~mitosis	10	3.35E-04	4.56
GO:0000087~M phase of mitotic cell cycle	10	3.83E-04	4.48
GO:0048285~organelle fission	10	4.50E-04	4.38
Annotation Cluster 2: Enrichment Score = 3.3			
GO:0006268~DNA unwinding during replication	4	3.27E-04	28.40
GO:0032508~DNA duplex unwinding	4	7.11E-04	22.09
GO:0032392~DNA geometric change	4	7.11E-04	22.09
Annotation Cluster 3: Enrichment Score = 2.3			
GO:0006270~DNA replication initiation	4	4.95E-04	24.85
domain:MCM	3	1.73E-03	46.44
IPR018525:DNA-dependent ATPase MCM, conserved site	3	1.80E-03	45.47
IPR001208:DNA-dependent ATPase MCM	3	2.31E-03	40.41
SM00350:MCM	3	3.09E-03	34.60
IPR012340:Nucleic acid-binding, OB-fold	3	6.76E-02	6.99
GO:0044454~nuclear chromosome part	4	1.09E-01	3.43
Annotation Cluster 4: Enrichment Score = 2.1			
GO:0005663~DNA replication factor C complex	4	1.66E-05	69.24
PIRSF004274:phage T4 DNA polymerase accessory protein 44	3	5.37E-04	77.09
GO:0006297~nucleotide-excision repair, DNA gap filling	4	5.97E-04	23.39
GO:0033170~protein-DNA loading ATPase activity	3	7.29E-04	68.74
GO:0003689~DNA clamp loader activity	3	7.29E-04	68.74
hsa03430:Mismatch repair	4	2.63E-03	13.92
hsa03420:Nucleotide excision repair	4	1.64E-02	7.27
GO:0006289~nucleotide-excision repair	4	1.67E-02	7.36
GO:0008094~DNA-dependent ATPase activity	3	8.71E-02	6.03
GO:0006281~DNA repair	5	3.04E-01	1.78
GO:0016887~ATPase activity	4	5.51E-01	1.38
GO:0042623~ATPase activity, coupled	3	6.84E-01	1.27

Supplemental Table A4.11. DAVID GO functional annotation clusters of genes upregulated genes by RFP Spn4A WT-R expression. Parameters are as described in Supplemental Table A4.2.

Term	Count	p-value	Fold Enrichment
Annotation Cluster 1: Enrichment Score = 2.2			
GO:0004033~aldo-keto reductase activity	3	1.06E-03	60.01
nadp	4	9.44E-03	9.01
hsa00980:Metabolism of xenobiotics by cytochrome P450	3	2.53E-02	11.46

Supplementary Table A4.12. Top 10 networks generated from genes differentially regulated by RFP Spn4A WT-R expression as identified by Ingenuity Pathway Analysis. Networks were generated using Ingenuity Pathway Analysis. Score is the negative log of the significance, which is based on number of focus molecules and size of network. The most annotated functions from molecules in the network are listed.

ID	Score	Focus Molecules	Top Functions
1	38	23	DNA Replication, Recombination, and Repair, Embryonic Development, Drug Metabolism
2	38	23	Lipid Metabolism, Small Molecule Biochemistry, Behavior
3	35	22	Cell-To-Cell Signaling and Interaction, Tissue Development, Cellular Movement
4	32	21	Cellular Growth and Proliferation, Cellular Development, Cell Cycle
5	27	19	Cell Cycle, Cancer, Cell Death
6	27	18	Infectious Disease, Cell Death, Cell Morphology
7	19	14	Genetic Disorder, Skeletal and Muscular Disorders, Cellular Growth and Proliferation
8	18	14	Cellular Development, Connective Tissue Development and Function, Skeletal and Muscular System Development and Function
9	14	11	Cancer, Dermatological Diseases and Conditions, Gene Expression
10	7	7	Cellular Assembly and Organization, Nervous System Development and Function, Infectious Disease

Supplemental Table A4.13. DAVID GO functional annotation clusters of unique and downregulated genes in response to RFP Spn4A WT-S compared to RFP Spn4A WT-R. Parameters are as described in Supplemental Table A4.2.

Term	Count	p-value	Fold Enrichment
Annotation Cluster 1: Enrichment Score = 3.5			
GO:0031974~membrane-enclosed lumen	28	9.97E-05	2.14
GO:0043233~organelle lumen	27	1.94E-04	2.10
GO:0031981~nuclear lumen	22	7.81E-04	2.15
GO:0070013~intracellular organelle lumen	25	8.62E-04	1.99
Annotation Cluster 2: Enrichment Score = 2.9			
GO:0022403~cell cycle phase	11	1.08E-03	3.50
GO:0022402~cell cycle process	13	1.09E-03	3.02
GO:0000278~mitotic cell cycle	10	1.89E-03	3.55
Annotation Cluster 3: Enrichment Score = 2.2			
GO:0000279~M phase	9	3.35E-03	3.60
GO:0000280~nuclear division	7	6.40E-03	4.17
GO:0007067~mitosis	7	6.40E-03	4.17
GO:0000087~M phase of mitotic cell cycle	7	6.98E-03	4.10
GO:0048285~organelle fission	7	7.75E-03	4.01

Supplemental Table A4.14. DAVID GO functional annotation clusters of unique and upregulated genes in response to RFP Spn4A WT-S compared to RFP Spn4A WT-R. Parameters are as described in Supplemental Table A4.2.

Term	Count	p-value	Fold Enrichment
Annotation Cluster 1: Enrichment Score = 3.2			
GO:0005578~proteinaceous extracellular matrix	9	2.81E-04	5.21
GO:0031012~extracellular matrix	9	4.70E-04	4.83
extracellular matrix	7	1.71E-03	5.47
Annotation Cluster 2: Enrichment Score = 2.6			
domain:GST N-terminal	4	1.80E-04	35.50
IPR004045:Glutathione S-transferase, N-terminal	4	2.32E-04	32.58
IPR010987:Glutathione S-transferase, C-terminal-like	4	5.35E-04	24.71
IPR017933:Glutathione S-transferase/chloride channel, C-terminal	4	5.92E-04	23.89
domain:GST C-terminal	4	7.06E-04	22.59
PIRSF000503:glutathione transferase	3	3.24E-03	33.89
hsa00980:Metabolism of xenobiotics by cytochrome P450	4	4.25E-03	11.59
hsa00982:Drug metabolism	4	4.66E-03	11.21
IPR004046:Glutathione S-transferase, C-terminal	3	5.91E-03	25.60
GO:0004364~glutathione transferase activity	3	6.04E-03	25.20
IPR012335:Thioredoxin fold	4	1.79E-02	7.17
hsa00480:Glutathione metabolism	3	3.09E-02	10.43
GO:0016765~transferase activity, transferring alkyl or aryl (other than methyl) groups	3	3.22E-02	10.50
Annotation Cluster 3: Enrichment Score = 2.4			
cell adhesion	9	1.75E-03	4.00
GO:0007155~cell adhesion	11	6.04E-03	2.73
GO:0022610~biological adhesion	11	6.10E-03	2.73

Supplemental Table A4.15. DAVID GO functional annotation clusters of unique and downregulated genes in response to RFP Spn4A WT-R compared to RFP Spn4A WT-S. Parameters are as described in Supplemental Table A4.2.

Term	Count	p-value	Fold Enrichment
Annotation Cluster 1: Enrichment Score = 4.2			
hsa03030:DNA replication	5	9.79E-06	33.34
dna replication	5	1.45E-04	18.44
GO:0005657~replication fork	4	1.94E-04	34.33
Annotation Cluster 2: Enrichment Score = 2.9			
GO:0022402~cell cycle process	9	7.46E-04	4.40
GO:0000279~M phase	7	1.01E-03	5.89
GO:0022403~cell cycle phase	7	3.18E-03	4.69

Supplemental Table A4.16. DAVID GO functional annotation clusters of shared and downregulated genes in response to RFP Spn4A WT-R and RFP Spn4A WT-S. Parameters are as described in Supplemental Table A4.2.

Term	Count	p-value	Fold Enrichment
Annotation Cluster 1: Enrichment Score = 3.1			
dna replication	6	7.71E-05	13.56
GO:0006260~DNA replication	8	1.66E-04	6.76
GO:0006259~DNA metabolic process	8	3.62E-02	2.54
Annotation Cluster 2: Enrichment Score = 2.3			
Term	Count	PValue	Fold Enrichment
GO:0051174~regulation of phosphorus metabolic process	10	3.24E-03	3.25
GO:0019220~regulation of phosphate metabolic process	10	3.24E-03	3.25
GO:0042325~regulation of phosphorylation	9	8.71E-03	3.04
Annotation Cluster 3: Enrichment Score= 2.3			
GO:0032103~positive regulation of response to external stimulus	5	7.08E-04	12.21
GO:0032101~regulation of response to external stimulus	6	2.98E-03	6.05
GO:0048584~positive regulation of response to stimulus	5	6.09E-02	3.34
Annotation Cluster4: Enrichment Score= 2.2			
GO:0009967~positive regulation of signal transduction	8	2.56E-03	4.25
GO:0010740~positive regulation of protein kinase cascade	6	4.00E-03	5.65
GO:0010627~regulation of protein kinase cascade	6	2.01E-02	3.79
Annotation Cluster 5: Enrichment Score= 2.1			
GO:0033273~response to vitamin	5	7.96E-04	11.84
GO:0007584~response to nutrient	5	1.19E-02	5.58
GO:0009991~response to extracellular stimulus	6	1.28E-02	4.26
GO:0031667~response to nutrient levels	5	3.62E-02	3.97

Appendix 5: Gene lists and annotations

Supplemental Table A5.1. Lists of genes downregulated and upregulated by secreted or retained RFP Spn4A WT and mutants. Differentially regulated genes in response to RFP Spn4A WT (RFP WT-S and RFP WT-R) were compared against mutants (RFP H338R-S, RFP S52R-R, and RFP H338R-R) and the shared genes reported.

Downregulated genes	Upregulated genes
PTGS2	AKNA
PLAU	ARMET
ACOX2	SDF2L1
RGS2	C1orf24
F2RL1	TMEM50B
TFAP2C	FAM129A
HOXA5	SELS
PTPRE	PDIA6
WDR79	PLAC8
VGF	HERPUD1
ARHGAP19	FICD
TRIB2	DNAJB9
PPAP2B	WARS
MSX1	HYOU1
SLC35A2	DNAJB11
TMEM158	NUCB2
CD55	TRA1P2
COL8A1	HSP90B1
ALDH1A3	AKR1C2
CDH11	SEC11C
TMEM100	DNAJC3
RDH10	PDIA3P
CCL2	HSPA5
SEMA3A	CRELD1
C10orf58	SASS6
CBX1	TRIB3
FBXO32	CDK2AP2
TGFBR2	PDIA4
ICAM3	ANG
TNFRSF11B	TAC1
SNHG5	CRELD2
PAPPA	BEX2
COL4A1	DDIT3
ST8SIA4	S100P
GNG2	CDH15
NOV	
SYTL2	
AADACL1	
GCHFR	
ADAM19	
S1PR3	

Supplemental Table A5.2. List of genes downregulated and upregulated by Spn4A WT-S that are associated with DAVID GO annotations. Genes from Table 3.1 and Table 3.2 are reported. One annotation term with the most number of genes from each cluster, up to ten clusters, are listed.

Cluster	Downregulated annotation	Genes
1	GO:0022402~cell cycle process	ADCY3,KIF23,RP11-553N16.2,KNTC1,TTK,PKMYT1, AURKA,TGFB2,ACVR1B,CCNE1,C18ORF24,RAD21,CDCA2 ,DAQB-126H3.5,C11ORF82,CDCA5,MYC,ASPM,DAAP-57C1.3,KIF11,RP11-42J4.2,CDC2,SGOL2,SGOL1, CCNF, KIF15,TPX2,NUSAP1,MND1,PBK,RBBP8,CCND1,MAD2L1, TIMELESS,HAUS8,NUP43,CCDC99,NEK2,TIPIN,POLA1,AN LN,SPC24,SPC25,RP11-262H5.1,NCAPG2,CENPA, FBXO5, HELLS,ERCC6L,IL8,RP11-101P17.12,BIRC5, CENPE,GAS1, CDC25C,SMC2,SMC3,CDC25A,BRCA1,CCNB1,AC132812.1; KPNA2,PSMC4,KIF20B,RP5-1163J1.2,RAD54B,BARD1
2	kinetochore	CENPO,CCDC99,CTA-250D10.18,NEK2,SGOL2,SGOL1,KNTC1,RP11-101P17.12,NUP85,CENPE,CENPK,MLF1IP,SPC24,SPC25,RP1 1-262H5.1,C18ORF24,MAD2L1,CENPA,NUP43,ERCC6L
3	GO:0031974~membrane-enclosed lumen	KIF23,E2F2,RP11-475E11.4,GRPEL2,MRPS35,RP4-686C3.1,LYAR,RP1-261G23.1,EZH2,PDLIM3,RP4-686B20.1,PKMYT1,MCM10,TGFB2,CDT1,CCNE2,PRIM1,CC NE1,MCM8,MCM7,PTGES,FANCI,FOXF1,AEN,DDX21,MY C,EXOSC8,EXOSC9,CDC2,USP1,ENC1,TPX2,NUSAP1,TOP BP1,MCM2,MCM3,MCM4,HMGA1,MCM5,MCM6,RFC5,CC ND1,RFC3,RFC4,RFC2,NAV2,NOL11,KIF4A,HMGB2,LMNB 1,NEK2,TH1L,NOC3L,POLA1,BOP1,POLA2,HNRNPA3,MRP L11,HNRNPL,RP11-262H5.1,DDX46,KDELC2 ,CDC45L,POLE2,RP11-230F18.1,CACYBP,BRIX1,ORC6L, FBXO5,ETV4,SRGN,PHLDA1,XPOT,CEBPB,BIRC5,CDC25C ,WWTR1,HNRNPA1,SMC3,CDC25A,BRCA1,SF3A3,FXR1,C CNB1,DUSP4,TXNDC12,AC132812.1;KPNA2,ATF4,PLK4,C DKN2AIP,PHF15,KIF20B,PCNA,TBL1X,PARP2,CHAF1B
4	IPR012340:Nucleic acid-binding, OB-fold	MCM8,YARS,MCM7,MCM2,MCM3,MCM4,MCM5,MCM6
5	GO:0001882~nucleoside binding	ADCY3,KIF23,GRPEL2,RP5-1054A22.2,PFTK1,FIGNL1,RP4-686B20.1,PKMYT1,TTK,AURKA,ACVR1B,MCM8,MCM7,RP 5-902P8.8,MKKS,DDX21,MLKL,DAQB-126H3.5,DDX10 ,KIF14,IRAK2,DAAP-57C1.3,YARS,KIF11,CDC2,KIF15, TPX2,PBK,MCM2,PRKCE,MCM3,MCM4,RP11-8N6.1,MCM5,MCM6,RFC5,RFC3,RFC4,RFC2,NAV2,FLAD1, UBE2T,PRPS2,KIF4A,NEK2,DCK,POLA1,ASNS,NP,PFAS,T RIB1,EPHB2,DDX46,KIF21B,HELLS,ERCC6L,MARS,TGFB R2,ATAD2,CENPE,SMC2,SMC3,GART,TXNDC12,PLK4,PS MC4,KIF20B,RAD54B,MYO19
6	GO:0006268~DNA unwinding during replication	HMGB2,MCM7,MCM2,MCM4,HMGA1,MCM6
7	IPR007875:Sprouty	SPRY2,SPRY1,SPRED2,SPRED1,SPRY4
8	domain:Kinesin-motor	KIF23,KIF14,KIF4A,KIF11,KIF15,KIF20B,CENPE,DAQB-126H3.5,KIF21B
9	GO:0005663~DNA replication factor C complex	RFC5,RFC3,RFC4,RFC2,PCNA
10	cyclin	CCNE2,CCNB1,CCNE1,CCND1,RP5-973N23.3,CACYBP,CCNF

Cluster	Upregulated annotation	Genes
1	GO:0044421~extracellular region part	HAPLN1,LUM,RP11-157P1.6,COL3A1,MGP,POSTN,DCN,SPARC,COL16A1,NTN3,RP11-54O7.13,METRN,CRISPLD2,KAL1,SFRP4,COL6A1,SEPP1,EPYC,MFAP4,RP1-238D15.1
2	GO:0005581~collagen	LUM,COL3A1,COL6A1,COL16A1,RP1-238D15.1
3	GO:0005539~glycosaminoglycan binding	HAPLN1,CRISPLD2,POSTN,DCN,GPNMB,EPYC
4	IPR018244:Allergen V5/Tpx-1 related, conserved site	CRISPLD1,CRISPLD2,PI15
5	leucine-rich repeat	LUM,LRRN3,LRRC17,DCN,LRRC4C,EPYC,SLITRK5

Supplemental Table A5.3. Genes associated with cell growth and proliferation as annotated by Ingenuity Pathway Analysis molecular functions in response to Spn4A WT-S. Gene symbols, gene names, and fold changes are listed.

Gene Symbol	Gene Name	Fold Change
IL8	interleukin 8	-5.319
ITGA2	integrin, alpha 2 (CD49B, alpha 2 subunit of VLA-2 receptor)	-4.695
TGFA	transforming growth factor, alpha	-3.846
GDF15	growth differentiation factor 15	-3.236
EMP1	epithelial membrane protein 1	-3.106
SPP1	secreted phosphoprotein 1	-2.959
MT2A	metallothionein 2A	-2.950
ITGA6	integrin, alpha 6	-2.857
PHLDA1	pleckstrin homology-like domain, family A, member 1	-2.778
ENC1	ectodermal-neural cortex (with BTB-like domain)	-2.667
F3	coagulation factor III (thromboplastin, tissue factor)	-2.545
E2F2	E2F transcription factor 2	-2.532
CCND1	cyclin D1	-2.519
VEGFA	vascular endothelial growth factor A	-2.500
PSMC4	proteasome (prosome, macropain) 26S subunit, ATPase, 4	-2.494
CDCA7	cell division cycle associated 7	-2.481
TFAP2C	transcription factor AP-2 gamma (activating enhancer binding protein 2 gamma)	-2.481
JAG1	jagged 1 (Alagille syndrome)	-2.469
GPRC5C	G protein-coupled receptor, family C, group 5, member C	-2.451
SH2B3	SH2B adaptor protein 3	-2.404
MT1A	metallothionein 1A	-2.392
CDT1	chromatin licensing and DNA replication factor 1	-2.381
HES1	hairy and enhancer of split 1, (*Drosophila*)	-2.315
IER3	immediate early response 3	-2.315
DCBLD2	discoidin, CUB and LCCL domain containing 2	-2.288
TGM2	transglutaminase 2 (C polypeptide, protein-glutamine-gamma-glutamyltransferase)	-2.278
IRF1	interferon regulatory factor 1	-2.268
PRNP	prion protein	-2.262
FHL2	four and a half LIM domains 2	-2.252
PLA2G4A	phospholipase A2, group IVA (cytosolic, calcium-dependent)	-2.247
TPX2	TPX2, microtubule-associated, homolog (Xenopus laevis)	-2.212
GAS1	growth arrest-specific 1	-2.203
PTGES	prostaglandin E synthase	-2.193
SPRY2	sprouty homolog 2 (*Drosophila*)	-2.193
PNP	purine nucleoside phosphorylase	-2.169
PTGER4	prostaglandin E receptor 4 (subtype EP4)	-2.165
PBK	PDZ binding kinase	-2.155
ATF4	activating transcription factor 4 (tax-responsive enhancer element B67)	-2.146
MCM3	minichromosome maintenance complex component 3	-2.146
HMGA1	high mobility group AT-hook 1	-2.128
PHLDA2	pleckstrin homology-like domain, family A, member 2	-2.114
HEY1	hairy/enhancer-of-split related with YRPW motif 1	-2.110
KIF23	kinesin family member 23	-2.110
DDX21	DEAD (Asp-Glu-Ala-Asp) box polypeptide 21	-2.101
STIL	SCL/TAL1 interrupting locus	-2.083
TFPI2	tissue factor pathway inhibitor 2	-2.083
KIF20B	kinesin family member 20B	-2.075
PLAUR	plasminogen activator, urokinase receptor	-2.070
ADORA2B	adenosine A2b receptor	-2.058
IL11	interleukin 11	-2.049

Gene Symbol	Gene Name	Fold Change
SF3A3	splicing factor 3a, subunit 3, 60kDa	-2.049
AURKA	aurora kinase A	-2.045
NAMPT	nicotinamide phosphoribosyltransferase	-2.037
BARD1	BRCA1 associated RING domain 1	-2.033
CCNE1	cyclin E1	-2.024
MAD2L1	MAD2 mitotic arrest deficient-like 1 (yeast)	-2.024
SMOX	spermine oxidase	-2.020
ATAD2	ATPase family, AAA domain containing 2	-2.016
EFNB2	ephrin-B2	-2.012
BCAR3	breast cancer anti-estrogen resistance 3	-1.988
EIF2C2	eukaryotic translation initiation factor 2C, 2	-1.965
PTPRF	protein tyrosine phosphatase, receptor type, F	-1.961
MYC	v-myc myelocytomatosis viral oncogene homolog (avian)	-1.957
BMP7	bone morphogenetic protein 7	-1.949
TFPI	tissue factor pathway inhibitor (lipoprotein-associated coagulation inhibitor)	-1.949
CDK1	cyclin-dependent kinase 1	-1.946
CDCA7L	cell division cycle associated 7-like	-1.942
ADCY3	adenylate cyclase 3	-1.923
CCNB1	cyclin B1	-1.919
TGFB2	transforming growth factor, beta 2	-1.919
FOXM1	forkhead box M1	-1.908
NEK2	NIMA (never in mitosis gene a)-related kinase 2	-1.894
PMEPA1	prostate transmembrane protein, androgen induced 1	-1.890
SPRED1	sprouty-related, EVH1 domain containing 1	-1.887
BST2	bone marrow stromal cell antigen 2	-1.883
DCK	deoxycytidine kinase	-1.883
DTL	denticleless homolog (*Drosophila*)	-1.883
PTPN13	protein tyrosine phosphatase, non-receptor type 13 (APO-1/CD95 (Fas)-associated phosphatase)	-1.880
TFDP1	transcription factor Dp-1	-1.873
UHRF1	ubiquitin-like with PHD and ring finger domains 1	-1.873
AK3L1	adenylate kinase 3-like 1	-1.869
CDC45L	CDC45 cell division cycle 45-like (S. cerevisiae)	-1.869
ATP6V0E2	ATPase, H+ transporting V0 subunit e2	-1.862
BRCA1	breast cancer 1, early onset	-1.855
CTSC	cathepsin C	-1.848
IDO1	indoleamine 2,3-dioxygenase 1	-1.848
TRIB1	tribbles homolog 1 (*Drosophila*)	-1.845
TSC22D1	TSC22 domain family, member 1	-1.842
CDC25A	cell division cycle 25 homolog A (S. pombe)	-1.825
VLDLR	very low density lipoprotein receptor	-1.821
CDKN2AIP	CDKN2A interacting protein	-1.818
SERPINE2	serpin peptidase inhibitor, clade E (nexin, plasminogen activator inhibitor type 1), member 2	-1.818
TIPIN	TIMELESS interacting protein	-1.818
ORC6L	origin recognition complex, subunit 6 like (yeast)	-1.815
CD44	CD44 molecule (Indian blood group)	-1.808
EZR	ezrin	-1.799
PLAT	plasminogen activator, tissue	-1.799
TTK	TTK protein kinase	-1.799
PLIN2	perilipin 2	-1.792

Gene Symbol	Gene Name	Fold Change
KIF11	kinesin family member 11	-1.779
CCND3	cyclin D3	-1.776
NFRSF10B	tumor necrosis factor receptor superfamily, member 10b	-1.773
DUSP5	dual specificity phosphatase 5	-1.767
PCNA	proliferating cell nuclear antigen	-1.767
COL6A3	collagen, type VI, alpha 3	-1.764
PRKCE	protein kinase C, epsilon	-1.764
USP10	ubiquitin specific peptidase 10	-1.764
ANLN	anillin, actin binding protein	-1.761
SUV39H1	suppressor of variegation 3-9 homolog 1 (*Drosophila*)	-1.757
SMC3	structural maintenance of chromosomes 3	-1.748
ACVR1B	activin A receptor, type IB	-1.745
BCL6	B-cell CLL/lymphoma 6	-1.745
CDK14	cyclin-dependent kinase 14	-1.742
CDC25C	cell division cycle 25 homolog C (S. pombe)	-1.739
KIF15	kinesin family member 15	-1.739
ITGB5	integrin, beta 5	-1.727
EZH2	enhancer of zeste homolog 2 (*Drosophila*)	-1.724
MCM5	minichromosome maintenance complex component 5	-1.724
CDCA4	cell division cycle associated 4	-1.721
SFRP1	secreted frizzled-related protein 1	-1.721
CEBPB	CCAAT/enhancer binding protein (C/EBP), beta	-1.718
HMMR	hyaluronan-mediated motility receptor (RHAMM)	-1.718
CAST	calpastatin	-1.712
PPAP2C	phosphatidic acid phosphatase type 2C	-1.712
POLA1	polymerase (DNA directed), alpha 1, catalytic subunit	-1.709
BIRC5	baculoviral IAP repeat-containing 5	-1.706
MCM2	minichromosome maintenance complex component 2	-1.706
TGFBR2	transforming growth factor, beta receptor II (70/80kDa)	-1.706
WWTR1	WW domain containing transcription regulator 1	-1.706
TIMELESS	timeless homolog (*Drosophila*)	-1.704
MCM7	minichromosome maintenance complex component 7	-1.701
SLC22A18	solute carrier family 22, member 18	1.716
GSTM1	glutathione S-transferase mu 1	1.719
GPER	G protein-coupled estrogen receptor 1	1.721
SPARC	secreted protein, acidic, cysteine-rich (osteonectin)	1.737
COL6A1	collagen, type VI, alpha 1	1.738
ACTG1	actin, gamma 1	1.758
VAV3	vav 3 guanine nucleotide exchange factor	1.763
IFITM1	interferon induced transmembrane protein 1 (9-27)	1.783
MGP	matrix Gla protein	1.785
RARRES3	retinoic acid receptor responder (tazarotene induced) 3	1.814
POSTN	periostin, osteoblast specific factor	1.850
MAGED2	melanoma antigen family D, 2	1.854
SOX4	SRY (sex determining region Y)-box 4	1.862
CDKN2C	cyclin-dependent kinase inhibitor 2C (p18, inhibits CDK4)	1.911
LAMA5	laminin, alpha 5	1.916
FOLR1	folate receptor 1 (adult)	1.930
MXD4	MAX dimerization protein 4	1.951
TMEFF2	transmembrane protein with EGF-like and two follistatin-like domains 2	1.973
NR3C1	nuclear receptor subfamily 3, group C, member 1 (glucocorticoid receptor)	2.007

Gene Symbol	Gene Name	Fold Change
NFE2	nuclear factor (erythroid-derived 2), 45kDa	2.141
MUC1	mucin 1, cell surface associated	2.150
CD24	CD24 molecule	2.283
S100A4	S100 calcium binding protein A4	2.364
CDKN1C	cyclin-dependent kinase inhibitor 1C (p57, Kip2)	2.578
SOCS2	suppressor of cytokine signaling 2	2.643
BMF	Bcl2 modifying factor	2.762
ALDH3A1	aldehyde dehydrogenase 3 family, memberA1	2.892
SFRP4	secreted frizzled-related protein 4	2.997
GUCY1A3	guanylate cyclase 1, soluble, alpha 3	3.054
GPNMB	glycoprotein (transmembrane) nmb	3.122
CD36	CD36 molecule (thrombospondin receptor)	3.329
LUM	lumican	3.379
ALDH1A1	aldehyde dehydrogenase 1 family, member A1	4.080
DCN	decorin	4.215

Supplemental Table A5.4. Genes associated with cell movement as annotated by Ingenuity Pathway Analysis molecular functions in response to Spn4A WT-S. Gene symbols, gene names, and fold changes are listed.

Gene Symbol	Gene Name	Fold Change
IL8	interleukin 8	-5.319
ITGA2	integrin, alpha 2 (CD49B, alpha 2 subunit of VLA-2 receptor)	-4.695
ETV5	ets variant 5	-4.348
TGFA	transforming growth factor, alpha	-3.846
GDF15	growth differentiation factor 15	-3.236
SPP1	secreted phosphoprotein 1	-2.959
ERRFI1	ERBB receptor feedback inhibitor 1	-2.933
AJAP1 (includes EG:55966)	adherens junctions associated protein 1	-2.924
ITGA6	integrin, alpha 6	-2.857
RGS1	regulator of G-protein signaling 1	-2.710
F3	coagulation factor III (thromboplastin, tissue factor)	-2.545
CCND1	cyclin D1	-2.519
VEGFA	vascular endothelial growth factor A	-2.500
TFAP2C	transcription factor AP-2 gamma (activating enhancer binding protein 2 gamma)	-2.481
JAG1	jagged 1 (Alagille syndrome)	-2.469
SDC1	syndecan 1	-2.445
STX16	syntaxin 16	-2.392
ETV4	ets variant 4	-2.387
DCBLD2	discoidin, CUB and LCCL domain containing 2	-2.288
TGM2	transglutaminase 2 (C polypeptide, protein-glutamine-gamma-glutamyltransferase)	-2.278
PRNP	prion protein	-2.262
FHL2	four and a half LIM domains 2	-2.252
MMP3	matrix metallopeptidase 3 (stromelysin 1, progelatinase)	-2.232
SPRY2	sprouty homolog 2 (*Drosophila*)	-2.193
PTPN12	protein tyrosine phosphatase, non-receptor type 12	-2.188
PBK	PDZ binding kinase	-2.155
HMGA1	high mobility group AT-hook 1	-2.128
HEY1	hairy/enhancer-of-split related with YRPW motif 1	-2.110
KIF23	kinesin family member 23	-2.110
TFPI2	tissue factor pathway inhibitor 2	-2.083
KIF20B	kinesin family member 20B	-2.075
PLAUR	plasminogen activator, urokinase receptor	-2.070
ECT2	epithelial cell transforming sequence 2 oncogene	-2.062
IL11	interleukin 11	-2.049
AURKA	aurora kinase A	-2.045
NUSAP1	nucleolar and spindle associated protein 1	-2.024
EFNB2	ephrin-B2	-2.012
TGFBR2	transforming growth factor, beta receptor II (70/80kDa)	-1.996
BCAR3	breast cancer anti-estrogen resistance 3	-1.988
CCL26 (includes EG:10344)	chemokine (C-C motif) ligand 26	-1.965
PTPRF	protein tyrosine phosphatase, receptor type, F	-1.961

Gene Symbol	Gene Name	Fold Change
DIAPH3	diaphanous homolog 3 (*Drosophila*)	-1.957
MYC	v-myc myelocytomatosis viral oncogene homolog (avian)	-1.957
BMP7	bone morphogenetic protein 7	-1.949
TFPI	tissue factor pathway inhibitor (lipoprotein-associated coagulation inhibitor)	-1.949
CDK1	cyclin-dependent kinase 1	-1.946
KIF14	kinesin family member 14	-1.934
PPAP2B	phosphatidic acid phosphatase type 2B	-1.934
CCNB1	cyclin B1	-1.919
TGFB2	transforming growth factor, beta 2	-1.919
FOXM1	forkhead box M1	-1.908
EPHB2	EPH receptor B2	-1.848
NUP85	nucleoporin 85kDa	-1.848
TRIB1	tribbles homolog 1 (*Drosophila*)	-1.845
KIF4A	kinesin family member 4A	-1.818
SERPINE2	serpin peptidase inhibitor, clade E (nexin, plasminogen activator inhibitor type 1), member 2	-1.818
CD44	CD44 molecule (Indian blood group)	-1.808
EZR	ezrin	-1.799
PLAT	plasminogen activator, tissue	-1.799
GNG12	guanine nucleotide binding protein (G protein), gamma 12	-1.786
DEK	DEK oncogene	-1.776
YARS	tyrosyl-tRNA synthetase	-1.767
PRKCE	protein kinase C, epsilon	-1.764
ANLN	anillin, actin binding protein	-1.761
ITGB5	integrin, beta 5	-1.727
EZH2	enhancer of zeste homolog 2 (*Drosophila*)	-1.724
SFRP1	secreted frizzled-related protein 1	-1.721
HMMR	hyaluronan-mediated motility receptor (RHAMM)	-1.718
CAST	calpastatin	-1.712
KIFC1	kinesin family member C1	-1.706
WWTR1	WW domain containing transcription regulator 1	-1.706
NDRG1	N-myc downstream regulated 1	1.730
SPARC	secreted protein, acidic, cysteine-rich (osteonectin)	1.737
ACTG1	actin, gamma 1	1.758
VAV3	vav 3 guanine nucleotide exchange factor	1.763
CITED2	Cbp/p300-interacting transactivator, with Glu/Asp-rich carboxy-terminal domain, 2	1.764
MGP	matrix Gla protein	1.785
MYLK	myosin light chain kinase	1.785
POSTN	periostin, osteoblast specific factor	1.850
LAMA5	laminin, alpha 5	1.916
AMOT	angiomotin	1.984
MUC1	mucin 1, cell surface associated	2.150
KAL1	Kallmann syndrome 1 sequence	2.182
C5ORF13	chromosome 5 open reading frame 13	2.203
ALPP	alkaline phosphatase, placental (Regan isozyme)	2.206

Gene Symbol	Gene Name	Fold Change
CD24	CD24 molecule	2.283
S100A4	S100 calcium binding protein A4	2.364
SOCS2	suppressor of cytokine signaling 2	2.643
PPAP2A	phosphatidic acid phosphatase type 2A	2.717
GUCY1A3	guanylate cyclase 1, soluble, alpha 3	3.054
CD36	CD36 molecule (thrombospondin receptor)	3.329
OLR1	oxidized low density lipoprotein (lectin-like) receptor 1	3.630
DCN	decorin	4.215

Supplemental Table A5.5. Genes associated with significant canonical pathways identified by Ingenuity in response to Spn4A WT-S. Fisher's exact test was used to calculate the p-value. Ratio represents the ratio of focus molecules to total molecules in the canonical pathway.

Ingenuity Canonical Pathways	-log(p-value)	Ratio	Molecules
Role of CHK Proteins in Cell Cycle Checkpoint Control	6.67	0.29	PCNA, CDC25C, RFC4, RFC2, RFC5, BRCA1, CDK1, E2F2, CDC25A, RFC3
Aryl Hydrocarbon Receptor Signaling	4.54	0.11	HSPB3, GSTM1, TFDP1, POLA1, CCND1, MYC, TGM2, CCNE1, NCOA7, GSTM2, ALDH1A1, CCND3, TGFB2, ALDH3B1, ALDH3A1, MCM7
Cell Cycle: G1/S Checkpoint Regulation	3.79	0.16	MYC, CCNE1, CCND3, TFDP1, SUV39H1, TGFB2, CCND1, E2F2, CDC25A
Role of BRCA1 in DNA Damage Response	3.73	0.15	RFC4, FANCG, BARD1, RFC2, RBBP8, RFC5, BRCA1, E2F2, RFC3
Mitotic Roles of Polo-Like Kinase	3.66	0.16	KIF23, CDC25C, PLK4, CCNB1, PPP2R2B, PKMYT1, CDK1, KIF11, CDC25A
ATM Signaling	3.24	0.15	SMC3, CDC25C, CCNB1, SMC2, ATF4, BRCA1, CDK1, CDC25A
Hereditary Breast Cancer Signaling	2.52	0.09	CDC25C, CCNB1, RFC4, FANCG, BARD1, RFC2, RFC5, BRCA1, CCND1, CDK1, RFC3
Pancreatic Adenocarcinoma Signaling	2.31	0.09	VEGFA, TGFBR2, CCNE1, TFDP1, SUV39H1, TGFA, TGFB2, CCND1, E2F2, BIRC5